NUREG/CR-0578
UCRL-52633

HIGH LEVEL WASTE REPOSITORY SITE SUITABILITY STUDY — STATUS REPORT

Richard A. Heckman
Donald F. Towse
Dana Isherwood
Ted Harvey
Thomas Holdsworth

7968080 467

Prepared for
U. S. Nuclear Regulatory Commission
by
Lawrence Livermore Laboratory

506 086

NOTICE

This report was prepared as an account of work sponsored by an agency of the United States Government. Neither the United States Government nor any agency thereof, or any of their employees, makes any warranty, expressed or implied, or assumes any legal liability or responsibility for any third party's use, or the results of such use, of any information, apparatus, product or process disclosed in this report, or represents that its use by such third party would not infringe privately owned rights.

The views expressed in this report are not necessarily those of the U. S. Nuclear Regulatory Commission.

Available from National Technical Information Service Springfield, Virginia 22161

506 087

NUREG/CR-0578
UCRL-52633

HIGH LEVEL WASTE REPOSITORY SITE SUITABILITY STUDY — STATUS REPORT

Richard A. Heckman
Donald F. Towse
Dana Isherwood
Ted Harvey
Thomas Holdsworth

Manuscript Submitted: February 1979
Date Published: July 1979

Prepared for
Office of Nuclear Material Safety and Safeguards
U.S. Nuclear Regulatory Commission
Washington, D. C. 20555
Under Interagency Agreement DOE 40-550-75
NRC FIN No. A 0277-7
by
Lawrence Livermore Laboratory
Livermore, CA 94550

operated by University of California

for the U.S. Department of Energy

506 088

FOREWORD

This report covers the progress made during the work period October, 1976 to January, 1978, by the Waste Management Technical Support Project of the Lawrence Livermore Laboratory for the Nuclear Regulatory Commission, under FIN A0277-7.

Delays in publication have been the result of the document review process in an evolutionary regulatory environment and changes in programmatic priorities.

506 089

PREFACE

The Nuclear Regulatory Commission is currently developing a framework of regulations, criteria, and standards, within which it can effectively and efficiently regulate management and disposal of radioactive wastes.

This framework is an evolving one, involving the development of many different aspects of waste management. As part of this framework, during FY77 the Nuclear Regulatory Commission sponsored work on:

1. performance criteria for solid high-level waste (SHLW),
2. SHLW repository/storage facility design criteria,
3. site suitability criteria for SHLW repositories, and
4. classification and disposal criteria for radioactive wastes.

During FY77, the Lawrence Livermore Laboratory (LLL) provided broad technical support on a continuing basis to aid in the development of this framework.

As the need for regulations, standards, and models emerged, LLL capabilities provided technical support towards the development of disposal criteria for radioactive wastes in general. This report describes progress made in particular on site suitability criteria for SHLW repositories.

This report, a composite of several working papers, has been through a number of draft stages. Each draft contains more technical detail than the preceding one, reflecting continuing progress on the project.

The initial report was first issued as a draft working paper for a programmatic review held at LLL on March 22 and 23, 1977. At that time, it was used for the briefing on the preliminary results of the work on site suitability criteria. Another draft was generated as a briefing document for the meetings with NRC at LLL on August 16-18, 1977.

506 090

On September 30, 1977, a draft report on the status of this work was prepared and sent to an NRC peer review panel. The report was used by the panel in their deliberations on the proposed NRC draft regulations on site suitability criteria for SHLW repositories. The NRC staff forwarded comments and suggestions on format and these were incorporated into a May, 1978 draft. A final technical editing of the May, 1978 draft has resulted in this revised status report for FY 77.

This report describes, in turn, 1) a physical model which simulates the natural environment of many potential sites, 2) mathematical models for the calculation of the performance of hypothetical repository sites, 3) a parameter data base representative of the natural environment, and 4) analyses and results. The appendices give details of the mathematics and of the analytic methods employed.

506 091

TABLE OF CONTENTS

506 092

506 093

506 094

506 095

LIST OF ILLUSTRATIONS

506 097

LIST OF TABLES

506 098

506 099

506 100

SUMMARY

The disposal of high-level waste (HLW) in an underground repository requires a method for determining the suitability of the repository site while considering potential hazards to public health and safety. The main purpose of our study is to identify and analyze the physical factors that are important for making this determination. This work entails the analysis of relevant geologic events and their effects on geohydrologic parameters, the modeling of waste transport through the hydrologic system, and the calculation of associated radiologic risk.

PHYSICAL MODEL

A six-layer hydrologic model was developed whose parameters and dimensions can be varied to simulate the natural environment of many potential sites. The variables define the environment that detemines the configurations and lengths of flow paths, as well as the properties that influence flow rates and waste concentrations. Composition and solubilities of the waste source and the influences of different water table levels, pressures, and pressure gradients can also be varied. This allows study of the effects of fractures around the repository, faults, solution breccia pipes, boreholes, and shorter aquifer paths to the biosphere.

MATHEMATICAL MODELS

A series of computer simulation programs representing the mathematical models was developed to calculate the performance of hypothetical repository sites. The Oak Ridge ORIGEN program was used to calculate the inventory of nuclides considered important. The WASTE program, the waste transport code, was used to calculate the amount of radioactive waste released to the biosphere via groundwater transport. Included are the effects of mass transport, chemical interactions between waste components and pathway media, hydrodynamic dispersion in the direction of flow, and radioactive decay. BIODOSE, our

biosphere transport and dose program, was used in conjunction with the WASTE program to calculate expected individual and population doses. Potential flow pathways that can be modeled include water wells, lakes, and a river, estuary, and ocean system. BIODOSE was derived from many models developed during the past 10 y to compute the consequences of radionuclide releases to the environment. Development has generally followed the methods outlined in NRC Regulatory Guide 1.109, but departs in two main respects from previous methods. First, it considers the buildup of radioactivity in soils and sediment, since radionuclide releases can occur over a period of 10 000 y or longer. Second, it computes population doses without referring explicitly to the local demography, since future population statistics are unknown. Our goal in developing the model was to furnish a means of evaluating the consequences and risk for conditions not too different from those we experience today.

PARAMETER VALUES

For our generic repository model, we specified parameters, events, and values that are representative of the natural environment, excluding rare extremes. Values were obtained from published and unpublished data on the sedimentary sequences of shale-sandstone and shale-evaporite-sandstone. Where laboratory and field data were inadequate, we relied on theoretical treatments and on the judgments of those experienced in the field. The model data base comprises: (1) geochemical processes, (2) hydrologic factors, (3) natural tectonic features, (4) man-made features, (5) seismic considerations, and (6) climatic effects.

One of the major factors influencing radionuclide migration in natural environments is retardation due to ion exchange. On the basis of available data and chemical theory, we have estimated retardation factors for three radionuclide groups: (1) the actinides, (2) the fission products, and (3) a separate group of fission products with no sorption characteristics represented by the radionuclides ^{129}I and ^{99}Tc.

506 102

Studies of water- and oil-bearing systems provide the major portion of our data base for hydrologic parameters. These data have been supplemented with the results of flow tests for civil engineering works, particularly tests in fractured rocks.

Features that affect hydraulic continuity include fracture zones with and without faults and solution-collapse breccia pipes. All these features may have a wide range of permeability and porosity. Our data are based on field measurements, the history of active faults, and the history of collapse features in terrains of soluble rocks. Dimensions, hydrologic values, and rates of change are provided.

Shafts, tunnels, and boreholes may form permeable pathways. From experience and rock mechanics analyses, we specified dimensions and hydrologic characteristics of the fracture zones formed around the man-made features, and estimated their changes with time. Seals have not yet been designed for the purpose of near-perfect sealing over long time periods. Therefore, we expect shaft and borehole seals to fail relatively early in the life of the repository, and have analyzed the effects of such failures.

We have assumed that seismic activity would not cause significant damage or change to the rock or the rock openings except in epicentral regions. Formation of a new fault on a repository site is an event of low probability. Reopening (or closing) of an existing fault is a more frequent occurrence.

Data from the CLIMAP project allow us to reconstruct climate regimes for the past one million years and to identify the wet and dry extremes. Correlation of past climate conditions with solar energy incidence provides a basis for projecting future climatic conditions to analyze their effect on the hydrology and waste isolation system of the repository model. Although we have changed hydrologic system parameters as a first step in this analysis, climatic change has not been explicitly introduced into the calculations.

SENSITIVITY ANALYSIS

By changing parameter values in the basic physical model, the breaching of barriers and radionuclide migration through different pathways can be simulated in shale and salt repositories. The resultant changes in dose and concentrations test the relative importance of the different parameters. Our studies have included "unflawed" and "flawed" environments.

In "unflawed" cases having no faults or other failure mechanisms, we varied simple parameters and combinations of parameters in 62 simulations. In the "flawed" cases we made 23 simulations with varied parameter values and added pathways. The "flawed" category included faults; failed borehole seals; failed backfill and shaft seals; and, in the case of the salt repository, the formation of a solution breccia pipe.

Three performance-measure formats are used to assess the parametric sensitivity analyses: peak individual dose for whole body and critical organ, population dose integrated over three million years following decommissioning, and the maximum groundwater concentration in an aquifer above the repository.

In the unflawed shale repository, actinide and fission product retardation, porosity, permeability of the tunnel and shaft fracture zone, thickness of the repository and barrier layers, and dissolution rate of the waste showed a major effect on individual dose to a critical organ. Except for the dissolution rate of the waste, the above parameters are related to transition time from repository to biosphere. These same parameters are valid in the salt repository, except that salt permeability replaces the fracture zone permeability in importance.

Integrated population dose is relatively insensitive to change in parameter values. Critical organ dose in most cases was between 0.16 and 0.51 man-rem/MWe-y to the gastrointestinal tract. Higher values occurred in the few cases where actinides migrated to the river within three million years. Once the waste reaches the river, the population dose depends on yearly use rates of the water system.

506 104

Aquifer concentrations showed the most sensitivity to changes in the model parameters, especially the transition time from the repository to the aquifer. This time dependence makes retardation the single most important parameter in the sensitivity analyses.

Excavation and backfilling can produce flow paths to the aquifer. Excavation creates a fracture zone around the shaft and tunnel, and backfill deteriorates with time. Increased levels of radionuclides in the above aquifer could result. Because of dispersion, however, they have little effect on concentration or dose some distance from the repository. This is also true for seal failures in exploration boreholes.

Two types of geologic events investigated to date are: the activation of a fault intersecting a repository, and the formation of a breccia pipe above a salt repository. In general, the doses did not differ significantly from what we calculated for the baseline models without geologic events. Expected values of dose were essentially unaffected by a change in probability of two orders of magnitude. Geologic events such as volcanos and major meterorites were excluded because their probability of occurrence was so low.

UNCERTAINTY ANALYSIS

Our estimates of HLW repository performance are subject to scientific uncertainties, both in the site descriptors and the mathematical models used to analyze future events. If, for the moment, the potential uncertainties associated with the mathematical model are ignored, a methodology can be established to determine the effect on the site performance of uncertainties associated with the site descriptors. To this end we have devised a Monte Carlo technique for the hydrology/geology radionuclide transport code, WASTE. This allows not only "best-estimate" prediction but also a measure of the data-induced uncertainty of the "best-estimate."

The Monte Carlo approach to the uncertainty analysis facilitates a statistical characterization of the precision of the site performance prediction. The technique is simple to implement, and can be modified to accommodate many parameter distributions and constraints.

506 105

ACKNOWLEDGMENTS

We acknowledge with thanks the efforts and contributions of all project team members who participated in this study. We appreciate, also, the input and guidance provided by W. M. Hewitt and N. Dayem of the NRC. The following people contributed to the technical work of the project and to the writing of this report.

Lawrence Livermore Laboratory
- D. Bernreuter
- S. Dreiss
- G. Potter

The Analytic Sciences Corporation (TASC)
- L. Berman
- C. Koplik
- B. Poss
- A. Sutherland

Golder Associates, Incorporated
- D. Pentz
- R. Plum

Geotechnical Engineers, Incorporated
- P. Davies
- B. Paulding

506 106

1. INTRODUCTION

The high-level waste management system has been defined as: solidification of high-level waste and interim storage, transportation to the repository site, handling and emplacement of the waste until the repository is sealed, and the future history of the sealed repository. Each component can be analyzed separately and modeled with a consistent set of assumptions. The risks associated with each component can then be minimized by identifying the critical factors. Thus, the overall risk from waste management processes can be minimized. Activities that could occur and initiate risk within the system must be considered in modeling.

Historically, the approach to a nuclear system has been to identify the components of a facility whose failure could threaten public health and safety, and to require multiple barriers against radiation release, strict quality control, and safety features that could be engineered into the facility. For containment of waste for geologic times substantial reliance must be placed on natural existing conditions. Physical characteristics, geologic behavior patterns of prospective sites, and estimated time constraints must be defined and analyzed. Therefore, assessing the suitability of a repository site for high-level waste storage becomes a complex problem with many interrelated, but not always well-defined, factors.

LLL is currently performing a multicycle systems analysis approach to the problem of site suitability through development of different models, including a physical model and mathematical models. This approach allows data development and model development to proceed in parallel. Each progressive cycle more clearly defines the parameters and their uncertainties, further refines the models developed, and validates assumptions and approximations used.

506 107

A six-layer horizontal model was developed whose parameters and dimensions can be varied to simulate the natural environment of many potential repository sites. The geologic-hydrologic properties that influence groundwater flow rates and waste concentrations, as well as variables that determine the configurations and lengths of flow paths were incorporated and analyzed.

The mathematical models were developed to calculate the performance of hypothetical repository sites. The ORIGEN, WASTE, and BIODOSE programs were employed to calculate and evaluate the inventory of important nuclides, the amount of radiactive waste released, and the expected individual and population radiation doses, respectively.

This report describes the analytical methods employed, the parameter data base used, and the preliminary results obtained.

506 108

2. PHYSICAL MODEL

A flexible model capable of simulating many geological environments was developed to investigate and calculate the consequences of high-level nuclear waste release and evaluate major parameters that control containment. In this way, parameters that can be measured or controlled might be used in developing site suitability criteria. The model, applicable only to bedded formations, is not intended to be explicit for any particular site; it simulates the natural environment of many potential sites. Because the model is sufficiently flexible for this purpose, it can also provide risk analyses of specific sites if the requisite data are provided.

Our model simulates release. Waste in deep geologic repositories would never escape, by natural events, if it were totally insoluble, if the rocks were totally dry or totally impermeable, or if there were no pressure differentials.

Since these conditions cannot be permanently guaranteed in the real world, we assume waste dissolution and transport in the hydrologic environment. Other release routes (gaseous, aerosol, and so on) might be possible, but the probabilities are so low we have deferred possible analyses to a later date.

In our model: (1) solution and waste release begin when the repository is saturated and the hydrologic regime reestablished; (2) hydraulic continuity (flow pathways with inherent permeability, however small) exists between the repository and the biosphere; and (3) a pressure gradient causes flow toward the biosphere. We assume an artesian head, in a water-bearing stratum below the repository, sufficient to cause flow upward to a permeable stratum connected to the biosphere. Other geometric and pressure configurations (e.g., downward flow to some pathway to the biosphere) would suffice. Our purpose is to simulate a pathway to man along which we can vary physical parameters and calculate the consequences. We assume a stable geologic and tectonic environment similar to that of large areas of the United States.

506 109

Effects of geologic features and their probability or rate of occurrence need only be analyzed until one can show the point at which the effect is negligible or the probability of occurrence is so low as to be impossible in a practical sense. Such results will allow us to truncate our analyses at that point and keep our task manageable.

Most of our analyses have been deterministic, i.e., analyzing the effect of the occurrence of a specific state. Calculation of expected values requires one to multiply a deterministic consequence at a certain state by the probability of that state occurring. In a physical system whose properties and processes are well known, predictions of future behavior or states can be made with a high degree of confidence. The more simple the processes acting and the slower the rate of change, the greater the confidence in predicted behavior. If we specify that geologic stability is a characteristic of our model, we are specifying a low rate of change. Geologic processes are extremely slow in human terms, and most of them follow well-documented habits that adhere to fundamental physical laws. The expression, "the present is a key to the past" (the doctrine of uniformitarianism), can be extrapolated to "the past is the key to the future," if near (in geologic terms) past and futures are specified and stability (slow rate of change) is assumed.

The history (changes in "state") of the Earth's geologic environment over the past 1 to 10 million y is well documented. (Detail in the past is lost increasingly as a function of time.) From this we can, in a "stable" area, predict with confidence that changes in geologic parameters will be small. With further documentation we can estimate the possible range of variation and be able to truncate our analyses.

By varying the geometry and characteristics of the flow paths, we can simulate the effects of fractures around the repository, faults, solution breccia pipes, boreholes, and shorter aquifer paths to the biosphere. In addition, we can simulate the effects of flowing or pumped wells, changes in fundamental regional water flow characteristics, erosion or deposition that decreases or increases path length to the biosphere, and so on. Factors such as a meteor strike, severe fault displacement at the site, or a drill hole or mine shaft placed directly into the repository can be simulated, but are not as likely to

occur as natural events. Releases with severe consequences have required us to model several multiple low-probability conditions or events occurring simultaneously.

DESCRIPTION

A simple six-layer horizontal model was designed as shown in Fig. 1. The physical parameters can be specified by preferred values and generic range, and include:

- Hydraulic factors
  Porosities
  Conductivities
  Cross sections of pathway
  ength of pathways and tunnels
  ressures
  Pressure gradient (horizontal)
  Dispersion coefficient
  Layer thickness
  Distance to surface water
- Chemical factors
  Retardation factor (K_f) of I and T_c
  Retardation factor (K_f) of other fission products
  Retardation factor (K_f) of actinides
  Rate of waste dissolution
- Geometric Factors
  Layer thickness
  Distance to surface water
  Length of tunnels and pathways

The selected parameter values simulate layered sedimentary environments with repository in either shale or salt, and with water flow through interstices or fractures. Our simulations to date have used values for hydrologic parameters

506 111

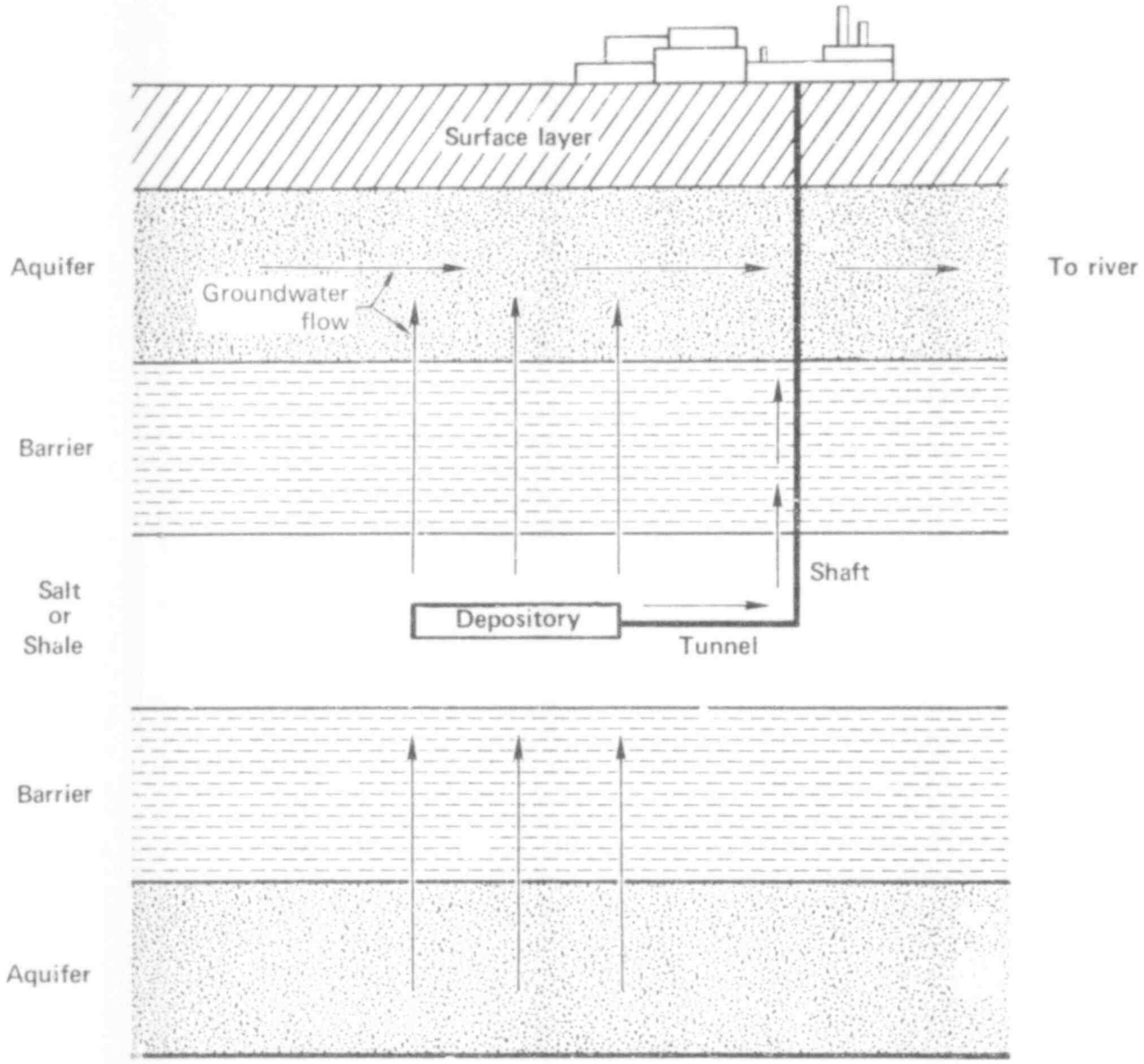

FIG. 1. Six-layered physical model; arrows show groundwater flow directions.

506 112

near the modal values of the real world, as shown in Table 1. A detailed model might be designed if more specific data were available as, e.g., at a thoroughly explored site. Except in the most simple geologies, building a sufficiently detailed generic model may be impractical, and, if more sophisticated models are desired, they may need to be made specific to a particular site.

Operation of the Model*

Parameter values and dimensions can be changed to simulate a variable number of strata and different media types and geometric configurations. These parameters and dimensions are important because they define the environment that determines flow path configurations, path lengths, and the properties that influence flow rates and waste product concentrations. By changing parameter values in the basic physical model, we simulated the results of radionuclide migration through many pathways and the breaching of several barriers in four basic sequences of sedimentary media: (1) sandstone-shale, with repository in shale and interstitial flow in the shales; (2) the same sequence with fracture flow in the shales; (3) sandstone-shale-salt, with repository in salt and interstitial flow in the shales; and (4) the same sequence with fracture flow in shales.

By changing values and different release mechanisms, waste containment and waste transport processes can be evaluated, and resulting doses can be calculated. The results obtained enable us to identify parameters and indicate their relative importance.

Areas and lengths of the zones were calculated from the dimensions of a reference repository described by Office of Waste Isolation Report #ONWI-SUB-76/16506. A fracture zone with a specified permeability is assumed to be formed around all tunnels and shafts because of excavation work.

*The model is applicable only to bedded formations, and simulates physical characteristics of many potential waste disposal sites.

506 113

TABLE 1. Comparison of model values and published ranges.

Parameter	Model[a] values	Published ranges
Conductivities (cm/sec)		
Shale	$10^{-10}(10^{-6})10^{-4}$	3.5×10^{-11} to 2×10^{-4}
Sandstone	$10^{-6}(10^{-4})10^{-2}$	10^{-7} to 1.1×10^{-2}
Salt	$10^{-10}(10^{-9})10^{-5}$	6.5×10^{-9} to 3.5×10^{-6}
Porosities		
Shale	0.01(0.05)0.10[b]	0.07-0.45
Sandstone	0.02(0.10)0.20[b]	0-0.51%
Salt	0.004(0.01)0.07[b]	<0.01
Dispersion constant(m)	10(50)100	11.6 - 38.1
Retardation Factor		
I and Tc	1 (1) 1	~1
Other fission products	1 (10^2) 10^3	1 - 10^4
Actinides	10^2 (10^4) 10^5	10 - 10^5

[a]Minimum value (preferred value) maximum value.

[b]Effective porosity (a fraction of total porosity).

Source: U. S. Geological Survey Open-File Report 74-158; Lawrence Livermore Laboratory, UCRL-52078.

506 114

Vertical flow in the repository area is assumed through a horizonatal area of 5×10^6 square meters, the area of a conceptual ERDA repository in bedded salt. Horizontal flow in the upper aquifer occurs through an area computed by multiplying the vertical thickness of the aquifer by 2000 m, which is the horizontal length of the repository. Variations in the baseline model are made by specifying additional flow paths by their location, dimensions, and hydraulic properties, e.g., porosity, permeability, and pressures. The added flow paths allowed us to simulate faults and breccia pipes, as well as man-induced features including failed seals and backfill in tunnels and shafts at the repository.

Geometry

Basecase thicknesses and other dimensions in our study are similar to those of the conceptual ERDA bedded salt repository. Different stratigraphy is simulated by changing thicknesses. Different geography or extreme erosion of the aquifer bed is simulated by changing the path length in the aquifer. The number of boreholes and the existence, or change in character, of faults and other features, such as breccia pipes in soluble rocks, can be simulated by changing the geometry and the dimsenions and characteristics of the flow paths.

Chemistry

Retardation factors, initial inventories, solubilities, solution rates, and other chemistry-related parameters can be varied independently of geometric and hydrologic factors. We are thus able to analyze a variety of waste materials and waste forms.

Hydrology

In addition to geometric considerations, such as pathway length and areas, the flow regime is specified by assigning values to properties of the rocks and hydraulic system. Rock properties include effective porosity and permeability. A preferred value and a generic range are assigned to both. Sensitivity studies have considered the preferred value and the highest values of permeability. Properties of the system include pressures and pressure

gradients in our model. By varying the excess artesian head in the lower aquifer and the horizontal pressure gradient, the flow velocities in the system are changed, which in turn influence retention time and dispersion.

Other Variables

Man-made features, including backfill and seals of boreholes and shafts, may have properties that vary in time; permeability and porosity, in particular, may increase with time as the engineered seals deteriorate. The hydraulic properties of natural features such as faults, fracture zones, and breccia pipes also vary with time. When faults and their associated fracture zones move, we expect them to become more permeable for a period and then return to a less permeable condition. Breccia pipes will form after the solution of the more soluble rocks has formed a cavity of some minimum critical size. Breccia pipes provide a new permeable flow path for a time.

Variations in climate may affect the hydrologic regime by changing water table levels, pressures, and pressure gradients. These can be modeled by changing the values of the appropriate parameters.

Seismic events sufficiently severe to affect integrity of the repository are so rare in stable geologic environments that we have deferred their consideration. These factors are discussed in a later section.

Uncertainties

Data-induced uncertainties may result from lack of precise measurement, a small data base, or imperfect understanding of a system--conditions that could exist in a generic model study such as ours. The first may be important in some cases of actual sites. The processes of hydrodynamic dispersion and radionuclide retardation are not well known. Their study needs a larger base of field measurements.

506 116

Few data exist on the hydraulic behavior of faults over long periods. We have had to extrapolate this behavior theoretically. The same is true for some natural features, such as breccia pipe formation and seismic activity. The behavior of man-made seals, tunnels, and shafts is better known; experience with these can be extrapolated and some technical progress can be assumed.

FLOW PATHS

We simulate two- and three-dimensional flow of groundwater with a network of pathway segments, in each of which the pressures and the flow velocities and volumes can be found by a one-dimensional analytical calculation.

We have specified a vertical gradient throughout, forcing flow of water up from below. In the permeable aquifer beds, we specify a horizontal pressure gradient that forces flow in the aquifers toward the biosphere (a river in simulations to date). Within the aquitards and aquicludes (the much less permeable repository and barrier beds), we specify only a vertical pressure gradient.

We examined the flow system in each case and specified a set of pathways. All pathway segments have been straight and either vertical or horizontal, connecting at right angles at all branches or changes in direction. The numerical code is capable of handling curved and other configurations, but in the simple cases analyzed to date this capability has not been invoked. Figures 2 through 5 show configurations of the flow paths. Areas, lengths, and hydrologic parameter values are specified in each segment of the flow path as it passes through the several rock types. Flow rate is calculated by Darcy's law, and the results are used in later stages of the calculation.

We consider that our assumption of vertical flow through less permeable aquitards and aquicludes to be an adequate representation for generic criteria development.

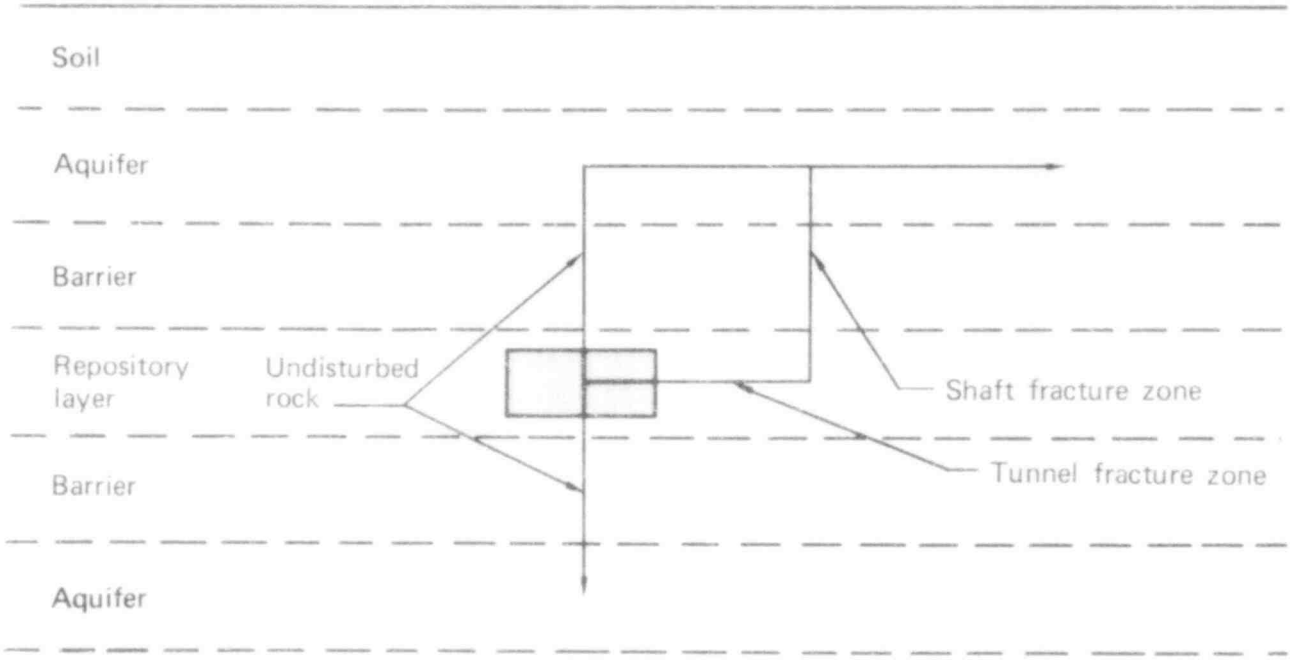

FIG. 2. Flow pathways for unflawed repository.

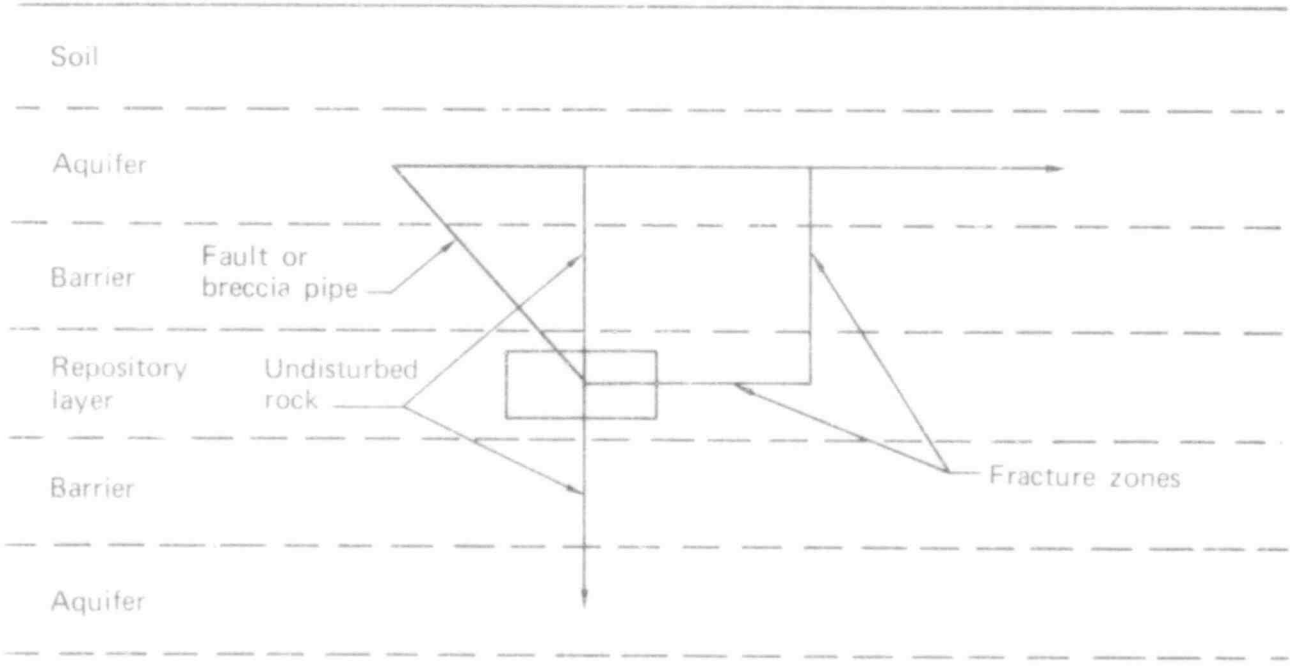

FIG. 3. Flow pathways for repository with fault or breccia pipe.

506 118

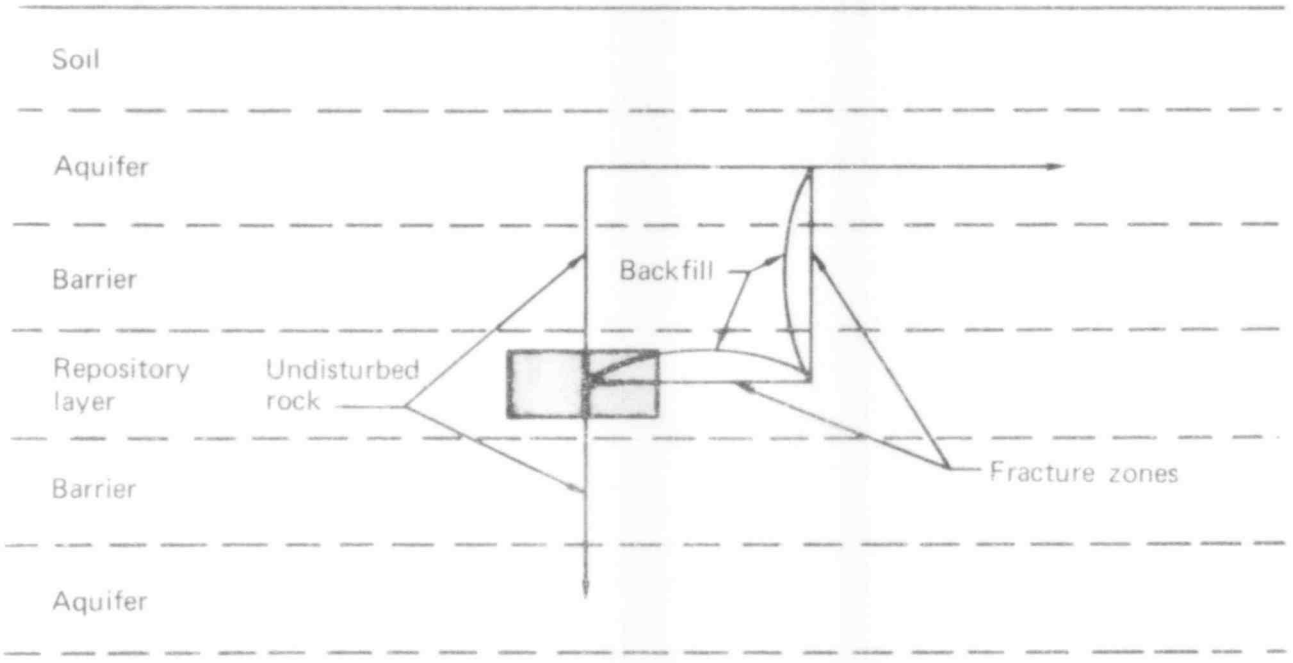

FIG. 4. Flow pathways for repository with deteriorated backfill.

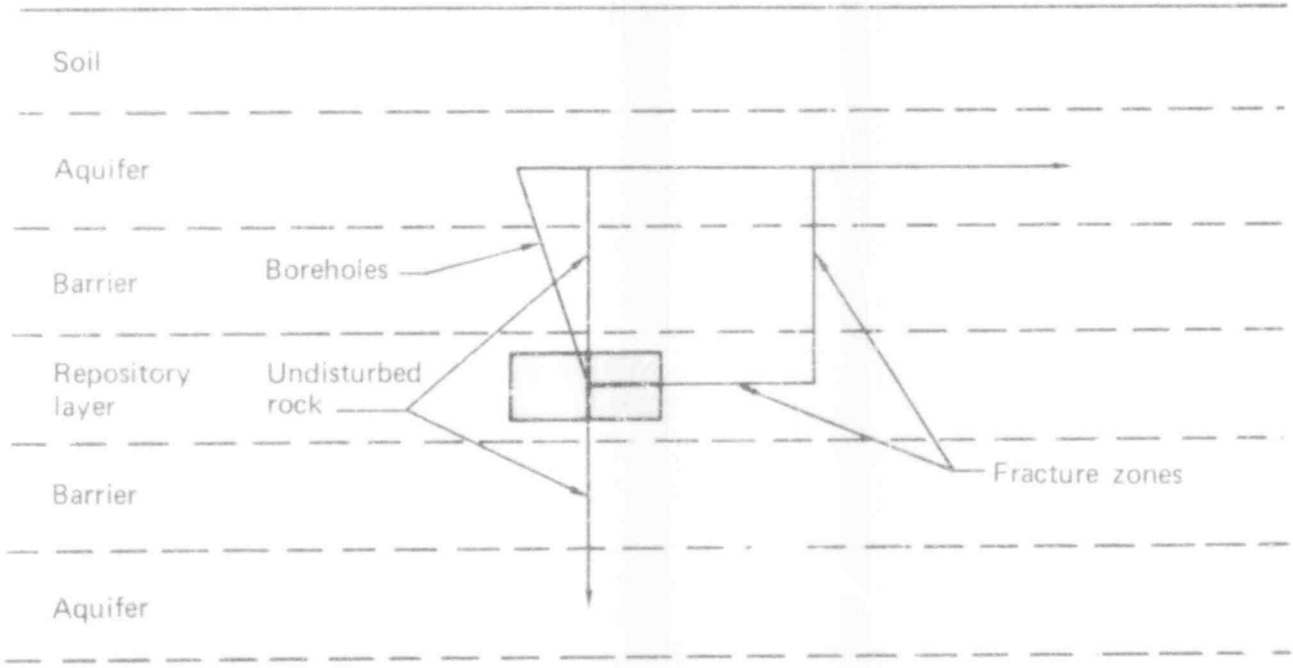

FIG. 5. Flow pathways for repository with failed borehole seals.

506 119

ONE-DIMENSIONAL ANALOG TESTS

This section presents the important factors and basic principles in water flow and solute transport, followed by assumptions and uncertainties in the simple transport model. Analytical and numerical methods for solving the transport problem in addition to alternative calculations to assess the possible errors induced by simplifying assumptions in our one-dimensional model are also given.

Tests of alternative calculations of travel time to river or retention time vs calculations used in our modeling indicate that model-induced error produced minimal effects considering the many assumptions and uncertainties in the modeling data at this time.

Hydrologic and Geologic Factors

Groundwater circulation is the major transport mechanism for radionuclides. The factors describing a repository site, therefore, are properties of the groundwater, the geologic materials, and the radionuclides, as well as the characteristics of the interactions of these three materials. Brief discussions of several important factors are presented here. Detailed discussions of these parameters can be found in the sources listed in the references.

Hydraulic conductivity, or effective permeability, describes the ability of a rock or soil to transmit a fluid. Effective permeability is a proportionality constant between the flow rate of water through a cross section of rock and the change in hydraulic pressure per unit length in the flow direction. It is related to lithologic characteristics of the rock, such as stratification, grain size, and porosity, as well as to the specific weight and dynamic viscosity of the fluid. Useful hydraulic conductivity values are determined in the field with well-pumping tests. These tests measure permeability resulting from flow in fractures and pores in relatively undisturbed conditions. Anisotropic permeabilities and extremely low or extremely high values of permeabilities are difficult to measure, even with elaborate field methods. Moreover, clasic groundwater techniques have been applied mainly to homogeneous, isotropic, porous media. Application of these techniques to fractured or highly anisotropic media must be done with caution.

506 120

Effective porosity is the ratio of the volume of voids open to groundwater flow to the total volume of the porous medium. Average velocity of flow through pores, U, is related to the average macroscopic velocity, V, through a cross section of rock by the relationship

$$U = V/\Phi \quad . \tag{2-1}$$

Empirical and theoretical arguments suggest that

$$D^1 = \alpha V \quad , \tag{2-2}$$

and where D^1 is the coefficient of mechanical dispersion, V is the average fluid flow velocity, and α is the dispersivity of the medium. In isotropic media, α can be described by two components with respect to the flow direction: the longitudinal dispersivity, α_L, and the transverse dispersivity, α_T. Useful estimates have been made for dispersivity in one dimension by calibrating mathematical models with observed transport. However, these coefficients have not been measured effectively for anisotropic or failed conditions.

Solute Transport Model

The transport model calculates the migration of radionuclides along various sequences of one-dimensional flow paths. For the basic case of an undisturbed repository, groundwater is routed through two paths: (1) vertically through the rock layers; and (2) through fractures around the repository, shaft, and tunnel. These paths join in the upper aquifer, where the waste travels in a horizontal path to the lake or river. For more complex scenarios such as faulting or borehole seal failure, a more complex set of paths is used and waste migration is calculated. Pressures at the ends of the paths, permeabilities, porosities, retardation factors, and dispersivities are specified from base data provided. Pressures at intermediate nodes on the path and velocities through the path are calculated by Darcy's law. Detailed descriptions of the transport model and the scenarios used in the model are discussed in the Mathematical Models section.

Present efforts include modification and improvement of the transport model to reduce uncertainties. To validate the model, we compare it with other multi-dimensional flow and solute tranport analyses. In realistic problems, flow and transport problems must be solved by numerical methods. The techniques usually applied are finite differences, finite elements, or methods of characteristics. Comparable results can be obtained using any of these methods. Finite element methods are preferred, however, if higher order approximations must be considered. Available codes suitable for solute transport modeling are summarized in Appendix A.

Two codes have been put on line at LLL for use in our study: a two-dimensional finite element flow code by Taylor and Brown (1967), and a two-dimensional finite element solute transport code by Duguid and Reeves (1976). These codes are suitable for comparison/validations of the present transport code, as well as for later application to specific sites. Other codes are listed in Appendix A. We are using the groundwater flow code to evaluate and validate the flow pathways used in our model. The first cases to be modeled with the Taylor code are: (1) the basic case with flow in fracture zones around the repository and shaft, (2) the case where a high-permeability fault intersects the repository, and (3) the case where a low-permeability fault intersects the repository. The two-dimensional groundwater flow code could become an integral part of the input procedure for our transport model.

Extension of modeling to include new parameters may be necessary as the project progresses. The two-dimensional transport code will be run for several flow cases to evaluate the effects of lateral dispersion. Other effects, such as thermal gradients, variable fluid densities, and long-range climatic changes may affect groundwater flow regimes. The importance of these effects and the technological limitations for their treatment will be evaluated.

The model considers only one-dimensional flow within each stream tube. The two major assumptions are that: (1) lateral dispersion across stream tube walls does not significantly affect ion concentrations and travel times and (2) the choice of stream tube paths through the media does not introduce significant errors in passage times of the ions.

506 122

The first assumption cannot be tested without calculations. Dispersion is poorly understood and difficult to measure experimentally, although limited experimental results, show that lateral dispersivity is significantly less than the longitudinal dispersivity. Given the limited state of knowledge of dispersion phenomena, one-dimensional treatment of dispersion is probably sufficient for our sensitivity analyses on a simple model. The second assumption can be tested partially by some simple calculations. This is carried out in Appendix L.

506 123

3. MATHEMATICAL MODELS

A series of computer simulation programs representing the mathematical models has been developed to calculate the performance of hypothetical repository sites as shown in Fig. 6. A program has also been developed for uncertainty analysis.

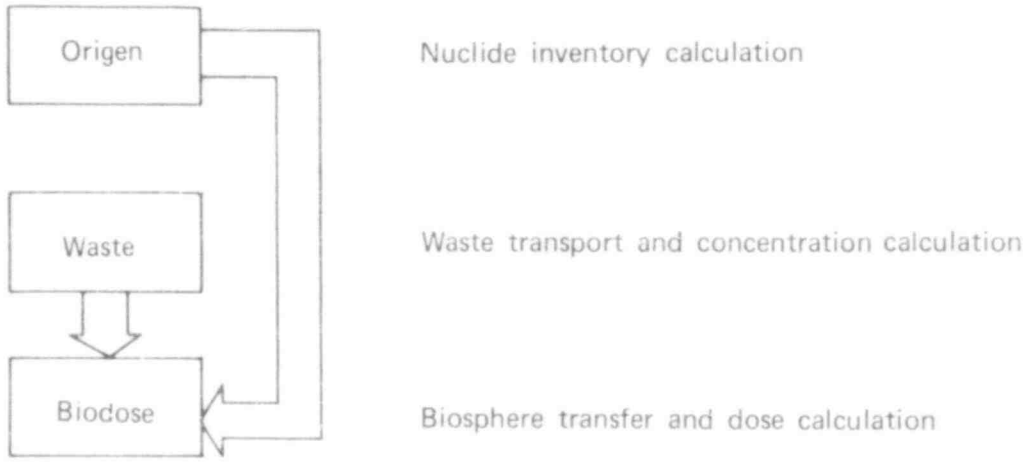

FIG. 6. Computer simulation codes used for analysis of mathematical models.

The WASTE program is used to calculate waste flow without considering radioactive decay. The results obtained are fractions of the total inventory of each nuclide, and must be multiplied by the inventories (radioactive decay is included) of the nuclides to provide numbers that directly measure concentration and risk. These inventories are derived from the Oak Ridge ORIGEN code. We reviewed the ORIGEN code. No modifications of the original ORIGEN code were necessary; however, only those nuclides considered to be important were analyzed (see Bell, 1973, for additional detail).

506 124

Defining the inputs to the WASTE program requires an understanding of the flow pattern of groundwater in the repository area. Currently the flow patterns are obtained by solving the hydrology problem analytically. More complex methods, including two- and three-dimensional models, will be used later as appropriate.

Doses to humans will depend on the waste movement through surface waters and waste concentration in the ecosystem, as well as on human diets and living habits and the biochemistry of the waste nuclides in the human body. These factors are modeled in the BIODOSE program.

Two subprograms that calculate doses and concentration multiply the outputs of the different programs and do final data manipulations.

WASTE PROGRAM

WASTE, the computer simulation program for subsurface waste migration, calculates the magnitude of release of buried radioactive waste to the biosphere resulting from groundwater transport. The program incorporates the effects of mass transport, chemical interactions between waste components and pathway media, and hydrodynamic dispersion. WASTE is used to simulate hydrogeological characteristics and perform sensitivity analyses. To maximize flexibility, WASTE avoids procedures such as finite element and finite difference methods that divide the regions of interest into a lattice of cells. Instead, the program approximates groundwater flow pattern by a network of simple flow paths, which need not be straight. More details appear in Appendix B. This approach increases computational efficiency and allows straightforward representation of small discontinuities (faults, boreholes, and so on) and regional flow patterns, and thereby avoids the difficulties of solving the time-dependent solute migration problem by finite-element or finite-difference methods.

Future events, such as faulting or failure of engineered seals, may affect the movement of groundwater and dissolved radionuclides. These events can be predicted only on a probabilistic basis; the model can account for future events by either of two analyses: (1) consequences can be calculated for

506 125

scenarios in which events occur at specified times, and (2) risk can be calculated for events that occur at random times with given probability of occurrence per year. Appendix C shows the statistical method that makes possible the second analysis.

The WASTE model approximates the groundwater flow pattern around a repository by a network of interconnected simple flow paths. The tabulation below lists the variables that describe each flow path.

$B(j,m_1,m_2,n)$	Retardation factor for nuclide type j in the flow path from node m_1 to m_2, in geologic state n (dimensionless). A state implies a set of parameter values that define the condition of the repository site.
$W(m_1,m_2,n)$	Cross section of flow path m_1, m_2 in state n (m^2)
$\alpha\ (m_1,m_2,)$	Dispersion constant (m)
$K(m_1,m_2,n)$	Permeability (cm/sec)
HEAD(m,n)	Hydraulic head at node m (m)
$Z(m_1,m_2)$	Distance from m_1 to m_2 (m)
$\epsilon(m_1,m_2,n)$	Effective porosity (dimensionless)

Each point in the network at which flow paths branch, or at which any of the variables listed above change value, is defined as a node. The nodes are numbered in such a way that water is shown as always flowing from lower-numbered to higher-numbered nodes. This method does not preclude situations where flow reverses when the state changes, because we artifically place more than one node at the same location. The WASTE program sequence is as follows:

First, the amount of waste leaving the repository (node 1) is calculated as a function of geologic state and time. Second, each node in the system of flow paths is examined in sequence. The rate at which waste arrives at a given node is calculated from the amounts of waste that had earlier left lower-numbered nodes. Time is divided into discrete intervals for digital calculations. Third, a quantity $F_j(\ell,m,n)$ that is the amount of waste of type j passing through node m during time interval ℓ is calculated, given that the system is in state n multiplied by the probability of the system being in state n.

The following equation calculates F for nodes other than the repository itself

$$F(\ell,m,n) = \sum_{m'<m} \sum_{\ell' \leq \ell} \sum_{n'} F(\ell',m',n') \times SP(m',m,n')\, G(\ell',\ell,m',m,n')\, TP(\ell',\ell,n',n) \quad . \tag{3-1}$$

In this formula, one begins with F(ℓ', m',n'), the amount of waste leaving node m' in state n' during interval ℓ'. This amount is multiplied by SP, the fraction of the waste leaving m' that enters a flow path leading directly from m' to m. (If there is no such flow path, SP equals zero.) G is the fraction of the waste entering the flow path during the interval ℓ' that reaches the end of the flow path (node m) during interval ℓ. This calculation assumes that the system is always in the same state, n', as it was in when the waste entered the flow path. Thus, the waste does not react to the system's change of state until it reaches a node. The factor TP accounts for changes of state when the waste reaches node m. Factor TP is the probability that the system, having been in state n' during interval ℓ', will be in state n during interval ℓ. The effect of multiplying by TP is to distribute waste, which migrated through the flow path from m' to m on the assumption that the system was still in state n', among all the states (including n') in proportion to the probability that the system went from state n' to state n while the waste was in the flow path.

The mathematical approximation (as compared to an exact solution of Eq. C-18) of delaying the effect of state changes on waste until the waste reaches a node greatly simplifies calculations. Its effect on uncertainty may be reduced by inserting intermediate nodes in flow paths. Waste will react to state changes when reaching these intermediate nodes. It will then proceed through the remainder of the flow paths at a velocity appropriate to the new state. The overall effect of the approximation may be analyzed by measuring the effect of adding such intermediate nodes. Such tests are planned as part of model validation.

The assumptions and methods used to calculate the factors SP, G, and TP are described in Appendix D.

RECONCENTRATION EFFECT

Reconcentration will be important for a parent-daughter pair in which the daughter has a smaller retardation factor than its parent. Our present model computes the flow rate of the daughter with the assumption that both members of the pair move at the same speed. If the daughter moves at a greater speed than the parent, the peak value of daughter entering the biosphere should be increased, since daughter created at a distance from the biosphere will move ahead and join with daughter created near the interface with the biosphere. The model will underestimate the peak value and total amount of daughter nuclide in the biosphere, because it does not include this additional contribution from farther back in the system.

The reconcentration effect has been analyzed for the case where the nuclides enter the biosphere through a flow path that is sufficiently long for any initial input of daughter to have decayed to an insignificant level in the time required for the parent to traverse the flow path. Cases where the daughter products have long half-lives will be analyzed in the near future. It is shown that the amount of daughter leaving the flow path during time periods when there is outflow of the parent is increased by an amount approximately equal to the ratio of the retardation factors.

High-level radioactive waste contains two parent-daughter pairs for which the reconcentration effect is of particular interest because large amounts of the following nuclides are present: ^{230}Th, with a half-life of 7.7×10^4 y, which decays to ^{226}Ra with a half-life of 1.6×10^3 y; and ^{93}Zr, with a half-life of 1.5×10^6 y, which decays to ^{93m}Nb with a half-life of 14 y. The analysis has been restricted to these two cases specifically. ^{230}Th and ^{226}Ra are part of a larger decay chain, which currently is being analyzed.

The reconcentration factor ρ is defined as the ratio of the flow rate of daughter entering the biosphere, when retardation factor differences are present, to the flow rate of daughter entering the biosphere when the retardation factor of the daughter equals the retardation factor of the parent. The WASTE program is used to calculate the flow rate of the daughter, assuming equal factors. Multiplying the model output by ρ corrects for the reconcentration effect in a computationally simple manner. Our computed reconcentration factor is based on three assumptions:

(1) The retardation factor of the daughter is significantly smaller than that of the parent.

(2) The half-life of the daughter is significantly shorter than that of the parent.

(3) The flow path is sufficiently long that any original input of daughter to the flow path will have decayed to an insignificant level in the time required for the daughter nuclide to traverse it.

Assumption 3 is especially significant for the calculation. When a large amount of input daughter nuclide is flowing out of the flow path, the factor ρ is small. The third assumption allows computation of the retardation factor without regard to the amount of input daughter, and guarantees that the calculated ρ will give the maximum effect.

Appendices E, G, and H present calculation details.

506 129

BIODOSE Program

The BIODOSE program is used in conjunction with the WASTE program to calculate expected doses to man resulting from radionuclide release to the biosphere. For example, water pathways considered in the BIODOSE program include water wells, lakes, and a river, estuary, and ocean system. Figure 7 illustrates the latter model and lists the exposure pathways considered.

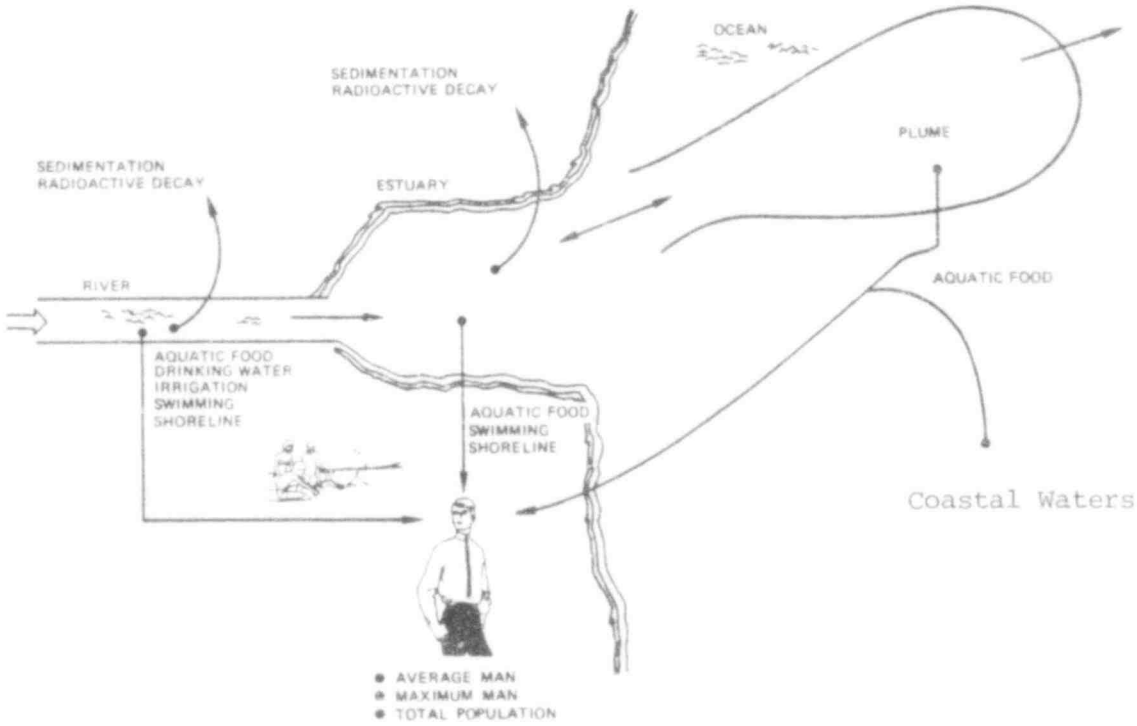

FIG 7. Radiation exposure pathways from contaminated river, estuary, and ocean system modeled in the BIODOSE program.

Following closely the methods outlined in NRC Regulatory Guide 1.109, BIODOSE was derived from numerous models that were developed during the past ten years to compute the consequences of radionuclide release (Fletcher and Dotson, 1971; Soldat et al., 1974; NRC, 1975; Booth et al., 1971). Our model differs on two major points from the previous models: first, we consider the problem of buildup in soils and sediment since radionuclide release can occur over a

506 130

long time period, i.e., 10 000 y or more. Second, we compute population doses without referring explicitly to the local demography, as future population statistics are unknown. The basic philosophy in developing the model was to provide a tool for evaluating the consequences of radionuclide release under conditions not significantly different from those we currently experience. The model is sufficiently general to accommodate a wide variety of assumptions including diet, irrigation use, water pathway characteristics and so forth.

Transport Model

The transport model is used to calculate the mean concentration of radionuclides occurring in sediment, topsoil, and water subsystems. Each parameter is modeled in a "compartment," which represents a particular section of the physical world as shown in Fig. 8. All relevant dynamic processes are converted into transfer coefficients between the compartments. The model is based on calculating the mass balance in each department. The basic equation is

$$V_p \frac{d}{dt} C_{rp} = \sum_j C_{rj} A_{jp} + V_p \sum_q \lambda_q C_{qp} + Q_{rp} - V_p \lambda_r C_{rp} \quad , \qquad (3\text{-}2)$$

where

C_{rp} = concentration of nuclide r in compartment p(Ci/m^3)

C_{qp} = concentration of nuclide q decaying into nuclide r in compartment p(Ci/m^3)

A_{jp} = flow rate from compartment j to compartment p for $p \neq j$

λ_r = radioactive decay constant for nuclide r

Q_{rp} = input rate of nuclide r into compartment p from outside the system (Ci/m^3)

V_p = volume of compartment p.

Dynamic processes that are modeled affecting radionuclide concentration in the water, sediment, and topsoil include:

- Dilution by mixing
- Diffusion between sediment and water
- Sedimentation
- Removal of water and food products by man
- Return flow from the topsoil to the water system
- Ion exchange and biogeochemical processes, which are expressed as distribution coefficients.

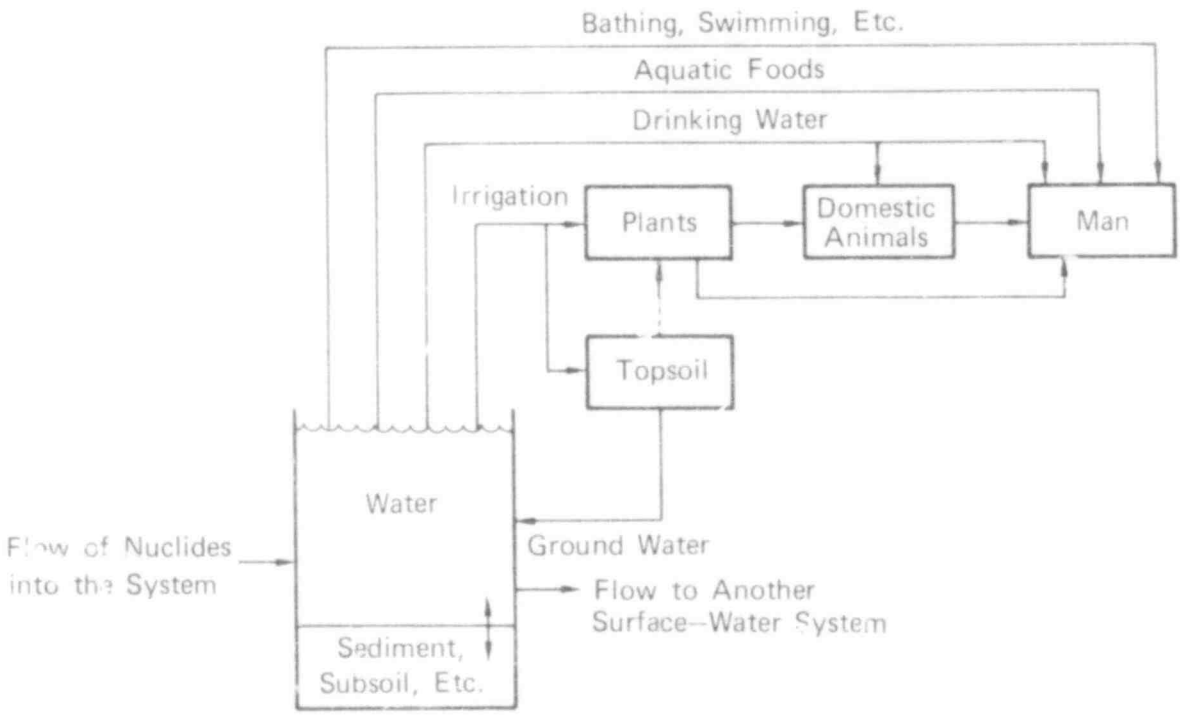

FIG. 8. The transport model.

506 132

Quasi Steady-State Model

Calculations for the quasi steady-state model can be simplified because it is assumed that the waste release from an aquifer is constant over a long period compared to the waste transition time through the water use system. The basic assumptions for all compartments of the transport model, except topsoil, are:

- The times V_p/A_{jp} associated with transfers between the compartments in the model are smaller than the time over which changes in Q_{rp} occur.
- Times V_p/A_{jp} are also much smaller than the times over which concentrations are affected by the combined processes of radionuclide production and decay.

These assumptions permit the use of a steady-state model in which all time dependence is contained in the input term for flow of waste from the aquifer into the water system. The terms in Eq. 3-2 expressing radioactive decay and the derivative of the concentration may be disregarded, so that

$$0 = \sum_j C_{rj} A_{jp} + Q_{rp}(t) \quad . \qquad (3\text{-}3)$$

Our assumptions yield a conservative estimate of the peak individual dose. This result occurs because water concentrations from a continuous source input rise from zero until they reach their equilibrium value, whereas the model assumes that the concentrations are always at an equilibrium value.

A less conservative analysis would be possible if there were a thorough understanding of the processes that remove contaminants from the biosphere. The main processes in river and estuary system are sedimentation and diffusion into the sediment. Radionuclides can reenter the biosphere from the sediment by physical, chemical, and biological means. Both the potential for remobilization and the time period over which it might occur are unknown, although it has been suggested that some radionuclides such as plutonium become irreversibly bound to the sediment.

506 133

For other radionuclides, recent evidence suggests that remobilization can occur (Bowen et al., 1975). Therefore, we have adopted the following conservative assumptions for our analysis:

- The water and sediment system are in dynamic equilibrium. For each radionuclide, the distribution coefficient gives the concentration in the sediment divided by the water concentration.
- No irreversible losses take place from the water system to the sediment.
- The time over which buildup in the sediment occurs is less than the time over which changes in Q_{rp} occur.

Radionuclide buildup in topsoil is not assumed to reach equilibrium. Topsoil is assumed to be irrigated at a constant rate for a fixed period, which was varied from 100 to 1000 y to test the sensitivity of the dose from direct exposure to the topsoil or from plant uptake. Except for ^{126}Sn, the dose from the topsoil was consistently less than doses from other pathways.

Concentration Equations

We divided the ocean pathway into two compartments: the coastal region and the river plume region. This division was necessary because the average fish harvest is usually greater closer to shore. Hence, the river plume contributes disproportionately to the net dose from the ocean. Concentration equations for the plume of contaminated water flowing from the estuary to sea are given in Appendix I. Site-specific calculations are based on data for the Columbia River system.

Dose Calculations

The concentrations calculated for the five transport media, sediment, river, estuary, ocean, and topsoil, are used with a simple ecosystem model to yield radionuclide dose rates to man. In the model, doses are received by ingestion and external exposure. The ingestion pathways include drinking water, aquatic foods, irrigated crops, and farm animals; the external exposure pathways include water related activities and topsoil contact.

Further assumptions are that: (1) each adult drinks all his water and eats all his aquatic food from the river or lake system into which radioactive material was released; (2) each adult's diet consists solely of food products that were either directly or indirectly contaminated by the river or lake water; and (3) all water-related recreation time is spent somewhere within the river, estuary, and ocean system. These assumptions ensure that no important exposure pathways for each nuclide are excluded from the system.

The basic dose equation is (Burkholder, 1975)

$$R_{rpu} = C_{rp} U_p D_{rpu} , \qquad (3\text{-}4)$$

where

R_{rpu} = dose rate to organ u from nuclide r via pathway p

C_{rp} = concentration of nuclide r in pathway p

U_p = use rate associated with pathway p

D_{rpu} = radiation dose factor for nuclide r in pathway p for organ u.

The dose calculations for water withdrawn directly from the aquifer through a well are identical to those for wastes flowing into a river or lake, except that the aquatic food, shoreline, and swimming pathways are eliminated.

Dose factors used in the model represent the accumulated dose over 50 y to an individual adult resulting from chronic ingestion and exposure to radiation. We calculated dose factors, using those already tabulated by Burkholder (1975), and multiplied them by a dose accumulation factor. The tabulated factors represent a one year accumulated dose from a single intake of radionuclides on the first day of the year. The basic equations for the 1-y and 50-y dose factors for chronic ingestion of radionuclides are

$$D = 18.7 \frac{f_w \varepsilon}{m} \frac{1 - e^{-\lambda}}{\lambda} \quad (3\text{-}5)$$

$$D50 = 18.7 \frac{f_w \varepsilon}{m} \frac{50\lambda + e^{-50\lambda} - 1}{\lambda^2} \quad , \quad (3\text{-}6)$$

where

D = 1-y dose factor (mrem/pCi)

D50 = 50-y dose factor $\left(\frac{\text{mrem}}{\text{pCi/y}}\right)$

f_w = fraction of the ingested nuclide reaching the organ

m = mass of the organ in grams

ε = effective energy of the nuclide in the organ under consideration (MeV/disintegration) (rem/rad)

$\lambda = \underline{\Delta} (0.693/\text{BHL} + 0.693/\text{AHL})$

BHL = biological half-life for the nuclide in the organ (y)
AHL = atomic half-life for the nuclide (y).

The appropriate dose accumulation factor is

$$DAF = \frac{50\lambda - 1 + e^{-50\lambda}}{(1 - e^{-\lambda})\lambda} \quad . \quad (3\text{-}7)$$

Values for λ were taken from Burkholder (1975).

The same 50-y dose factor was used to calculate individual and population dose. This method results in a measure of the accumulated dose to a population over a 50-y period. The population dose per year was calculated by

506 136

dividing the above measure by 50. This dose was used in our calculation of the integrated population dose, and represents the population as consisting of adults evenly distributed over a 50-y age range. Doses were calculated for the whole body and seven organs: gastrointestinal and lower large intestine (GI-LLI), thyroid, bone, liver, lung, kidney, and skin. The means of exposure included water-related recreation as well as ingestion.

Table 2 shows average and maximum use rates for calculating individual dose. The table gives use rates for water and food products, and the amount of time spent in water-related recreation for an adult. The values reflect those given in NRC Regulatory Guide, 1.109 (March 1976); however, we expanded the number of food products considered, using the data given by Burkholder (1975). Therefore, while the totals for a given source, e.g., meat and poultry, are stated in the NRC regulatory guide, the breakdown within that category is determined from the Burkholder data.

The aquatic diet for an individual was apportioned according to the contributions from the river, estuary, and ocean pathways. Results were obtained by multiplying the aquatic food intake in each pathway by $F_{\ell p}$, the fraction of food product ℓ (fish, crustacean, or mollusk) consumed from pathway p (river, estuary, plume, or ocean). The sum of $F_{\ell p}$ over all pathways for a fixed ℓ was set equal to one. Table 3 lists the values used for $F_{\ell p}$. They are estimated from the fish harvest data given in Appendix J, Table J-1. Other assumptions can easily be implemented, but they will not materially change the final calculated dose.

506 137

TABLE 2. Average and maximum use rates for an average adult.[a]

Diet and Recreation	Use rate, U_p/y	
	Average	Maximum
Milk, l	110	310
Fish, kg	6.9	21
Mollusk, kg	0.5	2.5
Crustacean, kg	0.5	2.5
Water, l	370	730
Eggs	487	730
Berries, kg	5	10
Melons, kg	7	14
Orchard produce, kg	43	90
Wheat, kg	50	113
Other grains, kg	4	12
Beef, kg	39	45
Poultry, kg	17	45
Pork, kg	39	20
Leafy vegetables, kg	5	32
Other above-ground vegetables, kg	5	32
Potatoes, kg	44	131
Other root vegetables, kg	28	86
Shoreline recreation, hr	8.3	12
Swimming and boating, hr[b]	5	200

[a]Appendix K presents the calculations of radionuclide concentrations in vegetable and animal food products.

[b]Burkholder, 1975.

506 138

TABLE 3. Fraction of food product consumed.

Water system	Fish	Crustacean	Mollusk
River	0.1	0	0
Estuary and near shore	0.4	1	1
Plume and ocean	0.5	0	0

Individual Doses

Some of the doses computed for an average individual appear in Figs. 9 and 10. The annual steady-state input of waste into the river is set at 1 MWe-y. The radionuclide selection and composition of solidified high-level waste (SHLW) from reprocessing (assuming uranium and plutonium recycle) and of spent fuel was determined by use of the ORIGEN code developed at Oak Ridge. Figures 13 and 14 aggregate the doses according to major types of radionuclides, based on their rates of migration in groundwater. Dissolution is assumed to be instantaneous.

In both figures, the fission products dominate the dose initially. After about 600 y, the actinides become the principal hazard as the ^{90}Sr and ^{137}Cs decay. Peak actinide dose occurs at about 100 000 y, as a result of ^{226}Ra production.

Our sensitivity analysis showed that the dose to an individual is almost inversely proportional to the river flow rate. This result is expected, since dose is proportional to concentration and river water concentration is approximately inversely proportional to the river flow rate.

506 139

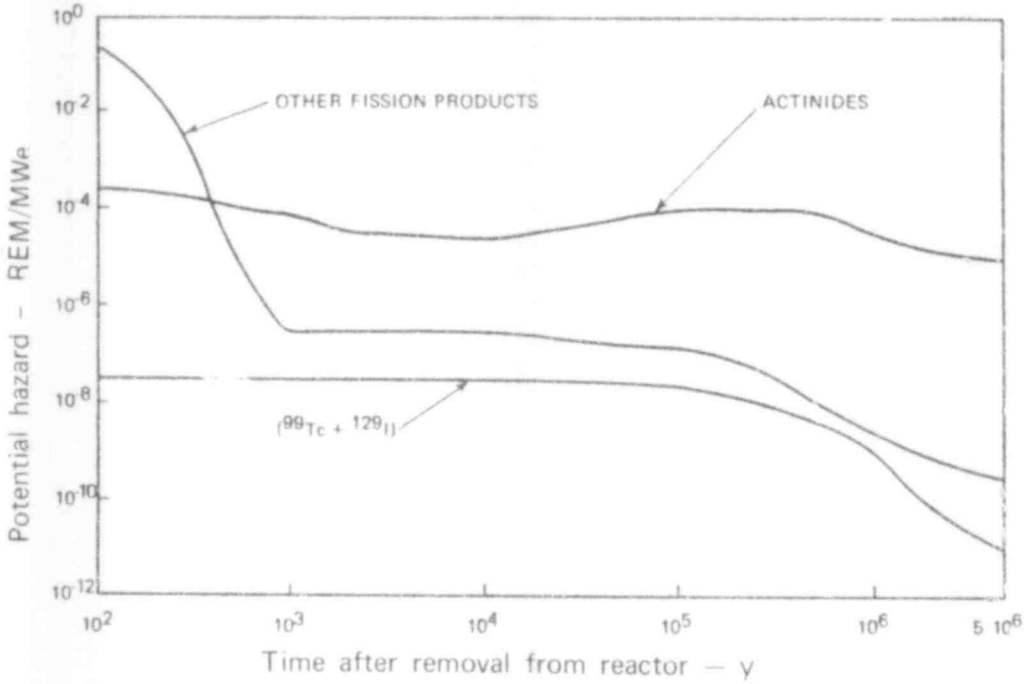

FIG. 9. Fifty-year dose to the whole body to an average individual from HLW.

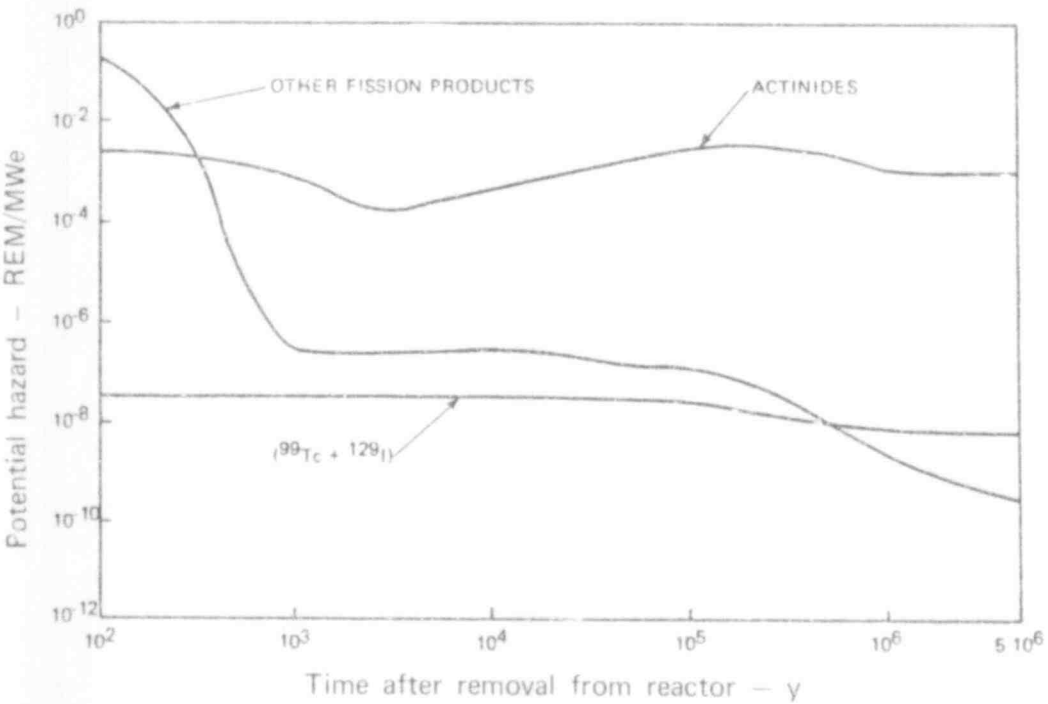

FIG. 10. Fifty-year dose to the whole body to an average individual from spent fuel.

506 140

Population Dose

Population doses (50-y dose commitment) are calculated by integrating the individual dose over an entire population. The integrated population dose is obtained by integrating the population dose over the entire lifetime of the repository. Since doses are proportional to the concentrations in each compartment, we can integrate Eq. 3-2 directly. For a repository lifetime of 3×10^6 y, integration gives

$$V_p C_{rp}(t = 3 \times 10^6 y) = \sum_j \left[C_{rj}\right] A_{jp} + V_p \sum_q \lambda_r \left[C_{qp}\right] + V_p \lambda_r \left[C_{rp}\right] + \left[Q_{rp}\right] , \quad (3\text{-}8)$$

where $[\ ]$ is defined as

$$\left[f\right] = \int_0^{3\times10^6 y} f \, dt \quad .$$

One may neglect the quantity on the left hand side of Eq. 3-8 for nuclides that have either decayed to negligible amounts or left the ecosystem by 3×10^6 y. If, in addition, the terms involving radioactive decay are neglected, Eq. 3-8 reduces in form to Eq. 3-3. Equation 3-8 is independent of the assumptions made in deriving the steady-state relation, Eq. 3-3.

Population dose is often calculated for a real or assumed population within a given radius of the contaminated region. For calculations of projected future population doses, it is difficult to make realistic estimates. However, total doses from some pathways will be essentially independent of the size of the receiving population. For example, the aquatic food pathway depends on the net fish harvest; the vegetable and animal food pathway depends mainly on the yearly irrigation rate; therefore, population dose from these pathways is independent of how those products are distributed. The parameters in the equations used for calculating population doses in appendix J are essentially independent of the size of the population living near the river system.

Population dose is usually independent of water system flow rate, in contrast to the individual dose, which is inversely proportional to the flow rate. This conclusion assumes that:

- Potential use of the water system is proportional to the average flow rate.
- Actual use is equal to the potential use.
- Concentrations within the water system are almost inversely proportional to the flow rate.

The use rates for drinking water and irrigation are influenced by water system flow rate. Maximum potential use rate of the water system is difficult to estimate. Theoretically it could amount to more than 100% of the water flow if there were considerable recycling. The following factors militate against high use rates:

- Extensive water reuse implies the removal of waste products. Presumably radionuclides would also be removed during water treatment.
- About 60% of the water used for irrigation is consumed and does not return to the water system. This water is not available for reuse.
- About 30% of the water used for municipal supplies is consumed and does not return to the water system. Furthermore, only a small amount (0.2%) of municipal water is used for drinking.

Aquatic food and recreational pathways are influenced by area and volume of the water system, and only indirectly on the flow rate. These latter pathways are of secondary importance in determining the total dose, except for ^{126}Sn and ^{93m}Nb. The water system characteristics and the aquatic food harvests used in the model were based on data collected from the Columbia River system (Barnes et al., 1972; Neal, 1972; Pruter, 1972). Irrigation use rates for river, lake, and underground water were based on values typical of the western United States (Kazmann, 1965; Todd, 1959). Appendix J gives values used and their sources.

Figures 11 and 12 illustrate population doses for SHLW from the reprocessing of spent fuel (with uranium and plutonium recycle) resulting from 1 MWe-y/y of waste flowing into the river system. Aquatic food is an important pathway only in determining the dose from the other fission products after ^{90}Sr and ^{137}Cs have decayed. The fission products that then contribute to the dose are primarily ^{126}Sn and ^{93m}Nb.

506 142

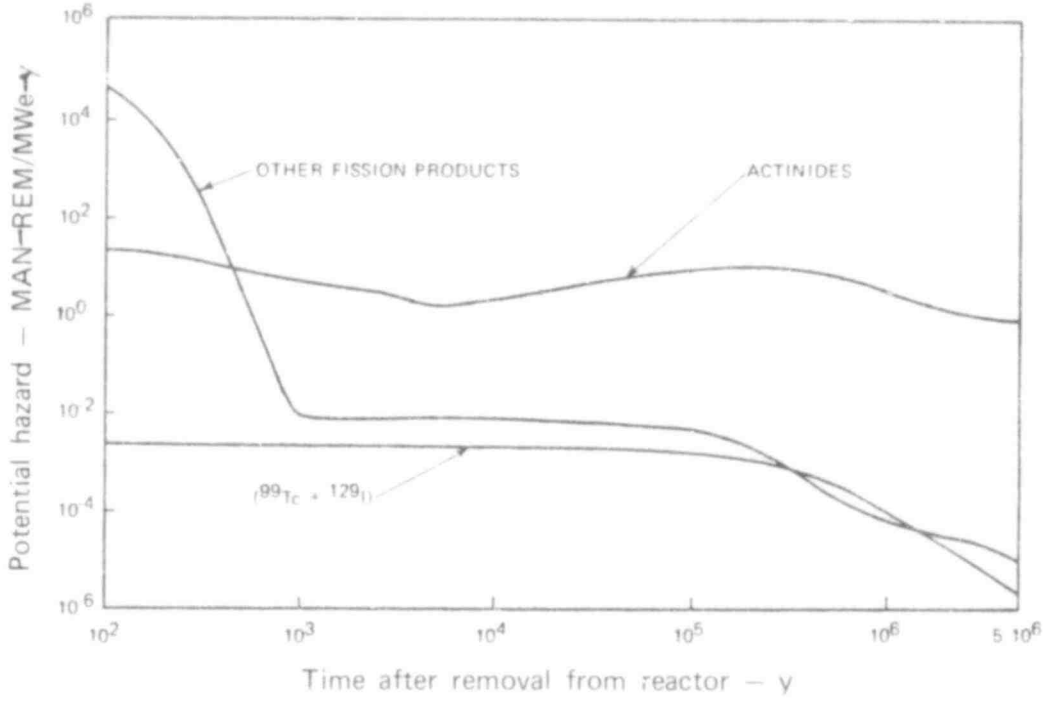

FIG. 11. Population dose per year to the whole body from high level waste.

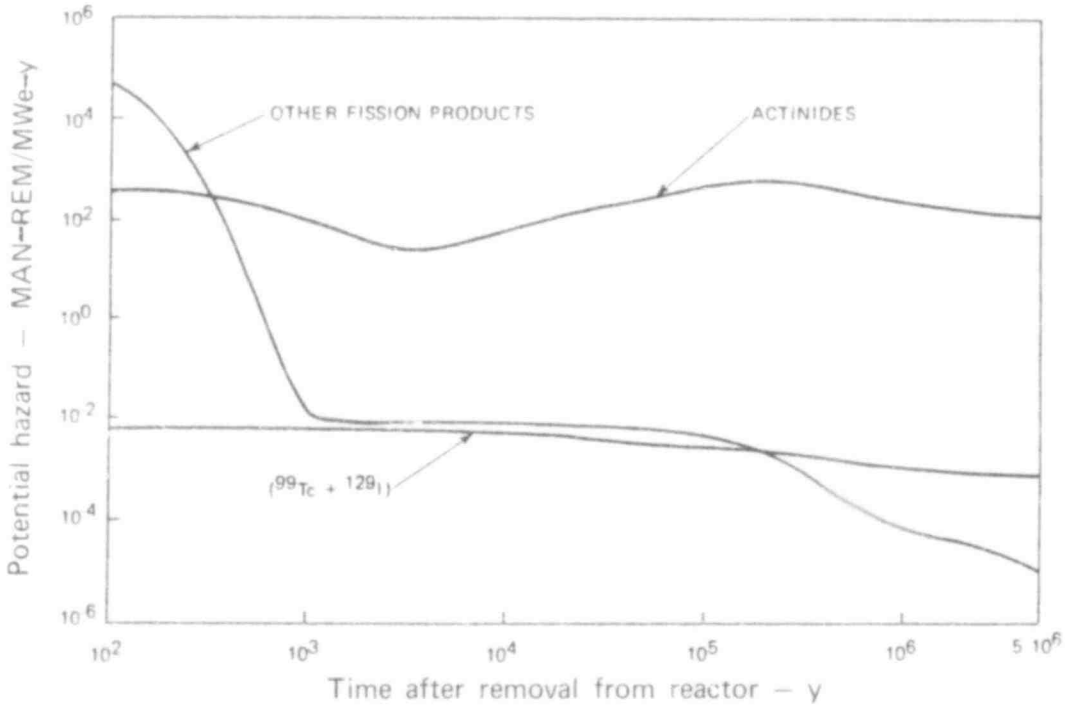

FIG. 12. Population dose per year to the whole body from spent fuel.

Figures 11 and 12 are similar to Figs. 9 and 10 for individual dose. The major difference is the increased importance of ^{99}Tc and ^{129}I in comparison to the other fission products. The critical pathways for ^{129}I and ^{99}Tc are those of vegetables and animals.

UNCERTAINTY ANALYSIS

We are developing a methodology to predict HLW repository performance. These predictions are subject to scientific uncertainties, both in the site descriptors and predictive model. Every scientific result consists of a scientific estimate (preferred value) and a characteristic range that indicates the precision of the estimate. The accuracy of the estimate is a measure of how close the estimate is to its "real" value. The uncertainty of a result is a combination of both the accuracy and the precision of the scientific estimate.

Uncertainty of HLW repository performance predictions results from a combination of imprecise data, inaccurate data, and invalid modeling. Imprecise data cause prediction uncertainties because the range in values of a site descriptor usually leads to a corresponding range in the site performance predictions. The uncertainty in a prediction can be no better than the precision of the prediction. The precision of the HLW predictions is obtained by propagating the descriptor uncertainties through the model to the predictions via a Monte Carlo technique.

Inaccurate data, when used in a valid predictive model, lead to inaccurate predictions. This fact is of concern only when the precision of the data is relatively good. Otherwise, the inaccuracies in the prediction are hidden by the data imprecision.

Invalid modeling is the most troublesome of our three concerns. It can reside in incomplete, insufficiently detailed, or erroneous numerical modeling. Incomplete modeling suggests that it is extremely difficult to determine when all the important processes have been included in a predictive model. In fact, because of the synergistic effects that frequently occur between different physical processes, caution must be used in simplifying the

506 144

analysis of a particular physical process. Insufficient detail refers to the scientific necessity of choosing a physical size scale of interest, then lumping smaller size-scale phenomena into larger size-scale parameters. In some cases the effects of smaller-size scale phenomena on larger size scales can be great. When this occurs, the choice of size scale can produce inaccurate predictions. Erroneous numerical modeling is not as subtle as the previous two concerns, but sufficient care should be taken to ensure that untoward numerical results are not generated. Careless formulation of analytical expressions has frequently led to erroneous and misleading results.

Low-confidence predictive models are easy to obtain. High-confidence models can only be obtained in a careful and insightful program by expending the technical expertise required to ensure, as much as current technology allows, that one is not surprised by a forgotten process, insufficient detail, or numerical blunders. The invalid predictive model, without all the important physical processes, is the most difficult problem to deal with. It is rooted in man's lack of omniscience, and is why supposedly well-engineered bridges are blown down and buildings tumble in earthquakes. Obviously, important physical processes were not considered in these instances. To develop high-confidence predictions, careful consideration must be given to the predictive model assumptions, both implicit and explicit.

Scientific error analysis gives us scientific confidence in our predictions. This procedure requires us to determine our prediction accuracy and precision. A careful analysis also tells whether the accuracy and precision can be improved, and where the most improvement can be made.

For a good perspective on scientific error analysis, it is instructive to see a symbolic analog error analysis. By perceiving all its facets, one obtains a complete set of uncertainty concepts applicable to our program.

To this end, we define H(X) as the prediction probability distribution function (PDF) obtained for the set of site descriptors (X) = (X_1, X_2,...X_n). Each subscripted term represents a preferred value and a distribution about the preferred value for one of the site descriptors. H is the symbolic

506 145

predictor model. The prediction for a baseline case is a one-to-one mapping of X_0 to $H(X_0) = (X_{1,0}, X_{2,0}, \ldots X_{n,0})$. For the sake of this analog discussion, we assume that there is a set of mean descriptors $(\overline{X})$ such that $H(\overline{X}) \equiv \overline{H}$, the mean of the prediction PDF.

The precision (σ_H) is found by considering the spread of values from the individual j mappings

$$H_j = H(X_j) = H(X_{1,j}, X_{2,j} \ldots X_{n,j}).$$

In the limit of an infinite number of measurements, $N \to \infty$, the variance of H, which is the square of the standard deviation σ_H is

$$\sigma_H^2 = \frac{1}{N} \sum_{j=1}^{N} (\Delta H_j)^2$$

where $\Delta H_j = H_j - \overline{H}$ is the predicted deviation of H_j from the mean prediction $\overline{H}$.

The predicted deviations can be expressed in terms of the descriptor deviations by use of a generalized n-dimensional Taylor's expansion about $\overline{X}$,

$$\Delta H_k = \sum_{i=i}^{n} \frac{\partial H(\overline{X})}{\partial X_i} \Delta X_{i,k} + \frac{1}{2!} \sum_{i=1}^{n} \frac{\partial^2 H(\overline{X})}{\partial X_i^2} \Delta X_{i,k}^2$$

$$+ \sum_{\substack{i,j=1 \\ i \neq j}}^{n} \frac{\partial^2 H(\overline{X})}{\partial X_i \partial X_j} \Delta X_{i,k} \Delta X_{j,k} + \text{higher order terms},$$

where

$$\Delta X_{i,k} = X_{i,k} - \overline{X}_i$$

and

$\frac{\partial H(\overline{X})}{\partial X_i}$ means that this partial derivative is evaluated at $\overline{X}$.

506 146

If the deviations $\Delta X_{i,k}$ are sufficiently small, the higher order terms can be neglected, then, to good approximation, the first order Taylor's expansion, which is linear in the deviations, would be adequate to describe our prediction space. Under these conditions, a sensitivity study would require only n + 1 computations by H to map the space. This is not the case for the site descriptors. Thus, if one does not wish to be surprised, the total space must be mapped out, baseline case by baseline case, until one has sufficient experience to gain a heuristic understanding of the site performance in every portion of the n-dimensional space. As the ΔX_i become large, terms like $\partial^2 H/\partial X_i \partial X_j$ become important, and correlations between the parameters must be considered. Because many of the parameters such as porosity and permeability are known to be correlated, a simplistic analytical description is likely to mislead in its predictions. Our only way to determine the precision of the predictions is a Monte Carlo type investigation on a full-blown numerical model.

If we use the expression for the covariance of X_1 and X_2

$$\sigma_{X_1 X_2} = \frac{1}{N} \sum_{j=1}^{N} \left[(X_{1,j} - \overline{X})(X_{2,j} - \overline{X}) \right],$$

we obtain the familiar statistical form of the standard deviation of H in terms of the standard deviations and covariance of the site descriptors,

$$\sigma_H = \sqrt{\sum_{i=1}^{n} \sigma_{X_i}^2 \left(\frac{\partial H(\overline{X})}{\partial X_i} \right)^2 + 2 \sum_{i \neq j=1}^{n} \sigma_{X_i X_j} \frac{\partial H(\overline{X})}{\partial X_i} \frac{\partial H(\overline{X})}{\partial X_j}} + \text{higher order terms}$$

σ_H and the partial derivatives in this expression are the analytical analogs of the unknowns we are looking for in our numerical sensitivity and Monte Carlo studies. Obviously, our other two concerns must be the understanding of the σ_X's and the validity of H. Assuming H is valid, one gains greater scientific knowledge as σ_H is reduced. Knowing the partial derivatives and the σ_X's, one can determine the dominating terms in σ_H. This procedure allows one to formulate a strategy that maximizes the rate of reduction in σ_H.

506 147

We have assumed to this point that our descriptor space is adequate, but this need not be the case. The descriptor space may not be sufficiently expansive, realistic, nor detailed enough. In particular, for the site suitability criteria program the set of n descriptors may need to be expanded to m descriptors, where m > n. Several reasons, for example, may be that: the salinity of the water must be included in the model, the permeability of a layer may have to be made nonuniform to be realistic, or the sedimentary rock may need a more detailed description of its microstructure. These descriptor-space changes may become justified as the program progresses, probabily requiring a reactionary change in the predictor H. This change, in turn, could alter the sensitivities of the descriptors and lead to a change in the direction of the technical data base development.

In summary, improvements in accuracy of H and precision, σ_H, in our analog data base will occur when: (1) H(X), the prediction space, is mapped out; (2) research is done to reduce or better understand the σ_X's; (3) research is done to establish more realistic site descriptors; and (4) validations of H, the prediction operator, are made. These procedures are exhaustive in the sense that complete, high-confidence technical information about our analytical analog would follow from these efforts. They imply three closely coupled development efforts for the actual data base, which include:

- Developing physically realistic descriptors and their uncertainties. Initially the descriptors are generic idealizations.
- Developing a predictor model that is valid in the descriptor space. Initially only the physical processes considered the most important will be included.
- Mapping the prediction to obtain information on the descriptor sensitivity, the precision of the predictions, and the magnitude of the predictions. Results of this indicate where resources can be optimally appropriated to improve the data base as quickly as possible.

Appendix L presents a discussion of the uncertainties associated with the development of the site descriptors, a description of the uncertainties in the prediction model, and a discussion of the Monte Carlo method used to establish the precision of the predictions.

506 148

4. THE PARAMETER DATA BASE

This section describes parameters of the important barriers to radionuclide release: geochemical processes, hydrologic factors (system and rocks), and natural tectonic features. In addition man-made flow pathways produced by construction and exploration are discussed, as well as the possible effects of seismic events and climate changes.

For a generic respository model development, parameters and values that are representative of the natural environment must be specified, excluding rare extremes. A comprehensive literature search was performed to establish a data base on sedimentary rock environments with (1) shale-sandstone sequences, and (2) shale-evaporite-sandstone sequences. Other environments are being investigated. Where no satisfactory laboratory or field data were available, we have relied on experience and on informed judgment. The quality of data for hydrologic systems operating in low-permeability rocks and those with flow through fractured rock, as well as the understanding of these systems, are not as reliable as those concerning more common hydrologic systems. Chemical factors are understood in theory, but more empirical data are needed to establish valid quantitative relationships. Systems analysis and a statistical approach demand data on, or estimates of, probabilities, frequency distributions, process rates, and the frequency of events. These kinds of data and concepts are not common in the geological sciences or in geotechnical engineering. Some of the data that may be required are not currently available. Our estimates, based on theoretical considerations or informed engineering judgment and experience, provide a set of statistical parameter values whose quality will remain lower than that of more traditional physical values pending major advances in geostatistics.

506 149

GEOCHEMISTRY

The main geochemical barrier to radionuclide migration from a high-level waste repository is ion exchange. Other geochemical barriers are ion filtration, hydrolysis, and solubility.

The retention of radionuclides via sorption processes is represented in the hydrologic model as a retardation factor (K_f); that is, the velocity of the groundwater relative to that expected for the individual radionuclide. Retardation factors are based on the rock's physical properties and on the ion exchange distribution coefficients determined experimentally for the individual radionuclides.

To provide input to the mass transport hydrologic model, we had to estimate retardation factors on the basis of available data for distribution coefficients. The radionuclides were divided into three goups: fission products with no sorption ($K_f = 1$), fission products with sorption ($K_f = 10^2$), and the actinides and their daughter products ($K_f = 10^4$). Minimum and maximum values were assigned the latter two groups. Uncertainties as a function of time were estimated at $\pm$ one order of magnitude, as discussed in Appendix L.

Retardation Factors

The retardation factor, $K_f = \frac{\text{water velocity}}{\text{nuclide velocity}} = 1 + rk_d$.

K_d is the ion exchange distribution coefficient, that is,

$$K_d = \frac{\text{amount of nuclide in solid phase} \;/\; \text{mass of solid}}{\text{amount of nuclide in liquid phase} \;/\; \text{volume of liquid}} = \frac{\text{ml}}{\text{g}} ,$$

and

$$r = \frac{\rho}{\theta} \qquad \rho = \text{rock density}, \quad \theta = \text{effective porosity} .$$

506 150

Thus, when there is no sorption, $K_d = 0$ and the retardation factor is 1. Also, as porosity increases, K_f decreases (see Fig. 13).* Although the retardation factor is defined primarily as a function of the ion exchange distribution coefficient, retardation factors as used in the transport model represent the combined effects of ion exchange and adsorption of charged colloidal species on silica surfaces. Other processes that also affect radionuclide concentrations (e.g., low solubilities) are not accounted for in the retardation factor.

The retardation factors used in the transport model originally came from Burkholder's (1976) estimated values** for sorption in a western U.S. desert soil, and are given in the tabulation below. Our recent evaluation of these retardation factors based on published values of K_d shows that Burkholder's results are applicable to sedimentary rocks as well.

Radionuclide	Retardation factor K_f	Radionuclide	Retardation factor K_f
Technetium	1	Zirconium	10^4
Iodine	1	Promethium	10^4
Strontium	10^2	Niobium	10^4
Antimony	10^2	Lead	10^4
Polonium	10^2	Protactinium	10^4
Neptunium	10^2	Uranium	10^4
Rubidium	10^3	Plutonium	10^4
Tin	10^3	Americium	10^4
Cesium	10^3	Curium	10^4
Radium	10^3	Europium	10^4
Yttrium	10^4	Thorium	10^5

*For more complete discussions on sorption and the relative movement of radionuclides in groundwater, see Borg et al. (1976) and Levy (1972).

**Rounded to the nearest order of magnitude.

506 151

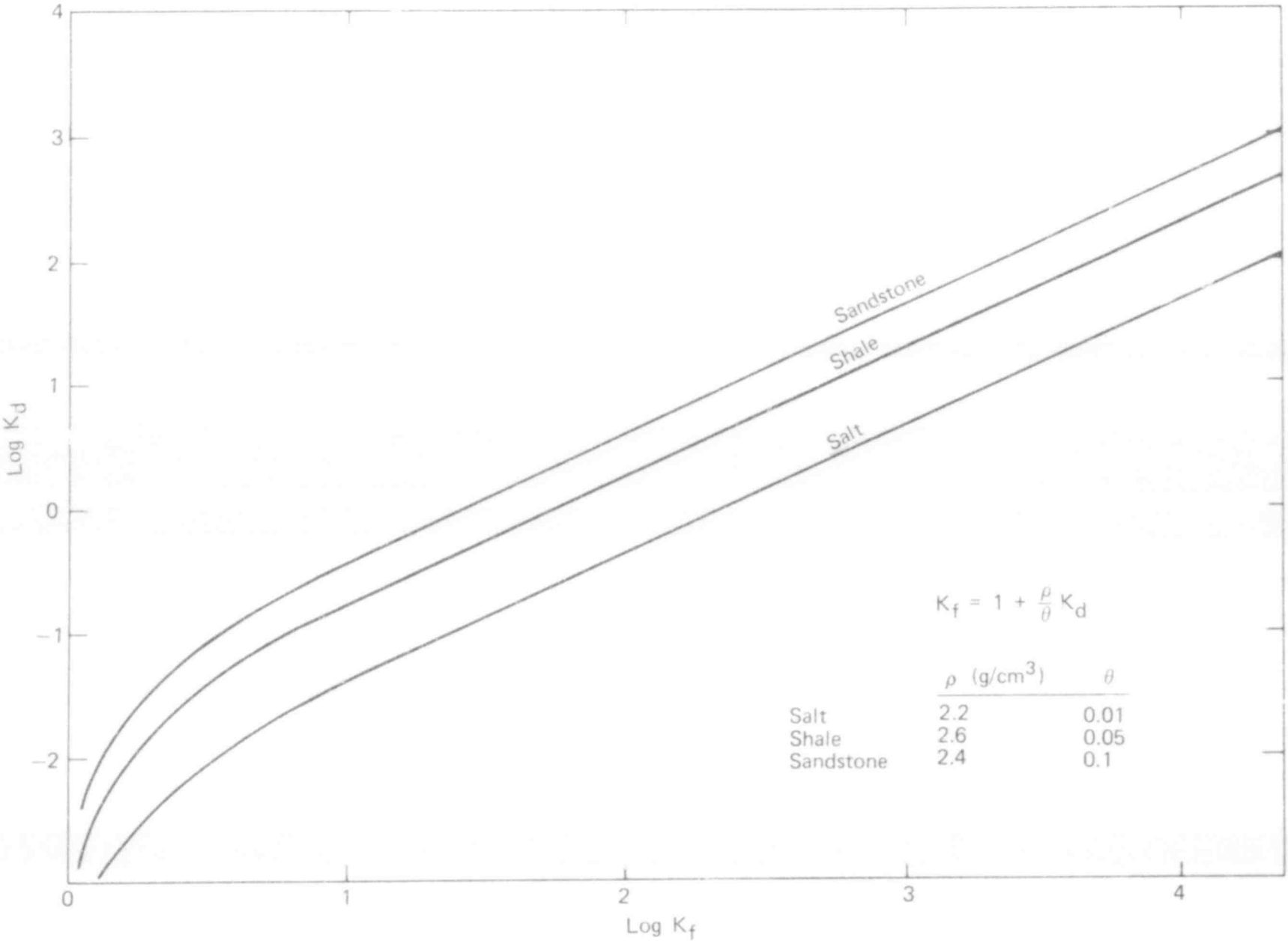

FIG. 13. Retardation factor (K_f) as a function of the distribution coefficient (K_d).

506 151

Because it was not practical to treat each radionuclide separately in the transport model, the 23 biologically significant nuclides in Table 4 were divided into three groups: (1) fission products with no sorption properties, (2) fission products with sorption, and (3) the actinides and their daughter products. The division between fission products and actinides separates the alpha emitters into one group. Each group was assigned maximum, minimum, and preferred values for shale and salt repositories as shown in Table 5. The uncertainties for retardation factors were taken as ± one order of magnitude. This includes the possibility that the chemical properties of the rock (e.g., ion exchange capabilities) may vary slightly over the next million y or so.

For the salt repository, sorption was modeled only in the aquifer (i.e., $K_f = 1$ in the salt layer and barrier bed). Salt has essentially no ion exchange capacity. We assumed that the high salt content of the groundwater* in the barrier bed would saturate the exchange sites to the extent that sorption would be severely limited. We assumed further, that dilution of the salty groundwater in the aquifer would decrease the salinity effect on ion exchange, and that sorption would occur as the radionuclides move through the aquifer.

The same retardation factors were used for interstitial and fracture flow. This assumption is based partly on Pu retardation experiments with artificial fissures in basalt by Fried et al. (1977). Whether retardation factors are actually the same for both interstitial and fracture flow depends on the rate of ion exchange, that is, whether the passage time through the sorbing medium is sufficiently long for equilibrium to occur. Unfortunately, rates of reaction for radionuclide ion exchange are unknown. Although the flow rates for interstitial and fracture flow differ greatly (e.g., 10^{-3} m/y vs 10^{3}m/y, respectively), we assumed that equilibrium would exist.

The bases for our assumed retardation factors (Table 5) are discussed in the following paragraphs.

---

*Data from the Salado and Castille Formations of the Delaware basin show local groundwater with more than 300 000 ppm total dissolved solids.

TABLE 4. Biologically significant nuclides from 10 to 10^6 y after irradiation.

Nuclide	Half-life, $T_{1/2}$ (y)	Specific (Ci/g) activity	MPC_w(Ci/m^3)[a]	MPC_w(moles/litre)[a]	Time of significance (y)[a]
^{90}Sr	28	1.42×10^{2}	3×10^{-7}	2×10^{-14}	10 - 100
^{90}Y	64[c]	5.44×10^{5}	2×10^{-5}	4×10^{-16}	10 - 100
^{93}Zr	1.5×10^{6}	2.56×10^{-3}	8×10^{-4}	3×10^{-6}	10^{3} - 10^{6}
^{93m}Nb	14	2.75×10^{-2}	3×10^{-4}	2×10^{-7}	10^{3} - 10^{6}
^{99}Tc	2.1×10^{5}	1.72×10^{-2}	3×10^{-4}	2×10^{-7}	10^{3} - 10^{5}
^{126}Sn	1.0×10^{5}	2.84×10^{-2}	2×10^{-5}	6×10^{-9}	10^{3} - 10^{5}
^{129}I	1.7×10^{7}	1.63×10^{-4}	6×10^{-8}	3×10^{-9}	10^{3} - 10^{6}
^{134}Cs	2.0	1.33×10^{3}	9×10^{-6}	2×10^{-9}	10
^{137}Cs	30	8.7×10^{1}	2×10^{-5}	2×10^{-12}	10 - 100
^{210}Pb	20	8.52×10^{1}	1×10^{-7}	6×10^{-15}	10^{4} - 10^{6}
^{210}Po	38	4.49×10^{3}	7×10^{-7}	7×10^{-16}	10^{4} - 10^{6}
^{226}Ra	1.6×10^{3}	9.90×10^{-1}	3×10^{-8}	1×10^{-13}	10^{4} - 10^{6}
^{229}Th	7.3×10^{3}	2.0×10^{-1}	7×10^{-6}	2×10^{-10}	10^{5} - 10^{6}
^{230}Th	8.0×10^{4}	2.0×10^{-2}	2×10^{-6}	4×10^{-10}	10^{5} - 10^{6}
^{231}Pa	3.3×10^{4}	4.7×10^{-2}	9×10^{-7}	8×10^{-11}	10^{6}
^{233}U	1.6×10^{5}	9.6×10^{-3}	3×10^{-5}	1×10^{-8}	10^{5} - 10^{6}
^{237}Np	2.1×10^{6}	7.19×10^{-4}	3×10^{-6}	2×10^{-8}	10^{3} - 10^{6}
^{238}Pu	86	1.75×10^{1}	5×10^{-6}	1×10^{-12}	10 - 100
^{239}Pu	2.4×10^{4}	6.2×10^{-2}	5×10^{-6}	3×10^{-10}	10^{3} - 10^{5}
^{241}Pu	6.6×10^{3}	2.26×10^{-1}	5×10^{-6}	9×10^{-11}	10^{3} - 10^{4}
^{241}Am	4.6×10^{2}	3.23	4×10^{-6}	5×10^{-12}	10 - 10^{4}
^{242}Am	8.0×10^{3}	1.84×10^{-1}	4×10^{-6}	8×10^{-11}	10 - 10^{4}
^{244}Cm	18	8.14×10^{1}	7×10^{-6}	4×10^{-13}	10 - 100

[a]Maximum permissible concentration in water

[b]After irradiation

[c]Hours

EQUATIONS:

$$\text{Specific Activity} = \frac{N \times 1.873 \times 10^{-11}}{T_{1/2}\,(\text{sec})} = \text{S. A.}$$

$$N = \frac{\text{atoms}}{\text{mole}} \qquad \text{S. A.} = \frac{1.12755 \times 10^{1}}{M \times T_{1/2}\,(\text{sec})} = \frac{\text{Ci}}{\text{g}}$$

$$M = {}^{\text{g}}/_{\text{mole}}$$

$$MPC_w\left(\frac{\text{moles}}{\ell}\right) = \frac{MPC_w\left(\frac{\text{Ci}}{\text{g}}\right)}{\text{Spec. Act.} \times 10^{3} \times M}$$

506 154

TABLE 5. Assumed retardation factors for the transport model.

Nuclide group	Retardation factor, K_f		
	Minimum	Preferred	Maximum
Shale repository			
Iodine and technetium	1	1	1
Other fission products	1	10^2	10^3
Actinides	10^2	10^4	10^5
Salt repository			
Iodine and technetium	1	1	1
Other fission products			
Salt repository and barrier bed	1	1	1
Aquifer	1	10^2	10^3
Actinides			
Salt repository and barrier bed	1	1	1
Aquifer	10^2	10^4	10^5

Group 1, Iodine and Technetium

Our sorption value of zero for iodine and technetium is based on theoretical and experimental evidence. Both elements exist in natural waters as negative ions I^- and TcO_4^-, respectively. Because soils and rocks generally exhibit no anion exchange capacity except that sometimes shown by soil organic matter, sorption should be zero.*

*Natural anion exchange materials include kaolinite, apatite, and hydrous aluminum oxide. All have low anion exchange capacities, and are limited in their distribution in rocks and soils.

506 155

Soil experiments by Wildung et al. (1974) gave K_d values of 2.8 and 0.007 (essentially zero for our purposes) for TcO_4^-. Values of K_d for I^- were in the range of 0.08 to 52.6. The value of 52.6 was attributed to Fe and Al oxide coatings on the soil particles, otherwise I^- showed no sorption. Gast et al. (1977) at the University of Minnesota reported similar K_d values for TcO_4^- in soils. In an earlier study of radionuclide migration at Hanford (Brown, 1967), Tc migrated at about the same rate as groundwater (i.e., $K_f = 1$). Values of K_d for Tc were found to be zero over a wide range of $NaHCO_3$ concentrations for a South Carolina topsoil (Routson et al., 1975).

Group 2, Other Fission Products

Fission products with sorption characteristics include ^{90}Sr, ^{90}Y, ^{93}Zr, ^{93m}Nb, ^{126}Sn, ^{134}Cs, and ^{137}Cs. The preferred retardation factor of 10^2 given this group is a conservative estimate based on the sorption characteristics of Sr and Cs, the only major contributors among the fission products to the waste inventory. The nuclide ^{90}Y, in secular equilibrium with ^{90}Sr, has a half-life of 64 h. The $^{93}Zr \rightarrow {}^{93m}Nb$ pair's inventory is 2×10^5 that of the combined inventory of ^{90}Sr plus ^{137}Cs in 10-y-old waste. The ^{126}Sn inventory is less than ^{93}Zr.

A compilation of distribution coefficients for Sr and Cs shows a wide range of values (Table 6). Note that the values for Sr vary from 0.19 in salt to 4000 in tuff. The values for Cs show a variation from 0.027 in salt, and 17 800 in tuff. With exception of Amchitka basalts, the coefficients for Cs are larger often by one order of magnitude, than those for Sr. Of the K_d values in Table 6, only the following are applicable to the geology used in the transport model (i.e., sedimentary rocks, excluding carbonates).

506 156

	K_d(Sr)	K_d(Cs)
Shale siltstone	8	309
Sandstone	1.4	102
Sands	1.7-43	22-314
Sediments	50	300
Soils	9-282	250 - 53

Based on the above, a value of 10 was chosen as an average distribution coefficient for Sr. This gives a retardation factor of approximately 10^2 in sandstone (see Fig. 13). Although Cs should have a retardation factor greater than 10^2, it was assumed to have the same value to simplify calculations in the transport model. The prefered value of 10^2 is used for both shale and sandstone units. The maximum and minimum values reflect the range commonly found for Sr in sediments and sedimentary rocks. The estimated uncertainty in the retardation factor as a function of time is ± one order of magnitude.

506 157

TABLE 6. Reported distribution coefficients for Sr and Cs.

Data source	Distribution coefficient, K_d		
	Sr	Cs	Conditions
Angelo et al., 1962	16-135	792-9520	Basalt, 32-80 mesh, synthetic groundwater
Baetsle and Dejonghe, 1972	1.7-3.8	22-314	Quartz sand, pH 7.7
Bertem et al., 1962	4-9	8-9	Granodiorite, 100-200 mesh, prep. groundwater
	11-23	1030-1810	Granodiorite, 0.5-1 mm, prep. groundwater
Brown, 1967	50	300	Hanford sediments
Dlouhy, 1967	45-75	800-1000	Tuff
Essington and Nork, 1969	220	39	Basalt, 0.5-4 mm, 300 ppm TDS
	1220	280	Basalt, 0.5-4 mm, 300 ppm TDS
	1.1	6.5	Basalt, 0.5-4 mm, sea water
Godse et al., 1967	143-282	617-1053	Soil, pH 6.8
Goldberg et al., 1962	2070-3480	12,000-17,800	Tuff, 100-200 mesh, synthetic groundwater
Hajek and Knoll, 1966	19-43	189-420	Soils
Hoffman et al., 1977	10^4	>5000	Tuff, chimney rubble, groundwater
Inoue, 1967	9.4-71	250-1000	Soils, Ca groundwater
Nork and Fenske, 1970	260	1020	Tuff, >0.4 mm, prep. water
	0.19	13.5	Carbonate, >4 mm, prep. water
	1.7	34.3	Granite, >4 mm, groundwater
	8.32	309	Shaley siltstone, >4 mm, well water
	1.37	102	Sandstone, >4 mm, well water
	0.19	0.027	Salt, >4 mm, saturated salt water
Nork et al., 1971	48-2454	121-3165	Alluvium, 0.5-4 mm, groundwater
Parsons, 1961	13-43	100	Sands
Robertson & Barroclough, 1973	3	-	Basalt, in situ measurements
Stead, 1963	5-14	-	Dolomite, 4000 ppm TDS
	4000		Tuff

Taken in part from Borg et al., 1976, Table 23.

506 159

Group 3, Actinides and Daughter Products

The biologically important actinides in Table 4 are the products of four interrelated decay chains:

$$^{244}Cm \rightarrow {}^{240}Pu$$

$$^{243}Am \rightarrow {}^{239}Pu \rightarrow {}^{231}Pa$$

$$^{241}Pu \rightarrow {}^{241}Am \rightarrow {}^{237}Np \rightarrow {}^{233}U \rightarrow {}^{229}Th$$

$$^{242}Cm \rightarrow {}^{238}Pu \rightarrow {}^{234}U \rightarrow {}^{230}Th \rightarrow {}^{226}Ra \rightarrow {}^{210}Po\ {}^{210}Pb$$

Because the transport model does not differentiate between parent nuclides and their daughters, all of the actinides are treated alike with regard to their retardation factors. For example, ^{239}Pu is the daughter of ^{243}Am. Although there is evidence that Am migrates faster than Pu (Fried et al., 1977; Hajek, 1966; Hajek and Knoll, 1966), in the transport model, Pu and Am are treated alike. It seems reasonable to do so, since the difference in retardation between them is probably less than the uncertainty in the retardation factor for actinides (Table 5).

In the pH range of 5 to 8 for natural waters, the reported values of K_d for the actinides (see Table 7) vary greatly:

Americium	2×10^2 to 5×10^4
Neptunium	3.2×10^2
Plutonium	2.5×10^2 to 3.8×10^5
Thorium	40 to $>10^5$

From the above values, a conservative estimate for an average K_d is 200 to 300. From Fig. 13, this value for K_d gives a retardation factor of approximately 10^4. Our minimum and maximum K_f values of 10^2 and 10^5 represent possible K_d values of 10 and 10^4, respectively. Uncertainties as a function of time are estimated as ± one order of magnitude.

506 159

TABLE 7. Reported distribution coefficients for actinides.

Data source	Distribution coefficient, K_d (ml/g)	Conditions
	Americium	
Hajek and Knoll, 1966	1	Sand, 5N NO_3^-, oil, org., pH 3
	2×10^2	Sand, 5N NO_3^-, oil, org., pH 7
	5×10^2	Sand, sludge, pH 7
Van Dalen et al., 1975	5×10^4	Illite/kaolinite, 90% sat. NaCl, pH 7-8
	4×10^2	River sand, 90% sat. NaCl, pH 7-8
Routson et al., 1975	$>1.2 \times 10^3$	Desert sand, 0.2M Ca, pH 2.5-3.1
	$>1.2 \times 10^3$	Desert sand, 0.002M Ca, pH 2.5-3.1
	67	Sandy clay, 0.002M Ca, pH 2.5-3-1
	1	Sandy clay, 0.2M Ca, pH 2.5-3.1
	1.6	Sandy clay, 3M Na, pH 2.5-3.1
	280	Sandy clay, 0.015M Na, pH 2.5-3.1
Fried et al., 1977	$K_f = 10^4$	Limestone, pH 6.7
	Neptunium	
Dahlman et al., 1976	3.2×10^2	Clay soil, pH 6.5, 5mM $Ca(NO_3)_2$
Routson et al., 1975	2.37	Sand, 0.002M Ca, pH 2.5-3.1
	0.36	Sand, 0.2M Ca, pH 2.5-3.1
	3.9	Sand, 0.015M Na, pH 2.5-3.1
	3.2	Sand, pH 2.5-3.1, 3.0M Na
	0.25	Sandy Clay, pH 2.5-3.1, 0.002M Ca
	0.16	Sandy clay, pH 2.5-3.1, 0.2M Ca
	0.7	Sandy clay, pH 2.5-3.1, 0.015M Na
	0.4	Sandy clay, pH 2.5-3.1, 3.0M Na

506 160

TABLE 7. (Continued).

Data source	Distribution coefficient, K_d (ml/g)	Conditions
	Plutonium	
Bondietti et al., 1976	$1\text{-}1.7 \times 10^5$	Soil clays, pH 6.5 Pu(IV), 5mM Ca
	7.5×10^4	Soil clays, pH 6.5 Pu(VI), 5mM Ca
	2.1×10^4	Montmorillonite, pH 6.5, Pu(IV), 5mM Ca
	2.5×10^2	Montmorillonite, pH 6.5, Pu(VI), 5mM Ca
Dahlman et al., 1976	3×10^5	Clay soil, pH 6 5 Pu(IV), 5mM Ca
Dursuma and Parsi, 1974	$1\text{-}9 \times 10^4$	Mediterranean sediment
Glover et al., 1976	35 to 1.4×10^4	17 soil samples, Pu(10^{-6},10^{-7},10^{-8}M)
Hajek, 1966	$K_f = 10^4$	Surface soil groundwater
Hetherington et al., 1975	$2\text{-}4.8 \times 10^4$	5% clay, 50% silt, 45% sand
Miner et al., 1974	$>4.3 \times 10^2$	Soils
Mo and Lowman, 1975	$0.16\text{-}3.8 \times 10^5$	Calcareous sediment
Noshkin et al., 1976	2.5×10^5	Average value for Eniwetok groundwater particulates
Noshkin, 1977	1.1×10^5	Coral soil and sediment
	8×10^4	Clay silt particulates
Pillai and Mathew, 1976	9×10^4	Average value for suspended silt
Wahlgren et al., 1976	3×10^5	Lake Michigan particulates
Van Dalen et al., 1975	10^4	Illite/kaolinite,90% sat. NaCl,pH 7-8
Fried and Friedman, 1976	$K_f = 10^4$	Tuff, Pu(IV), pH 6.7
	$K_f = 3 \times 10^2$	Tuff, Pu(VI), pH 6.7
Fried et al., 1977	$K_f = 3 \times 10^4$	Limestone, pH 6.7, Pu(IV)
	$K_f = 2 \times 10^4$	Basalt "fissure", pH 6.7, Pu(IV)

TABLE 7. (Concluded).

Data source	Distribution coefficient, K_d (ml/g)	Conditions
	Thorium	
Nishiwaki et al., 1972	40-130	Med. sand, pH 8.15
	310-470	v. f. sand, pH 8.15
	2700-10^4	silt/clay, pH 8.15
Rancon, 1973	8	Schist soil, pH 3.2, 1 g/l Th
	60	Schist soil, pH 3.2, 0.1 g/l Th
	120	Illite, pH 3.2, 1 g/l Th
	10^3	Illite, pH 3.2, 0.1 g/l Th
	$>10^5$	Illite, pH >6, 0.1 g/l Th
Dahlman et al., 1976	1.6×10^5	Clay soil, pH 6.5,, 5m$\underline{M}$ $Ca(NO_3)_2$
Bondietti et al., 1976	1.6×10^5	Silt loam, pH 6.5, Ca sat. clay
	4×10^5	Montmorillonite, pH 6.5, Ca sat. clay
	Uranium	
Rancon, 1973	3×10^2	Clay soil, pH 5.5, 1 ppm UO_2^{+2}
	2×10^3	Clay soil, pH 10, 1 ppm UO_2^{+2}
	2.7×10^2	Clay soil, pH 12, 1 ppm UO_2^{+2}
Dahlman et al., 1976	4.4×10^3	Clay soil, pH 6.5, U(VI), 5m$\underline{M}$ $Ca(NO_3)_2$
Bondietti et al., 1976	6.2×10^4	Silt loam, pH 6.5, U(VI), Ca sat.

506 162

The literature suggests that the actinide retardation factors may be related as follows: Th > Pu > Am > Np > Ra*. The actual differences depend on repository characteristics, e.g., rock type, flow rates, and groundwater composition. For the generic repository, treating the actinides as a group seems justified. It should be remembered, however, that Pu in particular may have a retardation factor as high as 10^7--an important consideration in modeling a repository for spent fuel.

Other Geochemical Barriers

Two geochemical barriers to radionuclide migration not included in the hydrologic model are ion filtration and solubility. Their importance in protecting the biosphere from contamination depends on the physical and chemical properties of the repository system.

Clays in shale beds act as semipermeable membranes retarding to varying degrees the passage of dissolved species with respect to water. The membrane properties of shales result from negative charges on the surface and edges of the clay particles. As the clays are forced together during compaction of formation, anions in the pore space are excluded, thereby creating a positively charged barrier. Later, as groundwater moves through the pore space, anions are attracted and cations repulsed, but because of the requirement of electrical neutrality, neither cations nor anions can move readily through the field. Neutral water molecules do move, thus increasing the concentration of the charged ions on the input side of the shale. The

*As the daughter of ^{230}Th, the alkaline-earth element ^{226}Ra is included with the actinides. There is evidence from the deep-sea cores that Ra migrates relative to Th by a factor of 10 to 100. Currently, we are evaluating reconcentration effects caused by these differences (see Appendix E).

506 163

degree of retention of the various charged species is a function of charge density, concentration, compaction pressure, temperature, and so on (Kharaka and Berry, 1973). At present, we cannot estimate how this process contributes to the retardation factor for inclusion in the hydrologic model.

Calculated concentrations of Sn, Th, Pu, and Am at node 1 (i.e., leaving the repository) exceed their theoretical solubilities (Table 8). If the theoretical solubilities are correct, the groundwater concentrations of these radionuclides could be restricted to some maximum value at the repository, thereby reducing the concentrations reaching the biosphere. Isotopic dilution of Sn and Th, plus stable nuclides that coprecipitate with radionuclides could also reduce the environmental risks by lowering the radioactivity of groundwater saturated with those elements.

TABLE 8. Radionuclide concentrations exceeding solubilities.

Nuclide	MPC_w (Ci/m^3)	Groundwater concentration[a] (Ci/m^3)	Solubility (Ci/m^3)
^{126}Sn	2×10^{-5}	2×10^{-2}	4×10^{-12}
^{229}Th	7×10^{-6}	9×10^{-5}	1×10^{-8}
^{239}Pu	5×10^{-6}	8×10^{-2}	1×10^{-7}
^{240}Pu	5×10^{-6}	3×10^{-1}	5×10^{-7}
^{241}Am	4×10^{-6}	6.6	4.5
^{243}Am	4×10^{-6}	6×10^{-1}	3×10^{-1}

[a]Maximum ground water concentration at node 1 (i.e., leaving a repository of 6×10^6 MWe-y).

[b]Maximum theoretical solubility in groundwater (pH = 5-8 Eh = 0): no isotopic dilution.

506 164

The theoretical solubilities in Table 8 are based on the formation of the relatively insoluble oxides and hydroxides. We did not consider the formation of soluble inorganic complexes, mainly because the data are limited or not available. To include solubility as a geochemical control, we need to know more about radionuclide solubility in natural waters. The importance of unknown complexes in determining solubility can be illustrated by comparing the theoretical solubilities of Sn and Th to concentrations found in natural waters (Table 9). For example, the solubility of Sn at pH 6.8 (a common value for fresh water) is 4×10^{-18}M. Yet the value given for filtered samples from the Saale River in Germany is 2×10^{-9}M. Until we can identify the actual species likely to exist in natural water systems, solubility limits as a way to control radionuclide concentrations must be used with caution.

TABLE 9. Theoretical solubilities of Sn and Th concentrations in natural waters.

Element	Solubility (M) at pH = 8.15	Concentration in sea water (M)	Solubility (M) at pH = 6.8	Concentration in fresh water (M)
Sn	2×10^{-15}	8×10^{-9}[a]	4×10^{-18}	2×10^{-9}[b]
Th	7×10^{-26}	1×10^{-10}[c]	2×10^{-20}	4×10^{-7}[d]

[a] Heide and Reichardt, 1975.

[b] Hamaguchi et al., 1964.

[c] Bernat and Goldberg, 1969.

[d] Lawrence Livermore Laboratory, 1976.

506 165

Hydrologic parameters include systems that must be measured in the field e.g., pressures, pressure gradients, and dispersion coefficients; and rock factors that can be measured in the field or in the laboratory, e.g., porosity, permeability or transmissivity, and saturation. In this section we first deal with the system and rock parameters and then discuss flow through fractures.

Pressures and Gradients

Table 10 gives the values assumed for the vertical head between the aquifers in our model (Fig. 14). We derived our range of head differences from observed values reported for deep aquifers in sedimentary basins, and set the preferred value to reflect a substantial upward driving gradient. A very small upward gradient for the model would have tended to mask other effects and limit the usefulness of the sensitivity analysis. We assumed that the entire upward gradient would be available to cause flow. The effects of salinity variations and osmotic potentials were not considered.

TABLE 10. Assumed values for aquifer gradients and head.

Parameter	Value	
	Preferred	Range
Horizontal gradient:		
Layers 2 and 6	0.005	0.0005-0.05
Layers 3, 4, and 5	0	-
Vertical head between		
Layers 2 and 6	60 m	3-150 m

506 166

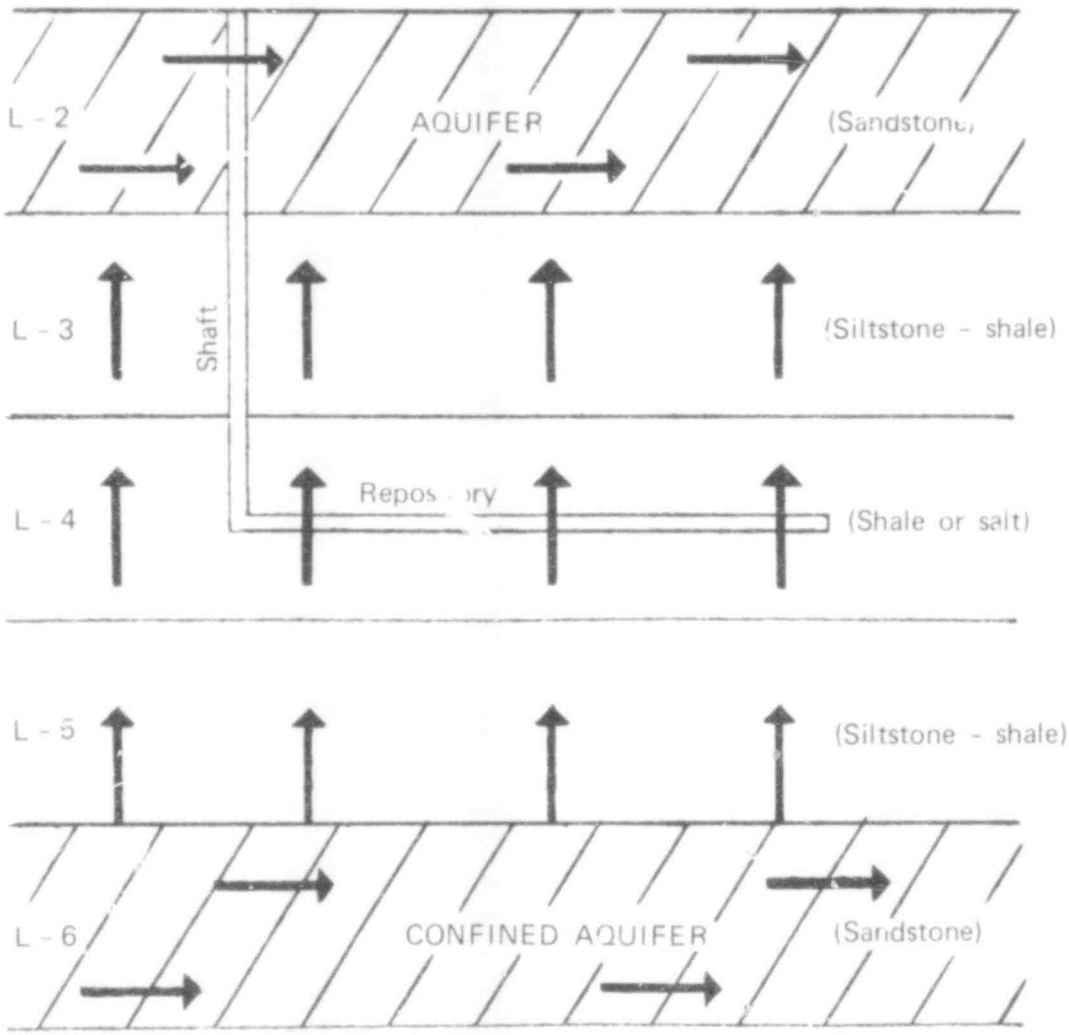

FIG. 14. General flow pattern for unflawed repository, layers 2 through 6 (layer 1 is a surface soil layer).

506 167

In the Williston basin, vertical head gradients between aquifers vary significantly depending on location and depth. Reported head differentials include 100 to 400 ft (30 to 122 m) between the Fox Hills and Dakota aquifers (Crosby, Armstrong, and Paulson, 1973), and 300 to 350 ft (91 to 107 m) between the Dakota and Madison aquifers (Swenson, 1968). The lower aquifer in each case was under the greater pressure. Claiborne and Gera (1973) reported that a downward gradient exists in the vicinity of the Waste Isolation Pilot Plant site in New Mexico. An equivalent freshwater head differential of 148 ft (45 m) was measured between the formations above the Salado and the underlying Delaware aquifer. However, significant variations in salinity throughout the formation make it difficult to determine the actual flow direction.

Horizonal gradient information is obtained also from sedimentary basin data. For example, Crosby, Armstrong, and Paulson (1973) report horizontal gradients in the Williston basin ranging from 0.0006 to 0.008 with an average of 0.002. Significantly greater gradients (0.02 or greater have been observed in the Delaware basin (McNeal, 1965). Horizontal gradients range from 0.0005 to 0.05 with a preferred (baseline) value of 0.005. The preferred value constitutes a horizontal head drop of about 25 ft/mi (4.7 m/km), which is representative of sedimentary basins. For simplicity, we assumed a horizontal gradient of zero for the less permeable layers. Although not consistent with the horizontal gradients in the aquifer, the assumption has minimal effect on the hydrology of the model.

Dispersion

Hydrodynamic dispersion is a nonsteady irreversible mixing process (Borg et al., 1976). It reflects: (1) external forces such as hydraulic head potential, (2) the geometry of the pore system, (3) molecular diffusion, (4) liquid properties, (5) changes in solute concentration, and (6) liquid-solid interactions.

The coefficient of hydrodynamic dispersion describes the complex process in an unspecific manner and can be evaluated only by experiment. Table 11 lists dispersivity values obtained by calibration of transport models against field

506 168

data. Note that there is minimal apparent correlation of rock type, porosity, and dispersivity. We assumed a coefficient of longitudinal dispersivity of 50 m, which can be compared with the values in Table 11.

Resaturation

It is important to estimate the time required for groundwater to fill the repository after abandonment, since dissolved waste will not flow out before refilling is completed. We estimated a generic case; a real site would require more precise calculations using the appropriate data and a detailed repository design.

The time required for groundwater to resaturate the repository depends on the nature of the original groundwater regime, the effectivenes of the shaft seal, and the porosity of the tunnel backfill and fracture zones. Assuming the shaft seal remains competent (i.e., permeability in the shaft remains equal to or less than that in the surrounding formation), one can estimate the time for resaturation by groundwater flowing from the formation above and below the mined zone. The total volume of water necessary to resaturate the repository equals the mined volume of the repository (HLW area × 24% extraction ratio × height) times the porosity of the backfill (assumed to be 10%). Flow rates into the repository from the top and bottom are computed using Darcy's equation $Q = KIA$, where Q is the inflow rate, K is the vertical permeability of the formations, I is the vertical gradient after abandonment and before saturation, and A is the total area of the HLW repository. Because the gradient and flow rates were assumed to be constant in this simple case, the flow rate and therefore the resaturation time, will vary directly with the formation permeability. A conductivity of 10^{-9} cm/sec yields a time of about 100 y, which is our preferred value. A value of 10^{-8} cm/sec yields about 20 y and 10^{-10} cm/sec about 1 000 y, which gives the assumed range of values.

Permeability and Porosity

We determined our values for porosity and permeability by examining field data and laboratory measurements. Some of the data are given in Appendix M,

506 169

TABLE 11. Dispersivity values obtained by calibration of transport models against observed groundwater solute transport.

Aquifer and location	Longitudinal dispersivity, a_L (m)	Transverse dispersivity, a_T (m)	Effective porosity of aquifer (%)	Reference
Cook Mountain Limestone, Tatum Dome, Mississippi	11.6	---	23	Fenske, 1973
Ocala Limestone, Brunswick, Georgia	61	20	35	Bredehoeft and Pinder, 1973
Pleistocene glacial outwash sand and gravel, Long Island, New York	21.3	4.3	35	Pinder, 1973
San Andres Limestone Roswell Basin, New Mexico	21.3	---	1-10	Rabinowitz and Gross, 1972
Culebra dolomite member of Rustler Formation, near Carlsbad, New Mexico	38.1	---	12	Grove and Beetem, 1971
Basalt lava flows and interbedded sediments of the Snake River Plain aquifer, near Idaho Falls, Idaho	91	137	10	Robertson and Barroclough, 1973
Bonanza King Formation (lower carbonate aquifer) near Nevada Test Site	15	---	At least 1.5	Claassen and Cordes, 1975

NOTE: From Borg et al., (1976), P. 157.

506 170

which discusses parameters in general and presents a basis for the parameter values used in our model.

The special case of porosity and permeability in fractured rocks is discussed below. The hydrology and parameter values associated with natural characteristics, i.e., tectonic and structural, and those associated with man-made features are discussed later in separate sections.

In general, theories, practices, and field measurements in groundwater hydrology have been developed for materials of permeability sufficiently high to provide a usable water resource or to constitute a dewatering problem. A fluid moving through low permeability rocks can flow between individual grains (interstitial flow) or through fractures or other flaws in the rock (fracture flow). Practical theories used in flow analysis usually relate to homogeneous, isotropic porous media. Thus, the hydrology of media with low permeabilities and fracture porosity has not been well documented.

Because we could not generalize regarding the type of groundwater flow (interstitial, fracture, or both) for our generic model, we developed two sets of values for permeability and porosity (see Table 12). Note that the values for layers 3, 4, and 5 are different; values for layers 2 and 6 are the same. Our values for a repository layer (layer 4) in salt are shown in Table 13.

Note also that in no case did we use a permeability value of zero, although near zero permeability is possible in some shale deposits exhibiting unusual conditions. However, measurement limitations may make it impossible to detect, and thus confirm, values lower than about 10^{-8} or 10^{-9} cm/sec. Therefore, it seems wise, to assume a finite lower bound for permeability at this time.

We adopted values for permeability and porosity to reflect the ranges found in nature. Layers 2 and 6 were assumed to be sandstone. Layers 3 and 5 were assumed to be a siltstone-shale sequence, and layer 4 was assumed to be shale or salt. Although values above or below our ranges can be found, they would be atypical for the types of rock assumed.

506 171

Cross-sectional areas of flow through the undisturbed cases are based on a conceptual repository design by Parsons et al. (1976). We assumed vertical flow through a horizontal area of 5×10^6 m^2. We assumed horizontal flow in the upper aquifer (layer 2) across an area equal to the vertical aquifer thickness times 2000 m, the horizontal length of the repository across the flow. Our values for horizontal permeability are based on experience and on a wide variety of representative measurements for different rock types (see Tables M-1, M-2, and M-3 of Appendix M).

TABLE 12. Assumed permeability and porosity values for shale repository.

Horizontal permeability (cm/sec)			Porosity	
Layer	Preferred	Range	Preferred	Range
		Interstitial flow		
2	10^{-4}	10^{-2} to 10^{-6}	0.10	0.02-0.20
3	10^{-6}	10^{-4} to 10^{-8}	0.05	0.01-0.10
4	10^{-8}	10^{-6} to 10^{-10}	0.05	0.01-0.10
5	10^{-6}	10^{-4} to 10^{-8}	0.05	0.01-0.10
6	10^{-4}	10^{-2} to 10^{-6}	0.10	0.02-0.20
		Fracture flow[a]		
2	10^{-4}	10^{-2} to 10^{-6}	0.10	0.02-0.20
3	10^{-5}	10^{-3} to 10^{-7}	10^{-4}	10^{-3}-10^{-5}
4	10^{-7}	10^{-5} to 10^{-9}	10^{-5}	10^{-4}-10^{-6}
5	10^{-5}	10^{-3} to 10^{-7}	10^{-4}	10^{-3}-10^{-5}
6	10^{-4}	10^{-2} to 10^{-6}	0.10	0.02-0.20

[a]Porosity and permeability are correlated physical variables. For example, in layer 4: with the preferred permeability value, use a porosity of 10^{-5}; with the maximum permeability value, use a porosity of 10^{-4}; with the minimum permeability value, use of porosity of 5×10^{-6}. Use similar combinations for layers 3 and 5.

506 172

TABLE 13. Assumed permeability and porosity values for salt repository.

Parameter	Value	
	Preferred	Range
Permeability (horizontal and vertical)[a]	10^{-7} cm/sec	10^{-10} to 10^{-4} cm/sec
Porosity[b]	0.01	0.004-0.07

[a]The end points of the range are the minimum (excluding zero) and maximum values in the literature reviewed to date. Because no distribution of values was available, the middle of the range was taken as the preferred value.

[b]The end points of the range are the minimum and maximum values in the literature reviewed to date. The distribution in reported values was used to determine the preferred value.

Permeability can vary significantly between the horizontal and vertical directions, particularly in stratified sedimentary rock. Few field tests of entire rock masses (as opposed to laboratory tests) have been conducted to evaluate vertical permeability. The horizontal and vertical permeabilities in Table 14 calculated from pumping tests in the Uinta and Green River formations, Piceance basin, Colorado, serve as an example of the variability possible.

TABLE 14. Permeability values calculated from field tests.

Rock type	K_H(cm/sec)	K_v(cm/sec)	K_v/K_H
Shale	2×10^{-6}	1×10^{-6}	0.5
Siltstone-shale	1.5×10^{-4}	3×10^{-6}	0.020
Shale	1.2×10^{-5}	1×10^{-7}	0.008
Siltstone-shale	2.1×10^{-4}	2.1×10^{-5}	0.1
Siltstone-shale	2.8×10^{-5}	3.0×10^{-6}	0.107
Sandstone	3.4×10^{-5}	3.4×10^{-5}	1.0

Note: From Golder Associates (1977).

506 173

The K_V/K_H ratio in our model ranges from 1.0 to 0.01, with a preferred value of 0.1, approximately the same values as observed in actual tests. Under some conditions the effective horizontal permeability may be equal to or greater than 1000 times the vertical permeability. This might be the case in a bedded salt deposit that contains continuous horizontal beds of fractured shales or siltstones.

Measured values of interstitial porosity are included with the permeabilities listed in Tables M-1 through M-3, Appendix M. The porosity values are effective porosity (rather than total porosity). Effective porosity is a measure of the void space that actively contributes flow through a porous medium. In particular, fine-grained rocks such as siltstones and shales can have total porosities of 30 to 50% with only a fraction of the void space contributing to flow. Our preferred values and ranges for interstitial porosity are estimates based on experience and the limited field measurements found in the literature.

We will now discuss the general problem of flow through fractures, and analyze the relation of fracturing to porosity and permeability. Tables M-4, M-5, and M-6 of Appendix M present laboratory and field data on permeability of fractured rocks. Table M-7 presents computed values relating fracture dimension, porosity, and permeability.

Laboratory permeability tests generally reflect the interstitial permeability of the core sample tested, while field tests, especially full-scale pumping tests, reflect the combined effect of interstitial and fracture flow. Data specifically relating the interstitial flow to fracture flow are generally lacking. By comparing laboratory permeabilities with field permeabilities, a relation between fracture and interstitial flow can be developed. However, even this procedure is questionable, because it is difficult to sample sufficient quantity to obtain an average permeability. Thus, it is difficult to determine whether the permeabilities derived from field tests, as reported in the literature, are predominantly fracture or interstitial. Our fracture permeability values are based on the same data and rationale as the interstitial permeabilities. The fracture permeabilities are specified

506 174

somewhat higher than the associated interstitial permeabilities for layers 3, 4, and 5. Flow in layers 2 and 6 (the aquifers) was assumed to be interstitial in all cases.

Values for fracture porosity dominate the calculation of flow velocities in fractured rocks, and their porosity is difficult to measure. We obtained our values using a method developed by Snow (1967) for estimating fracture porosity from measured values of permeability and fracture spacing. Our basic assumptions include the existence of the following conditions:

- Isotropic fracture permeability
- Three mutually orthogonal and similar sets of fractures (cubic fracturing).
- The numbers of open fractures intersected by equal lengths of random boreholes obey a Poisson distribution.

The fracture porosity n is given by $n = 3(3k/2)^{1/3}(2/S)^{2/3} = 5.45 (k/S^2)^{1/3}$, where k is the permeability in units of length squared and S is the fracture spacing (2.25 times the observed spacing, due to an adjustment factor). The representative aperture width 2b is given by $2b = nS/3$.

Snow (1967) indicates that for a rock of given permeability, the fracture porosity depends most on the fracture spacing and average aperture width. He concludes that neither aperture width nor fracture spacing are notably different from one rock type to another, nor are the porosities and permeabilities that depend on them. He found that fracture porosity decreases approximately logarithmically with depth. The upper porosity limit is 0.05% near the surface, decreasing to 0.0005% at 400 ft (122 m). In a few cases fracture porosity decreased less rapidly than one order of magnitude per 200 ft (61 m). The minimum spacing of open fractures increased from 4 to 24 ft (1.2 to 4.3 m) in this interval. Only fractures in competent rock were corsidered, thus excluding weathered zones, fault breccia, overburden, and so on. Fracture openings range from 400 to 75 μm in the upper 30 ft (9.1 m), but decrease to 250 to 50 μm at depths of 50 to 200 ft (15 to 61 m).

Webster et al. (1970) found two types of fracture common in crystalline rock (predominantly chlorite-hornblende schist and gneiss) at the Savannah River

506 175

nuclear reprocessing plant near Aiken, South Carolina. The first type pervades the entire rock mass, but transmits very little water. The second type is restricted to definite zones and transmits substantial quantities of water. Permeability of the entire rock mass (including both types of fracture) was 5×10^{-5} m/sec as determined from a two-well tracer test. Fracture porosity was calculated to be 0.08%. The fracture porosity of the rock containing only the first type of fracture was thought to be 0.01% or less.

Several calculations of fracture porosity and fracture width are given in Table M-7 of Appendix M using Snow's analysis. In the table, permeabilities in the range given for layers 3, 4, and 5 are used in conjunction with a wide range of probable fracture spacings. Figure 15 illustrates the calculated relationship between permeability and porosity in fractured media with different fracture spacings.

A significant assumption in this analysis is the fracture spacing. The preferred values reflect fracture spacing of about 100 to 200 cm, which seems reasonable. A study conducted by Ward (1968) of joint patterns in gently dipping sedimentary rocks in south central Kansas agrees with these assumptions.

NATURAL FEATURES

In modeling natural features that form permeable paths for groundwater, we considered fault zones and solution-breccia pipes. Other features can be modeled by changing parameter values, or analogous features can be analyzed by extrapolating results previously obtained. The model requires input of the features' dimensions, hydraulic properties, and the time-dependent variation in these, if present. Transition rates and probabilities are needed for probabilistic calculations. These requirements also apply to models of man-made features.

The flow and transport pattern analog is a three-dimensional network of one-dimensional path segments. For the initial model, the analog required to simulate the anticipated groundwater movements was developed primarily from experience, available field information, and judgment rather than detailed

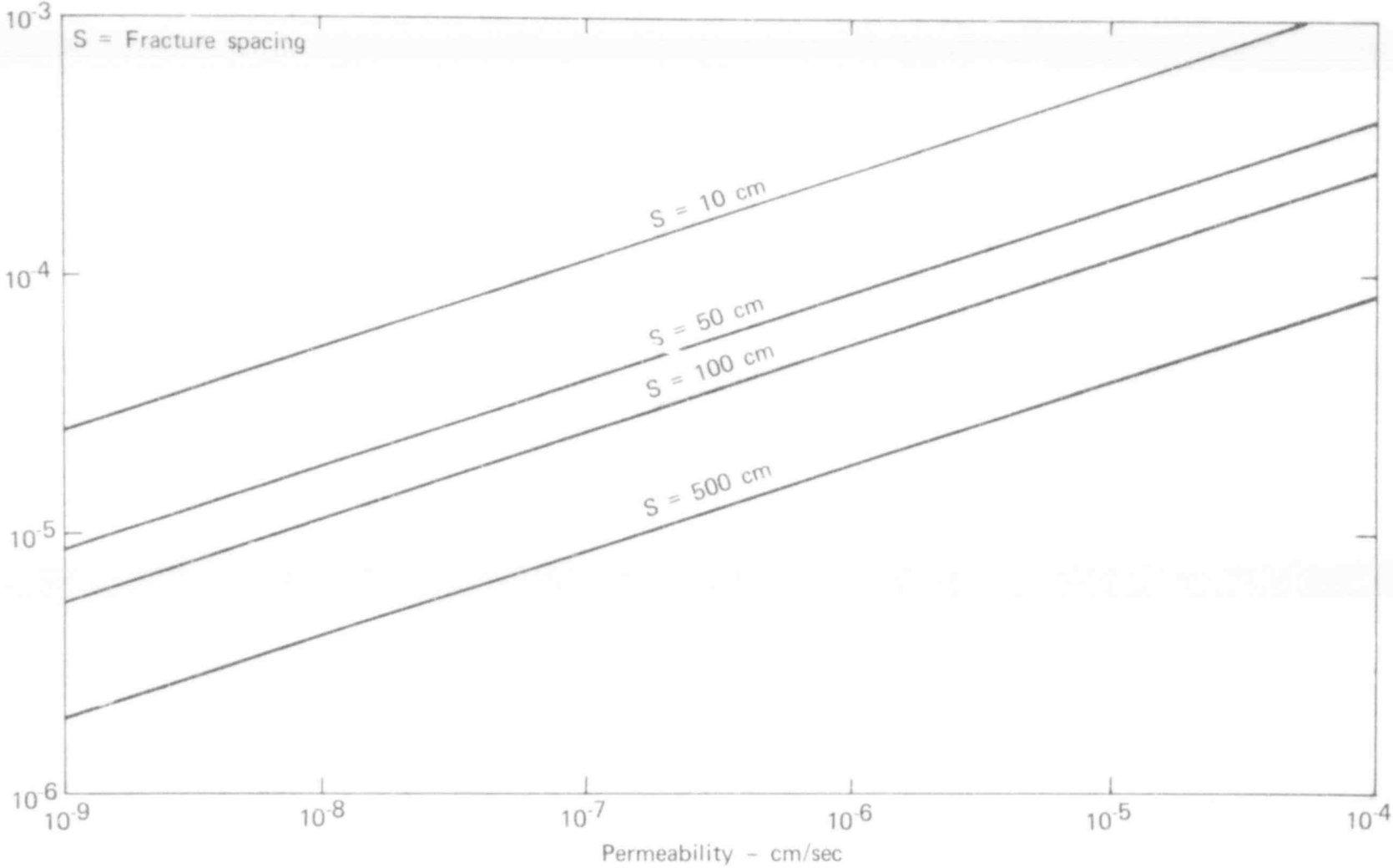

FIG. 15. Porosity vs permeability for various fracture spacings.

506 177

theoretical analysis. The hydrologically simple model makes this approach feasible. Future, more complex models may require numerical groundwater analysis to develop an appropriate analog.

The most difficult problem associated with the geology-hydrology model as used for a generic study is to construct an appropriate flowpath network. (The networks we used are shown in Figs. 3 to 5.)

The steps used in flowpath modeling are to:

1. Develop a schematic of the flow, identify the potential flow paths and directions anticipated.
2. Evaluate any constraints on the flow via any pathways such as limitations on mixing of flow along different flow paths.
3. Develop a network that best depicts the anticipated flow path.
4. Develop hydrologic parameters to describe the different paths.

Faults

Faults are fractures in the crust along which there has been displacement parallel to the fracture surface. By contrast, joints are fractures along which there has been no apparent displacement parallel to the rupture surface. Faults can vary in length from a few inches to hundreds of miles, with corresponding minor to major displacements. The magnitude and direction of movement and size of the fault zone depend on the size and orientation of the stress field and the mechanical properties of the rocks. Few faults have been mapped in three dimensions. The fault zone itself may range in width from a single, knife-edge crack to a zone of associated faults more than a mile wide. Within this zone, the fault may be cemented with calcite or quartz, or may contain clay gouge, sand or breccia. A zone of multiple associated faults may consist of several zones of gouge separated by relatively large unbroken blocks.

The fault is treated as a zone of increased vertical permeability due to fracturing of the rock adjacent to the fault. Currently, there are no reliable data available on time dependent changes in hydrologic properties along a fault zone caused by a single large event; however, limited data are available relating short-term hydrologic effects to seismic events (Walker,

506 178

1966) and the hydrologic effects to existing fault zones. Our estimates for the consequences of a seismic event are based on these data.

We assumed that a seismic event of Modified Mercalli (MM) intensity VIII or greater would cause movement along a new or recurring vertical fault that cuts through all the repository layers. New fault formation totally unrelated to existing fractures, would require a stress field sufficient to cause the rock to fail, i.e., greater than that needed to overcome frictional resistance on existing fracture surfaces. Once formed, faults tend to be reactivated even under stress conditions different than those causing the original rupture.

For our analyses, we assumed parameter values for a new fault and for recurrent faulting along existing faults. The probability of occurence of a new fault at the repository site is developed in the discussion on seismology. We assume that any examination of a prospective waste repository site would find, and thus help to avoid, major fault zones. The width of the hydraulically affected zone represents our estimate of a small-to-medium fault in plastic rocks (i.e., one with limited extent and minimal or no surface expression). Information on faulting and fault cataclastic zones at depth in great thicknesses of shale is very scarce in the literature.

Initial permeability is a function of fault type and history. After formation, the fault zone may retain some fracture permeability in addition to that of the parent rock. Recurrent fault zones start out with some fracture permeability. With each additional movement, the size of the cataclastic zone and any ancillary fractures will increase.

Our range of values includes the possibility of the fault remaining at maximum permeabilities. In salt, the permeability is initially that of the parent rock. Fracture permeability develops at the time of the faulting event and then decreases, due to salt flowage and recrystallization, until the affected zone is sealed.

In our analysis we considered only faults in shales and assumed that the permeability did not decrease with time after the fault movement.

Faults in salt are represented as fractures filled with broken material that become slightly more permeable due to the shearing of crystals before an event. In our model, the salt quickly flows plastically to close the opening, and recrystallization seals the entire feature. Some sealed fractures are found in potash mines of New Mexico and in salt domes. In some cases, however, fractures in salt do remain open.

Transition times represent the periods during which the stress buildup and release affect the permeability within the zone influenced by the fault. There are three periods of concern: (1) an initial period during which the stress is building, but has not yet induced fracturing or increased permeability; (2) an interim period during which stresses open fractures and feather joints, and increase permeability; and (3) a final period reflecting the long-term permanent change in the permeability. During the buildup of the associated stress field, microfractures and feather joints along the margins of the fault dilate, probably slowly at first then more rapidly just before movement. Fault movement releases the stress, and the dilated fractures return almost to their original state. Some cracks remain open and account for the permanent increase in permeability.

Because no applicable data are available for midcontinent sedimentary basins, we used estimated rates of change to reflect the periodicity of major movements. For example, the San Andreas Fault zone has had numerous earthquakes along its length. Earthquakes and associated movement have also occurred on associated fault zones (e.g., the 1952 Kern County and 1971 San Fernando earthquakes). Major movement in the San Andreas zone occured 1838, 1857, and 1906. These movements indicate a periodicity of about 50 y; minor movements occur almost constantly (Stevens, 1977). Though this fault zone represents a special case, it provides the best data available.

The values we used for shale and siltstone represent a fault with recurrent movement with periods about 10 times longer than those of the San Andreas. We thus simulated locations in regions that are tectonically less active.

506 180

The area of flow related to a fault is 2500 m times the width of the affected zone. We assumed that the fault zone cuts the repository parallel to its long axis. The length of the HLW area corresponds to that reported by Parsons et al. (1976).

For the MM VIII seismic event, we estimated a 90% probability of movement along an existing fault zone and only a 10% probability that it would cause an entirely new fault unrelated to any previous faulting. We assumed, basically, that the fault would result in an associated zone of high vertical permeability that could transmit water to the upper aquifer. The hydrologic effect of this phenomenon has many of the same uncertainties as the effect of borehole seal deterioration. The models are simplified solutions intended to represent upper and lower bound approximations.

Tables 15 and 16 list the recommended parameter values for recurrent faulting along existing faults and for new faults. Initial and residual permeabilities are given as percentages of the corresponding peak values. Except for initial permeabilities, preferred values and ranges are specified. The transition times are the periods over which the fault zone permeability increases from its initial value to the peak and then decreases to the residual value. Both a range and a preferred value are given for the times. Permeabilities are estimates based on considerations of the rock materials and on the pumping tests in fracture zones.

Solution Breccia Pipes

The existence of breccia pipes is of concern relative to the integrity of repositories in salt because the possibility of fluid flow and migration of the radioactive waste within the breccia pipe is potentially an important permeable conduit, and is present in salt basins like the Delaware basin in New Mexico (Vine, 1960). We made literature and field surveys of this feature and performed theoretical studies.

506 181

TABLE 15. Parameter values for recurren. faulting along existing fractures.

Layer	Width of hydraulically affected zone (m)	Initial (% of peak)	Permeability Peak (cm/sec)		Residual (% of peak)		Transition times (y)			
							Increase		Decrease	
			Range	Pref.	Pref.	Range	Range	Pref.	Range	Pref.
3 (barrier) siltstone	0.6-50	1	10^{-6} to 10^{-3}	10^{-4}	2	0-100	10-1000	50	1-100	10
4 (repository) shale	0.3-30	1	10^{-7} to 10^{-4}	10^{-5}	2	0-100	10-1000	50	1-100	20
4 (repository) salt	0.01-1	0	10^{-5} to 10^{-2}	10^{-3}	0	0-1000[a]	0.01-10	1	0.01-1	0.5
5 (barrier) siltstone	0.3-30	1	10^{-6} to 10^{-3}	10^{-4}	2	0-100	10-1000	50	1-100	20

[a]Solution opening of fault.

Note: Porosity range is 10^{-4}-10^{-1}; preferred value is 10^{-3}.

506 182

TABLE 16. Parameter values for new faults unrelated to previous fault movement.

Layer	Width of hydraulically affected zone (m)	Initial (% of peak)	Permeability Peak (cm/sec)		Residual (% of peak)		Transition times (y) Increase		Decrease	
			Range	Pref.	Pref.	Range	Range	Pref.	Range	Pref.
#3 400-600m Siltstone	0.3-7	0	10^{-6} to 10^{-3}	10^{-4}	1	0-100	100-10 000	1000	1-100	20
#4 600-800m Shale	0.15-3	0	10^{-7} to 10^{-4}	10^{-5}	1	0-100	100-10 000	1000	1-100	50
#4 600-800m Salt	0.03-1	0	10^{-5} to 10^{-2}	10^{-3}	0	0-1000[a]	0.01-10	1	0.01-1	0.5
#5 800-1000m Siltstone	0.15-3	0	10^{-6} to 10^{-3}	10^{-4}	1	0-100	100-10 000	1000	1-100	20

[a]Solution opening of fault.

Porosity range is 10^{-2} to 10^{-1}; preferred value is 10^{-3}.

506 183

A breccia pipe is formed when groundwater dissolves a portion of the rock and the overlying rock then collapses to form a rubble chimney. The following tabulation gives our assumed values for breccia pipe parameters. The probability of formation of breccia pipes is the same as for the associated faulting.

Parameter	Value
Dimensions:	
Base area (m^2)	10^5[a]
Height	From bottom of repository layer 4 to base of upper aquifer layer 2[b]
Permeability (cm/sec)	
Preferred	0.1
Range	0.001-1.0
Porosity	
Preferred	0.15
Range	0.05-0.20

From our present understanding of how collapse breccia originate, their rate of formation, and frequency of occurrence appear to be directly proportional to the rate of formation of dissolution cavities in salt. Thus, a better understanding of the factors controlling the rate of formation of dissolution cavities would improve our ability to estimate the rate of formation, and possibly the geological distribution, of collapse breccia. It has been noted that collapse breccias are associated with dissolution in some cases at the top of a salt unit and in others at the bottom. Some recent work on salt dissolution suggests that the rate of dissolution may be substantially different for th two (Snow and Nielsen, 1970; Snow and Chang, 1975).

Dissolution cavities and associated collapse breccia are formed by certain geologic and hydrologic processes. One factor that seems to have a strong effect on the location of dissolution cavities is the presence o. permeable rock adjacent to the bedded salt. Furthermore, the occurrence of areas of substantial surface subsidence seems to be highly correlated with the

---

[a] Vine (1960) reports an average diameter of approximately 1500 ft (457 m).

[b] This gives a pathway 300 m long from the center of layer 4.

existence of major underlying aquifers or features of relatively high permeability. An excellent example is the large area of surface subsidence known as the San Simon Swale, which overlies the Capitan Reef limestone, a coral reef of high permeability. Another example is the association of the dissolution breccia blanket at the top of the Salado formation (the major salt stratum of the Delaware basin) where it is in contact with the Rustler formation, which contains sedimentary rock zones of high permeability.

Additional data on this association should be sought relative to: (1) the distribution of the channel sands of the Bell Canyon formation; (2) the thinning, fracturing, or absence of the overlying, thin, tight shale units (the Trap and Lamar) of the Bell Canyon formation; and (3) the distribution of the breccia pipes in the Delaware basin. These data would strengthen our understanding of the mechanics and distribution of the dissolution process.

The work by Anderson (1977), which documents the existence of dissolution activity at depths of approximately 3000 ft (914 m), represents a substantial departure from earlier concepts that the dissolution phenomena are limited to depths of a few hundred or possibly a thousand feet.

Salt dissolution processes have been studied extensively, primarily by the solution mining industry (Durie and Jessen, 1964a and 1964b; Snow and Nielsen, 1970; Snow and Chang, 1975). This research includes laboratory studies, computer simulations, and limited field experimentation. The parameters controlling the dissolution process can be categorized as follows:

- Conditions of the solid
  - Solubility
  - Impurity content
  - Surface roughness
- Conditions of the fluid
  - Diffusivity
  - Flow behavior
  - Salinity of influent water

506 185

- Physical setting
  - Orientation of the salt face
  - Temperature
  - Pressure.

Rock salt (halite) is the most soluble of common rock types. At $20^{o}C$, the solubility of salt is 264 g/litre or 264 000 ppm (Borchert and Muir, 1964). This is approximately a dissolving capacity of 0.022 ft^3 of salt per gallon of fresh water. The solubility of salt increases significantly with temperature, e.g., at $300^{o}C$ the solubility is 373 g/litre. Changes in pressure do not significantly change the solubility, e.g., at 4000 bars and $30^{o}C$, the solubility increases only to 267 g/litre.

Dissolution occurs at the salt face, with diffusion of salt molecules away from the face allowing dissolution to continue. This effect causes an increase in the density of the brine concentrated near the salt face. The high-density brine tends to flow downward creating a natural convection boundary layer flowing along the salt surface. As stated by Snow and Nielsen (1970, p 342):

> Free or natural convection is the most important phenomenon in the cavity. It is caused by the increased density of concentrated brine near the salt face compared with the density of brine in the bulk of the cavity. The downward flow of dense brine, and simultaneous molecular diffusion, govern the concentration profile adjacent to the salt face and determine the rate of solution. Flow, in turn, is limited by drag of the fluid against the salt face and drag against the bulk fluid. Thus a balance of forces determines the velocity profile against the salt face. If the flow increases to the point where it becomes turbulent, this causes additional mixing which in turn affects the concentration profile and the solution rate (usually increasing it).

Over long periods of time, the bulk fluid in the cavity will approach saturation, and the quantity and rate of water inflow and its salinity will determine the volume and rate of salt removal. Because the least dense, least saline water will occur at the top of the fluid column, the dissolution

506 186

process will be most active in the upper portion of the cavity. A number of important implications about the salt dissolution process under natural conditions can be drawn from the cited research:

- The water in deep, saline-water-bearing units is usually not fully saturated with salt and, therefore, has significant salt-dissolution potential. In most parts of the Delaware basin the salinity of the water of the uppermost Delaware Mountain sandstones (underlying the salt-bearing evaporite formation) ranges from 50 000 ppm to 250 000 ppm total dissolved solids (McNeal, 1965) compared to a salinity at full saturation of about 264 000 ppm.
- Dissolution at the top of a salt unit tends to form shallow, wide flaring cavities because dissolution will be concentrated at the uppermost lateral edges. This may be why blanket, horizontal solution collapse breccias are most commonly found at the top of a salt unit.
- Dissolution at the base of a salt unit tends to form large discrete cavities with dissolution readily propagating upward as well as outward. This occurs because dissolution is most active at the roof and upper walls. This type of cavity development is conducive to the formation of collapse chimneys.

The rate of breccia pipe formation was calculated in terms of two components:

1. Critical dissolution rate--the fraction of total salt dissolution that contributes to the formation of large volume cavities resulting in collapse.
2. Critical cavity size--the minimum volume of salt dissolution in the immediate vicinity below the repository necessary to cause collapse of the overlying strata and consequent connection of the repository to the aquifer (layer 2).

Using the solubility given previously, we obtained critical dissolution rates by (1) calculating the potential dissolving capacity of deep, saline groundwater; and (2) using flow paths in or adjacent to the salt to compute the rate of salt dissolution and cavity formation.

As mentioned above, the salinity of the water of the uppermost Delaware Mountain sandstone (underlying the salt-bearing evaporite formations) ranges

506 187

from 50 000 ppm to 250 000 ppm over most of the basin. Based on this range the average salinity for our calculations is assumed to be 50% of total saturation at 25°C, or 136 000 ppm. (The value of 25°C was chosen as a reasonable approximation of the temperature at the depth of the salt layer.) This gives dissolving capacity of 0.0117 ft^3 of salt per gallon of Delaware Mountain formation water.

Using this figure, we considered three different scenarios:

1. Salt dissolution associated with flow through an open fault in the salt unit (Case I).
2. Salt dissolution associated with flow along an existing fault (with low residual permeability) in the barrier layer adjacent to the salt (Case II).
3. Salt dissolution associated with flow along a channel sandstone located between the base of the salt and the top of the lower barrier layer (Case III).

Because there are no data on the mechanisms of flow from a underlying permeable unit up into a developing cavity (Case II), we made several different sets of calculations. The question is: What is the quantity of flow through the developing cavity? In other words, to what depth in the underlying permeable unit is the water diverted upward through the developing cavity? For Case II, several different depths have been assumed. Salt dissolution rates and critical cavity formation times are presented in Table 17. To evaluate cavity size, we used data on cavity sizes and length of resultant collapse chimneys from eleven underground nuclear detonations. Boardman, Rabb, and McArthur (1963) found the cavity size to be a function of nuclear device yield, confining pressure, and the amount of gas-producing materials that condense at low temperatures in the immediate shot environment. They found the chimney height to be related to cavity size, nature and orientation of structural weaknesses, and the strength of the unfractured rock.

In all cases of chimney formation, collapse occurred within hours after the nuclear device was detonated.

506 188

TABLE 17. Critical cavity formation rate.

Case description			Salt dissolution rate (ft^3/y)	Time required to form critical cavity[a] (y)
I	Open fault passing through layer 4 (salt)		9.4×10^4	3.2×10^2
II	Existing fault in barrier adjacent to layer 4 (salt); fault assumed to have low residual permeability			
	Depth of discharge into cavity:			
	A	200 m	2.0×10^1	1.5×10^6
	B	100 m	1.0×10^1	3.0×10^6
	C	10 m	1.0	3.0×10^7
	D	1.0 m	0.1	3.0×10^8
Preferred		50 m	5.0	6.0×10^6

[a]For repository layer thickness of 200 m.

From the underground detonation data, we calculated the ratio of the diameter (original cavity) to the height (resultant chimney) and the overall porosity of the resultant collapse breccia. The average diameter-to-height ratio is 0.356; the average overall porosity of the resultant collapse breccia is 0.204. Our values of critical cavity size for different repository layer thicknesses (all other layers assumed as 200 m) are:

Thickness of repository layer (m)	Critical cavity size (m^3)
200	8×10^5
1000	2×10^7
20	1×10^5

506 189

Also, on the basis of the underground detonation data, we assumed the following porosity values for collapse breccia:

Preferred - 0.20
Range - 0.10 to 0.35.

Case I, an open fault passing through the salt unit, represents an extreme dissolution rate, 9.4×10^4 ft^3 (2700 m^3) NaCl/y. However, it is most likely a less probable event than cases II or III. We assumed, as a preferred value, that this fault would remain open for only 1.5 y, at which time 1.4×10^5 ft^3 (4000 m^3) of salt will have been removed. For the high end of the time range, we assumed this fault would remain open for 11 y, at which time 10^6 ft^3 (2.8×10^4 m^3) of salt will have been removed.

All cavities of comparable volumes (10^6 ft^3) in the underground nuclear detonations collapsed, forming chimneys with an average height less than 100 m (above the shot point). A breccia pipe of this height would breach the repository and radionuclides could leave the repository through lower flow paths. Later analyses should consider similar scenarios e.g., a smaller cavity and resultant breccia pipe sufficiently large to breach the repository to lower aquifers, and so on.

Case II, dissolution due to flow along an existing fault with residual permeability adjacent to the salt unit, is a realistic possibility. The preferred value of time to form a critical cavity is 6.0×10^6 y.

We originally considered the possibility of a breccia pipe being resealed by subsequent groundwater precipitation of a tight cementing matrix because the literature described this phenomenon and because tightly cemented breccias were observed in the Delaware and Michigan basins. A preliminary review of the chemistry of salt solution vs precipitation (Adams 1931; Helgeson, 1964; Stanton, 1966; Borchert, 1968; Braitsch, 1971) has shown that changes in temperature or pressure with depth are probably not sufficiently large, over the distance being considered, to cause significant precipitation of salt from upward moving solutions.

506 190

One possibility deserving further consideration is that the repository itself might cause a significant temperature rise of salt-bearing solutions. This would allow more salt to go into solution at the repository level, and the temperataure drop moving away from the repository would cause some salt precipitation. However, another consideration is that the water would have other elements in solution, which would strongly affect the precipitation behavior of the various constituents, including the salt.

Both cemented and uncemented collapse breccias occur in the Mackinac Straits region of Michigan (Landes, 1945). The cemented breccias are all composed predominantly of limestone fragments. The cement is calcium carbonate. Uncemented breccias are more common, and fragments usually consist of limestone, dolomite, shale, and chert. The uncemented breccias are approximately 4×10^8 y old.

MANMADE FEATURES

Man's exploration and construction activities at the repository would result in additional permeable pathways, e.g., fractures around shafts, tunnels and boreholes, and faulty or deteriorated seals in shafts, boreholes, and other openings. The data requirements are similar to those for modeling natural features, and the process for specifying flow pathways is the same as that explained earlier.

FRACTURE ZONES

The construction of an underground repository would result in some degree of disturbance to the rock mass, which could change the repository's ability to prevent hydrologic transport of radionuclides to the biosphere. Rock-mass disturbance would be a function of:

- Damage caused by the excavation process
- Magnitude of the in situ stress field
- Strength and deformability characteristics of the rock
- Geometrical layout of the repository

506 191

- Damage resulting thermally from induced loadings
- Performance of support or reinforcement structures during repository operation and backfill after sealing

For each model parameter we assumed a preferred value and a range of values in shale and bedded salt. We employed simple calculations based on elasticity theory and experience with rock mechanics. We compensated for the elastic assumption in the range beyond failure by taking a strength/stress ratio of 3 to indicate the extent of the zone of disturbance, which allows for the stress redistribution processes that occur on local failure. The effects of time-dependent deformation (particularly for rock salt at higher temperatures) has been handled in an entirely empirical manner for the purpose of this study. The nature of the disturbance zone depends on the type of failure that develops: brittle fracture with crack formation, or ductile flow that maintains the integrity of the material.

As previously described, our repository layout consists of a vertical shaft and horizontal tunnels located some 500 m below ground level (Parsons et al., 1976). For analysis purposes, we assumed that the opening of the shaft is circular in shape, and that the horizontal repository chambers are far enough apart for the stress concentration fields not to interact to any significant extent.

Excavation Disturbance

We assumed the depth of excavation disturbance would range up to 1 m. This covers a range of excavation methods from machine tunnel boring to drill and blast methods. The effective radius of the excavation that must be considered for assessing the depth of disturbance from high stress levels ranges from r to (r + 1), where r is the actual excavated radius.

On the basis of in situ virgin stress data from tectonically quiet and topographically simple locations, we consider the following ranges of stress values appropriate to the particular depth of repository analyzed.

506 192

Repository tunnels and shaft in vicinity of repository

	Vertical stress (psi)	Horizontal stress (psi)
Lower limit	1300	1300
Preferred	2180	3260
Upper limit	2190	6380

Upper shaft at approximate depth of 100 m

	Vertical stress (psi)	Horizontal stress (psi)
Lower limit	174	522
Preferred	435	1305
Upper limit	1595	4780

For predicting failure zones, we assumed a pore water pressure of zero (dry) for the operational phase of the repository, and a pressure equal to the hydrostatic head after abandonment.

Rock Mass Strength

We assumed the generic shale to be essentially intact and horizontally bedded, demonstrating pronounced strength anisotropies. The strength for failure by shearing across the bedding is given by

$$\sigma_{Df} = \sigma_c \left(1 + \frac{\sigma_{3'}}{\sigma_c}\right)^{1/2} ,$$

where

σ_{Df} = maximum principal failure stress difference
σ_c = unconfined compressive strength
$\sigma_{3'}$ = effective minor principal stress.

The shear strength for failure along the bedding is given by

$$\sigma_f = 0.1\sigma_c + \sigma_{n'} \tan \phi \quad (\phi = 25^o) ,$$

506 193

where

σ_f = shear failure stress

$\sigma_{n'}$ = effective normal failure stress.

These relationships indicate that the minimum unconfined compressive strength for critical orientation of the bedding plane of weakness would be approximately one-third of σ_c (the unconfined compressive strength for loading normal to the bedding). Our assumed values for σ_c are as follows:

	Unconfined compressive strength, σ_c (psi)
Lower limit	3 625
Preferred	7 250
Upper limit	10 875

We assumed that during the initial construction phase, the bedded salt would fail in a brittle manner, and that the strength characteristics are homogeneous and essentially nonfrictional as expressed by

$$\sigma_{Df} = \sigma_c$$

Our assumed strength values are as follows:

	σ_{Df} (psi)
Lower limit	1900
Preferred	4350
Upper limit	5800.

506 194

Stress-Field Disturbance

We determined the depth of disturbance due to high *in situ* stress by comparing the stress concentration fields with strength data as previously described. The zone of rock lying within the strength/stress ratio of 3 was considered to be the region of disturbed material, and this area is indicated by an equivalent radius of disturbance. We determined the lower limit of disturbance by examining the effect of the lower *in situ* stress field on the upper strength value. The upper limit of disturbance was similarly calculated by combining the upper *in situ* stress field with the lower strength level.

Temperature-Induced Stresses

We examined the effect of thermally induced stresses around the shale repository by assuming a long-term temperature distribution of 190°C at the repository. The assumption is simplified, and we emphasize that our consideration of thermal stresses is tentative at this stage.

We added the thermal stress distribution to the stress field resulting from *in situ* loading and again examined the extent of overstress. The results indicated that the thermal loadings increase the effective radius of disturbance by approximately 15%. This factor has been applied to the radius of the disturbance zones calculated for shale.

At the temperatures in question, thermal loadings would tend to develop within salt, but the physical properties of the salt might change so as to preclude additional disturbance. The high temperatures might induce partial healing of the disturbance zone created during excavation and operation when temperatures in the vicinity of the repository are comparatively low.

We assumed that structural support during operation would be adequate to prevent progressive deterioration of the roof and upper sidewalls of the repository.

Our procedure allowed us to determine a range of disturbance zones for the salt and shale repositories and associated shafts. The disturbance within

506 195

these zones, as characterized by our permeability and porosity values, ranges from maximum disturbance in the vicinity of the excavation to original undisturbed in situ conditions at the extremity of the zone.

Postsealing Disturbance

After the shale repository is sealed, the structural support used during operation would probably eventually deteriorate and the backfill would have to provide the required support. The optimum backfill would consist of stiff material placed under pressure, such as postplacement high pressure grout, which would provide support without further disturbing the rock. Alternatively, the repository could be backfilled with a soft material. This would lead to local roof collapse and bulking of the failed material until there is sufficient backfill support to stabilize the rock mass around the opening. We estimated and expressed the volume of moderately disturbed and bulked material (typically with 10% porosity) as an equivalent radius of intensely fractured zone. Since gravitational failure around shafts appears not to be a significant problem, we assumed there would be no intensely fractured zones within the vertical shaft.

The high temperatures developed after backfilling of a bedded salt repository might permit additional natural closure without fracturing. They might also induce the healing of fractures in the vicinity of the repository prior to backfilling.

Tunnel and Shaft Permeability

There is insufficient data on which to base permeability evaluations of rock that has been fractured due to stress relief, or in which stress relief has occurred. Some experimental work has been performed (Huitt, 1956; Snow, 1968; Louis, 1969; Sharp, 1970; Maini, 1971) and it is clear that stress, degree of fracturing, fracture width, and permeability are all related. However, the details of this relationship are still poorly understood.

506 196

The theoretical relation between crack spacing, crack width, and permeability for a parallel plate model is

$$k = \frac{ge^3}{12v\,b},$$

where

k = permeability coefficient
g = gravitational acceleration (981 cm/sec^2)
e = width of cracks or fissures
b = spacing between cracks
v = coefficient of kinematic viscosity
(0.0101 cm^2/sec for pure water at 20° C).

Permeability varies linearly with joint intensity and as the cube of joint opening or width. As stress is relieved near a shaft or tunnel, the joint opening will widen, new jointing will probably occur, and permeability will increase.

Field evaluations of permeability changes near tunnels and shafts due to stress relief are lacking. One of the few studies involving permeability measurement after a stress change was undertaken by Boardman and Skrove (1966) in connection with permeabilities related to fracturing induced by underground nuclear test shots. The study found that permeabilities in a granitic mass increased from a base value of 2×10^{-5} cm/sec to 7×10^{-4} cm/sec. The tests were conducted at substantial depths and under a high degree of confinement and *in situ* stress.

Around a tunnel there would be stress relief in the floor and ribs and either some compressing or arching in the roof. Permeability changes in the roof would be one order of magnitude greater than in the floor and ribs. In shale, near the tunnel face, a narrow but intensely fractured zone might exist with an estimated permeability of 10^{-1} cm/sec, approximately that of gravel. Beyond from the face the permeability would be like the theoretical and test values presented above. The preferred permeability of this general fracture zone is estimated to be 10^{-4} cm/sec with a range of 10^{-3} to 10^{-6} cm/sec. The conditions around a shaft are somewhat better. Gravitational failure

506 197

apparently is not a significant problem, and an intensely fractured zone would probably not develop.

Backfill Behavior

To be considered suitable, a fill should meet the following criteria:

- A design life preferably equal to that of the repository. The minimum design life would be about 500 y, which appears to be the most critical containment period.
- Sufficient strength to prevent closure of the openings. The ideal situation of the fill preventing all closure is possible only if it has the same modulus as the rock. Thus, some closure would probably occur as the fill consolidates.
- A low permeability to prevent circulation of groundwater.

Initial permeability and deterioration of the backfill are a function of host rock type, groundwater flow, backfill type, placement methods, and time. It is impossible to project backfill behavior without some knowledge of the backfill type and placement method. Our parameters and transition times are based on engineering judgment. Our preliminary backfill concept for the salt repository is to use salt, but we have not yet evaluated a suitable backfill material for shale. Thanks to mechanical creep combined with precipitation and recrystallization, a properly placed salt backfill may result in minimal deterioration. We examined two basic cases: (1) an effectively impervious backfill with some time-related deterioration uncertainty and (2) a backfill that is relatively pervious initially and remains so.

Borehole Seal Failure

It is impossible to project the dissolution characteristics of borehole seals without some knowledge of the sealing method. Research to develop sealing techniques is continuing, but no one method has yet been chosen. There is some probability that any given borehole seal would be improperly installed and fail immediately. Experience indicates a relatively poor performance record for borehole seals. There is also a probable transition time during which the borehole seals would deteriorate, depending on sealing procedure and

506 198

quality of work. The long-term effectiveness of a seal may be difficult to demonstrate either by analysis or by monitoring. The problem may be further complicated by the possibility of a fracture zone developing around the borehole or the existence of instrumentation in the hole.

Parameter Values

Table 18 and 19 give our assumed values for the width, permeability, and porosity of zones around vertical shafts and horizontal tunnels. The maximum fracture zone values apply to a repository in low strength rock with a high *in situ* stress field and a poorly placed or nonrigid backfill. The minimum values apply to a repository in high strength rock with a low stress field and an ideal rigid backfill placed under pressure. Since the permeability within the fracture zones is expected to decrease exponentially with distance from the tunnel or shaft face, the effective conductivity of the fracture zone is computed by multiplying the peak permeability at the face by a reduced area for the fracture zone. We assumed a reduction factor of 0.20.

We assumed an intensely fractured zone would be formed from mining activities in shale tunnels, but not in salt. All excavations would be surrounded by a general fracture zone. We estimated a larger fracture zone around the lower part of the shaft where it penetrates the shale in the repository layer.

The values in Tables 18 and 19 are the maximum we believe would be reached in less than 50 to 100 y. The time dependent factors in salt are such that fractures might heal to reduce permeability to 1% of its original value.

Our preferred value of healing time is 50 y, and our range is 20 to 200 y. We do not expect the permeability of fractured shale to change significantly with time.

We approximated tunnel and shaft dimensions (see Table 20) from the design by Parsons et al. (1976). The tunnels have two segments: a longer-length and larger-area storage space more distant from the shaft; and a shorter, smaller-area tunnel that connects the storage space to the shaft. The shaft also consists of two segments: a lower section with a larger cross-sectional

506 199

TABLE 18. Assumed widths for fracture zones.

Description	Zone width (m)[a]			
	Shale (layers 3 and 4)		Salt (layer 4)	
	Preferred	Range	Preferred	Range
Intensely fractured zone in tunnels	1.05R	0 to 1.12R	None	
General fracture zone				
Shaft, lower zone	1.25(R+1/2)	R to 3.3(R+1)	2.7(R+1/2)	1.15R to 3.5(R+1)
Shaft, upper zone	1.1(R+1/2)	R to 3.3(R+1)	--	--
Tunnels	2(R+1/2)	1.45R to 4(R+1)	2.7(R+1/2)	1.15R to 3.5(R+1)

[a] R is radius (or one-half the width) of shaft or tunnel.

TABLE 19. Assumed values for permeability and porosity of fracture zones.

Description	Permeability (cm/sec)		Porosity	
	Preferred	Range	Preferred	Range
Intensely fractured zone	0.1	0.01 to 1.0	0.1	0.01 to 0.2
General fracture zone	10^{-4}	10^{-6} to 10^{-3}	10^{-3}	10^{-4} to 10^{-2}

506 200

area and length equal to half the thickness of the repository bed (layer 4); and a longer, smaller-diameter section extending through the barrier bed (layer 3) to the bottom of the aquifer, and whose length therefore equals the thickness of layer 3.

TABLE 20. Assumed tunnel and shaft dimensions, fracture zones.

Description	Length (m)		Effective cross-section Area (m^2)	
	Preferred	Range	Preferred	Range
Tunnel, storage area:				
Highly fractured shale	1200	---	316	0-785
Generally fractured shale	1200	---	1900	580-7950
Generally fractured salt	1200	---	3300	290-6400
Tunnel, connection to shaft	440	200-6000	[a]	[a]
Shaft:				
In shale repository layer	[b]	---	10	0-100
In salt repository layer	[b]	---	60	4-110
Above shale repository layer	[c]	---	5	0-100

[a] Storage tunnel values times 0.06.

[b] One-half thickness of layer 4.

[c] Thickness of layer 3.

Tables 21 and 22 give our assumed values relative to backfill deterioration and geometry. In Case I, we assumed a backfill with the same hydrologic characteristics as the surrounding rock, but whose permeability would increase with time. In Case II, the backfill is relatively pervious initially and remains so.

In the case of boreholes made for repository investigations, there is some probability that they would fail and provide a flow pathway. Technological improvements would lower the probability. Our estimates are based on engineering judgment only.

506 201

506 201

TABLE 21. Assumed values for backfill conditions.

Type	Probability of deterioration[a]		Final permeability (cm/sec)		Final porosity	
	Preferred	Range	Preferred	Range	Preferred	Range
Case I						
Layer 3, shale	0.5	0.2-0.8	10^{-4}	10^{-5} to 10^{-3}	10^{-2}	10^{-4} to 10^{-1}
Layer 4, shale	0.4	.2-0.5	10^{-4}	10^{-5} to 10^{-3}	10^{-2}	10^{-4} to 10^{-1}
Layer 4, salt	0.1	0.05-0.6	10^{-4}	10^{-5} to 10^{-3}	10^{-2}	10^{-4} to 10^{-1}
Case II (all layers)	0	---	10^{-3}	10^{-6} to 10^{-1}	10^{-1}	10^{-3} to 2×10^{-1}

[a]Transition (deterioration) times assumed for Case I are: preferred value of 500 y and range of 50 to 5000 y.

506 202

TABLE 22. Assumed backfill dimensions.

Description	Length (m)		Cross-section area (m^2)
	Preferred	Range	
Tunnel, storage area	1200	---	3100
Tunnel, connection to shaft	440	200-6000	150
Shaft, lower zone	a	---	64
Shaft, upper zone	b	---	64

[a]One-half thickness of layer 4.

[b]Thickness of layer 3.

We assumed 50 borehholes at the site and a range of 5 to 100. Of the total number, 20% (1 to 20 holes) were assumed to penetrate through the lower aquifer (layer 6), and 80% (4 to 80 holes) to penetrate the thickness of the repository bed (layer 4). We assumed, also, that initially the borehole seal has hydrologic characteristics like those of the surrounding rock, but that it would deteriorate linearly with time. Assumed values for borehole seal parameters are as follows:

	Preferred	Range
Area of each hole	0.02 m^2	--
Final permeability	10^{-4} cm/sec	10^{-6} to 10^{-2} cm/sec
Final porosity	10^{-2}	10^{-4} to 10^{-1}

Deterioration Time	Probability
Immediate	0.1
0-500 y	0.2
500-1000 y	0.2
Never	0.5

Seismology

Seismic activity could breach the seal around a repository and allow water to enter and leave. Small earthquakes could induce microfractures and extention of other fractures; large earthquakes could cause local faulting and opening of direct flow pathways. Consideration of far future requires a careful and

506 203

detailed seismic analysis. Our initial effort is directed toward developing meaningful estimates of the actual danger imposed by earthquakes to properly designed underground facilities located in different regions of the country. These estimates are needed for eventual input into a more comprehensive system model.

For input into the system model it is necessary to quantify the parameters defining the seismic hazard as probability distributions. However, it is difficult to define the required distributions for the reasons discussed briefly below. Our approach was to eliminate all but the most important parameters that fix the seismic hazard at different sites. To do this, we (1) determined the probability of excessive ground motion for different regions of the country, (2) developed useful criteria to translate typical ground motion parameters into damage, and (3) determined what the important parameters are.

Seismic Analysis

Three specific locations (which might well be potential sites) were chosen as scenarios. One site is in southeastern New Mexico and two are in Nevada. The Nevada sites are located at the Nevada Test Site and the other is near Tonopah. The Tonapah Site is more near a zone that has had major earthquakes. These seismicities will help determine if some parameters are more important in higher seismic areas than in low seismic areas. It will also show how sensitive the results might be to a local zone of high seismicity.

In our studies, we used the seismic analysis program developed by McGuire (1976). The program requires as input (1) a description of local and regional seismicity; and (2) a relation between the intensity parameter of interest, epicentral distance, and earthquake magnitude. For the initial studies, we modeled the tectonics using the results of Algermissen and Perkins (1969), who put much effort into developing a good tectonic model. Further detailed studies should not significantly alter these models.

We used different relationships between earthquake magnitude and resulting ground motion to assess the effect of different parameters on the risk of damage at the sites.

We used seismic modeling to: (1) specify the limits of the earthquake zones that could affect a given site, (2) define statistically the seismicity in each earthquake zone, and (3) specify the largest earthquake that can occur in each zone. Each of these tasks is difficult: it is much less difficult to define the major earthquake zones in highly seismic areas than in areas of low seismicity. For example, several massive earthquakes have occurred near New Madrid at the head of the Mississippi Embayment, but it is unknown what faults were involved (Ekren et al., 1974). The same is true for the other major earthquake areas of the east (Schneider and Platt, 1974). Thus, defining the seismic zones that could affect a given site is complex and controversial.

Given the earthquake zones, the statistics are somewhat less controversial. It is generally assumed that the relation between the number of earthquakes N within a given magnitude range M (usually taken as $M_0 \pm 0.5$) is given by

$$\log N = a + bM \quad . \tag{4-1}$$

Two basic assumptions must be made. First, that the past is a guide to the future, and second is that we know how earthquakes are distributed in time. For the latter, a Poisson distribution is usually assumed and in most cases, except active zones, it is adequate. Normally, one is interested only in projecting, at the most, 100 y into the future. For such a short time and with properly defined tectonic zones, using Eq. (4-1) to predict the future would introduce only "small" errors. This is valid because the rate of change of seismicity is a historically slow process. It is more difficult to predict the future from observation of the brief past. Geology may not be an adequate guide to earthquake activity; for instance, it is difficulty to correlate the major earthquakes in the east with observable faulting.

The final assessent required in seismic modeling is the upper limit earthquake that can occur in any given earthquake zone. McGuire (In Press) examined this question from a statistical point of view, and concluded that the data do not support upper limit cutoffs. The size of the maximum earthquake must be determined by geophysical means. This currently, is difficult to determine. Safety analyses for power reactors have assumed that the largest earthquake during the life of a reactor would be no greater than the largest one in

506 205

recorded history. Unlike a repository, however, the life of a reactor is assumed to be only 40 y.

From an earthquake's magnitude or location relative to a given site, we can estimate the ground motion parameters at the site. But magnitude is a poor measure of the strong ground motion possible from a given earthquake. Schneider and Platt (1974) studies show that earthquake magnitude is given by:

$$M = 3/2 \log L + \log \Delta\sigma + C_3 \quad , \tag{4-2}$$

where

L = fault length
$\Delta\sigma$ = stress drop
C_3 = empirical constant (e.g., for Southern California, $C_3 = 3.6$)

and the resultant spectra of the ground motion is of the form

$$FS(r,w) = f\left(\frac{1}{r}, w, L, \Delta\sigma\right) \quad , \tag{4-3}$$

where

r = epicentral distance
w = frequency.

Although the magnitude of an earthquake does not suffice to define its potential ground motion, currently all analyses are based solely on magnitude, epicentral distance, and site condidtions. It should be noted that the correlation between ground motion and intensity is poor.

In a risk assessment program these difficulties can partially be eliminated by including distribution functions and the standard deviations. The real problem arises near the earthquake epicenter because limited near-field data are available. We do not know how to make reasonable estimates of the peak ground motion parameters. This problem is discussed in some detail by Trifunac (1976), and is important because minor earthquakes can have larger peak ground motions in the near field. Because of its form, Eq. (4-1) could represent a larger number of minor events, some of which would be a significant distance to a given site.

506 206

We used typical correlations between magnitude and ground motion in our analysis. The results show that such correlations are not adequate and that it is important to consider the near field.

Ground motion is attenuated significantly more in some regions of the country than in others. In the west, the ground motion is attenuated most strongly. The attenuation of intensity can be obtained from historic data. However, we have ground motion data only for the far west and do not know how to correct these data for the lower attenuation typical in the east. We used both intermediate and western attenuation of intensity in our analysis, and did not correct the correlations between magnitude, epicentral distance, and ground motion for differences in attenuation.

A review of the damage caused by a number of earthquakes to underground tunnels, pipelines, and wells indicates that the damage is confined mainly to the epicentral region. Most of the damage is located in regions where active surface faulting occurred or where there was ground failure resulting from liquifaction or slides. There is not much evidence of damage to such facilities outside the zone of rupture and very strong shaking. It should be noted that at least one minor earthquake, which occurred in an oilfield, caused considerable damage along the fault plane even though the level of shaking was relatively low.

Depending on the level or type of ground motion, different ground motion parameters can be useful in obtaining a measure of damage. For example, along the actual fault, the ground displacement could be of a slow, creeping nature, giving rise to low peak accelerations or velocities, yet doing considerable damage. In fact, in all cases it is the relative displacement that is of interest, because it sets up the strains/stresses that cause failure. In general, one cannot easily predict relative displacement. For this reason, either acceleration or velocity are used to correlate with damage. If we integrate the one-dimensional wave equation once with respect to time, we find (in the absence of reflected waves) the peak velocity is proportional to the peak stress. When reflected waves occur, the relation holds only for a steep wave front.

506 207

The only published correlation between ground motion (in this case peak acceleration) and damage to underground facilities is in Katayama et al. (1977). Damage data are given for manholes and water, gas, and sewer pipelines based on three major earthquakes (Fig. 16). It is clear that damage occurs only in the strong ground motion region. However, the results cited may be somewhat misleading because these earthquakes caused intense ground motion. The results do show that outside the zone of faulting, it takes strong ground motion to cause pipes to fail.

There is much unpublished data on ground motion and the damage to tunnels and large boreholes caused by ground motion from underground nuclear explosions at the Nevada test site. For the reasons discussed above, peak velocity was used to correlate with damage. These correlations should be conservative because the wave front of underground nuclear explosion ground motion is typically steeper than for earthquakes, and has smaller radius of curvature, hence greater relative displacement. In addition, the peak stress and velocity are associated with the first arrival rather than later arrivals as in many earthquakes.

The Nevada test site data are in general agreement with other observations that ground motion is required to damage underground facilities. In the case of an HLW repository, damage is taken as rock falls in tunnels, sloughing of large uncased boreholes, and cased boreholes going out of round. Minor rock falls in the fractured zones of tunnels and sloughing of large-diameter boreholes in desert alluvium set the threshold of damage at a peak velocity of 2 ft/sec (0.6 m/sec). Most facilities can withstand more ground motion if some added protection is provided. At this stage the 2 ft/sec criterion seems adequate because, as for earthquakes, typical correlations (Schneider and Platt, 1974) suggest that (peak velocity)/ (peak acceleration) = 2 ft/sec/g (0.6 m/sec/g) for hard rock and 3 ft/sec/g (0.9 m/sec/g) for soils.

Figure 17 gives the range of the average dislocation at the fault plane as a function of Richter magnitude. In general, these values are calculated; when comparison between calculated and direct field measurements is possible, the comparison is fairly good. These data indicate that minor earthquakes can cause damage to underground facilities.

506 208

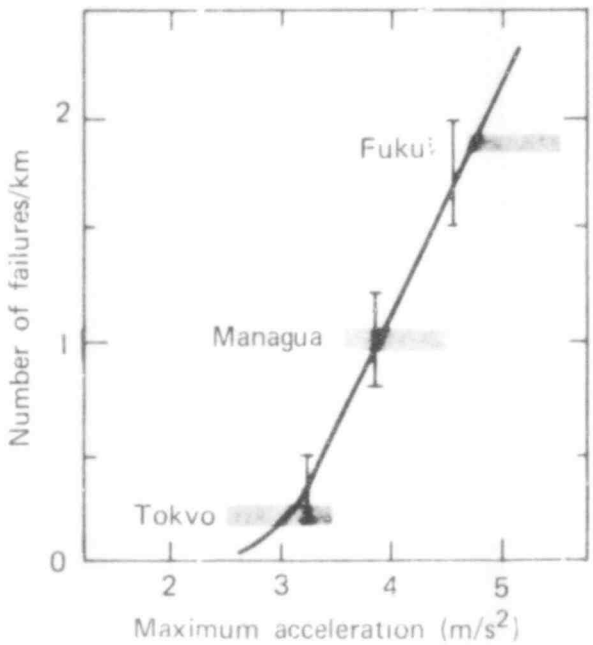

FIG. 16. Failure of pipes vs ground shaking intensity, based on data from several major earthquakes (after Katayama et al., 1977).

As discussed above, three sites were examined to identify the critical parameters. Different parameters were changed, and several attenuation laws were used at the New Mexico site. It was determined that the seismicity of the region in which the site is located is the most important factor. Available data on failure of underground facilities strongly suggest that damage is confined to the region where the faulting occurred. For the distant and more active regions, significant ground motion at a site requires that major (thus low probability) earthquakes occur.

506 209

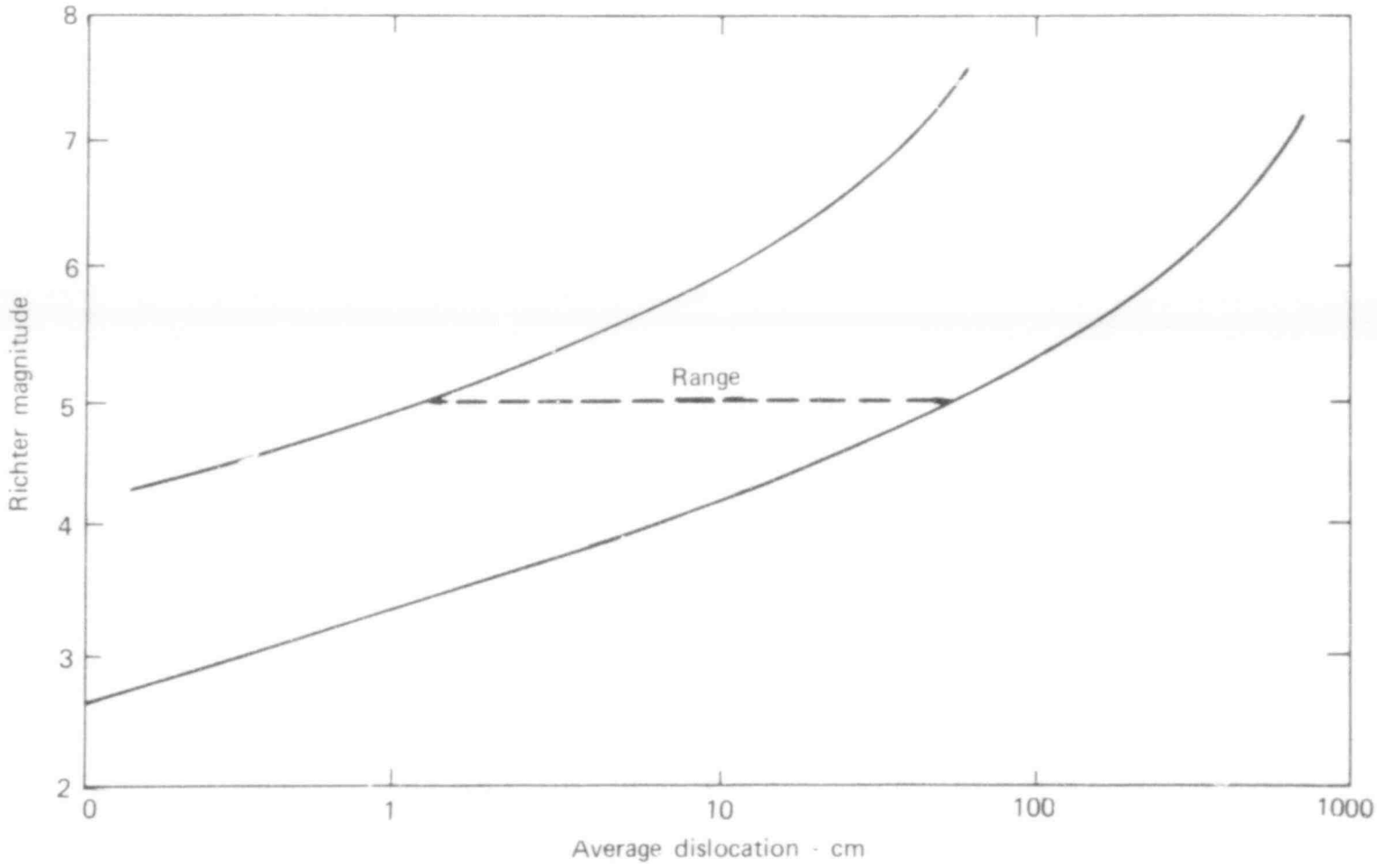

FIG. 17. Range of calculated dislocations for a number of California earthquakes (after Trifunac, 1976).

506 210

One interesting result is that there is a considerable difference between ground motion calculated by an accepted correlation between intensity and ground motion and the ground motion obtained by direct calculation. Table 23 gives the results of such a comparison for the New Mexico site.

TABLE 23. Ground motion velocities for New Mexico site.

Probability of occurence	MM	Velocity from MM correlation (cm/sec)	Velocity calculated directly (cm/sec)
10^{-2}	2	1	3
10^{-3}	4	2.4	9
10^{-4}	5	5.6	23
10^{-5}	7	16.5	60

It is evident that the magnitude of a major local earthquake is important, especially for sites in low seismicity regions. For sites in a region of higher seismicity, this consideration is of lesser importance. The boundaries of the distant tectonic provinces (relative to a given site) are not significantly important--this fact makes the analysis both more simple and more difficult. For example, the local seismicity at the Nevada sites is sufficiently well defined so that the analysis is reasonably simple; however, the local seismicity at the New Mexico site is poorly defined, although it governs the analysis.

Estimates of earthquake intensity and frequency (Ekren et al., 1974)[A,B] give the expected numbers of intensity VIII earthquakes per 100 y per 10^5 km^2 as:

Entire United States	1.67
East Coast	0.23
California and western Nevada	6.72
United States (except	

[A,B] See notes A to E at the end of this section.

506 211

California; western Nevada; Montana; Idaho; Utah; Arizona; and Puget Sound, Washington)	0.40.

We used the East Coast value to calculate our minimum transition rate. The value for California and western Nevada was used for the maximum, and the value for the United States excluding the three most active seismic areas was used for the preferred rate. If the data are to serve our purposes, we must assume that:

- Recurrence rates for 100 y can be extrapolated to transition rates over longer periods. Excluding the most active areas, this appears justified as a first approximation on the basis of past geologic history and the tetonic framework of the country.
- Earthquake centers and the "faulting" effects are randomly distributed.

These assumptions have been made by others in calculating earthquake risks and transition rates (Schneider and Platt, 1974).[C]

We can convert the frequency data for MM VIII intensity earthquakes to rate per y per square kilometer and, then estimate the frequency and area affected by more severe earthquakes. Published discussions of frequency vs severity and severity vs area affected (Press and Siever, 1974)[D] indicate that multiplying by a factor of 1.5 would account for most of the major earthquakes, as follows. The resulting earthquake transition rate for MM VIII earthquakes is:

MM VIII earthquake transition rate	
Minimum	3.5×10^{-8} y^{-1} km^{-2} 10^{-8} y^{-1} km^{-2}
Maximum	$10^{-6} = 10^{-6}$
Preferred	$0.6 \times 10^{-7} = 10^{-7}$.

506 212

With underground workings of nearly 10 km^2 and a total reservation site area of nearly 100 km^2,* transition rates for these areas can be compared with an earlier estimate for occurrence of a major earthquake as shown in the tabulation below.

	per 10 km^2	per 100 km^2
Minimum	10^{-7} y^{-1}	10^{-6} y^{-1}
Maximum	10^{-5}	10^{-4}
Preferred	10^{-6}	10^{-5}

Schneider and Platt (1974) give an estimate for a damaging earthquake at a "generic eastern site" as 2×10^{-5} y^{-1} km^{-2}.

*Office of Waste Isolation, "National Waste Terminal Storage Program Informational Meeting", Y/OWI/TM-11/1, p. 6-3, 1976, illustrates idealized control zones of about 2000 acres (1 mile radius) for underground workings, surrounded by about 16,000 acres (2 mile annulus) where all openings would be plugged and all drilling and mining would controlled. Converted to SI units, these areas are 8.1 km^2 and 64.8 km^2, a total of 72.9 km^2. For purposes of this report, these are listed as orders of magnitude 10^1 and 10^2 km^2. Other estimates of the required outer controlled zone have been about a mile annulus (total of about 8000 acres, or 32.6 km^2).

506 213

CONCLUSIONS

From our work to date, we can conclude the following:

- The local earthquake dominates the seismic hazard analysis for well-designed underground facilities.
- The relations between a nearby earthquake and the resultant ground motion must be studied in detail.
- Damage criteria should be improved and better documented. The data suggest that strong ground motion or actual fault movement is needed to cause extensive damage.
- The amount of fault movement that would cause a major flow path must be known so that the effect of minor local earthquakes causing a flow path via faulting can be included in the risk analysis.

506 214

NOTES

A. Ekren et al. (1974), Table 10, (p. 177) lists as some of the criteria for intensity VIII: "Sand and mud ejected in small amounts. Changes in well water..."
For intensity IX: "...ground cracked conspicuously. Underground pipes broken..."
For intensity X: "...ground badly cracked. Rails bent..."
For intensity XI: "...Bridges destroyed. Broad fissures in ground. Underground pipelines completely out of service..."
For intensity XII: "Damage total. Waves seen on ground surfaces..."
(Quoted original reference: Coffman, J. L., and Von Hake, C. A., "United States earthquakes. 1970," U.S. Dept. of Commerce, N.O.A.A., Silver Springs, MD., 81 pp., 1972. pp 4-7)

B. See Ekren et al. (1974), Table 13, p. 184, modified from original: Algermissen, S. T., Seismic Risk Studies in the U.S., in 4th World Conf. Earthquake Eng. Proc: Asociacion Chilena de Sismologia e Ingeneria Antisismica, Santiago, V. 1. p. 124-17. 1969.

C. Schneider and Platt (1974), pp. 3.27 and 3.28, show calculations of earthquake frequency for specific areas, and in: Lawrence Livermore Laboratory, "Determination of Performance Criteria for High-Level Solidified Nuclear Waste," UCID in press, these data are used for transition rates in a Markov chain analysis.

D. Larger magnitude earthquakes are less frequent than smaller ones (Press, F. and Siever, R., Earth, Freeman Co., San Francisco, Table 19-1, 1974) and in Schneider and Platt (1974), P. 3.28, area affected vs magnitude is discussed.

506 215

A combination of these leads to an estimate of 1.5 × Number of Intensity VIII earthquakes × area affected = Total earthquakes VIII to XII × area affected. Larger magnitude earthquakes, while much less frequent, affect larger areas.

E. Lawrence Livermore Laboratory, "Determination of Performance Criteria for High-Level Solidified Nuclear Waste", UCID in press.

CLIMATOLOGY

Climatology studies provide (1) regional precipitation patterns for discrete periods in the future, and (2) maximum and minimum changes in precipitation and temperature from the present day. Climatologic input can be applied to regional hydrology to determine changes in aquifer heads and local flow pathways. The hydrologic model can then be adjusted to reflect these changes and to assess the effect of climate on waste transport.

The earth's climate has been continually changing, and the magnitude of the changes has varied widely with respect to time and space. On the basis of past variations, the effect of climate on repository location could be profound. Different climatic regions may be wetter or drier and correspondingly affect the local hydrology, erosion rates, and, over long periods of time, sea level.

The main purpose of climatologic input into the repository simulations is to give reasonable estimates of the groundwater recharge based on the possible future climatic variation. The problem, then, is to estimate the regional responses. Secondary tasks entail estimates of future sea levels and cryospheric changes that will affect hydrologic and demographic patterns.

Predicting Climate

To predict the range of possible climatic regimes that may occur in the next 10^6 y, we have used the high degree of correspondence between the different

506 216

earth orbital parameters and past climate variation (Hays et al., 1976). Although the mechanism between solar variations due to earth orbital elements and major climate changes in the past is still under debate, more than one-half the variance in past temperature data is explained by this parameter. The orbital elements may be calculated by a relatively simple model, which can then be used to predict future global temperature and ice volume.

Shorter-term variations in climate are more difficult to predict. In the short term, the earth orbital parameters may still be controlling the natural climate fluctuations. However, with the increased anthropogenic release of CO_2 into the atmosphere, some researchers (Broecker, 1975) expect the earth to enter a "superinterglacial" similar to the postglacial optimum that occurred about 6×10^3 y ago.*

Global temperature ranges given by our predictive model give no indication of regional precipitation variations. Because the atmosphere is a nonlinear, highly coupled system, minimal information other than generally wetter or drier conditions can be deduced from mean temperature. We must rely on climatic reconstruction of different periods in the past that will then correspond to the future predictions of temperature.

Climate Data

Several major climatic regimes that are representative of the past 10^6 y are outlined in Table 24. These are based mainly on the work by Lamb (n.d.) and are related to the correlation between the earth orbital elements and global temperature/ice volume from Hays et al. (1976).

*Global temperatures 2°-2.5°K warmer than the present with generally wetter deserts and drier mid-latitudes.

506 217

We obtained temperature and precipitation patterns of the glacial climate regime from three-dimensional general circulation models that used ice age boundary conditions for initialization (Gates, 1976). The model output is limited by the grid structure and, in general, the predictability of the model. Basic patterns of regional precipitation become evident (see Fig. 18) and are consistent with the current estimates of actual precipitation during that period.

The remaining climatic regimes from Table 24 and the regional variations in precipitation will be constructed using data from Bernabo and Webb (1977) and Fritts (1977). The methods mainly entail eigenvector analysis of pollen and tree-ring data, respectively. Application of the climate data to the hydrologic model will require calculation of infiltration by balancing precipitation, evapotranspiration, and runoff.

TABLE 24. Climate regimes chosen as typical for future projections.

Time of representative patterns from past climate regimes	Characteristic	Location on time line
20,000-17,000 BC	Full glacial	Minimum eccentricity
7,000-6,000 BC	Boreal early warm	Few thousand y before peak in precession
4,000 BC	Atlantic moist postglacial-warm	Maximum in precession
2,000 BC	Sub-Boreal dry postglacial-warm	Maximum in precession
500 BC also 1550-1700 AD	Little Ice Age	Past maximum in precession

506 218

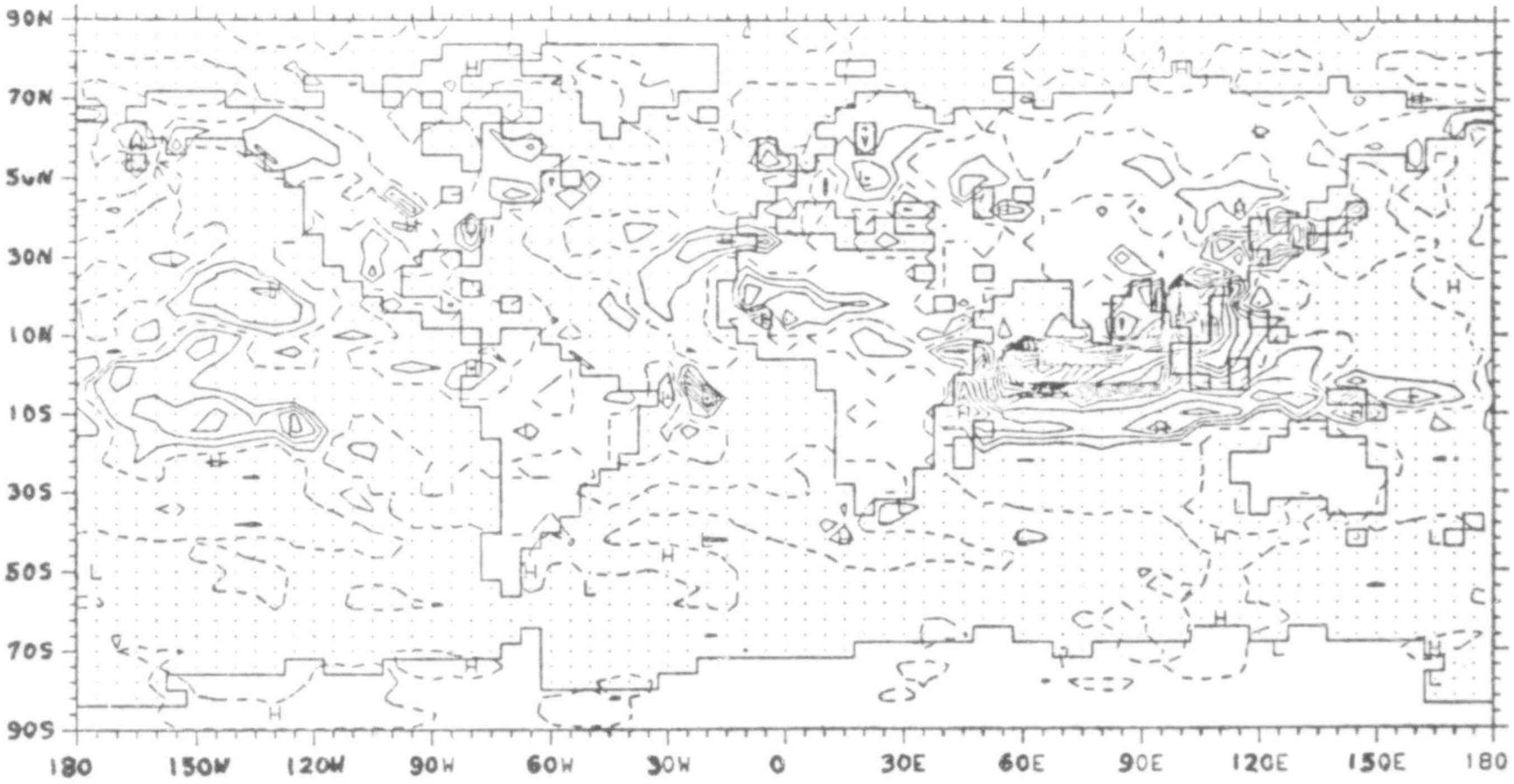

FIG. 18. Precipitation difference (mm/d) between model ice age and control run (ice age minus control). The dashed line is no difference; the contour interval is 5 mm/d. (From Gates, 1976.)

506 219

5. ANALYSES AND RESULTS

MULTIPLE-BARRIER CONCEPT

Results of analyses to date indicate that geometric, hydrologic, and geochemical parameters effect nuclear waste containment in deep geologic media. These parameters act as natural multiple barriers to waste transport from the repository to the biosphere. The important processes for each barrier that can be identified, measured, and possibly controlled will aid in defining a potential site's suitability for waste disposal. Barrier properties include:

- Geometric barrier
  - Layer thickness
  - Fracture zone area
  - Tunnel length
  - Aquifer length
- Hydrologic barrier
  - Rock properties
    - Porosity
    - Permeability (natural and induced)
  - System properties
    - Pressures and gradients
    - Disperson
    - Aquifer length
- Chemical barrier
  - Radionuclide retardation
  - Waste dissolution rate

A geometric barrier is one that physically isolates the waste by the thickness of the rock layers, the area of the fracture zone due to construction, and the distance groundwater must flow from the repository before intersecting a river or lake. A hydrologic barrier is more complex than the geometric barrier and comprises parameters determining the waste dilution factors (dispersion) and

506 220

groundwater flow rates (porosity, permeability, heads, gradients, and so on). In general, the hydrologic and geometric barriers isolate the waste by determining both the time required for resaturation of the repository after water begins to enter and the time required for groundwater to flow from the repository to the biosphere.

The geochemical barrier processes are identified as a series of waste/water/rock interactions involving sorption (ion exchange), membrane filtration, hydrolysis, precipitation, and complexing. The geochemical barrier inhibits migration of the radionuclides (retardation) and limits groundwater concentrations of radionuclides with low solubilities. Also influencing the geochemical barrier is the leach resistance of the waste, which lengthens the time necessary for dissolution.

Calculations of barrier interaction depend on whether the consequence or risk being measured is short term (such as concentration or individual dose) or integrated over time (such as integrated population dose or total amount of radioactivity released).

In the case of short term consequence or risk, dispersion over time (or dilution) joins radioactive decay as a controlling factor. Concentration or individual dose is inversely proportional to the duration of the pulse of waste reaching the environment. The contributions to pulse width from different barriers add, roughly, in quadrature (that is, the square root of the sum of the squares). This formula weights the final result strongly toward the largest single contribution. Thus, unless two barriers are of nearly equal effectiveness, the pulse width is governed by the most effective barrier alone and will be nearly equal to the total pulse width. When dose is integrated over time, the sensitivity analysis reveals the "plateaus and cliffs" structure, as shown in Fig. 19. This phenomenon results essentially from radioactive decay. Each nuclide generally escapes before it has decayed significantly, or it is contained until it has decayed to the point where a longer-lived nuclide is more important. The time interval during which the

506 221

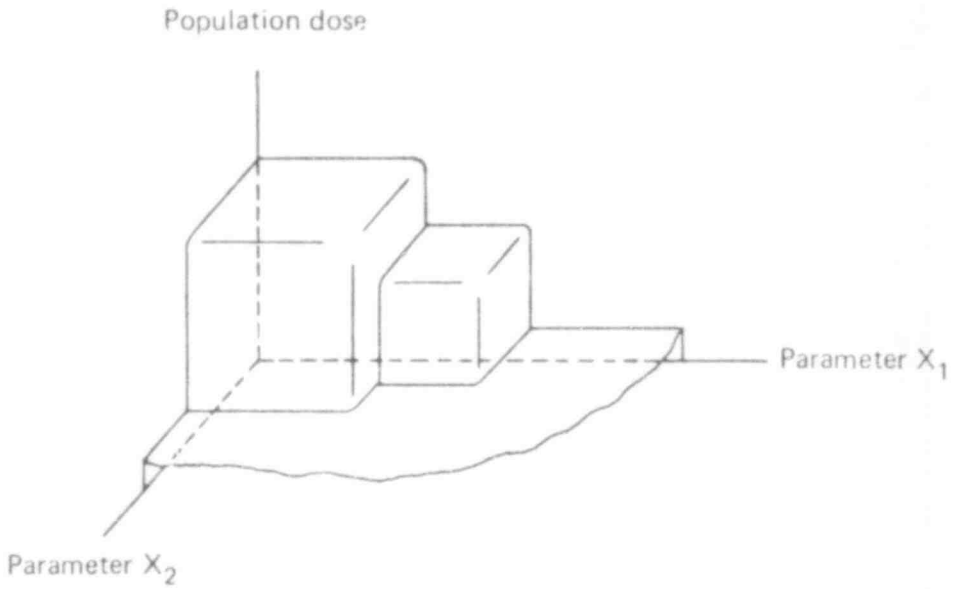

FIG. 19. Conceptual illustration of the general form of a plot of integrated population dose vs two of the parameters describing a repository.

decay of any individual nuclide significantly reduces the overall hazard of the waste is quite short on a logarithmic time scale ranging from hundreds to millions of y. The speed of exponential decay when viewed on a logarithmic scale is illustrated for the case of ^{239}Pu in Fig. 20.

Whether a particular nuclide is released to the biosphere may be determined by comparing its total transit or delay time in the system with the time required for it to decay into in significance. The total time delay is the sum of all the time delays in the system. For the same water velocity nuclides differ in velocity of movement through the ground because of geochemical factors (as measured by the retardation factors). Thus the time delays vary, and different barriers may be limited for different nuclides in the same system. One or more delays will usually be orders of magnitude larger than the others, and the barriers causing the delays are critical in reducing radionuclide release.

506 222

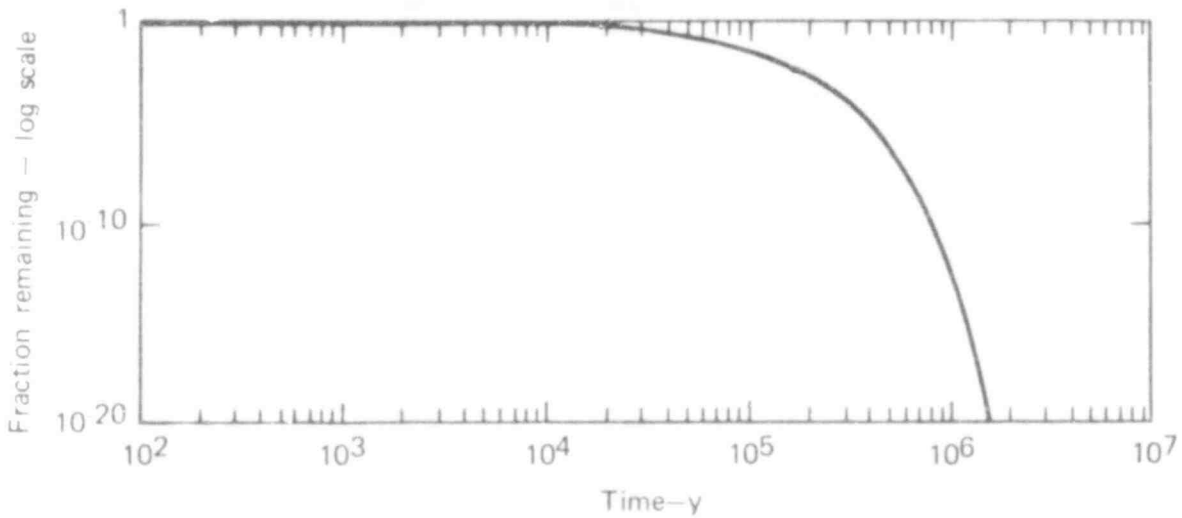

FIG. 20. Decay of ^{239}Pu.

GROUNDWATER FLOW VELOCITIES

The transport model approximates the groundwater flow pattern around a repository by a three-dimensional network of one-dimensional flow paths or stream tubes. Each point in the network at which stream tubes branch, or at which any of the variables change value, is defined as a network node, as shown in Fig. 21. By controlling permeabilities and porosities, flow can be described as interstitial (i.e., flow through the undisturbed rock) or fracture (e.g., in the unflawed repository there is flow through the fracture zone associated with the construction of the repository, shaft, and tunnel).

The groundwater flow velocities appearing in the transport equation are the interstitial velocities, sometimes referred to as the true velocities. They were calculated for individual stream tubes in the hydrologic model by the following equations derived from Darcy's law for flow through porous media:

506 223

$$V = \frac{V_m}{\epsilon}$$

and

$$V_m = -K\frac{\Delta H}{L} \quad ,$$

where

V = interstitial velocity
V_m = bulk velocity
ϵ = porosity
ΔH = head difference between two nodes
L = stream tube length
K = permeability.

Table 25 lists interstitial velocities for the baseline cases in the unflawed shale and salt repositores. Velocities are given between each node for both interstitial and fracture zone flow pathways. With the exception of flow in the lower section of the shaft (nodes 4-5), velocities are about the same in both repositories, assuming baseline values for the parameters.

Total travel time from the repository to the aquifer (Table 26) is 2.3×10^3 y for fracture zone flow along the tunnel/shaft and 1.6×10^5 y for interstitial flow with no retardation ($K_f = 1$). Another [illegible] are needed for flow from the aquifer directly above the repository to the river. Hence, waste will reach the aquifer first from the fracture zone flow. The velocities and travel times in Tables 25 and 26 show that the strongest part of the hydrologic barrier involving fracture zone flow is within the repository between nodes 1 and 2. The time for waste to travel the 1200 m from node 1 to 2 is about 2300 y with no sorption. This value depends on the major assumption that the waste is a point source at node 1. In the actual repository design, the waste will be distributed over most of the 5 km^2 of the repository. This could put waste within 50 m or so of the tunnel, rather than 1200 m. Travel time (t) for 50 m is about 100 y with no retardation; when $K_f = 10^2$, t = 10^4 y, and when $K_f = 10^4$, t = 10^6 y.

506 224

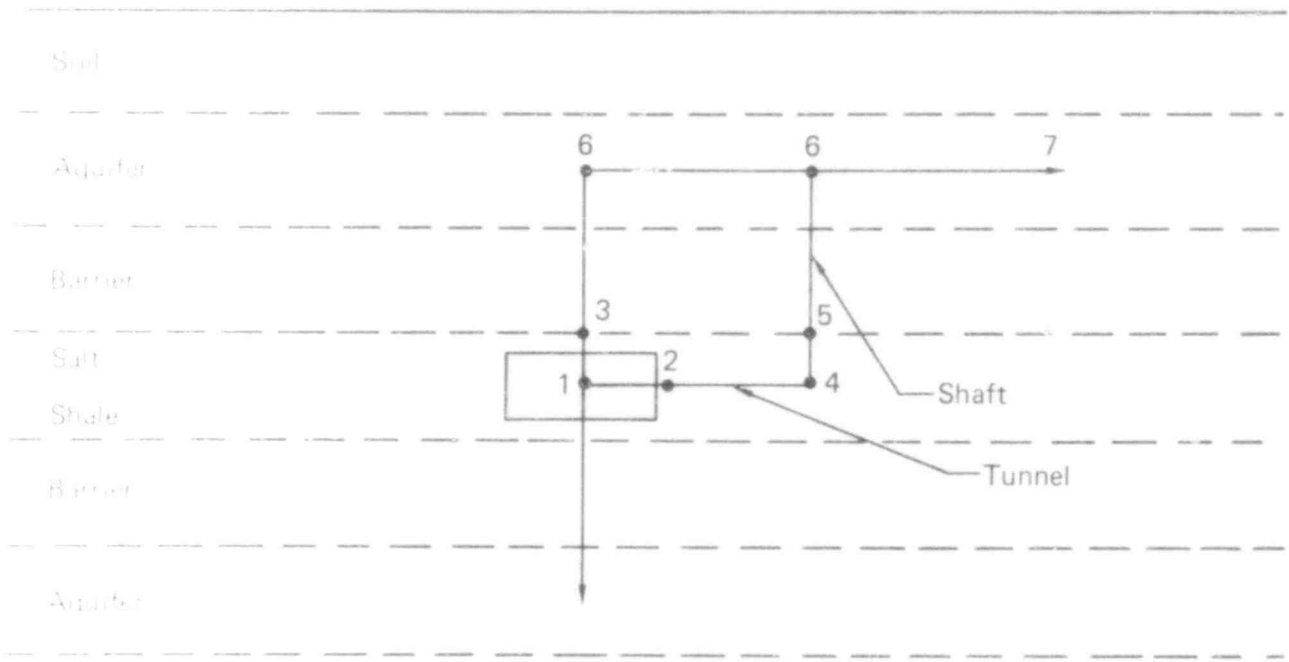

Fracture flow = nodes 1 → 2 → 4 → 5 → 6
Interstitial flow = nodes 1 → 3 → 6 → 7

FIG. 21. Node distribution for interstitial and fracture flow pathways in the transport model for the unflawed repository.

506 225

TABLE 25. Groundwater flow velocities.

Nodes	Flow type	Shale repository		Salt repository	
		Velocity (m/y)	Time (y)	Velocity (m/y)	Time
1-2	Fracture zone	5.36×10^{-1}	2.3×10^{3}	6.2×10^{-2}	1.9×10^{4}
2-4	Fracture zone	9.3	47	1.0	420
4-5	Fracture zone	1.9×10^{3}	0.05	3.3	30
5-6	Fracture zone	3.7×10^{3}	0.05	41	4.9
1-3	Interstitial	1.8×10^{-3}	5.5×10^{4}	9.3×10^{-3}	1×10^{4}
3-6	Interstitial	1.8×10^{-3}	1.1×10^{5}	1.9×10^{-3}	1×10^{5}
6-7	Interstitial	1.6	1.0×10^{4}	1.6	1×10^{4}

TABLE 26. Total travel time from repository (y).

Retardation	Flow path	Shale		Salt	
		To aquifer (node 6)	To river (node 7)	To aquifer (node 6)	To river (node 7)
$K_f = 1$	Tunnel/shaft[a]	2.3×10^{3}	1.2×10^{4}	1.9×10^{4}	2.9×10^{4}
	Interstitial[b]	1.7×10^{5}	1.8×10^{5}	1.1×10^{5}	1.2×10^{5}
$K_f = 10^{2}$	Tunnel/shaft[a]	2.3×10^{5}	1.2×10^{6}	1.9×10^{6}	2.9×10^{6}
	Interstitial[b]	1.7×10^{7}	1.8×10^{7}	1.1×10^{7}	1.2×10^{7}
$K_f = 10^{4}$	Tunnel/shaft[a]	2.3×10^{7}	1.2×10^{8}	1.9×10^{8}	2.9×10^{8}
	Interstitial[b]	1.7×10^{9}	1.8×10^{9}	1.1×10^{9}	1.2×10^{9}

[a]From nodes 1→2→4→5→6.

[b]From nodes 1→3→6.

506 226

In the shale repository, decreasing the effective length of the repository from 1200 m to 50 m for part of the waste has a significant affect only on the ^{129}I and ^{99}Tc concentrations and their contributions to dose calculations. Radionuclides ^{90}Sr and ^{137}Cs with a retardation factor of 10^2 will be retained within the repository for 10 000 y; however, in the salt repository, where retardation is assumed absent between the repository and the aquifer, changes in all radionuclide concentrations and doses are expected. Even then, the resultant change in values may not be significant. The amount of waste that flows from the salt repository is only about 0.5% of the total inventory. In the shale repository, about 0.4% of the waste is diverted through the tunnel/shaft.

With such limited amounts of waste flowing via the fracture zone pathway, the error related to the point source assumption is probably small, but future computer simulations will correct this problem by adding nodes between nodes 1 and 2 to simulate distribution of the waste throughout the repository.

HAZARD TIME DEPENDENCE

Figure 11 shows the potential hazard of high-level waste from reprocessing of light water reactor fuel as a function of time. Potential hazard in this figure is measured in terms of population dose to the whole body per MWe-y of waste. This quantity is defined as the total dose to the population that would be incurred if 1 MWe-y/y of waste in soluble form were to be dumped directly into the river. Curves for critical organs and for individual doses are similar in form.

Potential hazard is calculated here from the biosphere transport and dose model. The main difference between this hazard and the toxicity index calculated by the ORIGEN code (Bell, 1973) is that our model accounts for radionuclide transport in the ecosystem and bioaccumulation in the food chain. Note that the shape of these curves does not depend on the half-life of ^{239}Pu. There are, rather, two time periods during which the total potential hazard from the waste declines significantly:

506 227

- The period from 30 to 400 y during which ^{90}Sr and ^{137}Cs are decaying.
- The period from 500 000 to 2 million or 3 million y during which ^{226}Ra produced by the decay of ^{242}Cm and ^{238}Pu decays away. (The time constant governing this process is the quarter-million y half-life of ^{234}U.) After 3 million y, the remaining ^{226}Ra in the waste is that produced by decay of the original inventory of ^{238}U.

Given these time dependences, the life of the repository after decommissioning may be divided into three distinct periods. This division comes directly from the categorization of nuclides and the time dependence of their hazard illustrated in Fig. 11, and does not depend on the characterization of the repository site. The three periods are:

- An initial period lasting not more than 400 y. During this interval, the consequences of a release of radioactivity directly to the biosphere could be quite severe.
- An intermediate period following the initial period and lasting at least 500 000 y, but not more than 3 million y. The consequences of release during this period will be considerably less than during the earlier interval.
- A final period beginning not more than 3 million y in the future. At this point, the hazard of the waste will result primarily from natural ^{238}U and its decay products. The repository will contain little more than the equivalent that was mined near the surface and buried in a deep, stable formation.

506 228

PARAMETRIC SENSITIVITY ANALYSIS

By changing parameter values in the model, we simulated the results of release through a number of pathways and the breaching of barriers in four repository types:

- Sandstone-shale sedimentary sequence; repository in the shale layer with interstitial flow in the shales.
- Same as above with fracture flow in the shales.
- Sandstone-shale-salt sequence; repository in the salt layer, with interstitial flow in the shales.
- Sandstone-shale-salt sequence; repository in the salt layer, with fracture flow in shales.

In each of the above there is "fracture zone flow" about excavated features. This should not be confused with the "fracture flow" through the bulk rock. Appendix N presents the model assumptions and the results from 85 separate computer runs. The parameter values are tabulated in Appendix O.

Computer Simulations

In the unflawed cases (Tables N-1 through N-6) with no faults, breccia pipes, or seal failures, we varied single parameters in a total of 52 runs and varied 2 to 5 parameters simultaneously in 10 multiparameter runs. By observing the resultant changes in dose and concentrations, we gained an understanding of the relative importance of the parameters that define the multiple barrier system.

Parameters describing the rock and system hydrologic properties, chemistry, and geometry (path lengths) were varied from a preferred "base case" to the maximum or minimum limits in the direction that increased release. Further experiments are planned where values are varied so as to minimize release.

For release to occur, hydrologic pressures have to be such that they produce flow from the repository into a permeable zone and then along the permeable

506 229

zone in the direction of the biosphere. We assume that water will flow into the repository and that dissolution and transport of waste begins when the repository is filled (i.e., 100 y).

A fracture zone with a specified permeability is assumed to exist around tunnels and shafts in both the flawed and unflawed cases. Lengths of these zones were calculated from dimensions of a reference repository described by Office of Waste Isolation Report #Y/OWI/SUB-76/16506.

The remainder of the 85 simulations calculated the effect produced by introducing failure mechanisms. In the shale repository, we simulated (a) a fault (Table N-11), (b) failed borehole seals (Table N-9), and (c) failed backfill and shaft seals (Table N-7). In the salt repository, we simulated (a) failure of boring seals (Table N-10), (b) failed backfill and shaft seals (Table N-8), and (c) formation of a solution breccia pipe (Table N-12).

Planned sequences of simulations were truncated when it became clear that results would be similar to, or could be extrapolated from, other simulation runs. Additional single parameter and multiparameter variations are planned to test conclusions made from these runs.

Performance Measures

The consequences of release can be stated in a number of ways. They can be categorized along two dimensions: the period of time considered and the quantity to be measured. There are two fundamental approaches in the time domain:

- A time-varying measure of consequence, such as concentration at any instant or dose to a single individual.
- A measure integrated over the lifetime of the repository, such as integrated population dose or the total amount of a nuclide that is released.

With regard to the quantity to be measured, two main options have been generally considered:

506 230

- An estimate of the amount of radioactivity reaching some point, as in concentration or total amount released.
- An estimate of the dose to humans.

The three performance measure formats selected for assessing parameter sensitivity in this study are:

- The dose received by an individual consuming an "average" diet consisting entirely of contaminated food.
- The dose to the population integrated over the 3 million y period following decommissioning.
- The maximum groundwater concentration in an aquifer immediately above the repository cavity.*

Each measure depends quite differently on repository characteristics.

Individual Dose

The potential hazard of high-level waste released to the biosphere is determined by taking into account the pathways that might lead to man. This hazard can be reflected in the calculation of the dose to an individual. We calculated doses for releases into a river system at some distance from the waste repository. In all cases studied, the maximum dose was far below background.

The peak individual dose to the critical organ varied more than three orders of magnitude for the salt repository (see Tables N-3 and N-4) and two orders of magnitude for the shale repository (see Tables N-1 and N-2). Because individual parameters were changed by differing amounts (e.g., K_f varied two orders of magnitude while dispersion was only varied by a factor of 5), it is hard to suggest which of the parameters is most important. We can, however, evaluate those parameters that produce the greatest effect on the performance measures for the range of parameter values used. For example, in the unflawed

*We could not show all the radionuclide concentrations in the tables of Appendix N. Those shown represent the three groups of radionuclides used in the transport model.

506 231

shale repository with interstitial flow, the following parameters can be cited as having decreasing effect on the individual dose to a critical organ. (The dose was increased ~500% or more above baseline value in the sensitivity analysis):

- Shale permeability
- Area of fracture zones
- Fracture zone permeability
- Thickness of repository layer
- Actinide retardation factors.

Analysis of specific sites will change the ordering given. Each parameter will be strongly influenced by individual site characteristics. For a particular site, the permeability and area of the fracture zones and dissolution rate of the form will be strongly influenced by planning and engineering. The other parameters will be strongly influenced by the choice of the repository site and depth.

Population Dose

One can expect the dose to an individual to be far below background for any repository that isolates ^{90}Sr and ^{137}Cs for 400 y, and allows wastes to reach the biosphere only through a sizable surface water system. For such a repository, integrated population dose rather than individual dose may be a more appropriate measure of risk or consequence.

To measure the total effect, one integrates the population dose over the lifetime of the repository and assumes doses to be of equal concern, regardless of the time they occur. Total integrated dose is then limited by the repository inventory, radionuclide decay, existence of paths to the biosphere, the fraction of water from liquid pathways used for irrigation and drinking water, and the quantity of aquatic food harvested from the liquid pathways.

In the sensitivity studies, integrated population dose is relatively insensitive to changes in the baseline repository parameters. The critical organ dose in nearly all cases studied was between 0.16 and 0.51 man-rem/MWe-y

506 232

to the gastrointestinal tract and lower large intestine (GI-LLI). The few extreme off-baseline cases where the dose exceeded these values were due to the actinides reaching the river within the time span of 3 million y under consideration. For the actinides to affect the dose, the rock permeability and the head gradient along the flow pathway must be sufficiently high or the effective porosity sufficiently low to overcome ion exchange processes that retard actinide migration (see Tables N-4 and N-5).

The following can be concluded from the study to date:

- Population dose showed the least variation of the three measures of risk in the sensitivity studies.
- Population dose varied according to whether actinides were released. Among the parameters examined, population dose depended most strongly on actinide retardation due to sorption.
- Population dose depends on the yearly use rates of the water system, after waste reaches the river. It is independent of the river flow rate for fixed fractional use rates.

Concentration

Concentrations were calculated for radionuclides in the aquifer water at the downstream side of the repository cavity. All the waste is assumed to originate at the center of the facility. We calculated the concentrations assuming a line source in the aquifer with length equal to the width of the repository. Studies to date show that peak concentrations in the aquifer at this location often approach, and sometimes exceed, the maximum permissible concentrations in water. This situation will be important if the water in the aquifer is potable, and if wells are drilled near the repository.

As with the individual dose performance measure, concentrations are sensitive to parameters having a major effect on passage time from the repository to the aquifer. This is not surprising, as concentrations are mainly a function of the length of time over which radioactive decay and dispersion can occur.

Concentrations in the aquifer fall off at large distances from the repository because of dispersion. For a steady flux of waste into the aquifer, the peak

506 233

concentration in the direction of water flow far from the repository is inversely proportional to the square root of the distance from the repository, even if radioactive decay is not significant. Peak concentrations at large distances normal to the downstream aquifer flow fall off exponentially. Therefore, the hazard due to possibly high concentrations of waste in the aquifer depends on where this water becomes accessible to man.

Since the actinides are retarded more than the fission products, only the latter are released into the aquifer from the unflawed shale repository within the first 3 million y (as long as flow is assumed to be through pores and the fracture zone of the tunnel/shaft and not through fractures in undisturbed rock). However, relatively high concentrations of both the actinides and the long-lived fission products were calculated in the aquifer for the unflawed salt repository (Table 27). The difference in concentrations between the two repositories results primarily from the assumption that there is no geochemical retardation in the repository and barrier layers of the salt repository.

TABLE 27. Peak aquifer concentrations for baseline cases[a] (Ci/m^3).

Nuclide	MPCw	Salt repository	Shale repository
^{99}Tc	3×10^{-4}	1.6×10^{-4}	1.2×10^{-4}
^{126}Sn	2×10^{-5}	4.2×10^{-6}	7.8×10^{-8}
^{226}Ra	3×10^{-8}	3.4×10^{-7}	b

[a]From Tables N-1 and N-3.

[b]Peak occurred fter three million y and was not calculated.

506 234

For the concentration performance measure, the study to date indicates the following:

- Aquifer concentrations are the most sensitive to changes in the model parameters.
- Any decrease in concentrations caused by increasing aquifer flow rates will increase individual and population doses from use of a nearby surface water body.
- Peak aquifer concentrations are sensitive to barrier failures such as faults, boreholes, fracture zones, and breccia pipes.

Fracture Flow vs Interstitial Flow

The foregoing discussion relates to cases with interstitial flow in undisturbed rock. In cases with fracture flow rather than interstitial flow in the shale layers, baseline values are consistently higher and occur earlier (Table 28), primarily because flow velocities are higher in the fractured rock. Peak concentrations in Tables N-5 and N-6 show the actinides reaching the aquifer before 3 million y. The ^{126}Sn concentrations are increased by three orders of magnitude.

TABLE 28. Fracture flow vs interstitial flow for shale layers.[a]

Repository and flow type	Whole-body population dose (man rem/MWe-Y)	Whole-body individual dose (rem/MWe-Y)	Peak ^{99}Tc Conc. (Ci/m^3)
Shale repository			
Interstitial	1.3×10^{-3}	6.19×10^{-14} (14,400 y)[b]	2.02×10^{-11} (4000 y)[b]
Fracture	2.77×10^{-3}	1.86×10^{-12} (11,700 y)[b]	6.84×10^{-10} (230 y)[b]
Salt Repository			
Interstitial	1.63×10^{-3}	8.15×10^{-14} (149,000 y)[b]	2.58×10^{-11} (109,000 y)[b]
Fracture	2.56×10^{-3}	5.84×10^{-13} (25,600 y)[b]	1.86×10^{-10} (16,900 y)[b]

[a]From Tables N-5 and N-6.

[b]Time at which peak concentration occurs.

506 235

REPOSITORY CONSTRUCTION EFFECTS

There are two aspects of construction for which associated flow paths to the aquifer could be significant: (1) the method of excavation and the type of backfill, and (2) the backfill emplacement method used on decommissioning. Excavation produces a fracture zone around the shaft, tunnel, and repository cavity; the backfill may deteriorate with time.

The effects of construction are best understood in terms of the multibarrier concept introduced earlier. As long as radionuclides must pass through an aquifer, the aquifer could be considered a final barrier and these construction aspects could have only limited influence. If the aquifer is bypassed, however, they may have a large effect on risk.

The extent and the time-dependent behavior of backfill deterioration can be critical for peak aquifer concentrations and doses. Both factors are a function of host rock type, backfill type, flow patterns and flow rates (especially in the surrounding fracture zone), and emplacement method. To date we have yet to analyze these considerations completely, but they will affect the permeability and porosity of the tunnel and shaft as a function of time. To help understand the effect of this time dependence, we studied a series of cases in which complete backfill deterioration was assumed as the initial state, and the degree of deterioration of the tunnel and shaft was independently varied. These conditions served as a worst-case bound on the time dependence while providing quantitative insight into the effectiveness of the multibarrier concept in three distinct manifestations.

The first manifestation concerns the extent to which increasing the degree of backfill deterioration affects the peak concentrations and doses. Table 29, derived from Table N-8, shows that as the permeability is increased to 10^{-1} cm/sec, peak individual doses continue to increase but at a lower rate. The reason for this declining sensitivity is that the amount of water flowing through the repository becomes a function of the resistance to water flow of the rock between the lower aquifer and the repository. The flow resistance above the repository and below it can be thought of as resistors in series (Fig. 22).

506 236

TABLE 29. Peak individual dose vs permeability of backfill.

Tunnel/shaft backfill permeability (K)	Peak individual dose to critical organ (rem/MWe-y)
10^{-4}	4.5E-11
10^{-3}	1.6E-10
10^{-1}	2.2E-10

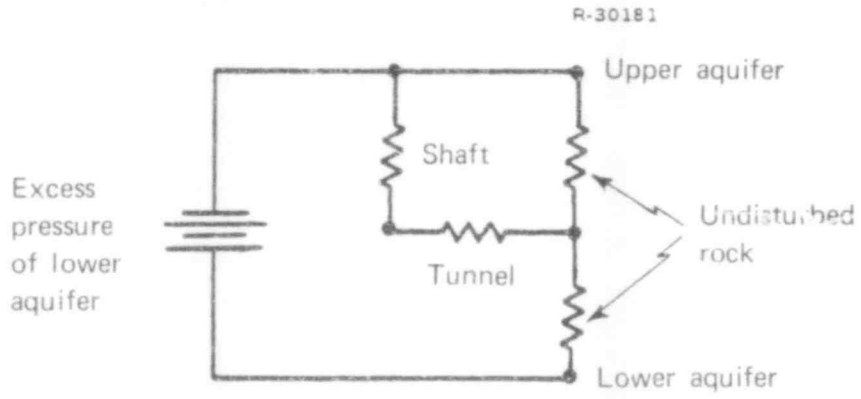

FIG. 22. Resistor network analogous to repository with permeable backfill.

Raising the permeability of the backfill is equivalent to reducing the size of its associated resistor. As one resistor decreases in size, reduction by additional orders of magnitude has diminishing effect on the total flow since it is the sum of the two resistances that determines the flow. The deteriorated backfill could allow more water to flow through it than can flow through the underlying rock. Therefore, increasing the permeability of the backfill has minimal effect beyond a certain point

506 237

The second manifestation concerns the degree to which either the shaft or the tunnel can independently serve as a barrier if the other has failed. When the permeability of the backfill in the shaft is decreased from 10^{-4} to 10^{-6} cm/sec (Table N-8) while allowing the tunnel backfill to remain highly permeable, the doses are almost identical to those in the case of no backfill deterioration (1.63E-3 vs 1.79×10^{-3} man-rem/MWe-y). The qualitative explanation of this phenomenon is identical to that of the preceding paragraph; the flow resistance of the shaft is greater than the resistance of the tunnel, and at the 10^{-6} cm/sec value only a negligible amount of water was able to pass through the shaft.

Finally, we consider why the variations in dose are so small among the different cases analyzed. The explanation lies in the long time (10^4 to 10^8 y required for radionuclides to flow from the region in the aquifer directly above the repository to the regions of discharge. It is assumed that the flow time is long because the horizontal head gradient is 0.005 and that there is a great distance (compared to repository dimensions) between repository and discharge regions. Aquifer length can have no affect on peak concentrations in the aquifer directly above the repository. This last observation makes the assumption of long discharge distance critical, since significant levels of nuclide discharge into the biosphere could occur if the aquifer were to be penetrated sufficiently close to the repository. Penetration could be in the form of wells, exploration, mining, and so on. The discharge could be particularly dangerous if it occurred during the initial 400-y period and other barriers failed; hence, administrative control of such activity can be important. Note, however, that the values for peak concentrations are based on the assumption that full backfill deterioration occurs immediately after decommissioning.

In reality, deterioration will increase to the fully deteriorated state over a time period probably comparable to the initial 400-y time period. This would considerably reduce the danger of aquifer penetration.

A discussion of fracture associated with excavation must distinguish between salt and shale repositories, because salt has plastic and recrystallization characteristics that may allow it to seal with time. In our salt model, the

506 238

period during which this occurs is shorter than the resaturation time of the depository, with a final value for permeability of 1% of the initial value. Given these assumptions, there is almost complete insensitivity to the state of the tunnel and shaft because almost all of the flow is through the undisturbed salt. The relative lack of flow through the tunnel and shaft derived from the facts that the tunnel and shaft occupy a smaller area than that of the overlying rock, and in the case of a salt repository the permeability of the fracture zone in the salt layer is relatively low at 10^{-6} cm/sec. As a result, even though the overlying rock is less permeable (10^{-9} cm/sec), it has a much larger cross-sectional area so that the flow through the overlying rock is two orders of magnitude greater than that through the tunnel and shaft. Therefore, changing the parameters of the shaft and tunnel within the given bounds has a negligible effect on the dose (see Table N-3). The above is not the case for the shale repository studied, since the permeability of the fracture zone in shale is assumed to be 10^{-1} cm/sec for the tunnel and 10^{-4} cm/sec for the shaft. This difference is sufficient to make the tunnel and shaft a significant flow path in shale under some conditions (see Table N-2).

EXPLORATION EFFECTS

Selection of a repository site will have to consider the detailed geologic structure of the proposed site and its vicinity; hence, the benefits and potential liabilities of borings must be investigated. The primary liability of a borehole is the possibility of nuclide flow to both the aquifer and the overlying biosphere if the borehole is not properly sealed or if the seal should fail. Our investigation to date has considered the effect of boreholes with a given probability of initial improper sealing and a subsequent time-dependent failure probability. (See Appendix O for rates and probabilities.) A substantial pressure gradient causing upward flow is assured.

Aquifer length is more relevant to boreholes than to backfill deterioration and construction effects. With an effective aquifer length, the effect of borings was negligible in the cases studied. Without that barrier, borehole-seal failure could have consequences much worse than those of the backfill failure cases discussed previously.

506 239

The doses for cases with borehole seal failures do not vary significantly from the baseline cases where only the flow through the overlying rock and through the fracture zone of the tunnel and shaft are considered (see Tables N-9, N-10). Peak concentrations in the aquifer do vary significantly, however. The ^{137}Cs and ^{90}Sr reach concentrations of 2.0×10^{-3} and 1.3×10^{-3} Ci/m^3, respectively, for the salt repository containing 6×10^6 MWe-y of waste. They result from the extremely high velocity of water flowing through the borings. The high velocity allows the ^{90}Sr and ^{137}Cs in a salt repository to get to the aquifer one y after the 100 y the repository is assumed to take to become saturated with water. For the shale repository with failed borehole seals the ^{90}Sr and ^{137}Cs reach the aquifer 100 y after the repository becomes saturated with water, increasing peak concentrations of these nuclides in the aquifer also.

The flow of ^{90}Sr and ^{137}Cs through the aquifer to the river takes so long that none of these short-lived nuclides reach the river soon enough to make a significant contribution to dose. Even though the barriers between the repository and the aquifer have been eliminated for some of the ^{90}Sr and ^{137}Cs, the distance from the repository to the river can be sufficient to prevent these nuclides from affecting dose.

GEOLOGIC EVENTS

Two types of geologic events have been investigated in the studies to date: the activation of a fault intersecting a portion of a repository and the formation of a breccia pipe within a salt repository. Although either of these events may provide a pathway for rapid flow from the depository to the aquifer, when treated probabilistically neither gave an expected value of dose significantly greater than the doses calculated for the unflawed repository.

Since the occurence of breccia pipes may be closely related to other relevant hydrologic phenomena, it was necessary to study a worst-case situation in which a permeable breccia pipe is present from the beginning. The calculations

506 240

of peak dose and integrated population dose for this case indicated that, although the flow to the aquifer was almost entirely through the breccia pipe (thus quite large and fast), the aquifer again provided the limiting barrier to man. The peak concentrations and doses were virtually identical to the high tunnel and shaft permeability case in the sensitivity analysis of deteriorated backfill in a slat repository (see Tables N-12 and N-8). The comments concerning the security of the aquifer mentioned in the two previous sections on borehole and backfill deterioration are again relevant. The peak aquifer concentrations were calculated to be well over the MPC_w values and shortening the flow path through the aquifer might create high individual doses.

When the breccia formation was assumed to be an event independent of other high flow phenomena, its probability of occurence was given an estimated baseline value of 5×10^{-7} events/y. The resulting calculations yielded the expected flow rates and doses based on this transition rate. The computed expected values did not differ significantly from those calculated from the baseline models without geologic events. An identical statement holds for the case of a fault in the shale repository. Furthermore, this result was essentially independent of an increase in probability of occurrence of two orders of magnitude.

The reason for the above result is that breccia pipe formation and faulting, under the stated assumptions, had such low probabilities of occurence that a large amount of time must pass before the probability the event has occurred would be large enough to meaningfully affect the expected values of doses.

506 241

REFERENCES

Adams, L. H., "Equilibrium in Binary Systems Under Pressure. I. An Experimental and Thermodynamic Investigation of the System, NaCl-H_2O, at 25^{o}," J. Am. Chem. Soc. 53, pp. 3769-3813 (1931).

Abramowitz, M., I. A. Stegun, Handbook of Mathematical Functions, (National Bureau of Standards, 1970), p. 298.

Algermissen, S. T. and D. M. Perkins, A Probabilistic Estimate of Maximum Acceleration in Rock in the Contiguous U.S., USGS Open File Report 76-416 (1975).

Anderson, R., Personal communication (1977).

Angelo, C., M. Goldberg, V. Janzer, and W. Beetem, Geology of the U 18a Site, Buckboard Mesa, NTS, Part VI: Summary of K_d's for Fission Products Between Groundwater and Basaltic Rocks, USGS Report, WT-1828 (1962), pp. 66-81.

Archie, G. E., "Introduction to Petrophysics of Reservoir Rocks," Amer. Assoc. Petrol. Geol. Bull., 34, pp. 943-961 (1950).

Baetsle, L. and P. Dejonghe, "Investigations on the Movement of Radioactive Substances in the Ground, Part III: Practical Aspects of the Program and Physicochemical Considerations," in Proc. Conf. Ground Disposal of Radioactive Wastes, 2nd, Chalk River, Canada, September, 1961, U.S. AEC, TID - 7628, pp. 198-210 (March, 1962).

Barnes, C. A., et al., "Circulation and Selected Properties of the Columbia River Effluent at Sea," in The Columbia River Estuary and Adjacent Ocean Waters, A. T. Pruter and D. L. Alverson, Eds., (University of Washington Press, Seattle and London, 1972), pp. 41-80.

Bear, J., Dynamics of Flow Through Porous Media, (American Elsevier, New York, 1972).

Beetem, W., V. Janzer, C. Angelo, and M. Goldberg, Summary of Distribution Coefficients for Fission Products Between Groundwater and Granite Rocks, Climax Stock, USGS, Denver, Colorado, USGS Tech. Letter NTS-13 (Jan. 11, 1962).

Bell, M. T., "ORIGEN - The ORNL Isotope Generation and Depletion Code," Oak Ridge National Laboratory, Oak Ridge, Tenn., ORNL-4628 (1973).

506 242

Bernabo, J. C. and T. Webb, III, "Changing Patterns in the Holocene Pollen Record of Northeastern North America: A Map Summary," Quat. Res., 8(1), pp. 65-96 (1977).

Bernat, M. and E. Goldberg, "Thorium Isotopes in the Marine Environment," Earth Planet. Sci., Letters, 5, pp. 308-312 (1969).

Bernreuter, D. L., Lawrence Livermore Laboratory, personal communication (March 18, 1977).

Bernreuter, D. L. and L. Wight, Analysis of Some of the Major Parameters Influencing the Response Spectra for the Diablo Canyon Site, Lawrence Livermore Laboratory, UCRL-52263.

Boardman, C. R., D. D. Rabb and R. D. McArthur, "Contained Nuclear Detonations in Four Media - Geological Factors in Cavity and Chimney Formation," Proc. of the 3rd Plowshare Symposium, pp. 109-126 (1963).

Boardman, C. R. and J. Skrove, "Distribution in Fracture Permeability of a Granitic Rock Mass Following a Contained Nuclear Explosion," Journal of Petroleum Technology, 18, pp. 619-623 (May, 1966).

Boast, C. W., "Modeling the Movement of Chemicals in Soils by Water," Soil Science, 115(3), pp. 224-230 (1973).

Bondietti, E., S. Reynolds and M. Shanks, "Interactions of Plutonium with Complexing Substances in Soils and Natural Waters," in Proc. Symp. Transuranium Nuclides in the Environment, San Francisco, Nov., 1976 (IAEA, Vienna, 1976).

Booth, R. S., et al., "A Systems Analysis Methodology for Predicting Dose to Man from a Radioactively Contaminated Terrestrial Environment," Proc. of the Third National Symposium on Radioecology, Oak Ridge, May, 1971, pp. 877-893.

Borchert, H. and R. O. Muir, Salt Deposits - the Origin, Metamorphism and Deformation of Evaporites (D. Van Nostrand Company, New York, 1964), p. 338.

Borchert, H., "Secondary Replacement Processes in Salt and Potash Deposits of Oceanic Origin: Geology of Saline Deposits," Proc. of the Hanover Symposium, 1968, pp. 61-68.

Borg, I. Y., R. Stone, H. B. Levy and L. D. Ramspott, Information Pertinent to the Migration of Radionuclides in Ground Water at the Nevada Test Site, Part 1, Lawrence Livermore Laboratory, Livermore, Calif., UCRL-52078, (1976).

506 243

Bowen, V. T., et al., "Distributions of Transuranium Nuclides in Sediments and Biota of the North Atlantic Ocean," Woods Hole Oceanographic Institution, Conf-721105-21, November 1975.

Braitsch, O., Salt Deposits - Their Origin and Composition (Springer-Verlag, New York, 1971) p. 297.

Bredehoeft, J. D. and G. F. Pinder, "Mass Transport in Flowing Groundwater," Water Resources Research 9(1), (1973).

Broecker, W. S., "Climate Change: Are we on the Brink of a Pronounced Global Warming?" Science 189, pp. 460-463 (1975).

Brown, D., "Migration Characteristics of Radionuclides Through Sediments Underlying the Hanford Reservation," in Proc. Symp. Disposal of Radioactive Wastes Into the Ground, Vienna, May 29 - June 2, 1967 (IAEA, Vienna, 1967).

Burkholder, H., "Nuclear Waste Partitioning Incentives," in Proc. NRC Workshop on Management of Radioactive Waste: Waste Partitioning as an Alternaive, June 8 - 10, 1976, Seattle NR-CONF-001 (1976), pp. 444-481.

Burkholder, H. and M. Cloninger, The Reconcentration Phenomenon of Radionuclide Chain Migration, for Presentation at the 69th Annual Meeting of the American Institute of Chemical Engineers, Nov. 2, 1976 Battelle/Pac. Northwest Lab., Richland, WA, BNWL-SA-5786.

Claassen, H. C. and E. H. Cordes, "Two-Well Recirculating Tracer Test in Fractured Carbonate Rock, Nevada," Hydrological Sciences Bull. 20(3) (1975).

Claiborne, H. C. and F. Gera, Potential Containment Failure Mechanisms and Their Consequences at a Radioactive Waste Repository in Bedded Salt in New Mexico, Oak Ridge National Laboratory, Oak Ridge, Tenn., ORNL-TM-4639 (Oct., 1973).

Cloninger, M. and H. Burkholder, "The Reconcentration Phenomenon of Radionuclide Chain Migration," Nuclear Waste Management and Transportation Quarterly Progress Report, April through June, 1976, BNWL-2126 pp. 1.2-1.7.

Crosby, Armstrong and Paulson, "Mineral and Water Resources of North Dakota." No. Dakota Geol. Survey Bull. 63, (1973).

Csanady, G. T., Turbulent Diffusion in the Environment, (D. Reidel Publishing Co., Hingham, Mass., 1973).

Dahlman, R., E. Bondietti and L. Eyman, "Biological Pathways and Chemical Behavior of Plutonium and Other Actinides in the Environment," in Proc. Symp. Transuranium Nuclides in the Environment, San Francisco, Nov. 17-21, 1976 (IAEA, Vienna, 1976).

Davis, S. N., "Porosity, Permeability of Natural Materials," in Flow Through Porous Media, R. J. M. DeWiest, Ed. (Academic Press, New York, 1969), pp. 54-88.

Davis, S. N., and R. J. M. DeWiest, Hydrogeology, (John Wiley and Sons, Inc., New York, 1966).

De Groot, S. R., Thermodynamics of Irreversible Processes, (North Holland Publ. Co., Amsterdam, 1951).

DeWiest, R. J. M., "Green's Functions in Flow Through Porous Media," in Flow Through Porous Media, R. J. M. DeWiest, Ed. (Academic Press, N. Y., 1969).

Dlouhy, Z., "Movement of Radionuclides in the Aerated Zone," in Proc. Symp. Disposal of Radioactive Wastes into Ground, Vienna, 1967 (IAEA, Vienna, 1967), pp. 241-249 (SM-93/18).

Duguid, J. O. and M. Reeves, Material Transport Through Porous Media: A Finite-Element Galerkin Model, Oak Ridge National Laboratory, Oak Ridge, Tenn., ORNL-4928, (1976) p. 198.

Durie, R. W. and F. W. Jessen, "Mechanism of the Dissolution of Salt in the Formation of Underground Salt Cavities," Soc. of Pet. Eng. J., pp. 183-190 (1964a).

Dursuma, E. and P. Parsi, "Distribution Coefficients for Plutonium Between Sediment and Seawater," in Activities of the International Laboratory of Marine Radioactivity, IAEA-163, (1974) pp. 94-96.

Essington, E. and W. Nork, Radionuclide Contamination Evaluation - Milrow Event, Teledyne Isotopes, Nevada Operations Office, Las Vegas, Nevada, NVO-1229-117 (1969).

Fenske, P. R., Hydrology and Radionuclide Transport Monitoring Well HT-2m, Tatum Dome, Mississippi, Desert Research Institute, University of Nevada, Project Report No. 25, NVO-1253-6 (1973).

Fletcher, J. F. and W. L. Dotson, HERMES - A Digital Computer Code for Estimating Regional Radiological Effects from the Nuclear Power Industry, Hanford Engineering Development Laboratory, USAEC Report HEDL-TME-71-168 (1971).

506 245

Fried, J. J. and M. A. Combarnous, "Dispersion in Porous Media," in Advances in Hydrosciences 7, pp. 169-282 (1971).

Fried, S. And A. Friedman, "The Retention of Plutonium and Americium by Rock," Science 196, pp. 1087-1089 (1977).

Fritts, H. C., Tree Rings and Climate, (Academic Press, New York, 1977).

Gard, L. M., et al., Hydrologic and Geologic Studies, Project Gnome Report, PNE - 130F (1962).

Gard, L., et al., Hydrologic and Geologic Studies, Project Gnome Report, PNE - 130F (1962).

Gast, R., E. Landa, L. Thornig, The Behavior of Technetium - 99 in Soils and Plants, Progress Report April 1 - March 31, 1977 for ERDA (COO - 2447-5) p. 76.

Gates, W. L., "The Numerical Simulation of Ice-Age Climate with a Global General Circulation Model," J. Atmos. Sci., 33, pp. 1844-1873 (1976).

Gera, F., Geochemical Behavior of Long-Lived Radioactive Wastes, Oak Ridge National Laboratory, Oak Ridge, Tenn., ORNL-TM-4881 (July, 1975).

Glover, P., F. Miner and W. Polzer, Plutonium and Americium Behavior in the Soil/Water Environment. I. Sorption of Plutonium and Americium by Soils, Battelle Pac. Northwest Lab., Richland, WA, BMWL-2117 (1976), pp. 224-254.

Gloyna, E. F. and T. D. Reynold, "Permeability Measurements of Rock Salt," J. of Geophys. Research 66, pp. 3913-3921 (1961).

Godse, V., A. Mohan, M. Singh, R. Amalraj and K. Thomas, "Characterization of Tromboy Soils for Disposal of Radioactive Wastes," in Proc. Symp. Disposal of Radioactive Wastes into the Ground, Vienna, 1967 (IAEA, Vienna, 1967).

Goldberg, M., V. Janzer, C. Angelo and W. Beetem, The Effects of Sodium Ion Concentration on Distribution Coefficients for Tuffs from NTS, USGS Tech. Letter, NTS-16, Denver, Colorado (Feb. 26, 1962).

Golder Associates, Water Management in Oil Shale Mining, prepared for U.S. Bureau of Mines, 1977b.

Golder Assoc., Report S74009, 1975.

Golder Assoc., Report S77202, 1976a.

Golder Assoc., Report S76008, 1976b.

Golder Assoc., Report S76015, 1976c.

Golder Assoc , Report S77011, 1977a.

Golder Brawner and Assoc., Report V76354, 1976a.

Golder Brawner and Assoc., Report V75304, 1976b.

506 246

Golder Brawner and Assoc., Report V76302, 1976c.

Golder Brawner and Assoc., Report V76349, 1976d.

Gondouin, M. and C. Scala, Streaming Potential and the SP Log, Am. Inst. Mining Metal. Eng. Petroleum Trans., Tech. Paper 8023 (1958).

Grove, D., A Method to Describe the Flow of Radioactive Ions in Ground Water, Sandia Laboratory, Albuquerque, NM, SC-CR-70-6139 (December, 1970).

Grove, D. and W. A. Beetem, "Porosity and Dispersion Constant Calculations for a Fractured Carbonate Aquifer Using the Two-Well Tracer Method," Water Resources Research 7(1) 1974.

Hadley, J. and J. Device, A Seismotectonics Map of the Eastern U.S., USGS, MF620 (1974).

Hajek, B., Plutonium and Americium Mobility in Soils, Battelle Pac. Northwest Lab., Richland, WA, BNWL-CC-925 (1966) p. 7.

Hajek, B. and K. Knoll, Disposal Characteristics of Plutonium and Americium in a High Salt Waste, Battelle Pac. Northwest Lab., Richland, WA, BNWL-CC-649 (1966).

Hamaguchi, H., et al., "The Geochemistry of Tin," Geochim. Cosmochim. Acta. 28, pp. 1093-1153 (1964).

Hanks, T. C. and D. A. Johnson, Geophysical Assessment of Peak Accelerations, BSSA 66, pp. 959-968 (1976).

Hays, J. D., J. Imbrie, N. J. Shackleton, "Variations in the Earth's Orbit: Pacemaker of the Ice Ages," Science 194, pp. 1121-1132 (1976).

Heide, F. and J. Reichardt, "Tin Content in the Water of the Saale River," in Recent Contributions to Geochemistry and Analytical Chemistry, A. Tugarinov, Ed., (Wiley, New York, 1975) pp. 371-382.

Helgeson, H. C., "Complexing and Hydrothermal Ore Deposition," International Series of Monographs on Earth Sciences 17, (MacMillan, 1964) pp. 91-93.

Hetherington, J., D. Jefferies, N. Mitchell, R. Pentreath, and D. Woodhead, Environmental and Public Health Consequences of the Controlled Disposal of Transuranic Elements to the Marine Environment, IAEA-SM-199/11 (1975).

Hoffman, D., R. Stone and W. Dudley, Jr., Radioactivity in the Underground Environment of the Cambric Nuclear Explosive at the Nevada Test Site, La-6877-MS (1977) p. 89.

Huitt, J. L., "Fluid Flow in Simulated Fracture," J. Am. Inst. Chem. Eng. 2, pp. 259-264 (1956).

506 247

Illinois Power Company, Chicago, Ill., (1973), Preliminary Safe Analysis Report for the CLINTON Nuclear Power Station.

Inoue, Y., "Prediction of Radionuclide Migration in Groundwater at the Japan Atomic Energy Research Institute," in Proc. Symp. Disposal of Radioactive Wastes into the Ground, Vienna, May 29 - June 2, 1967 (IAEA, Vienna, 1967).

Isherwood, D., Lawrence Livermore Laboratory, personal communication July 14, 1977.

Katayama, T., K. Kubo and N. Sato, "Quantitative Analysis of Seismic Damage to Buried Utility Pipelines," Proc. of the 6th World Conf. on Earthquake Eng., New Delhi, 1977.

Kaufman, W., An Appraisal of the Distribution Coefficient for Estimating Underground Movement of Radioisotopes, Report HNS-1229-21 (1963).

Kazmann, R. G., Modern Hydrology (Harper and Row, New York, 1965) p. 109.

Kharaka, Y. and F. Berry, "Simultaneous Flow of Water and Solutes Through Geological Membranes--I. Experimental Investigation," Geochim. Cosmochim. Acta 37, pp. 2577-2603 (1973).

Lamb, H. H., Lawrence Livermore Laboratory, unpublished paper.

Landes, K. K., "Mackinac Breccia, in Geology of the Mackinac Straits Region," Michigan Geological Survey, Pub. 44, Chap. 3, pp. 123-154 (1945).

Lang, J. W., Geohydrologic Summary of the Pearl River Basin, Mississippi and Louisiana, U.S. Geol. Survey, Water - Supply Paper 1899-M (1972).

Lawrence Livermore Laboratory, Site Suitability Criteria for Solidified High Level Waste Repositories, Preliminary Progress Report, August, 1977.

Levy, H., On Evaluating the Hazards of Groundwater Contamination by Radioactivity From an Underground Nuclear Explosion, UCRL-51278 (1972) p. 24.

Louis, C., A Study of Groundwater Flow in Jointed Rock and Its Influence on the Stability of Rock Masses (in German). Ph.D. Thesis, University of Karlsruhe, (1967). English trans.: Imperial College Rock Mechanics Research Report 10 (September, 1969).

Lowry, M. E., Ground-Water Resources of Sheridan County, Wyoming, U.S. Geol. Survey, Water-Supply Paper 1807 (1966).

Maini, Y. N., In Situ Parameters in Jointed Rock - Their Measurement and Interpretation, Ph.D. Thesis, University of London, Imperial College (1971).

Manger, G. E., Porosity and Bulk Density of Sedimentary Rocks. U.S. Geol. Survey, Bull. 1144-E (1963).

506 248

Marine, I. W., "Geohydrology of Buried Triassic Basin at Savannah River Plant, South Carolina," in 2nd International Symp. on Underground Waste Management and Artificial Recharge, New Orleans, La., Sept. 26-30, 1973. (Amer. Assoc. Petrol. Geol., Tulsa Okla., 1973) V. 1, pp. 481-504.

Maxey, G. B., "Hydrostratigraphic Units," Journal of Hydrology 2, pp. 124-129 (1964).

McGuire, R. K., FORTRAN Computer Program for Seismic Risk Analysis USGS Open File Report 76-67 (1976).

McGuire, R. K., "Effects of Uncertainty in Seismicity on Estimates of Seismic Hazard for the East Coast of the U.S.," BSSA, in press.

McNeal, R. P., "Hydrodynamics of the Permian Basin," in Fluids in Subsurface Environments, Amer. Assoc. Petrol. Geol. Memoir 4, pp. 308-326 (1965).

Miner, F., P. Glover and W. Polzer, "Plutonium Behavior in the Soil/Water Environment I. Sorption of Plutonium by Soils," Agronomy Abstracts, p. 35 (1974).

Mo, T. and F. Lowman, Laboratory Experiments on the Transfer Dynamics of Plutonium from Marine Sediments to Seawater and to Marine Organisms, CONF-750503-5, p. 35 (1975).

Muskat, M., The Flow of Homogeneous Fluids Through Porous Media (McGraw-Hill, New York, 1973).

Neal, V. T., "Physical Aspects of the Columbia River and its Estuary," in The Columbia River Estuary and Adjacent Ocean Waters, A. T. Pruter and D. L. Alverson, Eds., (University of Washington Press, Seattle and London, 1972), pp. 19-40.

Nishiwaki, Y., et al., "Behavior and Distribution of Radioactive Substances in Coastal and Estuarine Waters," in Radioactive Contamination of the Marine Environment, IAEA-SM-158/11, pp. 177-193 (1972).

Nork, W. and P. Fenske, Radioactivity in Water - Project Rulison, Nevada Operations Office, AEC, NVO-1229-131 (1970).

Nork, W., E. Forslow, and E. Essington, Radioactivity in Water, Central Nevada Test Area, Nevada Operations Office, AEC, NVO-1229-175 (1971).

Noshkin, V., K. Wong, K. Marsh, R. Eagle, G. Halladay and R. Buddemeier, "Plutonium Radionuclides in the Groundwaters at Eniwetok Atoll," in Proc. Sym. Transuranium Nuclides in the Environment, San Francisco, Nov. 17-21, 1976, (IAEA, Vienna, 1976) pp. 517-543.

Noshkin, V., Lawrence Livermore Laboratory, personal communication (1977).

506 249

O'Brien, L. J., J. R. Murphy and J. A. Lahoud, The Correlation of Peak Ground Acceleration Amplitude with Seismic Intensity and Other Physical Parameters, Computer Sciences Corporation, Washington, D.C., Final Tech. Report to U.S. NRC (March, 1976).

O'Neil, R. V., "Error Analysis of Ecological Models," in Proc. of the Third Nat'l. Symp. on Radioecology (Oak Ridge, Tennessee, May, 10, 1971).

Parsons, P., "Underground Movement of Radioactive Wastes at Chalk River," in Proc. Conf. Groundwater Disposal of Radioactive Wastes, 2nd, Chalk River, Canada, Sept. 1961, (U. S. AEC) TID - 7628 (March, 1962).

Parsons, Brinckerhoff, Quade and Douglas, Inc., Thermal Guidelines for a Repository in Bedrock. NTIS, Y/OWI/SUB-76/16504 (Sept., 1976).

Pfannkuch, H. O., "Contribution a l'etude des deplacements des fluides miscibles dans un milieu poreux," Inst. Francais du Petrole, (1962), cited in J. Bear, "Hydrodynamic Dispersion," in Flow Through Porous Media, R. J. M. DeWiest, Ed. (Academic Press, New York, 1969).

Pickens, J. F. and W. C. Lennox, "Numerical Simulation of Waste Movement in Steady Ground Water Flow Systems," Water Resources Research 12(2) pp. 171-180 (1976).

Pillai, K. and E. Mathew, "Plutonium in the Aquatic Environment: Its Behavior, Distribution and Significance," in Proc. Symp. Transuranium Nuclides in the Environment, San Francisco, Nov. 17-21, 1976 (IAEA, Vienna, 1976) pp. 25-45.

Pinder, G. F., "A Galerkin Finite-Element Simulation of Ground-Water Contamination on Long Island, New York," Water Resources Research 9(6) (1973).

Plum, R., Golder Associates, personal communication (June 22, 1977).

Pruter, A. T., "Review of Commercial Fisheries in the Columbia River and in Contiguous Ocean Waters," in The Columbia River Estuary and Adjancent Ocean Waters, A. T. Pruter and D. L. Alverson, Eds. (University of Washington Press, Seattle and London, 1972) pp. 41-81.

Rabinowitz, D. D. and G. W. Gross, Environmental Tritium as a Hydrometeorologic Tool in the Roswell Basin, New Mexico, Tech. Completion Report, New Mexico Water Resources Research Institute, Las Cruces, New Mexico, OWRR A-037-NMEX (1972).

506 250

Rancon, D., "The Behavior in Underground Environments of Uranium and Thorium Discharged by the Nuclear Industry," (in French) in Environmental Behavior of Radionuclides Released in the Nuclear Industry, IAEA-SM 172/55, pp. 333-346 (1973).

Rasmussen, W. F., "Permeability and Storage of Heterogeneous Aquifers in the U.S.," Int. Assoc. of Sci. Hydrology Pub. 64, pp. 317-325 (1963).

Robertson, J. and J. Barroclough, "Radioactive and Chemical - Waste Transport in Groundwater at National Reactor Testing Station, Idaho: 20 Year Case History and Digital Model," in Underground Waste Management and Artificial Recharge, J. Brounstein, Ed., (Amer. Assoc. Pet. Geol., 1973) pp. 291-322.

Routson, R., G. Jansen and A. Robinson, Sorption of ^{99}TC, ^{237}Np, and ^{241}Am on Two Subsoils from Differing Weathering Intensity Areas, BNWL-1889, p. 15 (1975).

Rowe, J., Golder Associates, personal communication (July 13, 1977).

Scheidegger, A. E., "On the Theory of Flow of Miscible Phases in Porous Media," Compt. Rend. Assem. Gen. Toronto, Assoc. Intern. Hydrol. Sci. 2, pp. 236-242 (1957).

Scheidegger, A. E., "General Theory of Dispersion in Porous Media," J. Geophysical Res. 66(10) (1961).

Scheidegger, A. E., "Statistical Hydrodynamics in Porous Media," Adv. Hydrosciences 1, (1964). pp. 161-181.

Schneider, K. J and A. M. Platt, High-Level Radioactive Waste Management Alternatives, Battelle Pa. Northwest Lab., Richland, WA, BNWL-1900 (1974).

Sharp, J. C., Fluid Flow Through Fractured Media, Ph.D. Thesis, University of London Imperial College (1970).

Snow, D. T., "Rock Fracture Spacings, Openings and Porosities," Journal Soil Mech. Foundation Div., 94, pp. 73-91 (1968).

Snow, R. H. and D. S. Chang, Prediction of Cavity Growth by Solution of Salt Around Boreholes, Union Carbide Corporation, Nuclear Division, IITRIC6313-14 (1975) p. 43.

Snow, R. H. and H. J. Nielsen, "IITRI-SMRI Solution Mining Studies," 3rd Symp. on Salt, N. Ohio Geo. Soc., Inc., 1970, pp. 341-359.

Soldat, J., et al., Models and Computer Codes for Evaluating Environmental Radiation Doses, Battelle Pacific Northwest Laboratories, Richland, WA, USAEC Report BNWL-1754, (February, 1974).

506 251

Soldat, J., et al., Food - An Interactive Code to Calculate Internal Radiation Doses from Contaminated Food Products, Battelle Pacific Northwest Laboratories, Richland, WA, USERDA Report BNWL-SA-5523 (February, 1976).

Stanton, R. J., "The Solution Brecciation Process," Geo. Soc. of Am. Bulletin 77, pp. 843-848 (1966).

Stead, F., "Distribution in Groundwater of Radionuclides from Underground Nuclear Explosions," in Proc. 3rd Plowshare Symp. (Lawrence Livermore Laboratory) TID - 7695 (1964).

Stead, F., "Tritium Distribution in Groundwater Around Large Underground Fusion Exploration," Science, 142, pp 1163-1165 (1963).

Stevens, P. R., Effects of Earthquakes on Underground Mines. USGS Open-File Report 77-313, 1977.

Streltsova, T. D., "Hydrodynamics of Groundwater Flow in a Fractured Formation," Water Resources Research 12(3) (June 1976) pp. 405-414.

Swenson, F. A., "New Theory of Recharge to the Artesian Basin of the Dakotas," Geol. Soc. Amer. Bull. 79(2) (1968).

Taylor, R. L. and C. B. Brown, "Darcy Flow Solutions with a Free Surface," Proc. Am. Soc. Civil Eng. Hydraulics Div., Vol. 93, No. HY2, March 1967, pp. 25-33.

Todd, D. K., Ground Water Hydrology (John Wiley and Sons, Inc., New York, 1959), pp. 5-7

Trifunac, M.D., Preliminary Analysis of the Peaks of Strong Earthquake Ground Motion - Dependence of Peaks on Earthquake Magnitude, Epicentral Distance and Recording Site Conditions, BSSA 66 (1976).

U.S. Department of Commerce, Fisheries Statistics of the U.S., 1972, Statistics and Market News Division, Washington, D. C., NOAA-NMFS.

U.S. Nuclear Regulatory Commission, "Reactor Safety Study: An Assessment of Accident Risks in the U.S. Commercial Nuclear Power Plants. Appendix VI. Calculation of Reactor Accident Consequences," WASH- 1400, October, 1975.

U.S. Nuclear Regulatory Commission, Office of Standards Development, "Calculation of Annual Doses to Man from Routine Releases of Reactor Effluents for the Purpose of Evaluating Compliance with 10 CFR Part 50, Appendix I," NRC Regulatory Guide 1.109 (March 1976)

U.S. Nuclear Regulatory Commission, Draft Liquid Pathways Generic Study, NUREG-0140 (September, 1976).

506 252

Van Dalen, A. F. deWitte and J. Wiskstra, "Distribution Coefficients for Some Radionuclides Between Saline Water and Clays, Sandstones, and other Samples from the Dutch Subsoil," Reactor Centrum Nederland, pp. 75-109 (1975).

[illegible], J. D., "Recent domal structures in Southeastern New Mexico", Am. Assoc. of Pet. Geo. Bull. 44 (12) pp. 1903-1911 (1960).

[illegible], M., J. Alberts, D. Nelson and K. Orlandi, "Study of the Behavior of Transuranics and Possible Chemical Homologues in Lake Michigan Water and Biota," in Transuranium Nuclides in the Environment, San Francisco, Nov. 17-21, 2975 (IAEA, Vienna, 1976) pp. 9-23.

[illegible], R. M., Effect of the March 1964 Alaska Earthquake on the Hydrology of South Central Alaska. USGS Prof. Paper 544-A (1966), p. 27.

[illegible], D. E., State-of-the-Art for Assessing Earthquake Hazards in the United States, Reports, Plate Tectonics and Earthquake Assessment, U.S. Army Eng. Waterways Experiment Station, CE, Vicksburg, Miss., Misc. paper S-73-1 (March 1976).

[illegible], T. R., A Study of the Joint Patters in Gently Dipping Sedimentary Rocks of South and Central Kansas. State Geological Survey of Kansas, Bulletin 191, Part 2 (1968).

[illegible], B. S., J. F. Proctor and I. W. Marine. Two-Well Tracer Test in Fractured Crystalline Rock. USGS Water-Supply Paper 1544-I (1970).

[illegible], G. E. and E. P. Weeks, Hydrologic Conditions Near Glendo, Platte County, Wyoming, USGS Water-Supply Paper 1971, (1965).

[illegible], R. et al., "Pertechnetate, Iodide and Methyl Iodide Retention by Surface Soils," in BNWL 1950, Part 2 (1974) pp. 37-40.

[illegible] Market Analysis, U.S. Statistical Atlas, 1973.

[illegible], W. O., H. H. Shearin, Jr., P. H. Masson and M. Williams, "Resistivity of Brine-Saturated Sands in Relation to Pore Geometry," Amer. Assoc. Petroleum Geol. Bull. 36, pp. 253-277 (1952).

[illegible], M. R. J. and M. B. Spangler. "Application of Electrical Resistivity Measurements to Problem of Fluid Flow in Porous Media," Am. Assoc. Petrol Geol. Bull. 36, pp. 359-403 (1952).

506 253

APPENDIX A

AVAILABLE SOLUTE TRANSPORT COMPUTER CODES

The following computer codes are suitable for solute transport modeling. Other programs are not as available as those discussed below, nor are they more appropriate for generic transport problems. Codes marked with asterisks are currently in use at Lawrence Livermore Laboratory.

Simple models. These codes operate in a maximum of two dimensions. The effects of variable temperature and salinity are not considered.

- USGS Program, written by D. Grove, U.S. Geological Survey, Denver. This model interfaces a finite difference flow model by Pinder and Bredehoft with transport solutions using finite elements, finite differences, or method of characteristics as desired. Documentation is poor, and input is inefficient. Porosity is considered constant. It is compiled on a CDC 7600.
- Waterloo Program, written by J. Pickens, University of Waterloo, Canada. This model solves transient transport problems in a steady-state flow field by finite element methods. Quality of documentation is unknown.
- ISOQUAD, developed at Princeton University. The program solves transient transport problems in a steady-state flow field by finite element methods. The quality of documentation is unknown.
- Oakridge Model*, written by J. Duguid and M. Reeves, Oak Ridge National Laboratory. This model solves transient solute transport problems in cross section using finite element methods. It can be coupled with a saturated-unsaturated flow model. The documentation is good.
- Taylor model*, written by R. Taylor, University of California, Berkeley. This model solves the 2-D steady-state flow field by finite element techniques.

506 254

Complex models. These codes can solve the transport problem in one, two, and three dimensions.

- TRUMP*, written by A. Edwards, Lawrence Livermore Laboratory. This code solves a set of simultaneous partial differential transport equations with four independent variables and three primary dependent variables using integrated finite difference techniques. Originally developed for geothermal applications, the program can be used to solve both flow and transport problems. Complex boundaries are easily handled, but permeability and dispersion coefficients are treated as scalars. Currently, TRUMP is being used on the NRC project by H. Cheung to model thermal gradients near the repository site.
- BIFEPS*, developed primarily by C. Voss, Princeton University. This code uses block iterative finite element methods to solve coupled nonlinear, second order, partial differential equations.
- DAVIS/3FE, written by S. K. Gupta jointly at Uuniversity of California, Davis and Princeton University. This program computes transient flow and salt transport in large multiaquifer basins using finite element methods.
- INTERCOMP, developed by Intercomp and U.S. Geological Survey for Sandia. This code is a transient, finite difference solution for deep-well waste-disposal systems. Viscosity and density are considered functions of pressure, temperature, and composition. Decay rates may be calculated at each time change or at the end of the program.
- OGRE*, written by J. Korver, Lawrence Livermore Laboratory. This code solves the coupled, time-dependent hydrology and material transport equations in two dimensions by finite difference techniques. It has variable grid scaling that allows fine-scale resolution of the central features being modeled.

506 255

APPENDIX B

ONE-DIMENSIONAL APPROXIMATION TO DISPERSIVE FLOW IN POROUS MEDIA

The WASTE model of flow through porous media comprises a series of interconnected one-dimensional flow paths. This approach eliminates the problem of solving two- or three-dimensional transport equations for an extensive variety of changing parameters and geologic states. The simplification is justified on both pragmatic and mathematical grounds. It is not practical to perform extensive sensitivity analysis on multistate generic repository models without such simplification. Further, modeling flow as a series of linear pathways is advantageous. The dynamics are decomposed into a fundamental form that makes the processes easier to understand.

Mathematically the flow paths represent stream tubes, and the complexity of the fluid flow defines the number and positioning of the flow paths. We chose simple flow fields for our initial models. More complicated and more realistic flow fields determined by two- and three-demensional hydrology programs can be considered at a later date.

Given certain constraints, the transport equation for dispersive flow reduces to a simple one-dimensional flow model in stream coordinates. Generally, transport of radionuclides in porous media is described by a diffusivity equation (Scheidegger, 1964). Hence, if the concentration of nuclide r in the interstitial water is $C_r(\underline{x}, t)$ and the interstitial fluid velocity is $\underline{v}$, then

$$-\frac{\partial C_r}{\partial t} = \frac{\partial}{\partial x_i} D_{ij} \frac{\partial}{\partial x_j} C_r - \frac{\partial}{\partial x_i} (v_i C_r) - \lambda r\, C_r$$

$$+ \sum_{s \neq r} \lambda_s^r C_s - \frac{\partial m_r}{\partial t} - \lambda_r m_r + \sum_{s \neq r} - \lambda_s^r m_r \qquad \text{(B-1)}$$

506 256

Here D_{ij} is the coefficient of convective dispersion, λ_r is the radioactive decay constant, λ_s^r is the production rate of nuclide r from decay of nuclide s, m_r is the amount of ion absorbed on the solid per unit volume, and the subscripts i and j refer to two of the three Cartesian coodinates. We have adopted the convention that when subscripts referring to coordinate axes are repeated in a term, they are to be summed over. This equation may be further simplified by dropping the r subscript to

$$B \frac{\partial c}{\partial t} = \frac{\partial}{\partial x_i} D_{ij} \frac{\partial c}{\partial x_j} - \frac{\partial}{\partial x_i} (v_i c) \quad , \tag{B-2}$$

where B is the retardation factor and $c(\underline{x},t)$ is C_r divided by the amount of nuclide r from repository waste in existence at time t.

We assume that D_{ij} reduces to a linear function of the flow velocity in the one-dimensional case (Grove, 1970; Scheidegger, 1957; Pfannkuch, 1969). This assumption requires some additional comment. We have implicitly assumed that flow due to diffusion is negligible when compared to dispersion. A linear relation between D_{ij} and $|\underline{v}|$ is acceptable in this regime. If diffusion becomes important, our equations do not apply: time would not be sufficient for the nuclide to migrate to the biosphere.

The most simple form of D_{ij} must now be

$$D_{ij} = \frac{a_{ij\ell m} v_\ell v_m}{V} \tag{B-3}$$

where $V = |\underline{v}|$ (Scheidegger, 1964).
The tensor $a_{ij\ell m}$ is called the dispersivity tensor of the porous medium. If it is now assumed that $a_{ij\ell m}$ is an isotropic tensor,

$$a_{ij\ell m} = (\alpha-2\mu)\, \delta_{ij}\, \delta_{\ell m} + \mu(\delta_{i\ell}\delta_{jm}+\delta_{j\ell}\delta_{im}) + \nu(\delta_{i\ell}\delta_{jm}-\delta_{j\ell}\delta_{im}) \quad , \tag{B-4}$$

506 257

where δ_{ij} is a Kronecker delta function; i, j, ℓ, and m are Cartesian coordinate indices; and α, μ, and ν are dispersion constants. Substituting Eq. B-4 into Eqs. B-2 and B-3 leads to

$$D_{ij} = (\alpha-2\mu)\ \delta_{ij}\ V + \frac{2\mu v_i v_j}{V}$$

and

$$B\ \frac{\partial c}{\partial t} + \frac{\partial}{\partial x_i}\ (v_i\ c) = (\alpha-2\mu)\frac{\partial}{\partial x_i}\ \nu\frac{\partial c}{\partial x_i} + 2\mu\ \frac{\partial}{\partial x_i}\ \frac{v_i v_j}{V}\ \frac{\partial c}{\partial x_j}\ . \qquad \text{(B-5)}$$

For steady, incompressible flow $\nabla\cdot\underline{v} = 0$ and the above equation simplifies to

$$B\ \frac{\partial c}{\partial t} + \underline{v}\cdot\nabla c = (\alpha-2\mu)\ \nabla\cdot(V\nabla c) + 2\mu(\underline{v}\cdot\nabla)\ \frac{1}{V}\ (\underline{v}\cdot\nabla)c\ . \qquad \text{(B-6)}$$

We now rewrite this equation in coordinates determined by the velocity field. The natural coordinates (S,N,T) are those where S represents the distance along a streamline in the direction of stream flow. The equation reduces to

$$B\ \frac{\partial c}{\partial t} + V\ \frac{\partial c}{\partial S} = \alpha\ V\ \frac{\partial^2 c}{\partial S^2} + \frac{(\alpha-2\mu)}{h_1 h_3}\ \frac{\partial}{\partial N}\ (h_1 h_3 V)\ \frac{\partial c}{\partial N} + \frac{(\alpha-2\mu)}{h_1 h_2}\ \frac{\partial}{\partial T}\ (h_1 h_2 V)\ \frac{\partial c}{\partial T}\ . \qquad \text{(B-7)}$$

Here h_1, h_2, and h_3 are the scale factors. The similarity of this equation to the familiar result for $\underline{v} = V\hat{i}$, and V constant is clear, i.e.,

$$B\ \frac{\partial c}{\partial t} + V\ \frac{\partial c}{\partial x} = \alpha\ V\ \frac{\partial^2 c}{\partial x^2} + (\alpha-2\mu)\ V\left(\frac{\partial^2 c}{\partial y^2} + \frac{\partial^2 c}{\partial z^2}\right)\ . \qquad \text{(B-8)}$$

We now wish to average Eq. B-7 across the stream tube. The rate at which velocity and the concentration gradient drop off in the N and T directions determines the area over which to integrate. For example, if a source introduces an impluse at time zero into a flow path in which V is a constant, the concentration falls off with radial direction r as $\exp(-r^2/4L(\alpha-2\mu))$. Here L represents the distance the pulse has traveled. For a flow path 200 m long and with $(\alpha-2\mu)$ = 10 m, the pulse would spread about 180 m by the time it left the flow path.

506 258

Returning to Eq. B-7, we note that in this formulation S, N, and T represent distances along coordinate axes. Hence, the order of differentiation cannot (in general) be interchanged. Introducing coordidnates (S*,N*,T*) where $dS = h_1 dS^*$, $dN = h_2 dN^*$, and $dT = h_3 dT^*$, and integrating over the cross-sectional area of the flow path we have

$$B \frac{\partial}{\partial t} \iint_A c h_1 h_2 h_3 dN^* dT^* + \frac{\partial}{\partial S^*} \iint_A V c h_2 h_3 dN^* dT^*$$

$$= \alpha \frac{\partial}{\partial S^*} \iint_A \frac{V}{h_1} \frac{\partial c}{\partial S^*} h_2 h_3 dN^* dT^* \qquad \text{(B-9)}$$

The area of the stream tube, the mean velocity, and the mean concentrations can now be defined as

$$W = \iint_A h_2 h_3 dN^* dT^*$$

$$\tilde{V} = \iint_A V h_2 h_3 dN^* dT^* / W$$

$$\tilde{c} = \iint_A V c h_2 h_3 dN^* dT^* / W \tilde{V} \qquad \text{(B-10)}$$

$$\langle c \rangle = \iint_A c h_2 h_3 dN^* dT^* / W$$

If h_1 is, to a first order approximation, independent of N* and T* across the flow path, it may be taken outside of the integrals and we have approximately

$$B \frac{\partial \langle c \rangle}{\partial t} + \tilde{V} \frac{\partial \tilde{c}}{\partial S^*} = \alpha \tilde{V} \frac{\partial^2 \tilde{c}}{\partial S^2} \qquad \text{(B-11)}$$

The constraint on h_1 is equivalent to requiring the integral of the curvature across the stream to be much less than one.

Several situations exist for which the averaged equation may not be a good representation of transport. Figure B-1 shows a stream tube branching into two parts. The initial concentration in each branch is the same, since the

506 259

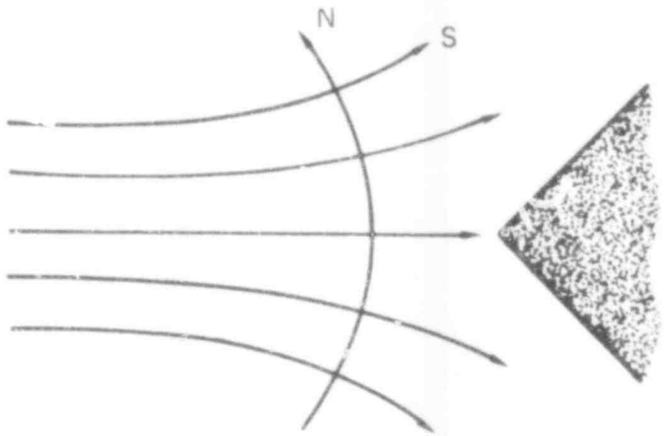

FIG. B-1. Branching of a stream tube.

506 260

concentration is averaged over the width of the stream. To represent situations in which the mixing is not expected to be complete at a given node, mixing factors can be included in the program. For example, the concentration of waste entering a borehole at the repository may not be the same as the mean concentration of waste over the entire repository.

Figure B-2 shows a possible situation not currently handled by the WASTE program. Here most of the waste flows laterally in a layer that only partially connects to the biosphere. The upper, faster-moving layer flows directly to a river or lake. Waste can migrate upward from the lower layer, because of dispersion, and enter the biosphere. Since our stream tube in this case consists only of the lower layer, the amount of waste entering the river is underestimated. Furthermore, since the upper layer is moving faster than the lower layer, waste will reach the river more quickly. This situation occurs only when a large fraction of the waste in the lower layer does not flow directly into the river. Therefore, this mechanism for release is, in general, of less concern than one in which all the waste in the lower layer enters the river.

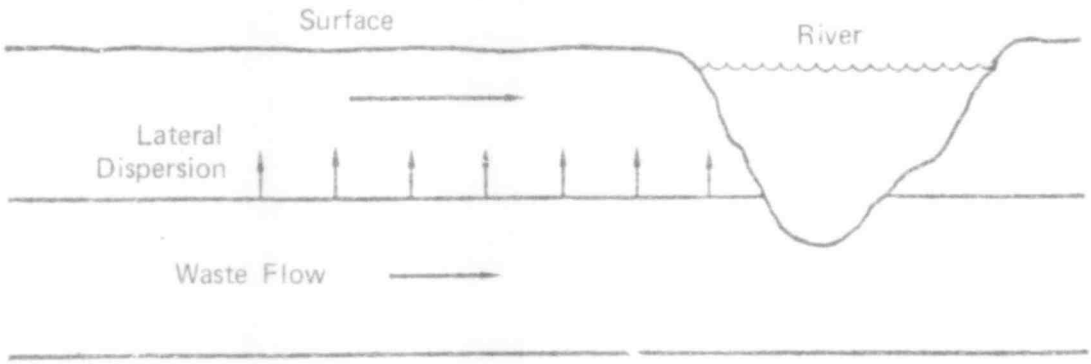

FIG. B-2. Dispersive flow into a river.

506 261

APPENDIX C

METHOD USED TO OBTAIN EXPECTED VALUES

INTRODUCTION

Migration of radioactive waste in the ground may be affected by future events, such as faulting or dissolution of engineered seals. Such events can usually be predicted only on a probabilistic basis. Their consequences depend on their sequence and timing. Therefore, a scenario-by-scenario study of waste transport would require study not merely of the possible events, but of the far greater number of possible histories that a repository might experience as it passes from state to state. To measure the overall potential hazard of a waste repository, one must calculate expected values of radionuclide releases. This appendix describes the method developed for that purpose.

A total system composed of the repository, the waste, and the different pathways by which the waste might reach the biosphere, is described by a geologic state and a waste distribution. The geologic state is defined by the condition of the rock layers in which the repository is located and of the pathways. For a given geologic state, all the system variables governing waste transport, such as the permeability and porosity of different rock layers and the velocity field of ground water, will be uniquely defined. The waste distribution describes the actual concentration of radioactive waste in the repository and the different pathways at any given time. This appendix derives an equation for the expected value of the waste distribution in terms of the equations for waste flow in each geologic state and the rates of transition between geologic states.

506 262

MATHEMATICAL DERIVATION

The derivation begins with the observation that the concentration of waste nuclides in groundwater at any point may depend on the whole history of the repository area from emplacement to the time being considered. Therefore, concentration at time t depends not only on the current geologic state g(t), but on the entire evolution of the geologic state from zero to t. The history of the geologic system will be denoted by h. Each value of h is an entire realization of the stochastic process whose value at time t is the random variable g(t). The expected value of the concentration of any radionuclide r at point $\underline{x}$, $C_r(\underline{x};h,t)$ will be given by integrating over all histories

$$E(C_r(\underline{x},t)) = \int C_r(\underline{x};h,t)\, p(h)\, dh \quad , \tag{C-1}$$

where p(h) is the probability density of history h.

We assume that waste transport is described by an equation of the form

$$\frac{\partial}{\partial t} C_r(\underline{x};h,t) = L^{(h)} C_r(\underline{x};h,t) + \sum_{s \neq r} \lambda_s^r C_s(\underline{x};h,t) \quad , \tag{C-2}$$

where for any h, $L^{(h)}$ operates on the spatial coordinates of C_r; λ_s^r is the rate at which nuclide s decays into nuclide r, and is equal to ln 2 divided by the half-life of nuclide s if nuclide s always decay into r. This assumption is consistent with the usual equation for flow of dissolved material in groundwater (Scheidegger, 1964), which in one dimension takes the form

$$\frac{\partial C_r}{\partial t} = \left[-V_{ion} \frac{\partial}{\partial x} + \alpha V_{ion} \frac{\partial^2}{\partial x^2} - \lambda_r \right] C_r \quad , \tag{C-3}$$

where V_{ion} is the advection velocity of the ions, α is the dispersion constant, and λ_r is the decay rate of nuclide r.

506 263

We wish to obtain an equation for waste transport that does not involve the history h, but only the current state g. To do so, we define a quantity ϕ_r by integrating over all histories h which reaches state g at time t.

$$\phi_r(\underline{x};g,t) = \int_{\Omega:\{h(t)=g\}} C_r(\underline{x};h,t)\, p(h)\, dh \qquad (C\text{-}4)$$

The integral is taken over all realizations h of the random process that takes the value g at time t. In subsequent equations this integration will be understood and the Ω and brackets will be omitted. ϕ_r may be interpreted physically as the expected value of concentration of nuclide r at point $\underline{x}$, given that the system is in state g, multiplied by the probability that the system is in g. This quantity is analogous to the previously defined $F(r,\ell,m,n)$; F_r is related to mass flux integrated over interval ℓ in the same way as ϕ_r is related to concentration. By comparing Eq. C-1 and Eq. C-4, we see that expected concentrations may be calculated from the relationship

$$E(C_r(\underline{x},t)) = \sum_g \phi_r(\underline{x};g,t) \qquad (C\text{-}5)$$

For this definition to be useful, we must derive an equation for the evolution of ϕ_r that does not depend on h. We begin by taking the time derivative of Eq. C-4. To deal with the summation over histories, we must explicitly use the definition of the derivative

$$\frac{\partial}{\partial t}\phi_r(\underline{x};g,t) = \lim_{\Delta t\to 0} \frac{1}{\Delta t}\left\{\int_{h(t+\Delta t)=g} C_r(\underline{x};h,t+\Delta t)\, p(h)\, dh - \int_{h(t)=g} C_r(\underline{x};h,t)\, p(h)\, dh\right\} \qquad (C\text{-}6)$$

To separate out the time dependence of C_r, we add and subtract identical terms

506 264

$$\frac{\partial}{\partial t}\ \phi_r(\underline{x};g,t) = \lim_{\Delta t\to 0}\ \frac{1}{\Delta t}\ \left\{ \int_{h(t+\Delta t)=g} C_r\ (\underline{x};h,t+\Delta t)\ p(h)dh \right.$$

$$- \int_{h(t+\Delta t)=g} C_r(\underline{x};h,t)\ p(h)\ dh + \int_{h(t+\Delta t)=g} C_r(\underline{x};h,t)\ p(h)\ dh$$

$$\left. - \int_{h(t)=g} C_r(\underline{x};h,t)\ p(h)\ dh \right\} \quad . \tag{C-7}$$

The first two terms are integrals over the same range of values of h, and thus can be combined and simplified by using Eq. C-2

$$\lim_{\Delta t\to 0} \int_{h(t+\Delta t)=g} p(h)\ \frac{C_r(\underline{x};h,t+\Delta t) - C_r(\underline{x};h,t)}{\Delta t}\ dh$$

$$= \int_{h(t)=g} p(h)\ \frac{\partial}{\partial t}\ C_r(\underline{x};h,t)dh$$

$$= \int_{h(t)=g} p(h)\ L^{(h)} C_r(\underline{x};h,t)dh$$

$$+ \sum_{s\neq r} p(h)\ \lambda_s^r\ C_s(\underline{x};h,t)\ dh \quad . \tag{C-8}$$

To simplify the two remaining terms of Eq. C-7, we must assume that the range of possible states g is countable. Canceling terms that appear in both integrals, we then obtain

$$\lim_{\Delta t\to 0}\ \frac{1}{\Delta t}\ \left\{ \int_{\substack{h(t+\Delta t)=g \\ \text{and } h(t)\neq g}} C_r(\underline{x};h,t)\ p(h)\ dh \right.$$

$$\left. - \int_{\substack{h(t)=g \text{ and} \\ h(t+\Delta t)\neq g}} C_r(\underline{x};h,t)\ p(h)\ dh \right\}$$

$$= \lim_{\Delta t\to 0}\ \frac{1}{\Delta t}\ \left\{ \sum_{g'\neq g} \int_{\substack{h(t+\Delta t)=g \\ \text{and } h(t)=g'}} C_r(\underline{x};h,t)\ p(h)\ dh \right.$$

$$\left. - \sum_{g'\neq g} \int_{\substack{h(t)=g \text{ and} \\ h(t+\Delta t)=g'}} C_r(\underline{x};h,t)\ p(h)\ dh \right\} \quad . \tag{C-9}$$

506 265

Proceeding further, we examine more closely the role of h. The variable h represents the geologic history over the entire time period of concern in the analysis. We define two partial histories, e and f, as the histories from time zero through times t and $t+\Delta t$, respectively. If each value of h is thought of a sequence of states, each value of e or f will be a shorter sequence. Each sequence e or f will be included in many different h's. Different partial histories f that are identical through time t and then reach different states at time $t+\Delta t$ will all include the same partial history e.

It is reasonable to assume causality, i.e.,that the concentration of waste at a given time will depend only on the previous geologic states of the system and not on what happens at subsequent times. For all histories h that include the same partial history f, $C_r(\underline{x};h,t)$ are then identical. All the terms in Eq. C-9 corresponding to the same f can be grouped together, and the right hand side of that equation can be written as

$$\lim_{\Delta t \to 0} \frac{1}{\Delta t} \left\{ \sum_{g' \neq g} \int_{S_{g'g}} C_r(\underline{x};f,t)\, p(f)\, df - \sum_{g' \neq g} \int_{S_{gg'}} C_r(\underline{x};f,t)\, p(f)\, df \right\} . \qquad \text{(C-10,}$$

We have denoted the space of partial histories f that pass through state a at time t and through b at time $t+\Delta t$ as S_{ab}. The membership of S_{ab} will change when the value of Δt is varied.

Each space S_{ab} may be partitioned into subspaces S^e_{ab}. Each subspace S^e_{ab} consists of all those partial histories f that follow a particular partial history e from time zero to t, at which time they have reached state a, and then reach state b at time $t+\Delta t$, as shown schematically in Fig. C-1. Since S_{ab} is equal to the union of all the S^e_{ab} corresponding to different e that reach state a at time t, we may rewrite our integrals to obtain

506 266

$$\lim_{\Delta t \to 0} \frac{1}{\Delta t} \left\{ \sum_{g' \neq g} \int_{e(t)=g'} de \int_{S^e_{g'g}} df\, C_r(\underline{x};f,t)\, p(f) - \sum_{g' \neq g} \int_{e(t)=g} de \int_{S^e_{gg'}} df\, C_r(\underline{x};f,t)\, p(f) \right\} \tag{C-11}$$

We now invoke causality again to make concentration C_r at time t a function only of e and not of f. Since only the integral over f depends on Δt, the order of operations can be altered to obtain

$$\sum_{g' \neq g} \int_{e(t)=g} de\, C_r(\underline{x};e,t) \lim_{\Delta t \to 0} \frac{1}{\Delta t} \int_{S^e_{g'g}} p(f)\, df - \sum_{g' \neq g} \int_{e(t)=g} de\, C_r(\underline{x};e,t) \lim_{\Delta t \to 0} \frac{1}{\Delta t} \int_{S^e_{gg'}} p(f)\, df \cdots \tag{C-12}$$

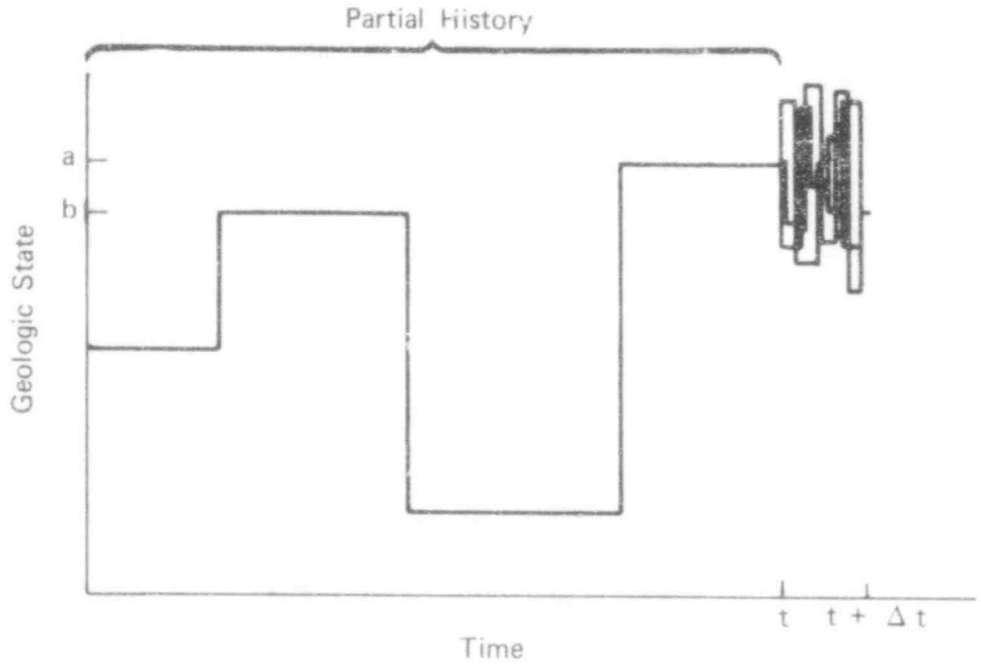

FIG. C-1. Schematic illustration of some partial histories belonging to the subspace S^e_{ab}.

506 267

The integral of p(f) over S^e_{ab} is simply p(e) multiplied by the conditional probability P(b,t+Δt|e) that the system, having experienced partial history e and having reached state a at time t, will reach state b at time t+Δt. We therefore have

$$\sum_{g' \neq g} \int_{e(t)=g} de\ C_r(\underline{x};e,t)\ p(e) \lim_{\Delta t \to 0} \frac{1}{\Delta t} P(g,t+\Delta t|e)$$

$$\sum_{g' \neq g} \int_{e(t)=g} de\ C_r(\underline{x};e,t)\ p(e) \lim_{\Delta t \to 0} \frac{1}{\Delta t} P(g',t+\Delta t|e) \qquad \text{(C-13)}$$

We may define the transition rate from a to b, Γ_{ba}, by

$$\Gamma_{ba}(e) = \lim_{\Delta t \to 0} \frac{1}{\Delta t} P(b,t+\Delta t)\ |a,t;e) \qquad \text{(C-14)}$$

The transition rate in this definition has been written so as to show that it may be a function of past history e; in what follows we will not explicitly show this dependence. In the cases we are considering, the value of e at time t is defined by the restrictions on the integrals over e; hence, we can substitute the definition directly to obtain

$$\sum_{g' \neq g} \int_{e(t)=g'} C_r(\underline{x};e,t)\ p(e)\ \Gamma_{gg'}\ de$$

$$- \sum_{g' \neq g} \int_{e(t)=g} C_r(\underline{x};e,t)\ p(e)\ \Gamma_{g'g}\ de \qquad \text{(C-15)}$$

The integrals over e may be expanded back into integrals over h to restore simplicity of notation. Substituting into Eq. C-7 the values we have calculated for its terms, a formula for the derivative of ϕ_r is obtained:

506 268

$$\frac{\partial}{\partial t}\,\phi_r\,(\underline{x};g,t) = \int_{h(t)=g} p(h)\,L^{(h)}\,C_r(\underline{x};h,t)\,dh$$

$$+ \sum_{g'\neq g} \int_{h(t)=g'} \Gamma_{gg'}\,p(h)\,C_r(\underline{x};h,t)\,dh$$

$$- \sum_{g'\neq g} \int_{h(t)=g} \Gamma_{g'g}\,p(h)\,C_r(\underline{x};h,t)\,dh$$

$$+ \sum_{s\neq r} \int_{h(t)=g} \lambda_s^r\,p(h)\,C_s(\underline{x};h,t)\,dh \quad . \qquad \text{(C-16)}$$

The first term in this equation represents both the flow through space and the decay of radionuclide r. The second term represents the increase in ϕ_r due to transitions into g from other states. The third term represents transitions out of state g. The fourth term describes the creation of nuclide r by the decay of parent nuclides.

We now make two assumptions about the transport operator L: that L depends only on g and not on h, and that it operates linearly on C_r. We may then move it outside the integral so that

$$\int_{h(t)=g} p(h)\,L^{(h)}\,C_r(\underline{x};h,t)\,dh$$

$$= L^{(g)} \int_{h(t)=g} p(h)\,C_r(\underline{x};h,t)\,dh$$

$$= L^{(g)} C_r(\underline{x},g,t) \quad . \qquad \text{(C-17)}$$

506 269

We assume further that the system described by the geologic states is a Markov process. The transition rates Γ will now be assumed independent of the past history. They, like the decay rates λ, also may be moved outside of the sum. Eq. C-16 for the evolution of ϕ_r reduces to

$$\frac{\partial}{\partial t}\ \phi_r(\underline{x};g,t) = L^{(g)}\phi_r(\underline{x};g,t)$$
$$+ \sum_{g'=g} \Gamma_{gg'}\ \phi_r(\underline{x};g',t) - \sum_{g'\neq g} \Gamma_{g'g}\ \phi_r(\underline{x};g;t)$$
$$+ \sum_{s\neq r} \lambda_s^r\ \phi_s(\underline{x};g,t)\ . \qquad \text{(C-18)}$$

Equation C-18 involves only the current state g and may be solved for the ϕ_r; Eq. C-5 may then be used to calculate expected values of concentration.

With this result, it is not necessary to calculate the motion of waste for each history. One may, instead, solve for the quantities $\phi_r(\underline{x};g,t)$. These were defined as the expected value of concentration of radionuclide r at point $\underline{x}$, given that the system is in geologic state g, multiplied by the probability of the system being in state g. These quantities represent an aggregation of the various histories that could lead to state g at time t. It is not necessary to solve an infinite number of partial differential equations corresponding to an infinity of possible histories. Instead, one need solve a system of as many equations as there are geologic states and radionuclides.

DISCUSSION

The main assumptions made in the above derivation are as follows:

1. The operator describing motion of waste must depend only on the current geologic state and not on past geologic states.
2. The operator describing waste motion in any given state must be linear in waste concentration.
3. The transition rates between geologic states cannot depend on the past history of the system.
4. The geologic system is restricted to a countable set of states.

506 270

The first two assumptions restrict waste transport to flows that can be described by linear instantaneous operators. These assumptions are satisfied by the most commonly used transport equation, as described above in the discussion of Eq. C-3.

The other two assumptions govern the geologic states. They require that the system of geologic states form a Markov chain. Whether this requirement is satisfied depends on the particular set of states used in a model.

506 271

APPENDIX D

WASTE MODEL CALCULATIONS

TRANSPORT EQUATION

The problem of predicting nuclide transport in groundwater in three-dimensional space has been approximated by estimating stream flow lines, then formulating a transport equation for a one-dimensional flow path. Water flow lines and velocities can be predicted with a two- or three-dimensional hydrology model using numerical techniques, given the spatial distribution of particular geological structures and properties.

The one-dimensional nuclide transport equation is solved explicitly with a Green's function (impulse response) approach (De Wiest, 1969). The resulting integral equation allows the use of a simple numerical integration technique that avoids the inherent difficulties of numerical dispersion associated with finite difference schemes. This approach is illustrated graphically in Fig. D-1.

506 272

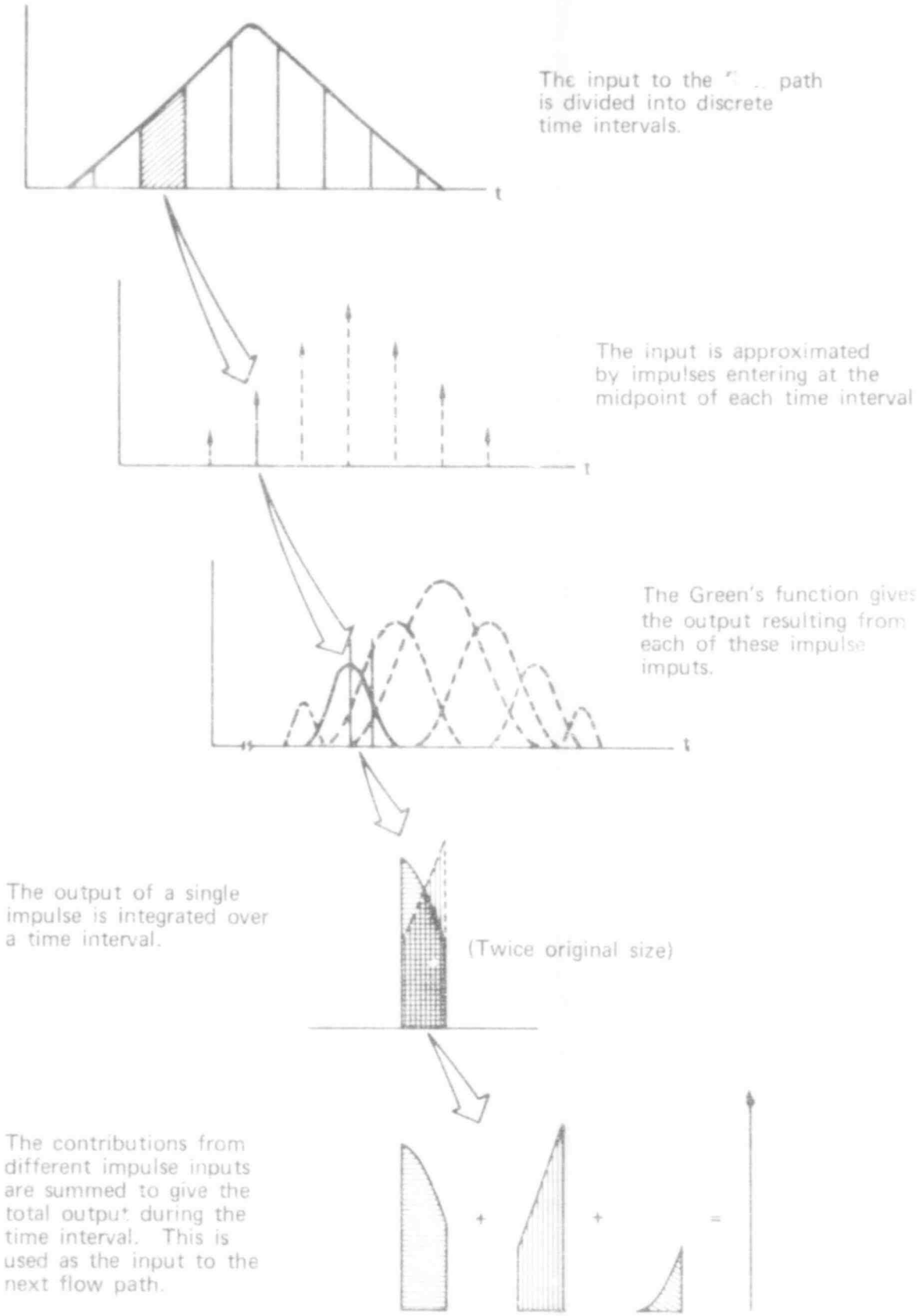

FIG. D-1. Procedure for calculating the output of a flow path.

506 273

HYDROLOGIC EQUATIONS

A fundamental equation governing transport and dispersion of ions in one-dimensional flow through porous media is

$$\frac{\partial m_r}{\partial t} + \frac{\partial C_r}{\partial t} + V \frac{\partial C_r}{\partial x} = \alpha V \frac{\partial^2 C_r}{\partial x^2} - \lambda_r C_r + \sum_{s \neq r} \lambda_s^r C_s - \lambda_r m_r + \sum_{s \neq r} \lambda_s^r m_s \quad \text{(D-1)}$$

Here λ_r is the radioactive decay constant of nuclide r (equal to ln 2 divided by the half-life), λ_s^r is the production rate of nuclide r from decay of nuclide s, V is the interstitial water flow velocity, C_r and C_s are the concentration of nuclides r and s in the interstitial water, α is the longitudinal dispersion constant, and m_r and m_s are the amount of ions r and s absorbed on the solid per unit volume.

The third term on the left side of Eq. D-1 represents simple convection. The first term on the right side is a hydrodynamic dispersion term where the dispersion coefficient is assumed to be a linear function of fluid velocity. Velocity V can be estimated from the hydrology program or from Darcy's law if the pressure differences (HEAD) in the flow path are known. Flow direction can be estimated from the hydrology program also.

Additional assumptions include:

- Flow is sufficiently slow for instantaneous ion exchange equilibrium to result, and the exchange adsorption isotherm is linear. That is, $m_r = \frac{\rho}{\varepsilon} K_d C_r$, where ρ is the bulk density, ε is the effective porosity, and K_d is the distribution coefficient.
- The dissolution rate R(t) of the waste form is independent of nuclide type.
- The retardation factor B_r is the same for all parent-daughter combination ($B_r = 1 + \frac{\rho}{\varepsilon} K_d$).
- All flow paths are considered to be infinite or semi-infinite in extent for the purpose of setting boundary conditions.

506 274

The first assumption allows us to write (Taylor and Brown, 1967)

$$B_r \frac{\partial C_r}{\partial t} + V \frac{\partial C_r}{\partial x} = \alpha V \frac{\partial^2 C_r}{\partial x^2} - B_r \lambda_r C_r + \sum_{s \neq r} B_s \lambda_s^r C_s \qquad \text{(D-2)}$$

Let $INV_r(t)$ be the total amount of radionuclide r at time t in the waste that was originally emplaced in the repository. Then, using the remaining assumptions and defining $c_r = C_r/INV_r$, we have for nuclides in the same decay chain

$$\frac{\partial c_r}{\partial t} + \frac{V}{B} \frac{\partial c_r}{\partial x} = \frac{\alpha V}{B} \frac{\partial^2 C_r}{\partial x^2} + \sum_s \lambda_s^r \frac{INV_s}{INV_r} (c_s - c_r) \qquad \text{(D-3)}$$

$$c_r = 0 \quad , \quad t = 0$$

$$c_r = 0 \quad , \quad x = \infty$$

$$Q \left(c_r - \alpha \frac{\partial c_r}{\partial x} \right) = R(t) + Q_\alpha \frac{\partial c_r}{\partial x} \quad x = 0 \quad ,$$

where Q is the flow rate of water through the repository. The last boundary condition results from conservation of mass flux across the boundary. Equation D-3 is derived by substituting $(c_r INV_r)$ for C_r in Eq. D-2 and using the decay equation for INV_r

$$\frac{d(INV_r)}{dt} = -\lambda_r INV_r + \sum_s \lambda_s^r INV_s$$

By the uniqueness theorem for differential equations, $c_r = c_s$ and the subcripts may be replaced with a single subscript j denoting a group of nuclides that have the same retardation factor. In the remainder of this chapter, we omit the subscript j. This simplification allows us to eliminate from our model a detailed analysis of nuclide decay chains. The assumption that the retardation factor is the same for all parent-daughter combinations is reasonable in comparison to overall uncertainty levels. That this assumption causes only minor perturbations in our results will be discussed later in this section.

506 275

The final set of equations is

$$\frac{\partial c}{\partial t} + \frac{V}{B}\frac{\partial c}{\partial x} = \frac{\alpha V}{B}\frac{\partial^2 c}{\partial x^2} \qquad x > 0 \qquad \text{(D-4)}$$

$$c = 0 \qquad t = 0$$

$$c = 0 \qquad x = \infty$$

$$Q\left(c - \alpha \frac{\partial c}{\partial x}\right) = R(t) + Q\alpha \frac{\partial c}{\partial x} \qquad x = 0 \ .$$

For the next flow path in the network, where the beginning of the flow path is at a distance z from the repository, we would have

$$\frac{\partial c'}{\partial t} + \frac{V'}{B'}\frac{\partial c'}{\partial x} = \frac{\partial' V'}{B'}\frac{\partial^2 c'}{\partial x^2} \qquad x > z$$

$$c' = 0 \qquad t = 0$$

$$c' = 0 \qquad x = \infty$$

$$\left(c' - \alpha' \frac{\partial c'}{\partial x}\right)\Bigg|_{x=z+o} = \left(c - \alpha \frac{\partial c}{\partial x}\right)\Bigg|_{x=z-o} \ . \qquad \text{(D-5)}$$

The last equation follows from conservation of mass flux across the boundary at z.

FORMULAS FOR DISCRETE TIME INTERVALS

The solution of Eq. D-4 can be written as

$$c(x,t) = \frac{V}{BQ}\int_0^t R(\tau)\, G'(x, t-\tau)\, d\tau \ , \qquad \text{(D-6)}$$

where the Green's function, or impulse response, is

$$G'(x,t) = \frac{1}{\sqrt{4\,\pi\,\alpha\,\frac{V}{B}\,t}} \exp\left\{-\frac{(x - \frac{V}{B}t)^2}{4\,\alpha\,\frac{V}{B}\,t}\right\}. \qquad \text{(D-7)}$$

To solve our problem on the computer, we have to modify this continuous-time solution so that it is compatible with discrete time intervals (as shown in Fig. D-1).

506 276

We first define

$$F(\ell) = \int_{T(\ell)}^{T(\ell+1)} Q\, c(z,t)\, dt \quad , \tag{D-8}$$

where Q is the volumetric water flow rate. $F(\ell)$ represents approximately the amount of waste leaving the flow pipe at x = z during the time period $(T(\ell), T(\ell+1))$, where ℓ is the time interval index. Substitution of Eq. D-6 into Eq. D-8 and reversal of the order of intergration yields

$$F(\ell) = \frac{V}{B}\int_{0}^{T(\ell)} \int_{T(\ell)}^{T(\ell+1)} R(\tau)G'(z,t-\tau, dt\, d\tau$$

$$+ \frac{V}{B}\int_{T(\ell)}^{T(\ell+1)} \int_{\tau}^{T(\ell+1)} R(\tau)G'(z,t-\tau)\, dt\, d\tau \quad . \tag{D-9}$$

We now move $R(\tau)$ outside the t integral and integrate the Green's function over a single time interval. Let

$$G_1(z,\tau,\ell) = \frac{V}{B}\int_{T(\ell)}^{T(\ell+1)} G'(z,t-\tau)\, dt \qquad \tau \leq T(\ell) \tag{D-10}$$

and

$$G_2(z,\tau,\ell) = \frac{V}{B}\int_{\tau}^{T(\ell+1)} G'(z,t-\tau)\, dt \qquad T(\ell)<\tau<T(\ell+1) \quad . \tag{D-11}$$

506 277

These functions give the fraction of an impulse of waste entering the flow path at time τ that would leave the flow path during the time interval $(T(\ell), T(\ell+1))$. $R(\tau)$ is the rate at which waste enters the flow path. The integrals of Eq. D-10 can be carried out explicitly, giving

$$\frac{V}{B}\int_{T(\ell)}^{T(\ell+1)} G'(z,\ t-\tau)\ dt = \frac{1}{2}\, e^{\frac{z}{2\alpha}} \left[g(z,\ T(\ell+1)\ -\tau) - g(z,\ T(\ell)\ -\tau)\right]$$

and

$$\frac{V}{B}\int_{\tau}^{T(\ell+1)} G'(z,\ t-\tau)\ dt = \frac{1}{2}\, e^{\frac{z}{2\alpha}} g(z,\ T(\ell+1)\ -\tau) \quad ,$$

where

$$g(z,t) = \text{erfc}\left\{\frac{z - \frac{V}{B}\,t}{\sqrt{\frac{4\alpha V t}{B}}}\right\} e^{\frac{z}{2\alpha}} - \text{erfc}\left\{\frac{z + \frac{V}{B}\,t}{\sqrt{\frac{4\alpha V t}{B}}}\right\} e^{\frac{z}{2\alpha}} \quad . \tag{D-12}$$

The quantity $F(\ell)$ from Eqs. D-9 and D-12 can now be used as the input to the next flow path. A new set of integrated Green's functions will then show the fraction of waste leaving the second flow path. This procedure, as generalized to more complicated networks, is described by Eq. 3-1.
We divide time into steps to calculate $F(\ell)$. Step size is

$$TD(\ell) = T(\ell+1) - T(\ell) \quad ,$$

where

$$T(\ell) = 10^{2 + \frac{4.5(\ell-1)}{\ell_{max}}} - 100 \quad . \tag{D-13}$$

Our choice of step size corresponds with our choosing to display the output on a log-log scale. This approach also puts greater emphasis on earlier times when releases may be more critical. The equation for the output of a given flow path becomes

506 278

$$F_D(\ell) \cong \sum_{i=1}^{i=\ell-1} \int_{T(i)}^{T(i+1)} R(\tau)\, G_1(z,\tau,\ell)\, d\tau$$

$$+ \int_{T(\ell)}^{T(\ell+1)} R(\tau)\, G_2(z,\tau,\ell)\, d\tau \quad , \qquad \text{(D-14)}$$

where $R(\tau)$ is the rate at which waste enters the flow path.

The integrals are usually evaluated by means of the midpoint rule. The computer program takes each input $R(\tau)\, d\tau$ to a flow path and computes the fraction that comes out of the flow path at all time intervals.

When the Green's function is narrower than the time steps, G' may be approximated by a delta function

$$G'(z,t) \cong \delta\left(z - \frac{V}{B}\, t\right). \qquad \text{(D-15)}$$

If the midpoint rule were then used to integrate Eq. D-14 with changing time steps, the sum for certain values of ℓ would contain two nonzero terms and for other values of ℓ it would only contain one nonzero term. Numerical noise would result, as illustrated in Fig. D-2. In such cases, it is more accurate to use Eq. D-15 directly to solve Eq. D-9. Appendix F discusses precise conditions under which this is done.

An additional procedure is necessary to avoid round-off errors. Both $g(z,t)$ and $G_1(z,\tau\ \ell)$ involve differences of complementary error functions. When these differences are small, the error functions are expanded so that accuracy may be maintained (see Appendix F).

Our program is written to minimize the number of necessary calls to the complementary error function routine. The result is an accurate and efficient calculation of nuclide migration.

506 279

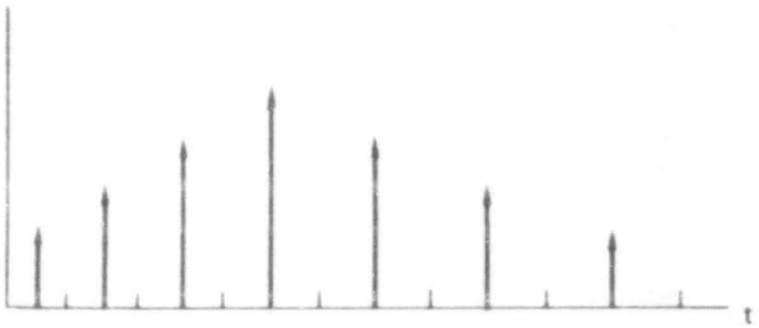

a) Entering flow path

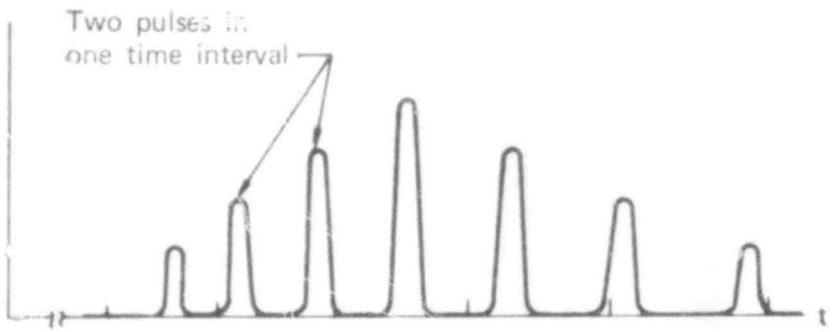

b) Leaving flow path

FIG. D-2. Numerical noise arises when the Green's function is narrower than the time interval and the duration of time intervals is not constant.

506 280

TREATMENT OF NODES WHERE FLOW PATHS BRANCH

Flow paths will branch at some nodes, and waste can migrate from the node by more than one route. For example, in our baseline models waste may leave the repository through the fracture zone and around the shaft and tunnel, through the bulk permeability of the surrounding rock, or by other pathways. It is necessary in these cases to determine how much of the waste enters each open flow path.

Our model divides the waste in proportion to the volumetric flow of water on each pathway. The proportion of the waste leaving node m_1 in state n that proceeds toward node m_2 is given by

$$SP(m_1,m_2,n) = \frac{V(m_1,m_2,n)\ W(m_1,m_2,n)\ \varepsilon(m_1,m_2,n)}{\sum_{m'} V(m_1,m',n)W(m_1,m',n)\varepsilon(m_1,m',n)} \quad , \qquad \text{(D-16)}$$

where V is the water velocity in each pathway, W is the cross section of the pathway, and ε is the effective porosity.

Retardation factors do not enter into this formula. Velocity is that of the water rather than of the waste. Waste transport is simply proportional to the water flow when streamlines branch in an area where rock chemistry, water impurities, and other parameters are homogeneous, and retardation factors change only after the waste has been irrevocably committed to a particular pathway. This situation leads directly to Eq. D-16.

The situation where streamlines branch in an area of inhomogeneous sorption is more complicated. Applicability of Eq. D-16 to this case will be analyzed in the future.

506 281

CALCULATING PROBABILITIES OF TRANSITION

The quantity $TP(\ell',\ell,n',n)$ used in Eq. 3-1 is defined as the conditional probability that the system, having been in state n' at time $T(\ell')$, is in state n at time $T(\ell)$. (n' may be equal to n.) When the program is used to analyze deterministic scenarios, TP is equal to unity if the system is in state n' at time $T(\ell')$ and is also in state n at time $T(\ell)$, otherwise TP equals zero. When the transitions among states are stochastic processes, more complicated formulas for TP must be used. The most simple case arises when the transition rates Γ (defined in Appendix C) are constant. For given ℓ' and ℓ, a matrix of TP(n',n) may be calculated from the equation

$$TP = \ell^{-M\left[T(\ell) - T(\ell')\right]} ,$$

where M is a matrix whose elements are the transition rates. If transition rates are not constant, formulas for TP must be derived by solving the appropriate differential equations.

LEACHING CALCULATION

Our model assumes that no waste leaves the repository until groundwater has resaturated the space resulting from mining operations. The interval required for this to occur (designated T_{fill}) is an input to the program. After the mine is resaturated, the rate at which waste leaves is assumed to be proportional to the amount remaining in the repository. The rate at which waste leaves the repository is therefore given by

$$R(t) = \Lambda q(t) , \qquad (D\text{-}17)$$

where Λ is the fractional dissolution rate of the waste, and q(t) is the amount of waste in the repository at time t.

The quantity used by our model is the input to the first flow path $F(\ell,1,n)$. This input represents the expected amount of waste leaving the repository during time interval ℓ if the system is in state n, multiplied by the

506 282

probability of the system being in state n. Since Eq. D-17 is linear in q, the expected rate of release is the expected amount in the repository multiplied by Λ. Integrating over a time interval, we have

$$F(\ell,1,n)\left\{- Q(\ell,n)\ \ 1 - \exp\left(\left[-\Lambda(j,n)\left[T(\ell+1) - T(\ell)\right]\right]\right)\right\} . \qquad \text{(D-18)}$$

Here $Q(\ell,n)$ is the expected amount of waste remaining in the repository at time $T(\ell)$ if the system is in state n, multiplied by the probability of the system being in state n. The following equation for $Q(\ell,n)$ may be derived from Eq. C-13.

$$Q(\ell,n) = \sum_{n} TP(\ell-1,\ell,n',n)\left[Q(\ell-1,n') - F(\ell-1,1,n')\right] . \qquad \text{(D-19)}$$

The initial values $Q(1,n)$ are inputs to the program. If the total amount of waste is normalized to one MWe-y, $Q(1,n)$ is the probability that the system is in state n at time $T(1)$.

Note that the dissolution rate Λ was written in Eq. D-18 as a function of both nuclide type j and geologic state n. This notation enables the program to handle dissolution rates that are affected by water flow, repository temperature, or other geologic state variables, or by chemical properties of different nuclides. However, as noted in the first section of this appendix, parent and daughter nuclides in any single decay chain are represented as having the same dissolution rate if both are present in the waste at the time it is dissolving.

506 283

CALCULATION OF MAXIMUM CONCENTRATIONS

The subprogram WSCONS, a portion of the WASTE program, is used to calculate the maximum concentrations of selected radionuclides in the interstitial water at the entrance to each flow path. WSCONS calculations are used to check the consistency of our physical assumptions as to the degree of ion solubility and the rate of ion-exchange reactions. These computations are made only for deterministic models, as actual concentrations, not expected concentrations, are required for these purposes. The formula used to compute the interstitial concentration at the entrance to flow path (m_1,m_2) at time $T(\ell)$ is

$$C_r(\ell,m_1,1) = \frac{F(\ell,m_1,1)\ INV_r(T(\ell))\ SP(m_1,m_2,1)}{(T(\ell+1)-T(\ell))\ V(m_1,m_2,1)\ W(m_1,m_2,1)\ \epsilon(m_1,m_2,1)} \quad . \qquad \text{(D-20)}$$

This formula is the flow rate $F/(T(\ell+1)-T(\ell))$, multiplied by the inventory of nuclide r, INV_r, and the fraction of waste flowing into flow path (m_1,m_2), SP, and divided by the flow rate of water in the flow path, VWε.

To calculate concentrations in the aquifer, we assumed mixing through an area equal to the height of the aquifer times the width of the repository. We have enhanced the program so that it can be used to calculate explicity the horizontal distribution of waste in the aquifer from point and plane sources.

506 284

APPENDIX E

RECONCENTRATION FACTOR CALCULATIONS

PROCEDURE

To calculate the reconcentration factor, it is necessary to calculate the flow rate of daughter out of the flow path. Let B denote the retardation factor and λ denote the decay constant. Let the subscript 1 refer to the parent and subscript 2 to the daughter. Let x denote the distance coordinate along the flow path.

Inputs to the flow path in the WASTE program are a sum of impulses. Response of the system to an impulse input is a Gaussian pulse traveling in the flow path (Burkholder and Cloninger, 1976). In this analysis the concentration of parent in the flow path is given as a single Gaussian pulse. The molar concentration of parent nuclide in the flow path is given by

$$C_1(x,t) = \frac{1}{B_1 \varepsilon \sqrt{4\pi\alpha \frac{v}{B_1} t}} \exp \left\{ - \frac{(x - \frac{v}{B_1} t)^2}{4\alpha \frac{v}{B_1} t} \right\} e^{-\lambda_1 t} \quad t > 0 \quad , \qquad \text{(E-1)}$$

where v denotes the velocity of the interstitial water, ε the porosity of the aquifer, and α the dispersion constant. The time scale is chosen so that t = 0 refers to the time when the impulse enters the flow path.

Let z denote the length of the flow path. Let f(t) denote the flow rate of the daughter to the biosphere as a result of the parent's decay. We obtain the flow rate by taking the product of the velocity of the daughter and the concentration of daughter at the far end of the flow path at time t. The concentration of daughter at x = z and time t is obtained by summing the decay product of the parent that occurs at each time τ and position $z - v(t-\tau)/B_2$,

506 285

since this decay product will reach the exit of the flow path at time t. Also this sum must take into account the decay of the daughter. The resulting expression is

$$f(z,t) = \frac{vB_1}{B_2} \lambda_1 \int_0^t C_1 \left(z - \frac{v}{B_2}(t-\tau), \tau\right) e^{-\lambda_2(t-\tau)} \, d\tau \quad . \tag{E-2}$$

Equation E-2 results in an underestimate of the daughter flow rate when the input pulse is near the beginning of the flow path. This error occurs because the dispersion of the daughter has been neglected. However, the effect of the daughter's dispersion will become insignificant as the input pulse nears the exit of the flow path. Therefore, Eq. E-2 accurately represents the rate of the daughter flow rate when the reconcentration effect is most important.

The result of integrating Eq. E-2 is given by Eq. G-1 of Appendix G. Let

$$\Omega^2 \triangleq \left(\frac{v}{B_1} - \frac{v}{B_2}\right)^2 - 4\alpha \frac{v}{B_1}(\lambda_2 - \lambda_1) \quad .$$

When either

$$\Omega^2 < 0 \quad , \tag{E-3}$$

or

$$\Omega^2 > 0 \text{ and } \left| z - \frac{v}{B_2} t \right| - \Omega t > \sqrt{4\alpha \frac{v}{B_1} t} \tag{E-4}$$

the flow rate may be approximated by

$$f(t) = \frac{v}{B_2} \lambda_1 C_1(z,t) \left[(\lambda_2 - \lambda_1) - \frac{\left(\frac{v}{B_2} - \frac{v}{B_1}\right)^2}{\alpha 4 \frac{v}{B_1}} + \frac{\left(z - \frac{v}{B_2} t\right)^2}{4\alpha \frac{v}{B_1} t^2} \right]^{-1} \quad . \tag{E-5}$$

As discussed in Appendix G, Eq. E-3 or E-4 will be satisfied in the thorium-radium or niobium-zirconium case except in a small time interval near $t = zB_2/v$. The size of the interval depends on the parameters of the case being studied; but, unless the interstitial water velocity is several kilometers per year, the interval will not be sufficienty large to affect the calculations at times when reconcentration is of greatest interest.

506 286

In the special case $B_1 = B_2$

$$f(t) = \frac{v}{B_1} \lambda_1 C_1(z,t) \left[(\lambda_2-\lambda_1) + \frac{\left(z - \frac{v}{B_1} t\right)^2}{4\alpha \, B_1 \frac{v}{} t^2} \right]^{-1} . \qquad \text{(E-6)}$$

When the parent pulse is near the exit of the flow path, t is large and $z - (v/B_1)t$ is small; hence, the flow rate is approximately

$$f(t) = \frac{v}{B_1} \frac{\lambda_1 C_1(z,t)}{\lambda_2-\lambda_1} . \qquad \text{(E-7)}$$

By assuming that the parent and daughter travel in secular equilibrium, we obtain the same result. The reconcentration factor $\rho(t)$ is the ratio of Eq. E-5 to Eq. E-6

$$\rho(t) = \frac{B_1}{B_2} \left\{ \frac{(\lambda_2-\lambda_1)\ 4\alpha \ \frac{v}{B_1} t^2 + \left(z - \frac{v}{B_1} t\right)^2}{(\lambda_2-\lambda_1)\ 4\alpha \ B_1 \frac{v}{} t^2 - \left(\frac{v}{B_1} - \frac{v}{B_2}\right)^2 t^2 + \left(z - \frac{v}{B_2} t\right)^2} \right\} . \qquad \text{(E-8)}$$

Let $t_1 = \frac{zB_1}{v}$, the time required for the parent pulse to traverse the flow path. Writing Eq. E-8 as a Taylor series about t_1 and disregarding the terms of second order and higher yields

$$\rho(t) \cong \frac{B_1}{B_2} \left[1 - \frac{\frac{v}{B_1} \left(\frac{v}{B_2} - \frac{v}{B_2}\right)(t-t_1)}{2\alpha(\lambda_2-\lambda_1)z} \right] , \qquad \text{(E-9)}$$

with error less than 1%.

506 287

Appendix H shows that when the half-life of the daughter is less than the time necessary for the daughter to travel the width of the output pulse (Eq. E-1) of the parent

$$\rho(t) \cong \frac{B_1}{B_2} \quad . \tag{E-10}$$

The width of the output pulse is $\sqrt{\alpha z}$.

The half-life of ^{226}Ra and that of ^{93m}Nb are sufficiently small for Eq. E-10 to be used. Hence, the reconcentration factor is approximately B_1/B_2 at all times near the transit time of the parent through the flow path.

Increasing the value of α in Eq. E-9 approximates the effect of a broader input pulse of parent. This increase improves the accuracy of Eq. E-10.

The reconcentration factor (Eq. E-10) is used to correct the daughter flow rate out of the flow path for the reconcentration effect when the parent input is a single impulse. In general, the input is a sum of impulses. Equation E-10 may be used to correct the daughter flow rate for each impulse. Because the correction is linear, ρ may be used to correct the flow rate computed by the model.

Equation E-10 applies when a pulse of parent is near the exit of the flow path. Since no daughter input can traverse the flow path, any flow of daughter into the biosphere occurs because the parent pulse is near the exit. Therefore, the reconcentration factor given by Eq. E-10 may be applied whenever there is daughter flowing out of the flow path. If the daughter flow rate is zero, multiplication by ρ will not affect it. Hence, the reconcentration factor ρ may be used at all times.

506 288

SUMMARY

The flow rate of daughter nuclide calculated by the WASTE program can be corrected for the reconcentration effect by multiplying the calculated flow rate by

$$\rho = \frac{B_1}{B_2} \quad . \tag{E-11}$$

Several conditions must be fulfilled to use this calculation:

1. The flow path is so long that any initial daughter input has decayed to insignificant levels in the time necessary for parent to traverse the flow path.
2. The retardation factor of the parent nuclide is much larger than the retardation factor of its daughter.
3. The daughter has a much smaller half-life than its parent.
4. The half-life of the daughter is much less than the time necessary for the daughter to travel the width of the parent input pulse.
5. Conditions in Eq. E-3 or E-4 are satisfied.

If neither Eq. E-3 nor E-4 is satisfied, a more complicated expression for ρ may be obtained by using the result of the integration of Eq. E-1 in the numerator of Eq. E-8.

506 289

APPENDIX F

FORMULAS USED TO CALCULATE THE INTEGRATED GREEN'S FUNCTION, G

The fraction of waste entering a flow path at time τ that leaves the flow path between $\tau + t$ and $\tau + t + \Delta t$ is given by

$$G = g(t+\Delta t) - g(t) \quad , \tag{F-1}$$

where $g(t)$ represents the fraction of waste passing through the flow path in less time than t. The formula for g is

$$\text{where } g_A(t) = \frac{1}{2} \left[\text{erfc}\,(\phi_-(t)) - e^{z/\alpha}\, \text{erfc}\,(\psi_+(t)) \right] \quad , \tag{F-2}$$

$$\phi_{\pm}(t) = \frac{z \pm \frac{V}{B} t}{\sqrt{4\alpha \frac{V}{B} t}} \quad , \tag{F-3}$$

Note that $g_A(t)$ is the exact formula for $g(t)$ and that other indices (B,C,etc.) are used to designate numerical approximations to g_A.

Numerical problems can arise if Eqs. F-1 and F-2 are used directly to calculate G. These problems can be resolved by using the asymptotic expansion of the complementary error function:

$$\text{erfc}(u) \xrightarrow[u \to \infty]{} \frac{e^{-u^2}}{\sqrt{\pi}\, u} \left(1 - \frac{1}{2u^2} + \frac{3}{4u^4} - \cdots\right) \quad . \tag{F-4}$$

506 290

This expansion possesses the useful property that the error is always less than the first excluded term.

Consider first the case $z/\alpha \gg 1$. If z/α is sufficiently large, the exponentiation in Eq. F-2 will yield a number that exceeds the storage capacity of the machine. (The criterion is $z/\alpha > 144$.) By expanding erfc $(\phi_+ (t))$, we obtain

$$g_B(t) = \frac{1}{2} \left[\text{erfc } \phi_- (t) - \frac{e^{-\phi_-^2 (t)}}{\sqrt{\pi}\, \phi_+ (t)} \right], \tag{F-5}$$

The fractional error introduced by dropping terms of order ϕ_+^{-2} and higher will always be less than $\alpha/2z$.

Roundoff errors can occur in the subtraction operation of either Eqs. F-2 or F-5. Both complementary error functions must then be expanded, and large terms occurring in both expansions must be canceled. The resulting formula is

$$g_C(t) = \frac{e^{-\phi_-^2 (t)}}{\sqrt{4\pi\alpha\, B/(Vt)}} \quad \frac{1}{\phi_+(t)\, \phi_-(t)} \times \left[1 - \frac{1}{2} \left(\frac{1}{\phi_+^2 (t)} + \frac{1}{\phi_+(t)\, \phi_-(t)} + \frac{1}{\phi_-^2(t)} \right) \right] . \tag{F-6}$$

Roundoff errors will exceed 1% when the computer calculates with six digit numbers and

$$\frac{g(t)}{\text{erfc } \phi_-(t)} \leq 10^{-5} .$$

506 291

When Eqs. F-4 and F-6 are substituted into this relation, one finds

$$\frac{1}{1+\frac{zB}{Vt}}\left[\frac{1-\frac{1}{2}-\phi_+^{-2}(t)+\phi_+^{-1}(t)\phi_-^{-1}(t)+\phi_-^{-2}+\cdots}{1-\frac{1}{2}\phi_-^{2}(t)+\cdots}\right]10^{-5}$$

As long as $\phi_-(t)>1$, this relation can only be satisfied when $Vt/zB\gtrsim 10^{-5}$. For $z\gtrsim\alpha$, this implies $\phi_+>10^2$ and the error in Eq. F-6 due to dropping additional terms will be less than 1%.

For large times when $Vt/Bz\gg 1$, on the other hand, roundoff errors can arise in in Eq. F-1. To deal with this, we rewrite Eq. D-12 as

$$\begin{aligned} G &= g_A(T(\ell+1)-\tau) - g_A(T(\ell)-\tau) \\ &= \frac{1}{2}\left\{\operatorname{erfc}\left(\phi_-(T(\ell+1))-\tau\right) - \operatorname{erfc}\left(\phi_-(T(\ell)-\tau)\right)\right. \\ &\quad \left. + e^{z/\alpha}\left[\operatorname{erfc}\left(\phi_+(T(\ell)-\tau)\right) - \operatorname{erfc}\left(\phi_+(T(\ell+1)-\tau)\right)\right]\right\} \\ &= g'_A(T(\ell+1)-\tau) - g'_A(T(\ell)-\tau) \quad , \end{aligned} \tag{F-7}$$

where

$$g'_A(t) = \frac{1}{2}\left[-\operatorname{erfc}(-\phi_-(t)) - e^{z/\alpha}\operatorname{erfc}(\phi_+(t))\right] \tag{F-8}$$

and ℓ is the time interval index.

In the limit $\frac{Vt}{zB}\longrightarrow\infty$, one has $\phi_-\longrightarrow-\infty$ and $\phi_+\longrightarrow+\infty$, and

$$\frac{G}{g_A(T(\ell)-\tau)} < 10^{-5}$$

and its precision will be governed by considerations similar to those of the preceding case.

506 292

This roundoff problem cannot arise when $\ell = \ell'$, because the substraction of Eq. F-1 is not carried out. F-2 or F-5 is then used as appropriate.

Finally, we have the case when the dispersion time $\frac{B}{V}\sqrt{4\alpha z}$ is much less than the time interval $T(\ell+1) - T(\ell)$. Calculating G in this case, we ignore dispersion altogether, but consider the width of the input pulse. Defining $T_f = zB/V$, the formulas used are:

If $T(\ell') + T_f < T(\ell)$ and $T(\ell'+1)+T_f > T(\ell)$, then

$$G(\ell',\ell) = \frac{T(\ell'+1)+T_f-T(\ell)}{T(\ell'+1)-T(\ell')} \qquad \text{(F-9)}$$

$$G(\ell',\ell-1) = 1-G(\ell',\ell) \; ; \qquad \text{(F-10)}$$

If $T(\ell')+T_f > T(\ell)$ and $T(\ell'+1)+T_f < T(\ell+1)$, then

$$G(\ell',\ell) = 1 \; ;$$

otherwise G = 0.

These formulas are used when 95% of the output from a impulse entered into the flow path will emerge during a single time interval. This event will occur when the time interval is longer than four times the variance of the Gaussian output pulse, i.e., when

$$4\frac{B}{V}\sqrt{2\alpha z} > T(\ell+1) - T(\ell) \quad .$$

However, dispersion cannot be neglected when the input pulse is more narrow than the Green's function. For that reason these formulas are not used when

$$\frac{F(\ell',m',n')}{F(\ell'+1,m',n')} < 0.05$$

or

$$\frac{F(\ell'+1,m'n')}{F(\ell',m',n')} < 0.05$$

506 293

Table F-1 summarizes the different cases, defines the conditions, and shows the formulas used in this discussion.

In table F-1

$$g_A(t) = \frac{1}{2}\left[\operatorname{erfc}\,\phi_-(t) - e^{z/\alpha}\,\operatorname{erfc}\,\phi_+(t)\right] \tag{F-11}$$

$$g_B(t) = \frac{1}{2}\left[\operatorname{erfc}\,\phi_-(t) - \frac{e^{-\phi_-^2(t)}}{\sqrt{\pi}\phi_+(t)}\right] \tag{F-12}$$

$$g_C(t) = \frac{e^{-\phi_-^2(t)}}{\sqrt{\frac{4\pi\alpha B}{Vt}}\,\phi_+(t)\,\phi_-(t)}\left[1 - \frac{1}{2}\left(\frac{1}{\phi_+^2(t)} + \frac{1}{\phi_+(t)\cdot\phi_-(t)} + \frac{1}{\phi_-^2(t)}\right)\right] \tag{F-13}$$

$$\phi_{\pm}(t) = \frac{z \pm \frac{V}{B}t}{\sqrt{4\alpha\,\frac{V}{B}\,t}} \tag{F-14}$$

and ℓ_{opt} is defined by $T(\ell_{opt} - 1) < T(\ell') + T_f \leq T(\ell_{opt})$, where $T_f = \frac{zB}{V}$.

506 294

TABLE . Formulas for integrated Green's function G

CASE NO.	CONDITIONS		FORMULA
0.1	$\ell = \ell'$ $z/\alpha < 144$ not Case 3		$G = g_A(T(\ell'+1) - T(\ell'))$
0.2	$\ell = \ell'$ $z/\alpha \geq 144$ not Case 3		$G = g_B(T(\ell'+1) - T(\ell'))$
1	$\ell \neq \ell'$ $e_{-}(T(\ell+1) - T(\ell')) > 1$ $\frac{g_A(T(\ell+1) - T(\ell'))}{\operatorname{erfc}(e_{-}(T(\ell+1)-T(\ell')))} < 10^{-3}$ not Case 3		$G = g_C(T(\ell+1) - T(\ell'))$ $- g_C(T(\ell) - T(\ell'))$
2	$\ell \neq \ell'$ $e_{-}(T(\ell) - T(\ell')) < -2$ $\frac{G}{g_A(T(\ell) - T(\ell'))} < 10^{-5}$ not Case 3		$G = g_C(T(\ell+1) - T(\ell'))$ $-g_C(T(\ell) - T(\ell'))$
3	$\ell \neq \ell'$ $z/c \geq 144$ not Cases 1, 2, or 3		$G = g_B(T(\ell+1) - T(\ell'))$ $-g_B(T(\ell) - T(\ell'))$
4	$\ell \neq \ell'$ $z/\alpha < 144$ not Cases 1, 2, or 3		$G = g_A(T(\ell+1) - T(\ell'))$ $-g_A(T(\ell) - T(\ell'))$
3.1	$4\frac{3}{\sqrt{\pi}}\sqrt{2\alpha z} < T(\ell_{opt}) - T(\ell_{opt}-1)$.	$T(\ell')+T_f < T(\ell_{opt}-1)$	$G(\ell', \ell_{opt}-2) = \frac{T(\ell_{opt}-1) - T(\ell') - T_f}{T(\ell'+1) - T(\ell')}$ $G(\ell', \ell_{opt}-1) = \frac{T(\ell'+1) - T_f - T(\ell_{opt}-1)}{T(\ell'+1) - T(\ell')}$
3.2	$\frac{F(\ell'+1,m',n')}{F(\ell',m',n')} > 0.05$ $\frac{F(\ell',m',n')}{F(\ell'+1,m',n')} > 0.05$	$T(\ell'+1) + T_f > T(\ell_{opt})$	$G(\ell', \ell_{opt}) = \frac{T(\ell'+1) + T_f - T(\ell_{opt})}{T(\ell'+1) - T(\ell')}$ $G(\ell', \ell_{opt}-1) = \frac{T(\ell_{opt}) - T(\ell') - T_f}{T(\ell'+1) - T(\ell')}$
3.3		$T(\ell')+T_f > T(\ell_{opt}-1)$ $T(\ell'+1)+ T_f < T(\ell_{opt})$	$G(\ell', \ell_{opt}-1) = 1$

506 295

APPENDIX G

DERIVATION OF THE DAUGHTER FLOW RATE

The result of the integration of Eq. E-2 has a complicated form. Let $t_2 = zB_2/v$, the transit time of an input daughter through the aquifer. The formal expression for the result of the integration changes according to whether the flow rate is being computed for a time before or after t_2. Let

$$\sigma(t) = \begin{cases} 1 \text{ if } t < t_2 \\ \\ -1 \text{ if } t \leq t_2 \end{cases}$$

Then

$$f(z,t) = \sigma(t)\,\frac{vB_1}{B_2}\,\lambda_1 Q e^{-\lambda_2 t}\,\frac{1}{2\Omega}\exp\left\{\frac{\left(\frac{v}{B_1}-\frac{v}{B_2}\right)\left(z-\frac{v}{B_2}t\right)}{2\alpha\,\frac{v}{B_1}}\right\}$$

$$\times\left[\exp\left\{\frac{-\Omega\left(z-\frac{v}{B_2}t\right)}{2\alpha\,\frac{v}{B_1}}\right\}\operatorname{erfc}\left(\frac{\left|z-\frac{v}{B_2}t\right|-\sigma(t)\,\Omega t}{\sqrt{4\alpha\,\frac{v}{B_1}t}}\right)\right.$$

$$\left.-\exp\left\{\frac{\Omega\left(z-\frac{v}{B_2}t\right)}{2\alpha\,\frac{v}{B_1}}\right\}\operatorname{erfc}\left(\frac{\left|z-\frac{v}{B_2}t\right|+\sigma(t)\,\Omega t}{\sqrt{4\alpha\,\frac{v}{B_1}t}}\right)\right] \qquad \text{(G-1)}$$

506 296

where

$$\Omega^2 = \left(\frac{v}{B_1} - \frac{v}{B_2}\right)^2 - 4\alpha \frac{v}{B_1}(\lambda_2 - \lambda_1) \quad . \tag{G-2}$$

Note that Ω^2 may be negative so that $\Omega = \sqrt{\Omega^2}$ may be imaginary.

Equation G-1 reduces to the more simple form

$$f(z,t) = \frac{vB_1}{B_2}\lambda_1 C_1(z,t)\left[\lambda_2 - \lambda_1 + \frac{\left(\frac{v}{B_1} - \frac{v}{B_2}\right)^2}{4\alpha \frac{v}{B_1}} + \frac{\left(z - \frac{v}{B_2}t\right)^2}{4\alpha \frac{v}{B_1}t^2}\right]^{-1} \quad . \tag{G-3}$$

when the asymptotic expansion

$$\operatorname{erfc}(w) \cong \frac{e^{-w^2}}{\sqrt{\pi}\, w} \tag{G-4}$$

is used.

The approximation Eq. G-4 is valid for complex numbers, w, with large modulus satisfying $|\arg w| < 3\pi/4$ (Abramowitz and Stegun, 1970, p. 298).

To use Eq. G-3 in the WASTE program, it is necessary to show that the approximation applies to the complementary error functions occurring in Eq. G-1. If

$$\left[\frac{v}{B_2} - \frac{v}{B_1}\left(\frac{z + 4\alpha z}{z - 4\alpha z}\right)\right]^2 \geq \Omega^2 \tag{G-5}$$

the approximations will cause an error in the value of $\rho(t)$ no greater than 10%.

506 297

For the thorium-radium and zirconium-niobium cases, the retardation factors and interstitial water velocity can be chosen so that the condition occurring in Eq. G-5 fails for times near $t_2 = zB_2/v$. However, when $B_1 >> B_2$ there will be no flow of daughter at times near t_2. At times when Eq. G-3 cannot be used, Eq. G-1 can be computed directly to find $\rho(t)$.

506 298

APPENDIX H

EFFECT OF A SHORT DAUGHTER HALF-LIFE ON THE RECONCENTRATION FACTOR

The reconcentration factor is given in Eq. E-9 as

$$\rho(t) = \frac{B_1}{B_2}\left[1 - \frac{\frac{v}{B_1}\left(\frac{v}{B_2} - \frac{v}{B_1}\right)(t - t_0)}{2\alpha(\lambda_2-\lambda_1)z}\right] , \qquad \text{(H-1)}$$

where $t_0 = \frac{z}{v}B_1$.

For times when the parent pulse is about one pulse width from the end of the flow path ($|t-t_0| \approx B_1/v\sqrt{\alpha z}$)

$$\rho(t) \approx \frac{B_1}{B_2}\left[1 \pm \frac{\left(\frac{v}{B_2} - \frac{v}{B_1}\right)}{2\sqrt{\alpha z}\,(\lambda_2-\lambda_1)}\right] . \qquad \text{(H-2)}$$

Suppose that the daughter half-life is much less than the time for the daughter to travel the width of the pulse, i.e.,

$$\frac{\ln 2}{\lambda_2} \ll \frac{\sqrt{\alpha z}}{\left(\frac{v}{B_2}\right)} ,$$

then the second term in the braces in Eq. H-2 may be neglected.
Hence,

$$\rho(t) \approx \frac{B_1}{B_2} . \qquad \text{(H-3)}$$

For ^{226}Ra and ^{93m}Nb the half-lives are sufficiently small that Eq. H-3 applies.

506 299

APPENDIX I

CONCENTRATION EQUATIONS FOR THE RIVER, ESTUARY, AND OCEAN SYSTEM

TIME-DEPENDENT MODEL

The concentration of nuclide r in a river or lake is given by

$$V_w \frac{d}{dt} C_{rw} = - \left[\lambda_r V_w + F + I + \frac{DA_s}{d} + v_{rs} A_s v_w \right] C_{rw}$$

$$+ Q_r + V_w \sum_q \lambda_r C_{qw} + \left[\frac{I + R - E}{K_{rt}} \right] C_{rt}$$

$$+ \left[\frac{DA_s}{K_{rs} d} \right] C_{rs} , \qquad \text{(I-1)}$$

where losses are due to radioactive decay, flow out of the system, irrigation withdrawals, diffusion into the sediment, and sedimentation. Inputs to the river or lake come from the aquifer, radionuclide production, runoff, and diffusion from the sediment.

The concentration in the sediment is given by

$$V_s \frac{d}{dt} C_{rs} = - \left[\lambda_r V_s + \frac{DA_s}{K_{rs} d} + A_s v_w \right] C_{rs}$$

$$+ \left[\frac{DA_s}{d} + K_{rs} A_s v_w \right] C_{rw} + V_s \sum_q \lambda_r C_{qs} . \qquad \text{(I-2)}$$

506 300

The concentration in the topsoil is given by

$$V_t \frac{d}{dt} C_{rt} = - \left[\lambda_r V_t + \frac{I + R - E}{K_{rt}} + M_r \right] C_{rt} + I C_{rw} + V_t \sum_q \lambda_r C_{qt} \qquad (I\text{-}3)$$

The concentration in the estuary is given by

$$V_e \frac{d}{dt} C_{re} = - \left[\lambda_r V_e + \frac{V_e}{T_e} + \frac{DA_e}{d} + K_{rse} A_e v_e \right] C_{re} + F C_{re} + V_e \sum_q \lambda_r C_{qe} + \left[\frac{DA_e}{K_{rse} d} \right] C_{rse} \; . \qquad (I\text{-}4)$$

The concentration in the estuarine sediment is given by

$$V_{se} \frac{d}{dt} C_{rse} = - \left[\lambda_r V_{se} + \frac{DA_e}{K_{rse} d} + A_e v_e \right] C_{rse} + \left[\frac{DA_e}{d} + K_{rse} A_s v_e \right] C_{re} + V_{se} \sum_q \lambda_r C_{qse} \; . \qquad (I\text{-}5)$$

The concentration in the ocean is given by

$$V_o \frac{d}{dt} C_{ro} = - \left[\lambda_r V_o + \frac{V_o}{T_o} \right] C_{ro} + V_o \sum_q \lambda_r C_{qo} + \frac{V_e}{T_e} C_{re} \; . \qquad (I\text{-}6)$$

506 301

We have adopted the following notation for our equations:

C_{rp} = concentration of nuclide r in pathway p (Ci/m^3) where w,e,o,t,s, and se represent the river (or lake), estuary, ocean, topsoil, river sediment, and estuarine sediment pathways, respectively

V_p = effective volume of pathway p (m^3)

T_p = flushing time for the estuary or the residence time for coastal waters (y)

A_p = area of the sediment (m^2)

K_{rp} = distribution coefficient for nuclide r in pathway p $\left(\frac{Ci/m^3 \text{ dry sediment}}{Ci/m^3 \text{ water}}\right)$

Q_r = input of nuclide r from the aquifer into the river or lake (Ci/y)

λ_r = radioactive decay constant of nuclide r (y^{-1})

v_p = net rate of sedimentation (m/y)

F = flow rate of the river (m^3/y)

I = average yearly rate at which water is withdrawn from the river for irrigation (m^3/y)

D = diffusion coefficient (m^2/y)

d = average diffusion depth for sediment and subsoil (m)

R = average yearly rainfall on the topsoil under irrigation (m^3/y)

E = average yearly evaporation from the topsoil under irrigation (m^3/y)

M_r = effective average yearly removal rate of nuclide r from topsoil that is taken up by plants and animals (m^3/y). This parameter is evaluated in Appendix J.

506 302

STEADY-STATE EQUATIONS

The equations used in the program BIODOSE to compute concentrations in the water, topsoil, and sediment are

$$C_{rw}\,(F + I) = Q_r + \left(\frac{I + R - E}{K_{rt}}\right) C_{rt} \qquad \text{(I-7)}$$

$$C_{re}\left(\frac{V_e}{T_o}\right) = F\, C_{rw} \qquad \text{(I-8)}$$

$$C_{ro}\left(\frac{V}{T_o}\right) = \left(\frac{V_e}{T_e}\right) C_{re} \qquad \text{(I-9)}$$

$$C_{rs} = K_{rs}\, C_{rw} \qquad \text{(I-10)}$$

$$C_{rt} = C_{rw}\left(\frac{I}{V_t}\right)\left(\frac{1 - e^{-L_r t_b}}{L_r}\right), \qquad \text{(I-11)}$$

where

$$L_r = \frac{I + R - E}{K_{rt} V_t} + \frac{M_r}{V_t} \qquad \text{(I-12)}$$

and t_b is time over which the topsoil is irrigated.

The notation is the same as for the time-dependent model. The input from Q_r measures the amount of waste flowing out of the aquifer from 1 MWe-y of nuclear power production as a function of time.

Values assumed for the various parameters are given in Tables I-1 and I-2, along with their references. Note that the values of the distribution coefficients for sediment and topsoil have a wide range in nature. Experimentally measured values, even within the same region, can vary by several orders of magnitude. A more accurate and dynamic model of these phenomena can be obtaired after additional experimental and theoretical work.

506 303

TABLE I-1. Data for water system equations.

Parameter	Value	Units	Reference
F	1.2×10^{11}	m^3/y	Booth et al., 1971
V_e	2.6×10^9	m^3	Booth et al., 1971
T_e	2.5	d	Booth et al., 1971
V_o	6×10^{12}	m^3	Taylor and Brown, 1967
T_o	122	d	Taylor and Brown, 1967
I	4% F	m^3/y	U.S. Dept. of Commerce, NOAA-NMFS, 1972
A_t	(I/1m/y)	m^2	U.S. Dept. of Commerce, NOAA-NMFS, 1972
V_t	0.15m A_t	m^3	Boast, 1973
R,E	R = E	m^3/y	Chosen for simplicity
M_r	---	m^3/y	See Appendix F
K_{rt}	Western desert soil	$\frac{Ci/m^3 \text{ sediment}}{Ci/m^3 \text{ water}}$	Fletcher and Datson, 1971

506 304

TABLE I-2. Concentration factors in fresh and salt water.

	K_{rs} $\left(\frac{Ci/m^3 \text{ Sediment}}{Ci/m^3 \text{ Water}}\right)$[a]		Reference number	
Nuclide	Fresh	Salt	Fresh	Salt
Sr	1.3×10^3	5.3×10^1	22	18, 21
Y	5.3×10^2		16	
Zr	1.0×10^5	1.0×10^5	16	18
Nb	3.0×10^3	1.0×10^5	22	18
Tc[b]	1.0×10^4			
Ru	2.0×10^3	1.6×10^4	22	18, 21
Sn	5.4×10^4		16	
I	1.0×10^4		22	
Cs	4.8×10^3	1.0×10^3	22	17
Ce	6.0×10^4	2.0×10^5	16	21
Pm		1.0×10^5		17
Eu[b]	1.0×10^4			
Pb	3.2×10^3			
Po	3.2×10^3			
Ra	3.2×10^3		22	
Th	5.0×10^3		22	
Pa[b]	1.0×10^4			
U[b]	1.0×10^4			
Np[b]	1.0×10^4			
Pu	3.8×10^5	2.1×10^5	19	21
Am	8.4×10^4	1.0×10^5	20	
Cm[b]	1.0×10^4			

[a] Sediment density assumed to be 1.6 kg/litre.

[b] Arbitrarily assigned values. Net dose is (virtually) insensitive to the concentration factor for these nuclides.

506 305

OCEAN PLUME DYNAMICS

Spatial distribution of radionuclides in the ocean may become important if biological activity is not uniform. The tabulation below shows how the commercial fish harvest in the United States falls off as distance from shore increases (see Ref. 3-14).

Distance from Shore (mi)	0-3	3-12	12-50
Average Harvest (g/m² d)	0.0193	0.0022	0.0003

The distribution of radionuclides in a plume may be calculated for a specific site using the following equation (Csanady, 1973)

$$C_{rp\ell}(x,y) = \left[\frac{C_{re}\ V_e}{T_e}\right] \frac{\exp\left(\frac{-y^2}{4Dx}\right) \exp\left(\frac{-\lambda_r x}{u}\right)}{2d\sqrt{\pi u}\ x\ D}\ , \qquad \text{(I-13)}$$

where

u = ocean velocity, about 15 cm/s for the Oregon and Washington coasts
d = plume depth, about 20 m for the Columbia River plume
D = lateral dispersion coefficient
x = distance parallel to the current
y = distance normal to the current
C_{rp} = concentration of nuclide r in the plume
C_{re} = concentration of nuclide r in the estuary
V_e = volume of the estuary, about 2.6×10^9 m^3 for the Columbia River estuary
T_e = flushing time of the estuary, about 2.5 d for the Columbia River estuary.

Values for the Columbia River estuary and plume were found in Barnes et al. (1972) and Neal (1972).

506 306

For use in the model, a mean plume concentration was calculated on the basis of the data presented in Barnes et al. (1972) for the Columbia River plume For a plume area of about $1.25 \times 10^{10}/m^2$, the mean plume concentration would be

$$C_{rp\ell} = \left[\frac{V_e}{10 \, T \, F_e} \right] r\ell \quad , \tag{I-14}$$

where F is the yearly flow rate of the river (m^3/y).

506 307

APPENDIX J

EQUATIONS USED TO CALCULATE POPULATION DOSE

The intake from irrigated crops is given by

$$p_r^{veg} = \frac{f^{veg} F \sum_v U_v C_{rv}}{\sum_v \frac{U_v IR_v t_e}{Y_v}} 1000 \quad , \qquad (J\text{-}1)$$

where

p_r^{veg} = intake rate from all plant products (Ci/y)

f^{veg} = fraction of the river or well flow rate that is used for irrigating crops for human consumption

F = average yearly flow rate of a river or well (m^3/y)

U_v = average yearly consumption of food crop v by an individual (kg/y)

C_{rv} = concentration of nuclide r in plant v (Ci/kg) as calculated in Appendix K

IR_v = irrigation rate during the growing season for vegetable v (litre/m^2-d)

Y_v = plant yield (kg/m^2)

t_e = time of above-ground exposure of crops to contamination during the growing season (d).

Vegetables were assumed to be grown in proportion to their use in an average diet, as given in Table 2. An adult population was assumed.

The intake rate from consumption of milk and beef products is given by

$$p_r^{milk} = f^{milk} FC_{rF} S_{rA} \left(\frac{Y_F A^{milk}}{IR_F t_e} \right) 1000 + f^{cow} FC_{rw} S_{rA} A^{milk} \qquad (J\text{-}2)$$

$$p_r^{beef} = f^{beef} FC_{rF} S_{rA} \left(\frac{Y_F A^{beef}}{IR_F t_e} \right) 1000 + f^{cattle} FC_{rw} S_{rA} A^{beef}, \qquad (J\text{-}3)$$

where

D_r^{milk}, D_r^{beef} = the intake rate from consumption of milk or beef (Ci/y)

f^{milk}, f^{beef} = fraction of the river or well flow rate that is used for irrigating crops for consumption by dairy cows or beef cattle

f^{cow}, f^{cattle} = fraction of the river or well flow rate that serves as drinking water for dairy cows or beef cattle

C_{rF}, IR_F, Y_F = as defined in Eq. J-1, and the subscript F refers to feed or forage

S_{rA} = transfer coefficient for nuclide r from daily intake of animal to edible portion of animal product d/litre(milk) or d/kg(beef)

A^{milk}, A^{beef} = production rate of milk or beef per animal per day litre/d(milk) or kg/d(beef) .

It is assumed that

$$I = \left[f^{milk} + f^{beef} + f^{veg} \right]$$

where I is the average yearly rate at which water is withdrawn from the river or well for irrigation.

It is now possible to obtain a relationship for M_r, the effective removal rate from topsoil, which is required in Appendix I.

$$M_r = \left\{ \frac{B_{rF}\, S_{rA}\, Y_F\, A^{milk}}{D_T\, IR_F\, t_e} f^{milk} + \frac{B_{rF}\, S_{rA}\, Y_F\, A^{beef}}{D_T\, IR_F\, t_e} f^{beef} + \frac{\sum_v B_{rv}\, U_v}{D_T \sum_v \frac{U_v\, IR_v\, t_e}{Y_v}} f^{veg} \right\} F\, 1000 \quad , \tag{J-4}$$

where B_{rv} and D_T are defined in Appendix K, and B_{rf} is the value of B_{rv} for feed or forage.

506 309

The value of A^{beef} was obtained from Booth et al. (1971), which quoted a production rate of 0.4 kg/d for a fattening steer. The value of A^{milk} was obtained by dividing the total U.S. milk production by the total number of dairy cows in the United States (Williams Market Analysis, 1973). This gives a value of about 15 litres of milk produced per cow per day.

The fraction of river water used for irrigation was obtained by dividing the amount of water used for irrigation in the United States by the total runoff per year (Kazmann, 1965). Account was taken of the fraction of irrigation water coming from underground sources (Todd, 1959). An estimated 4% of the yearly runoff in the United States is used for irrigation.

A similar calculations is necessary for groundwater. Based on Todd (1959), 85% of the groundwater used in the western United States is for irrigation. Therefore, I/F = 0.04 for rivers and I/F = 0.85 for wells.

The population dose resulting from the aquatic food pathway was calculated using the harvest data in Table J-1. Harvests for the river, estuary, and ocean pathways were based on data from the Columbia River system (Pruter, 1972). The lake harvest data, from NRC, NUREG-0140, 1976, typified the Great Lakes. Since the productivity of aquatic life is limited, large increases in these yields are not expected.

TABLE J-1. Aquatic food harvest.[a]

Aquatic Food	River	Estuary and near-shore	Ocean	Lake
Fish	1.5×10^5	1.2×10^7	2.0×10^8	7.5×10^6
Mollusk	--	4.5×10^6	--	--
Crustacean	1.0×10^4	1.7×10^6	--	--

[a]All weights are in edible pounds.

506 310

Population doses from the swimming, shoreline, and topsoil exposure pathways were based on the following assumptions:

1. Swimming and boating population use was 0.14 h/acre of water system per day (NRC, NUREG-0140, 1976).
2. Shoreline population use was 0.5 user-h/acre of water system per day (NRC, NUREG-0140, 1976).
3. The topsoil was assumed to be occupied 100% of the time. A shielding factor of one-third was included to take account of housing (NRC, WASH-1400, 1975). The area of the topsoil was estimated from the irrigation rate by assuming 1 m^3 of water for every 1 m^2 of land (Kasmann, 1965).

A population density of 500 people/km^2 was chosen to test the importance of the topsoil exposure pathway.

The population dose from drinking water is calculated from an assumed use rate for the river system. The rate was obtained by dividing the total quantity of drinking water used from above-ground resources in the United States per year by the annual runoff. This figure, 3.7×10^{-5}, was then multiplied by the river flow rate in our system to obtain the total quantity of water consumed.

Population dose from drinking water from underground resources is calculated by using an assumed use rate for wells. About 7% of well flow is used for municipal supplies (Todd, 1959). Only about 0.2% of this quantity is used for drinking purposes, assuming a 125 gal/d/capita water use for urban centers. Therefore, $W/F = 3.7 \times 10^{-5}$ for rivers and $W/F = 1.4 \times 10^{-4}$ for wells, where W is the quantity of drinking water used per year.

506 311

APPENDIX K

EQUATIONS USED TO CALCULATE RADIONUCLIDE CONCENTRATIONS IN VEGETABLE AND ANIMAL FOOD PRODUCTS

The method used to calculate concentrations in irrigated food was taken from Burkholder et al. (1975) and Soldat et al. (1976). It is essentially the same as that detailed in NRC Regulatory Guide 1.109. The following equations were used:

$$C_{rv} = \left[IR_v \frac{r C_{rw} T_v \left(1 - e^{-\lambda_{E_r} t_e}\right)}{Y_v \lambda_{E_r}} 1000 + \frac{C_{rt} B_{rv}}{D_T} \right]$$

$$C_{ra} = S_{rA} \left[C_{rF} Q_F + C_{rw} Q_{Aw} \right],$$

where

C_{rv} = concentration of nuclide r in plant v (Ci/kg)
C_{ra} = concentration of nuclide r in animal product a (Ci/unit)
C_{rF} = concentration of nuclide r in feed or forage calculated from C_{rv}(Ci/kg)
C_{rw} = concentration of nuclide r in the fresh water used for irrigation (Ci/m^3)
C_{rt} = concentration of nuclide r in the topsoil (Ci/m^3)
IR_v = irrigation rate during the growing season for vegetable v (ℓ/m^2-d)
r = fraction of deposited nuclide (activity) retained in crops, taken to be 0.25
T_v = fraction of deposited nuclide (activity ending up) in the edible portion of the plant--it assumed to be 1 for leafy vegetables and fresh forage, and 0.1 for other produce
λ_{E_r} = weathering removal constant = 0.693/14 (d^{-1})
t_e = time of above-ground exposure of crops to contamination during the growing season (d)
Y_v = plant yield (kg/m^2)
B_{rv} = plant concentration factor (Ci/kg)/(Ci/kg)
D_T = topsoil density (kg/m^3) assumed to be 1600 kg/m^3

506 312

S_{rA} = transfer coefficient for nuclide r from daily intake of animal to edible portion of animal product d/litre(milk) or d/kg(animal product)

Q_F = consumption rate of contaminated feed or forage by an animal (kg/d)

Q_{Aw} = consumption rate of water by an animal (litre/d).

The values of B_{rv}, S_{rA}, Q_F, and Q_{Aw} are taken from NRC Regulatory Guide 1.109. Table K-1 gives the values of IR_v, Y_v, and t_e.

Concentrations of radionuclides in the edible portions of aquatic foods are found by using the NRC Regulatory Guide 1.109 factors, which measure the ratio of the concentration in the biota to the radionuclide concentration in water at equilibrium.

TABLE K-1. Irrigation rate, plant yield, and growing period.

Plant product	IR_v (litre/m^2-d)	Y_v (kg/m^2)	t_e (d/y)
Leafy vegetables	5.0	1.5	90
Other above ground vegetables	5.3	0.7	60
Potatoes	6.0	4.0	90
Other root vegetables	5.0	5.0	90
Berries	5.0	2.7	60
Melons	5.0	0.8	90
Orchard fruit	5.0	1.7	90
Wheat	5.0	0.7	90
Other grain	5.0	1.4	90
Grass	5.0	1.3	30

506 313

Fresh water bioaccumulation factors were used for the river to calculate fish, mollusk, and crustacean concentrations. Salt water bioaccumulation factors were used for the estuary and ocean calculations.

The shoreline concentrations were modified to take account of the geometry of exposure, using the shore-width factor as given in NRC Regulatory Guide 1.109. Similarly, topsoil concentrations were multiplied by a shielding factor to account for housing.

506 314

APPENDIX L

REPOSITORY MODEL UNCERTAINTY ANALYSIS

SITE DESCRIPTOR UNCERTAINTIES

This section documents the geotechnical input uncertainty data used in this phase of the repository analysis. Our purpose is to provide the best available current information for use in the initial site suitability models, which called for definition of preferred values and probable ranges of all relevant parameters. Where data were poorly understood or not available we made the best technical estimate. The probable ranges of most parameters are reasonably well known. Where estimates had to be made, they are so noted. As the project develops, factors identified as being significant will be refined as appropriate for subsequent models.

The following had to be developed for the physical model data base: (1) descriptors and coefficients for the hydrologic analog of the mathematical model; (2) permeability and porosity values for the geologic formations; (3) occurrence and properties of the borehole seals, backfill, and mine fracture zones; and (4) properties of seismically induced faults. All parameters were assigned preferred values and maximum credible ranges. These values relate to a generic repository in a sedimentary basin and not to a specific site. Thus, the parameters are inherently less precise than those associated with a specific site. This approach is consistent with the philosophy for the generic site suitability model, that is, to evaluate the relative importance of descriptors and not to determine absolute prediction values. The approach used in developing input data reflected this philosophy and was primarily based on experience, available field information, and judgment, rather than on detailed analysis.

Much of the data relates to topics that are not well understood and do not lend themselves to a rigorous evaluation. The permeability of faults, size and permeabilities of mine backfill, borehole seal permeabilities and longevity, and other data are so poorly understood at this time or so variable

506 315

(depending on the details of a specific site or details of construction methods) that any attempt at a detailed evaluation would be inappropriate for a generic model. Thus, the primary rationale for much of the input data was simply technical judgment in an attempt to provide values that reflect the real world and will result in meaningful model output data.

The data relate only to the basic salt or shale model discussed elsewhere in this report. In general, the model is a simple layered system with water flowing vertically upward from a lower aquifer under higher pressure, through the repository zone, and to an upper aquifer. In the upper aquifer, the water flows horizontally to its discharge into a river or lake. Assumptions had to be made relative to the geometry of the repository to provide useful data. For the input data we assumed that the repository was similar to the conceptual design by Parson et al.(1976) Figure L-1 shows the basic layout of the conceptual repository. Changes in the basic geologic and hydrologic model and/or changes in the assumed conceptual repository design would alter many of the parameter uncertainties presented below.

Descriptors and Coefficients

In developing the data base for the physical model, we had to provide uncertainty ranges for the descriptors and coefficients used for this phase of the model analysis. Depending on the results of the initial uncertainty analysis, some of the more sensitive descriptors may be subjected to extensive evaluation and analysis in the future.

For a specific site and assumed level of exploration and instrumentation, there would be an uncertainty at a given confidence level associated with every parameter. The uncertainty arises from geologic variations, errors and limitations of testing techniques, and limitations in the evaluations of the tests or explorations. We considered the following general exploration levels appropriate:

1. Preconstruction Phase
   - Minimal: No boreholes, but research of available regional information and surface mapping,

506 316

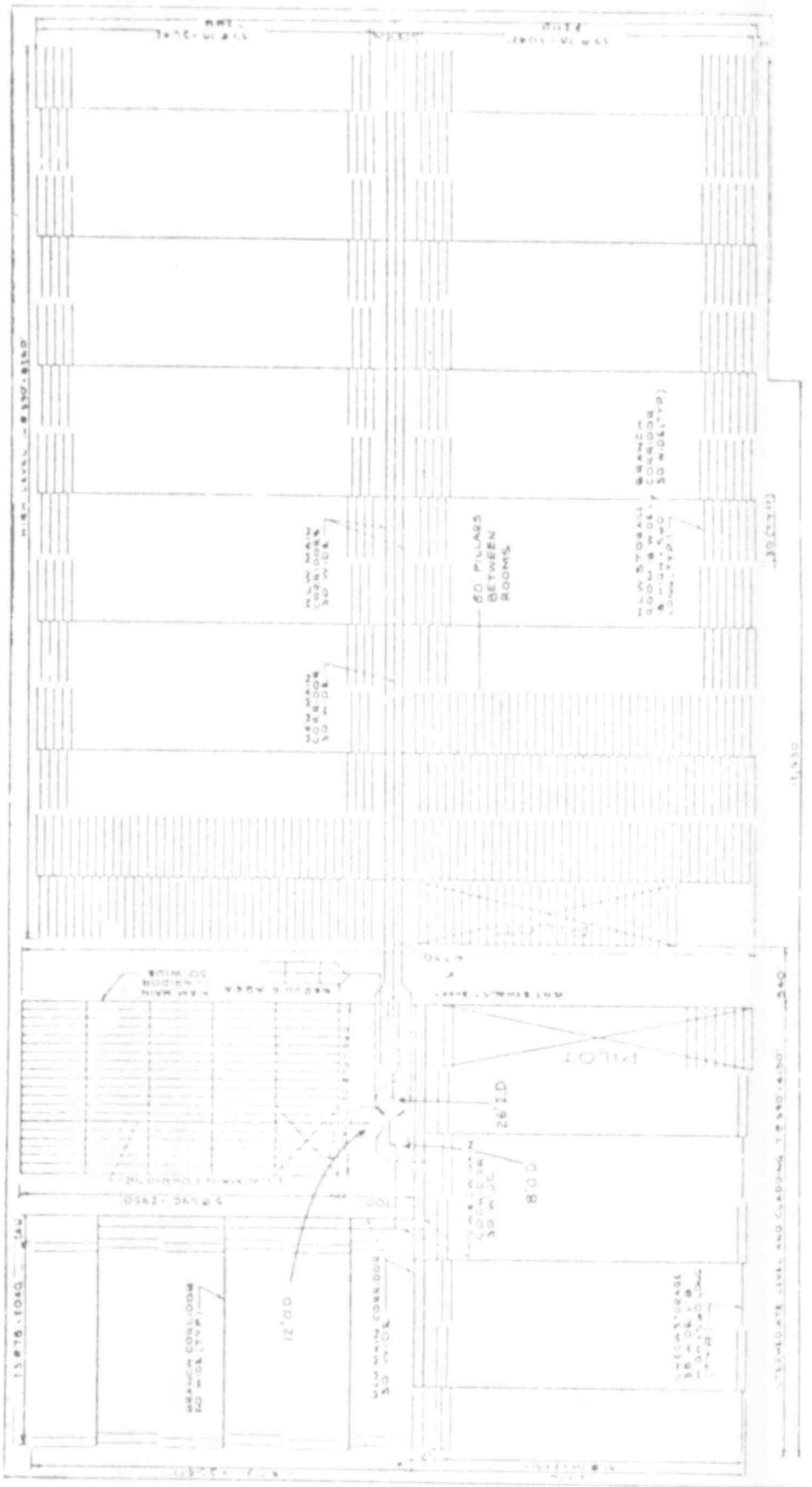

FIG. L-1. Mine master plan.

506 317

- Moderate: Approximately 40 shallow holes to level of repository and 10 deep holes through to underlying aquifers.
- Maximum: Extensive explorations with hydrologic testing.

2. Postconstruction Phase
   - After mining the shaft and main corridors, both with major instrumentation and testing and with instrumentation only.
   - Before backfilling, both with major instrumentation and testing and with instrumentation only.

The uncertainty values are expressed in terms of confidence limits on the median value. For example, if the 90% confidence limits for a parameter are A and B, it means that if the parameter were repeatedly sampled, the value obtained would lie between A and B 90% of the time. The geotechnical parameters were initially assumed to fit a log-normal distribution. The canonical unit for defining the uncertainty U of such a distribution corresponds to the standard deviation in the logarithm of the parameter. Thus, if the median value of the parameter is V, the definition of its uncertainty U is nearly two-thirds of the sample population of the parameter lies between V/U and VU, or alternatively, 95% of the sample population lies between V/U^2 and VU^2. All our uncertainty range values are given in terms of the value U.

Porosity and Permeability

The uncertainty attached to the parameters of permeability and porosity at a specific site depend primarily on the degree of exploration. Maximum exploration would reduce uncertainties, but might also create more pathways that on failure, could cause release of contaminants. In general, rock mechanics and hydrologic testing can be conducted during the premining phase, primarily through boreholes, and during the mining and waste emplacement phase by instrumentation within the mine. The recommended values of U are given in Table L-1.

506 318

TABLE L-1. Values of U for permeability and porosity.

Layer	Premine Phase Exploration			Mine Phase	
	Minimal	Moderate	Extensive	Shaft & Corridors[a]	30 Y[a]
			Permeability		
2	100	10	5	5(4)	5(3)
3	100	10	5	5(4)	5(3)
4	100	10	5	5(4)	4(2)
5	100	10	5	5	5(3)
6	100	10	5	5	5(4)
			Interstitial Porosity		
2	3	2	1.5	1.5	1.5
3	5	3	2	2	2
4	5	3	2	2	2
5	5	3	2	2	2
6	3	2	1.5	1.5	1.5
			Fracture Porosity		
3	10	8	5	5(4)	5(4)
4	10	8	5	4	4
5	10	8	5	5	5

[a]Numbers in parentheses represent uncertainties if extensive explorations are conducted in the mine.

Heads and Gradients

We can measure heads and, thus, compute horizontal and vertical pressure gradients. The effects of salinity complicate this measurement and, thereby, introduce uncertainty. Additional gradients resulting from osmotic potential, thermal potential, and so on are not included in these uncertainties. The values of U for the pressure gradients are given in Table L-2.

506 319

TABLE L-2. Values of U for horizontal and vertical pressure gradients.

	Premine Phase Exploration				Mine Phase	
	Layer	Minimal	Moderate	Extensive	Shaft & Corridors	30 y
Horizontal gradients	2	5	1.3	1.2	1.2	1.2
	6	10	1.3	1.2	1.	1.3
Vertical head between layers 2 and 6		5	1.3	1.2	1.2	1.2

Other Parameters

Preferred values and generic ranges were provided for fault sizes and properties, borehole seal dissolution, backfill dissolution and size, and properties of mine opening fracture zones. These are not measured values. To evaluate credibly the uncertainty related to these computed parameters would require a substantial analysis. In our opinion, such a substantial analysis was inappropriate in this phase. Rather than provide any estimates of U, we recommend that at this phase the full range of values given be assumed as the uncertainty. As we learn more about the sensitivity of these descriptors, we will develop these uncertainties as appropriate.

Relationship Between Permeability and Porosity

To do the Monte Carlo analysis on the predictive model, one has to know the functional relationship between permeability and porosity, otherwise the random input parameter generator could produce premeabilities inconsistent with the porosities. This could be particularly significant for fracture flow, since high permeabilities coupled with low porosities would yield unrealistic water velocities. A deterministic relationship between permeability and porosity does not exist because these properties are not directly related to each other. In a particular formation, however, and assuming only minor variations in other rock properties, it is feasible to construct a stochastic relationship between permeability and porosity.

506 320

Interstitial permeability depends somewhat on porosity. Many media and fluid properties other than porosity influence permeability, but average trends of permeability-porosity values can often be found for different formations. Figure L-2 is a plot of permeability and porosity measurements in two oil-bearing sandstone formations (Archie, 1950). Note that permeability can range over several orders of magnitude for a given porosity, but a general trend is indicated. Figure L-3 shows average trends in the permeability-porosity relationship for many oil-bearing formations. In general, the trend lines are straight and somewhat parallel. An equation can be written for the average trend lines in the form

$$K = A10^{Bn} \quad ,$$

where K is permeability, n is effective porosity, and A and B are coefficients.

Functional relationships can be synthesized by pairing the preferred values and ranges of interstitial permeability and porosity provided for the Monte Carlo model and by assuming that the paired values fall on a trend line similar to those in Fig. L-3. To do the synthesis, we plotted the paired permeability-porosity values as shown in Fig. L-4. The general equation for the trend line is

$$n = C \log_{10}(K/A) \quad ,$$

which is the previous equation solved for porosity rather than permeability. Values for the coefficients C and A are found from these trend lines. We held the coefficient A constant for each layer and varied the coefficient C to give a range of porosities for a given permeability. Recommended values of C are shown in Fig. L-4.

These permeability-porosity relationships are necessary for computational realism when used in the Monte Carlo data-induced uncertainty analysis. They are not meant to reproduce actual permeability-porosity measurements, which can be expected to vary widely from the trend line and ranges given by the above relationships.

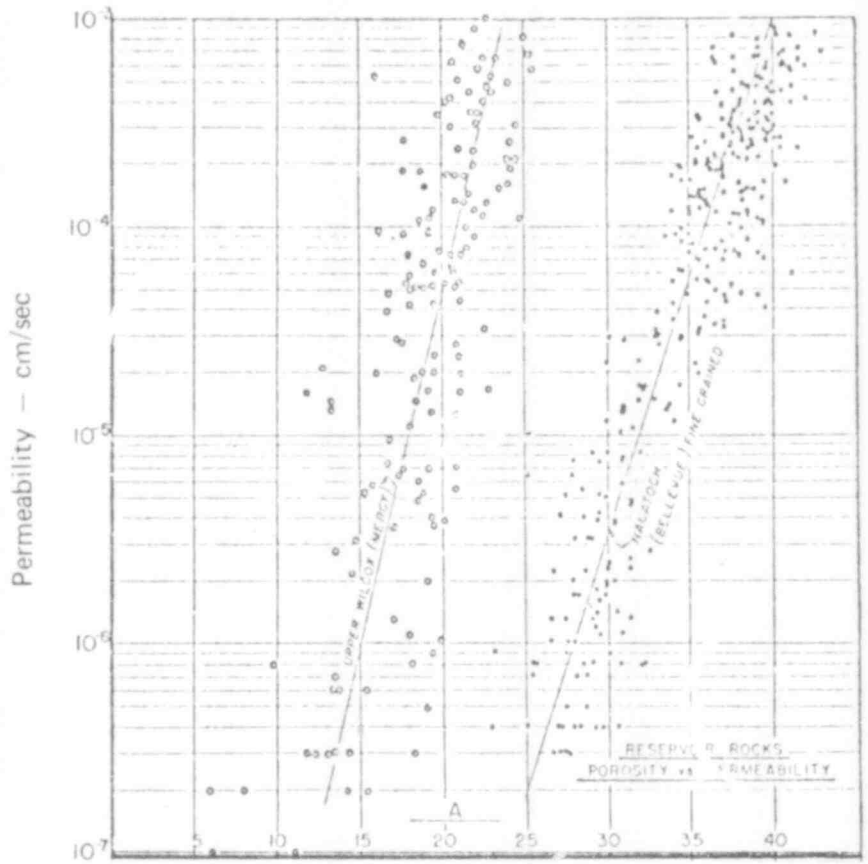

FIG. L-2. Average relation between porosity and permeability for different formations.

506 322

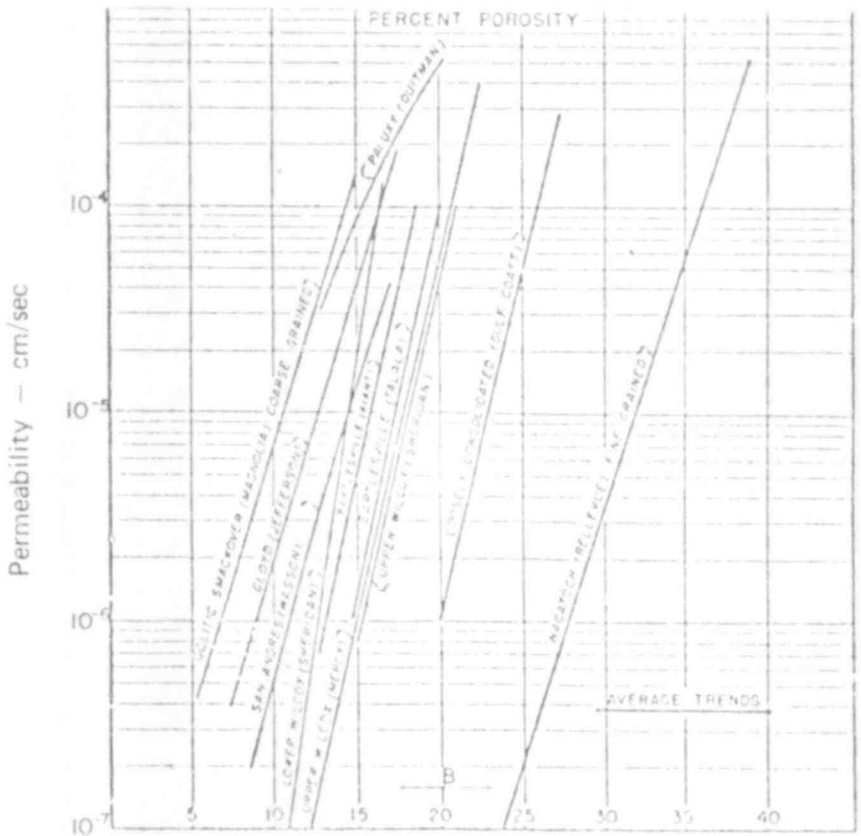

FIG. L-3. Average trends in porosity-permeability relationships.

506 323

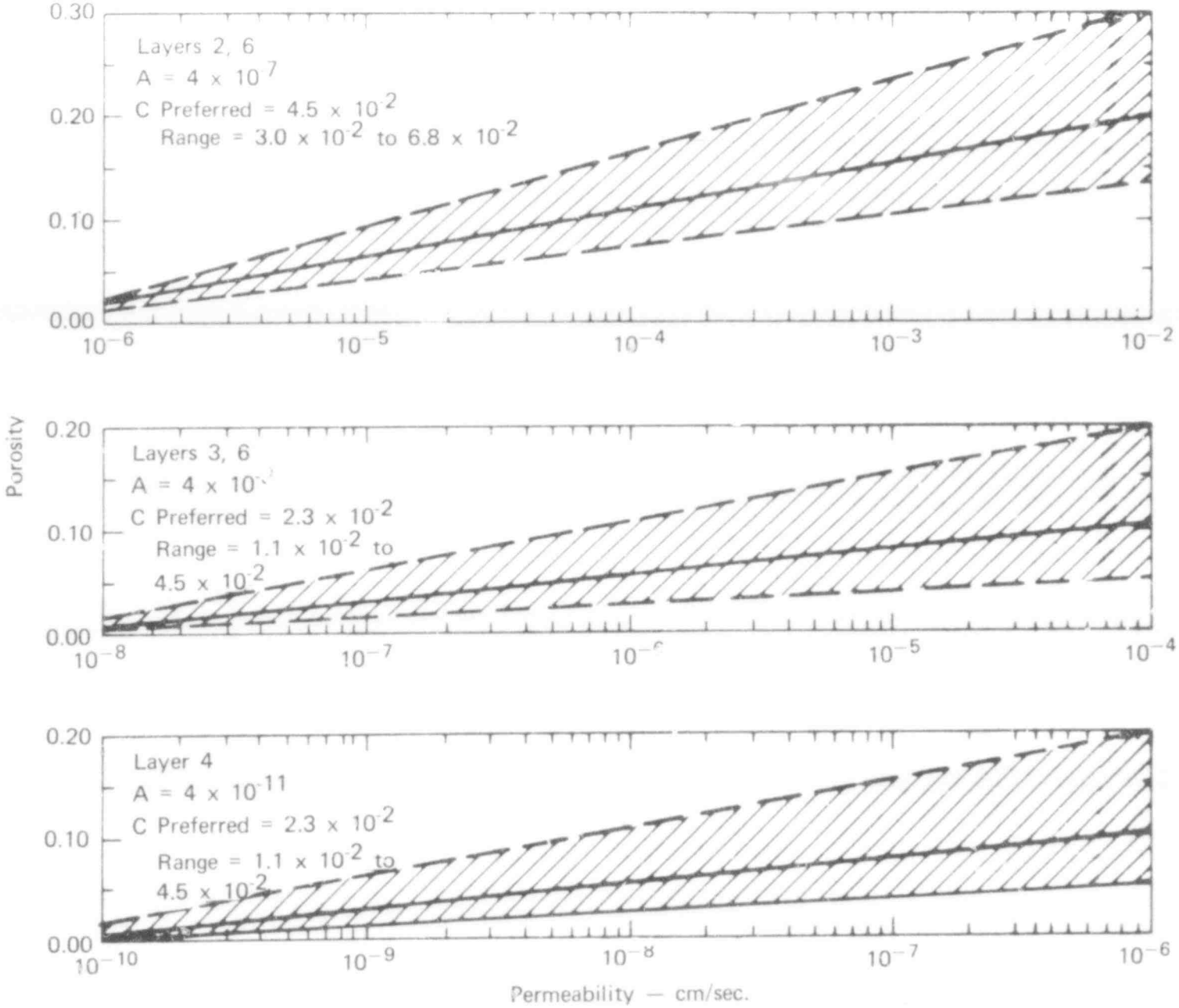

FIG. L-4. Assumed permeability-porosity relationship for interstitial flow.

506 324

The permeability-porosity relationship for fracture flow, in terms of metres and cm/sec, is

$$n = 5.45 \times 10^{-3}(K/S^2)^{1/3} ,$$

where n is porosity, K is permeability (cm/sec), and S is fracture spacing (m).

For the purposes of the uncertainty analysis, we selected a fracture spacing of 1 m with a range of 0.1 to 10 m.

Retardation Factors

Uncertainties in the retardation factors are a product of both the experimental uncertainties in the K_d measurements and the uncertainties related to modeling a generic site where there are no direct measurements of the rock properties. In evaluating the uncertainties, we must ascertain whether the values of K_d determined in the laboratory represent the retardation factors in the field. Unfortunately, there are no reliable in situ measurement techniques of absorption. Even the laboratory approach is fraught with confusion, and a standard methodology is nonexistent.

Experimental evidence shows that retardation factors are a function of rock type, pH, water composition, flow rates, and so forth. Yet how these parameters interrelate and how they quantitatively influence retardation is largely unknown. We do know that waste/water/rock interactions retard radionuclide migration. Theoretically we can calculate the relative velocities of the waste and groundwater, and apply them to the transport model. Based on the limited experience of others, the retardation factors used in our present model appear reasonable. The maximum and minimum values are within the range of expected values.

For the purpose of examining the geochemical barrier to radionuclide migration, the use of estimated retardation factors is adequate for the waste

506 325

model. However, future improvements to the transport model will require an expanded data base such that the retardation behavior of individual radionuclides is understood.

Seismicity

Our analysis indicates that only near-field earthquakes (both large and small) are possible as sources of damage to a well-designed facility. Sufficient data are not available to define the threshold of seismic damage to the site precisely. Establishing a well-defined uncertainty range for the results of our seismic risk analysis is only possible if the time frame of the prediction, geologically speaking, is short. However, a careful geologic investigation could give reasonable assurance that large displacements will occur with sufficiently low probability at a given seismically inactive site to make it useful for containment.

PREDICTIVE MODEL UNCERTAINTIES

The term "predictive model", as used here, refers to the governing physical laws that dictate the time evolution of the hazardous radionuclides in the repository, their analytical and numerical form, and the simplifying assumptions needed to put them into usable form. It also refers to its initial state, boundary conditions, and any time-dependent geological, hydrological, or chemical changes that occur or might occur. The computational form of the HLW predictive model for the repository must be numerical, as the time evolution of the system is too complex to solve in closed analytical form.

Our ongoing program ensures that the model is sufficiently realistic to make credible predictions. Simplifying and expediting assumptions that have been necessary to generate timely predictions are currently being evaluated. The ultimate believability of a model is determined by its ability to predict actual doses. It is impossible to provide timely predictions from a validated model if comparing with an actual system history is the only acceptable validation procedure. However, one can verify subsystems of the model and test some of the physical and numerical assumptions and processes. This effort will lead to a higher-confidence model.

506 326

Uncertainty in the predictive model is attributed mainly to the uncertainty in the model structure; a secondary source of uncertainty is numerical. Unless one carefully considers such things as numerical roundoff error, truncation error, and formulation of analytical expressions, the transformation of the analytical model into the numerical model can lead to serious disastrous errors. Moderate caution, however, can usually eliminate computational problems.

Currently, the predicted dose to humans is based on parametric simulation models for radionuclide inventory (ORIGEN), groundwater waste migration (WASTE), and dose intake (BIODOSE). Although the methodology of the present discussion applies to each of these subsystems, we have excluded ORIGEN from this discussion because it is well accepted by the technical community. We also excluded BIODOSE because it is based on established and validated methodology. However, the WASTE model is new, reasonably untested, and potentially controversial; thus, it certainly is a potential major source of predictive model uncertainty. WASTE has been used to predict repository performance for relatively simple geological and hydrological scenarios, and a substantial effort to expand its capabilities and improve its acceptability is underway. A concern is that models with insufficient complexity are known to produce inaccurate predictions; however, too detailed a model may be too specific for our purposes. We must ensure that a balance between too little and too much detail is met in WASTE. O'Neil (1971) presented a discussion of model complexity and how it relates to radioecological systems.

Assumptions in WASTE

The subsurface waste migration model, WASTE, is based on the following vector equation for dispersive flow through porous media:

$$B \frac{\partial c}{\partial t} + \underline{v} \cdot \nabla c = (\alpha - 2\mu)\nabla \cdot (V\nabla c) + 2\mu \, (\underline{v} \cdot \nabla) \frac{1}{V} (\underline{v} \cdot \nabla) c \quad ,$$

where

B = nuclide retardation factor

506 327

$\underline{v}$ = interstitial fluid velocity

c = nuclide concentration in interstitial flow

α,μ = coefficients of the dispersivity tensor

V = $|\underline{v}|$.

A number of physical assumptions, made in the derivation of this vector equation, contribute to model uncertainty: (1) pulse dilution due to diffusion is negligible when compared to dispersion, (2) the dispersivity tensor of the porous medium is isotropic, (3) the flow is incompressible ($\nabla \cdot \underline{v}=0$), and (4) the transport equation is valid for fracture flow.

Of these assumptions, the question of the validity of the transport equation for fracture flow may be of most concern to the evaluation of model uncertainty. Therefore, we are considering an investigation of fracture flow to examine the relation between effective dispersion and fracture spacing. Such an investigation can be facilitated by a fracture flow model consisting of a separate flow pathway for each fracture (e.g., perhaps 50 fracture flow paths for a segment of fractured rock).

Flow Pathway Model

The most important model-structure assumption in WASTE at present is that the geology/hydrology of the site can be simulated by a three-dimensional network of one-dimensional flow pathways. For the model, the analogs required to simulate the actual anticipated groundwater movements were developed mainly from experience, available field information, and judgment, rather than from a detailed theoretical analysis. This approach was feasible because the initial models were hydrologically simple. More complex models may require numerical groundwater analysis if an appropriate flow path analog is to be developed. Fundamentally, the flow path model is not a groundwater model and cannot solve groundwater flow problems; it is a nuclide transport model requiring the general hydrology to be solved external to the model with the results analogued into the model in the form of an appropriate flow path network.

506 328

Although each flow path segment is one dimensional, the network itself can be made to simulate two or three dimensions.

Theoretically, a suitable WASTE analogy can be developed to simulate closely almost any specific geologic and hydrologic condition. This would be accomplishedby using two- or three-dimensional transport codes to evaluate the nuclide concentrations at critical points. A flow path network could then be developed that would give the desired results. Most errors in WASTE relate to the development of the flow path analog and to the efforts needed to simplify the r work.

Testing Flow Pathway Model Assumptions

The flow path approach entails at least two major assumptions: (1) lateral dispersion across flow path walls does not significantly affect ion concentrations and travel times and (2) the choice of flow paths through the media does not introduce significant errors in passage times of the ions.

The first assumption cannot be tested without extensive calculations. Dispersion is poorly understood and difficult to measure experimentally. Limited experimental results, however, show that lateral dispersivity is usually a fraction of longitudinal dispersivity. Given the limited state of knowledge of dispersion phenomena, one-dimensional treatment of dispersion is probably sufficient for sensitivity analyses based on a conceptual model.

The second assumption can be tested partially by some simple calculations. Figure L-5 shows a two-layer system analogous to the six-layer repository model of Fig. 2. Velocities and travel times were calculated using Darcy's law for a vertical path through layer 1 and a horizontal path through layer 2. They were then recalculated to account for a horizontal gradient and horizontal permeabilities within layer 1 (Fig. L-6). The difference in the travel times between the first case and the second case was divided by the total travel time in the second case to obtain an estimate of the error in the "strictly vertical flow in the lower layer" assumption. The results are summarized in Table L-3. As the horizontal permeability in the lower layer increases and approaches the horizontal permeability of the upper layer, the

506 329

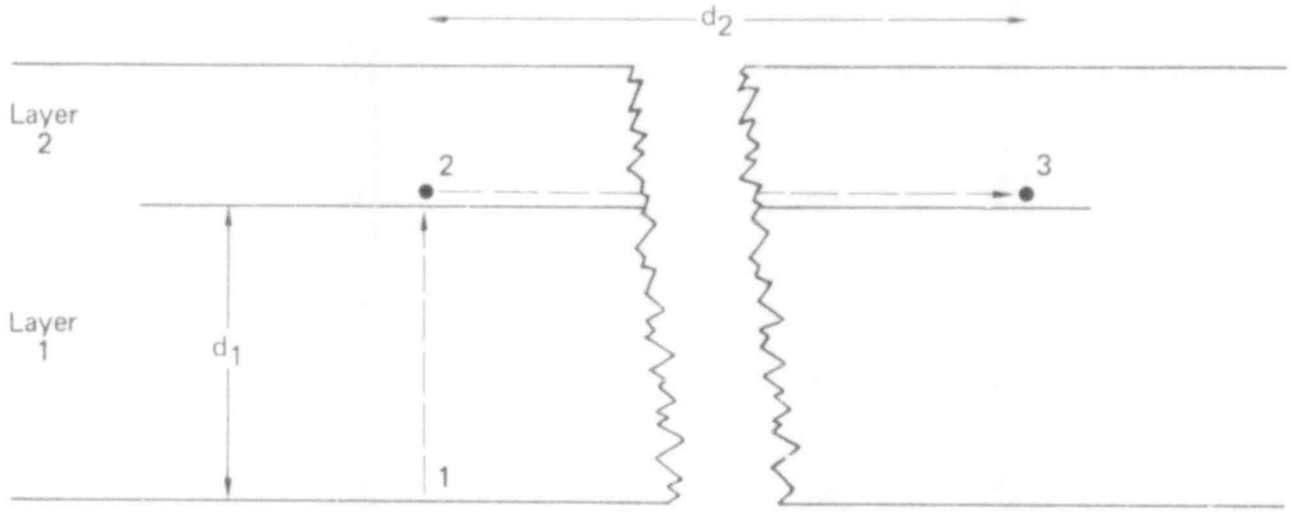

Vertical distance, d_1 = 400 m

Horizontal distance, d_2 = 16,000 m

Vertical permeability in layer 1, $K_{y_1} = 10^{-8}$ cm/sec , $K_{x_1} = 0$

Horizontal permeability in layer 2, $K_{x_2} = 10^{-4}$ cm/sec , $K_{y_2} = 0$

Pressure at node 1, P_1 = 140 m

P_2 = 80 m

P_3 = 0 m

FIG. L-5. Two-layer case with approximated vertical and horizontal paths.

506 330

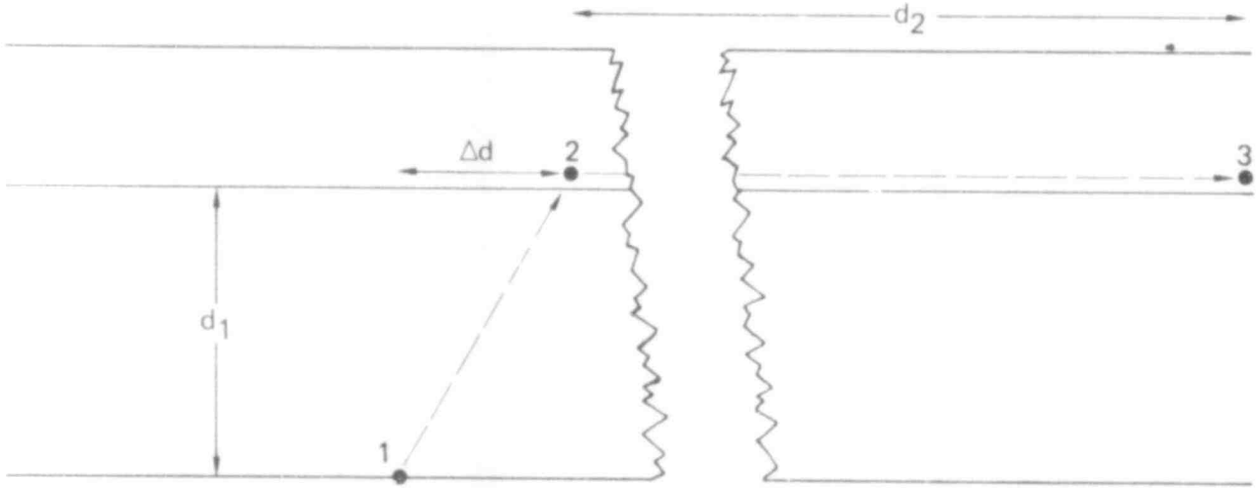

d_1 = 400 m d_2 = 16,000 m − Δd
Δd = distance of horizontal offset
K_{x_1} = 10^{-8} to 10^{-5} cm/sec
K_{y_1} = 10^{-8} cm/sec
K_{x_2} = 10^{-4} cm/sec
K_{y_2} = 0
P_1 = 140 m
P_2 = 80 m − 0.005 (Δd)
P_3 = 0 m

FIG. L-6. Two-layer case with both vertical and horizontal flow in layer 1.

506 331

TABLE L-3. Summary of two-layer flow calculations.[a]

Case	K_{y_1} ($\frac{cm}{sec}$)	K_{x_1} ($\frac{cm}{sec}$)	Distance of horizontal offset, Δd(m)	Distance of travel in layer 1 (m)	Velocity in layer 1 (m/y)	Total travel time (y)	Δt(y)	Error (%)
Without horizontal flow in layer 1	10^{-8}	0	0	400	4.7×10^{-4}	9.5×10^{-5}	0.0	0.0
With horizontal flow in layer 1	10^{-8}	10^{-8}	13.6	400	4.7×10^{-4}	9.5×10^{5}	85	0.009
	10^{-8}	10^{-7}	136	422	5.0×10^{-4}	9.4×10^{5}	1×10^{4}	1.1
	10^{-8}	10^{-6}	1 360	1 420	1.67×10^{-3}	9.4×10^{5}	1×10^{4}	1.1
	10^{-8}	10^{-5}	13 600	13 600	1.6×10^{-2}	8.65×10^{5}	8.5×10^{4}	9.8

[a] $K_{x_2} = 10^{-4}$ cm/sec and $K_{y_2} = 0$.

506 332

error becomes greater. This error remains small, however, for the ranges of values used in the sensitivity analyses.

Similar calculations were made for a three-layer case in Figs. L-7 and L-8. Values of permeability, distances, and pressure gradients in this case are the same as the unflawed repository model without flow in the repository and shaft. The error in travel time calculations in this case is only 0.6% (see Table L-4). The calculations indicated that the choice of a vertical flow path through barrier and repository layers does not introduce significant errors into the analyses. However, the cases considered are simple. More sophisticated methods or validation are necessary as more complex models are developed.

Comments on Flow Pathway Model

At this time it is difficult to assess rigorously the errors involved in using the flow path model. However, the following statements support the use of such a model for a generic site suitability study:

1. In a generic repository study, the uncertainties related to input parameters are inherently large. The range of many of these generic parameters (especially properties such as permeability and fracture porosity, which exhibit wide ranges) may exceed many orders of magnitude.
2. Because of the wide range in radioactivity exhibited by the high level waste as it decays and the anticipated time required for the nuclides to reach the biosphere, the general computed radiologic effects will be assessed in terms of orders of magnitude. Subtle variations in computed concentrations or dose will probably be of minimal consequence.
3. Uncertainties are associated with other phases of the site suitability program, including waste dissolution behavior, nuclide adsorption behavior, dispersion behavior, prediction of future geologic events, and evaluation of the effects on man of a given radiation release.
4. The advantages of complex two- or three-dimensional hydrology and nuclide transport codes (finite element or finite difference) may be

506 333

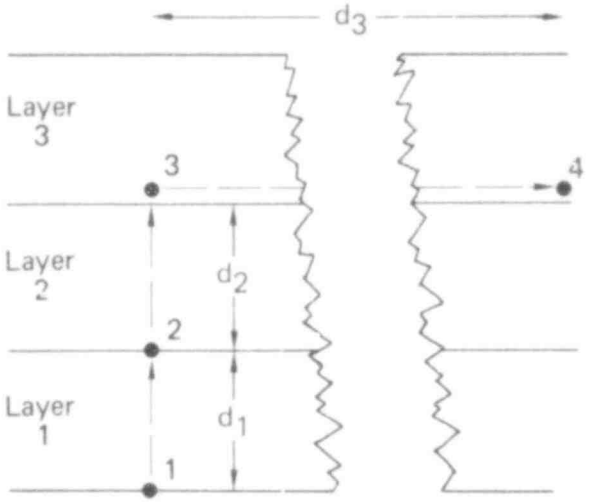

Case without horizontal flow in layers 1 and 2

$d_1 = d_2 = 200$ m
$d_3 = 16{,}000$ m
$K_{y_1} = 10^{-9}$ cm/sec, $K_{x_1} = 0$
$K_{y_2} = 10^{-7}$ cm/sec, $K_{x_2} = 0$
$K_{x_3} = 10^{-4}$ cm/sec, $K_{y_3} = 0$
$P_1 = 140$ m
$P_3 = 80$ m
$P_4 = 0$ m

FIG. L-7. Three-layer case without horizontal gradient in layers 1 and 2.

506 334

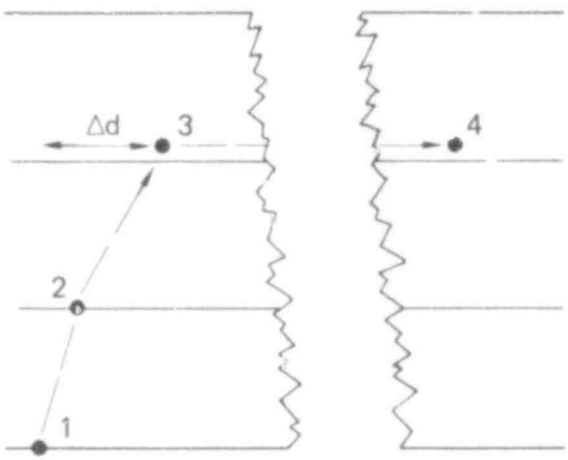

Case with horizontal
flow in layers 1 and 2

$d_1 = d_2 = 200$ m
$d_3 = 16{,}000$ m $- \Delta d$
$K_{y_1} = 10^{-9}$ cm/sec
$K_{y_2} = 10^{-7}$ cm/sec
$K_{y_3} = 0$
$K_{x_1} = 10^{-8}$ cm/sec
$K_{x_2} = 10^{-6}$ cm/sec
$K_{x_3} = 10^{-4}$ cm/sec
$P_1 = 140$ m
$P_3 = 80$ m $- 0.005(\Delta d)$
$P_4 = 0$ m

FIG. L-8. Three-layer case with horizontal gradients in layers 1 and 2.

506 335

TABLE L-4. Summary of three layer flow calculations.

Condition	K_{y_1} (cm/sec)	K_{y_2} (cm/sec)	K_{y_3} (cm/sec)	K_{x_1} (cm/sec)	K_{x_2} (cm/sec)	K_{x_3} (cm/sec)	Total Travel Time (y)	t(y)	Error(%) Error(%)
Without horizontal flow in layers 1 and 2	10^{-9}	10^{-7}	10^{-5}	0	0	10^{-4}	8.65×10^{6}	0	0
With horizontal flow in layers 1 and 2	10^{-9}	10^{-7}	10^{-5}	10^{-8}	10^{-6}	10^{-4}	8.59×10^{6}	5×10^{4}	0.6%

506 336

limited in a suitability evaluation for a repository site. Using these methods, it is difficult to model extreme variations in hydrologic properties such as repository backfill dissolution, borehole seal failure, or faults. These small-scale features may exhibit permeabilities several orders of magnitude greater than the adjacent rock formations. Unless properly incorporated into the model these features may result in numerical instabilities and erroneous results. In addition, as the models are refined to include numerous layers, complex geometry, complex gradients, and many anomalies (shafts, boreholes, mines, reefs, faults, and so on). Many simplifying assumptions may be required to keep the model from becoming too cumbersome to be useful. This situation would be particularly true of a three-dimensional code. However, the ability to handle complex situations with numerous anomalies is one of the strengths of the flow path model.

5. A preliminary error analysis that considered all the uncertainties related to a generic model study indicated that virtually no significant error would be introduced by using the flow path model instead of a true three-dimensional transport code. This conclusion is logical because of the large uncertainties in the input data and errors related to many of the other required analyses.

Probably the most serious problem associated with the flow path geology/hydrology model is the construction of a proper network. A network that fails to incorporate a major flow path or significant hydrologic mechanism would produce errors. Therefore, adequate validation of the network analogies is essential to the site suitability program. Validation techniques could include numerical solutions (finite element or finite difference hydrologic and transport codes), analytical solutions, or actual field data.

Alternative Model Structures

Alternative model structures to represent the waste flow are under consideration. We are investigating complex flow models using two- and three-dimensional finite element models. Future models should be aimed at: (1) validation of the present transport model, and modification and improvement of the model to reduce uncertainties; and (2) consideration of more realistic and complex repository models.

506 337

Validation and modification of the transport model entails implementation of two- or three-dimensional flow and solute transport analyses. In more than one dimension, however, fluid flow and solute transport problems must be solved using numerical methods. The numerical techniques usually applied are finite differences, finite elements, and methods of characteristics. Comparable results can be obtained using any of these methods. Finite element methods are preferable if complex geometries or higher-order approximations must be considered. Some available codes suitable for solute transport modeling are summarized in Appendix A.

A multidimensional groundwater flow code will be used to evaluate and validate the hydrologic input values used to date. The primary cases to be modeled are (1) the basic case with flow in fracture zones around the repository and shaft, (2) the case where a high-permeability fault intersects the repository, and (3) the case where a low-permeability fault intersects the repository. Other cases, such as borehole seal failures and multiple failure events, will be analyzed. A sensitivity analysis will be run for each of these cases for variable permeability, pressure gradients, and distances of travel. The multidimensional groundwater flow code could become an integral part of the input procedure for WASTE. Other inherently multidimensional aspects of the waste transport process, such as source configuration and lateral dispersion, will be modeled and the predictions compared with those obtained in WASTE.

Generally speaking, extension of modeling to include new parameters will be necessary as the project progresses. Low-priority effects, such as thermal gradients, variable fluid densities, and long range climatic changes, which have been neglected to date, may radically affect groundwater flow regimes. The importance of these effects should be evaluated along with the technological limitations for their treatment. Under some conditions, the steady-state hydrology model may not be appropriate and transient hydrological modeling may be necessary. If so, the modeling capabilities should also include a time-dependent hydrological model.

506 338

MONTE CARLO PREDICTION UNCERTAINTIES

The WASTE subsurface waste migration model is characterized by different geological and geochemical parameters, e.g., permeability and porosity of the geological layers and retardation factors for the different nuclides. The assumed parameter values used in the risk calculations are uncertain for a number of reasons, including measurement uncertainty and level of exploration. Uncertainty in the data parameters gives rise to uncertainty in the site performance predictions. Our approach is to view the underlying model values and their ranges to be specified by probability distribution functions (PDFs). A random-number generator is used to pick values from these PDFs. The chosen descriptor values are used in WASTE for many trials. The resulting distribution of predictions is then used to determine data-induced uncertainties in the prediction.

A Monte Carlo computer program (WSRAND) has been developed to generate random parameter values using specified probability distributions. These parameters are used as inputs for the WASTE program to simulate the flow of waste out of a repository with a particular set of random geological and geochemical characteristics. This process is repeated for a number of random parameter sets, e.g., 50, and statistical analysis may be performed on the ensemble of outputs. This procedure is illustrated in Fig. L-9.

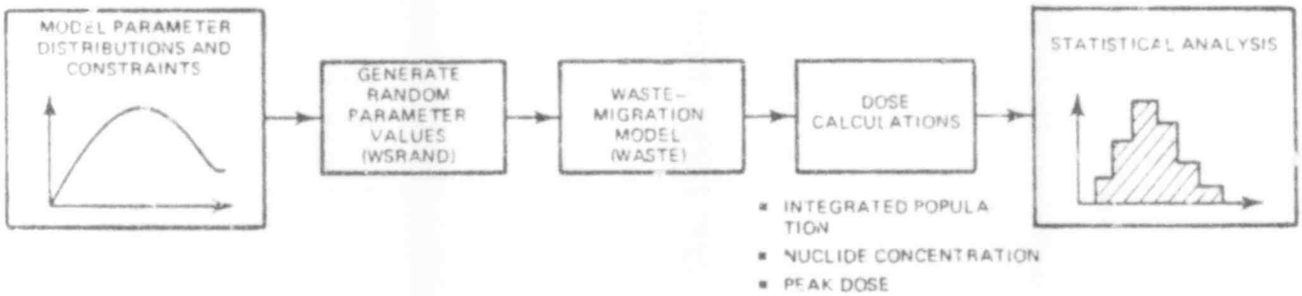

FIG. L-9. Data-induced uncertainty analysis for the geology-hydrology model.

506 339

The Monte Carlo approach to the uncertainty analysis facilitates a statistical characterization of the performance prediction uncertainty. Simple to implement, the technique is flexible in that it can be modified to accommodate a wide variety of descriptor distributions and constraints. A drawback might be the amount of computer time and costs required to perform the number of Monte Carlo trials needed to represent adequately the assumed parameter distributions. However, many may not be necessary because precise knowledge of the input parameter distributions is not currently available.

Baseline Repository

The baseline repository chosen for the initial Monte Carlo study is a shale repository with flow paths to the aquifer through a fracture zone surrounding the tunnel and shaft, and through the two overlying layers of shale. Flow through the shale is assumed to be interstitial. This repository, along with its descriptor preferred values, was described previously. For the Monte Carlo study, the effects of geologic state transitions have not been considered to date.

Generation of Random Parameters

We assumed, in developing the methodology, that the model parameters generated randomly have approximately lognormal distributions. In addition, we required them to satisfy certain constraints based on physical considerations. The following model parameters are generated randomly:

- Permeabilities
- Porosities
- Cross sections of the shaft and tunnel fracture zones
- Nuclide retardation factors
- Dispersion coefficients
- Horizontal head gradient in the aquifer
- Head difference of the underlying and overlying aquifers
- Dissolution rate of the waste
- Time required to saturate the repository void space.

Note that the assumption of a lognormal distribution may be incorrect in many cases. The available data base may not be sufficient to characterize adequately the low-probability tails of the distribution functions. The results of this study can serve as a baseline for definition of future work.

Statistical Analysis of Random Data

A statistical analysis has been performed on the random input data to the Monte Carlo analysis to check the consistency of the random sample distributions with the assumed population distributions, and to determine the impact of the parameter constraints on the sample statistics. In many cases, the parameter constraints result in significant modifications of the assumed unconstrained population distributions. Figure L-10 shows the procedure for generating and analyzing the constrained parameter distribution functions.

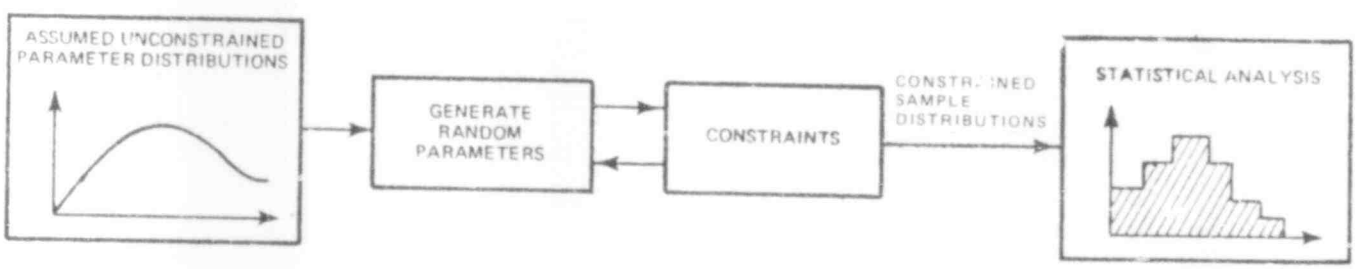

FIG. L-10. Analysis and generation of constrained distributions.

Table L-5 compares the constrained sample statistics with the assumed unconstrained statistics.

TABLE L-5. Constrained sample statiscics.

Variate	Sample mean	Sample Standard deviation	Assumed unconstrained mean	Assumed unconstrained standard deviation
	$\log_{10}$ (variate)	$\log_{10}$ (variate)	$\log_{10}$ (variate)	$\log_{10}$ (variate)
Actinide retardation factor, aquifer	3.5	0.4	4.0	0.5
Actinide retardation factor, fracture zone	3.5	0.4	4.0	0.5
Actinide retardation factor, shale (interstitial)	4.0	0.5	4.0	0.5

As an example of the significance of the model constraints let us consider the following. For each set of randomly generated data, it was required (Isherwood, 1977) that the retardation factors for actinides flowing through the fracture zone and the aquifer be less than or equal to the corresponding value for interstitial flow through shale. The distribution for interstitial flow in shale was not constrained, and the values for the fracture zone and aquifer that failed to meet the specified inequality constraint were rejected. As is evident from Table L-5, sample statistics for the unconstrained interstitial actinide retardation factor were in close agreement with the assumed probability distribution. However, the sample statistics for the constrained variates differed significantly from their assumed unconstrained distributions. Similar results have been observed for each of the constrained variates. In each case, the constraints tend to alter the shape of the assumed probability curves.

506 342

The effect of the model constraints on the sample probability distributions indicates that there may be a need to determine the underlying parameter distributions more accurately. An accurate assessment of data-induced uncertainty may not be possible without a more complete understanding of the underlying model constraints and correlations than is currently available.

Statistical Analysis of Data-Induced Uncertainty

Once the random data have been put through the subsurface waste migration programs and dose model programs, the ensemble of results will be subjected to a statistical analysis. Among the performance measures that will be considered are (1) peak dose to an individual, (2) integrated population dose, and (3) concentrations of various nuclides in the aquifer.

The analysis, including histograms and sample statistics (e.g., means and standard deviations), will indicate the range of the uncertainty indices. Various theorems from sampling theory (e.g., the central limit theorem) can be used to determine confidence intervals for estimates of the population statistics.

Constraints Used in the Monte Carlo Analysis

The Monte Carlo program (WSRAND) was designed to incorporate a variety of constraints and correlations into the generated sets of input parameters for the waste migration model. Each randomly generated variate, V, is assumed to have a lognormal distribution and is thus characterized by its median value, M, and scale factor uncertainty, U.

The scale factor uncertainty, U, has the property that $\log_{10}(U)$ is the standard deviation of the normal random variable $\log_{10}(V)$ with median $\log_{10}(M)$. Constraints incorporated into the Monte Carlo routine in some cases have the effect of modifying the sample distributions so that th deviate significantly from the assumed population distributions. The scale factor uncertainties we used reflect the assumed measurement uncertainties and ensemble parameter variations that exist after a moderate exploration of the repository before excavation (Plum, 1977).

506 343

Dispersion Coefficients

Table L-6 lists the median value and scale factor for the randomly generated dispersion coefficients, which were generated independently of each other and all other variates.

TABLE L-6. Assumed statistics for dispersion coefficients.

Pathway	Median value (m)	Scale factor uncertainty
First segment of tunnel fracture zone	50	2
Repository layer	50	2
Second segment of tunnel fracture zone	50	2
Shaft fracture zone in repository layer	50	2
Shaft fracture zone in shale layer	50	2
Barrier layer above repository	50	2
Aquifer	50	2

Stream Tube Cross Sections

Table L-7 lists the median values and scale factor uncertainties for the cross sections of the shaft and tunnel fracture zone.

506 344

TABLE L-7. Assumed statistics for pathway cross sections.

Pathway	Median value (m^2)	Scale factor uncertainty
First segment of tunnel fracture zone	316	2.5
Second segment of tunnel fracture zone	18.96	2.5
Shaft fracture zone in repository layer	10.0	10.0
Shaft fracture zone in shale layer	5.0	10.0

Nuclide Retardation Factors

Table L-8 lists the assumed statistics used to generate the random retardation factors. The retardation factor statistics are listed according to pathway and nuclide group, where the groups are numbered as follows:

I. ^{129}I, ^{99}Tc

II. Other Fission Products

III. Actinides

TABLE L-8. Assumed retardation factor statistics.

Pathway	Nuclide group	Median value	Scale factor uncertainty
Aquifer	I	1.0	0[a]
	II	10^2	3.16
	III	10^4	3.16
Fracture zone Shaft and tunnel	I	1.0	3.16
	II	10^2	3.16
	III	10^4	3.16
Shale Repository and barrier	I	1.0	3.16
	II	10^2	3.16
	III	10^4	3.16

[a]The retardation factor for group I was constrained to be unity in the aquifer, but is listed here for the sake of completeness.

506 345

A number of constraints were imposed (Isherwood, 1977) on the retardation factors. These constraints are described below using the following notation:

BS(j) = retardation factor for interstitial flow of the nuclide group j through shale; j = I, II, III.

BA(j) = retardation factor for flow of the nuclide group j through the aquifer; j = I, II, III.

BF(j) = retardation factor for flow of the nuclide group j through the fracture zone (shaft and tunnel); j = I, II, III.

- Constraints for iodine and technetium apply to the retardation factors for ^{129}I and ^{99}Tc (nuclide group I):

  $BS(I) \geq 1.0$

  $BF(I) \geq 1.0$

  $BA(I) = 1.0$

  $BF(I) \leq BS(I)$

- Constraints for fission products and actinides apply to the retardation factors for fission products (group II) and actinides (group III):

  $BS(II) \geq BS(I)$

  $BS(III) \geq BS(I)$

  $BF(II) \geq BF(I)$

  $BF(III) \geq BF(I)$

  $BA(II) \geq BA(I)$

  $BA(III) \geq BA(I)$

  $BA(II) \leq BS(II)$

  $BA(III) \leq BS(III)$

  $BF(II) \leq BS(II)$

  $BF(III) \leq BS(III)$

506 346

We assumed, in addition to the above constraints, that the fission product and actinide retardation factors are correlated random variables. Thus, variates $\log_{10}(BS(II))$, $\log_{10}(BS(III))$ were generated using an assumed bivariate normal distribution with a correlation coefficient $\rho = 0.5$.

Figure L-11 is a normalized histogram of 1000 random retardation factors for group I (^{129}I, ^{99}Tc) in shale, generated to satisfy the constraints specified earlier.

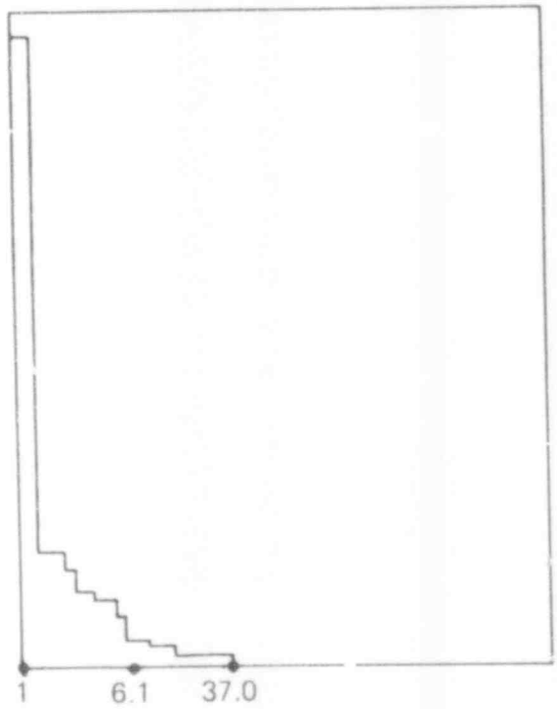

FIG. L-11. Sample probability density functions for retardation factors for ^{129}I and ^{99}Tc in shale, obtained from 1000 Monte Carlo trials.

Permeabilities and Effective Porosities

Because permeability and effective porosity are closely related quantities, the values used in this study were generated jointly. The constraints specified were obtained from Rowe (1977).

506 347

Fracture Zones

Tables L-9 and L-10 list the assumed statistics used to generate the random permeabilities and effective porosities for the fracture zone. For each pathway, we assumed that the random variates $\log_{10}$ (permeability) and $\log_{10}$ (porosity) have a bivariate normal distribution with a correlation coefficient $\rho = 0.8$.

TABLE L-9. Assumed permeability statistics for fracture zones.

Pathway location	Median value (cm/sec)	Scale factor uncertainty
Tunnel	10^{-1}	10.0
Shaft in repository layer	10^{-4}	10.0
Shaft in shale barrier layer	10^{-4}	10.0

TABLE L-10. Assumed effective porosity statistics for fracture zones.

Pathway location	Median value (cm/sec)	Scale factor uncertainty
Tunnel	10^{-1}	2.0
Shaft in repository layer	10^{-3}	10.0
Shaft in shale barrier layer	10^{-3}	10.0

Interstitial Flow

Table L-11 lists the assumed statistics used to generate the random permeabilities for flow in the bulk undisturbed rock.

506 348

TABLE L-11. Assumed statistics for permeability in the undisturbed rock.

Layer	Median Value (cm/sec)	Scale Factor Uncertainty
Repository layer	10^{-9}	10.0
Shale barrier layer above repository	10^{-7}	10.0
Aquifer	10^{-4}	10.0
Barrier layer below repository	10^{-5}	10.0

For this flow the effective porosities ε were generated from the horizontal permeabilities K_H by the relationship (Rowe, 1977)

$$\varepsilon = C \log_{10}\left(\frac{K_H}{A}\right) .$$

The constants C and A depend on the geologic medium and are listed in Table L-12. In addition, the interval constraint $0 < \varepsilon < 1$ was imposed to yield physically possible values of porosity.

TABLE L-12. Constants used to generate effective porosity from permeability.

Layer	C	A (cm/sec)
Aquifer	4.5×10^{-2}	4.0×10^{-7}
Shale barrier layer above repository	2.3×10^{-2}	4.0×10^{-9}
Repository layer	2.3×10^{-2}	4.0×10^{-11}
Shale barrier layer below repository	2.3×10^{-2}	4.0×10^{-9}

506 349

Figure L-12 is a normalized histogram of 1000 random permeabilities for the aquifer.

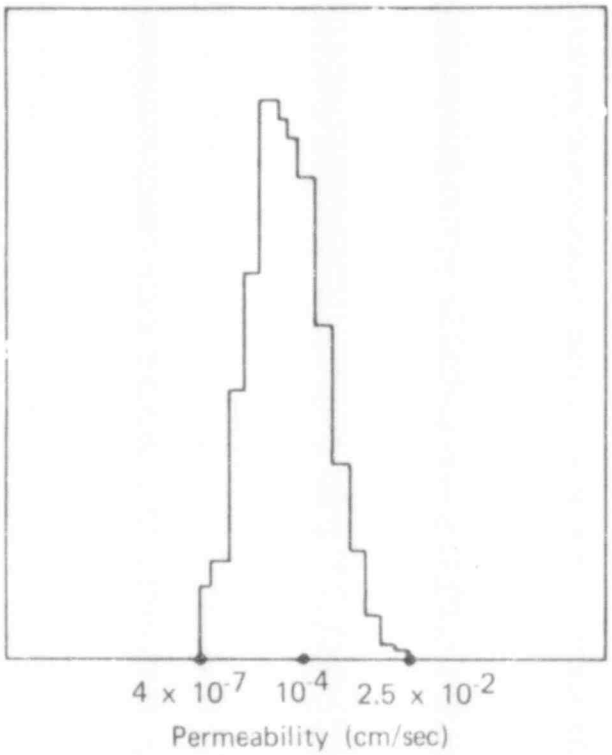

FIG. L-12. Sample probability density function for aquifer permeability obtained from Monte Carlo trials.

Additional Variates

Table L-13 lists the statistics used to generate the following random variates:

- Horizontal head gradient in the aquifer
- Vertical head of the underlying aquifer
- Dissolution rate of the waste (Λ)
- Time required to saturate the repository void space (T_{fill}).

506 350

TABLE L-13. Statistics of some random variates.

Variate	Median value	Scale factor uncertainty
Horizontal head gradient in the aquifer (m)	5.0×10^{-3}	1.2
Vertical head of the underlying aquifer (m)	60.0	1.2
Λ (y^{-1})	10^{-4}	10.0
$T_{fill}(y)$	10^{2}	10.0

506 351

APPENDIX M

PERMEABILITY, POROSITY, AND FRACTURE DATA FOR ROCKS

This appendix contains some of the laboratory and field data on which we based the permeability and porosity values assumed for our generic repository model.

TABLE M-1. Permeability and porosity of sandstone conglomerate

Description	Permeability (cm/sec)	Porosity	Type of test	Reference
Triassic Basin sandstone, mudstone, conglomerate	10^{-11} to 10^{-9}	--	Lab	Marine, 1973
Sandstone, Spraberry oil field, W. Texas	9.7×10^{-10} to 9.7×10^{-7}	<0.13	Field	Streltsova, 1976
Sandstone, sandy shales East Carpathians				Streltsova, 1976
Primary	$<10^{-6}$	0.08-0.10	Field	Streltsova, 1976
Secondary	10^{-4}			
Sandstone, Shebelinsky gas field - secondary	10^{-4} to 10^{-3}	0.05-0.27	Field	Streltsova, 1976
N. E. British Columbia sandstones, shales	10^{-8}		Field	Golder, Brawner & Assoc., 1976
N. W. Alberta sandstone, silty sandstone	5×10^{-6} to 2×10^{-4}		Field	Golder, Brawner & Assoc., 1976
effective	3×10^{-4}			
Uinta sandstone	3.4×10^{-5}	0.10	Field	Golder Assoc., 1977
Sandstone, N. W. Colorado	2.8×10^{-3} to 4.8×10^{-5}		Field	Golder assoc., 1976

506 353

TABLE M-1. (continued)

Description	Permeability (cm/sec)	Porosity	Type of test	Reference
Lazert Fm, S. W. Wyoming sandstone	6.7×10^{-6}		Field	Golder Assoc., 1976
sandstone	1.65×10^{-4}			
average	5.4×10^{-5}			
Lazert Fm, S. W. Wyoming sandstone/siltstone	1×10^{-5}		Field	Golder Assoc., 1976
Elk River Sandstone	1×10^{-5}		Field	Golder, Brawner & Assoc., 1976
Bradford Sandstone (Devonian)	2.7×10^{-6}	0.148	Lab	Wyllie and Spangler, 1952
Berea Sandstone (Mississippian)	3.83×10^{-4}	0.19	Lab	Wyllie and Spangler, 1952
Oil Creek Sandstone (Ordovician)	4×10^{-6}	0.067	Lab	Winsauer et al., 1952
Woodbine Sandstone (Cretaceous)	4.4×10^{-3}	0.256	Lab	Winsauer et al., 1952
Repetto Sandstone (Pliocene)	3.6×10^{-5}	0.191	Lab	Winsauer et al., 1952
Wilcox Sandstone (Eocene)	3×10^{-7}	0.153	Lab	Archie, 1950
Cambrian - Ordovician	1.3×10^{-3}		Field	Maxey, 1964

506 334

TABLE M-1. (concluded)

Description	Permeability (cm/sec)	Porosity	Type of Test	Reference
Catahoula sandstone	4.4×10^{-2}		Field	Lang, 1972
	3.3×10^{-2}			
Sandstone (Cretaceous)	1.5×10^{-4}		Lab	Davis, 1969
	4.8×10^{-2}			
Cromwell sandstone	4.1×10^{-1}	0.166	Lab	Muskat, 1937
Gilcrest sandstone	8×10^{-1}	0.274	Lab	Muskat, 1937
Prue sandstone	3.4×10^{-3}	0.114	Lab	Muskat, 1937
Wilcox sandstone	7.6×10^{-2}		Lab	Muskat, 1937
	8.8×10^{-2}			
Converse sand	4.1×10^{-3}		Field	Welder and Weeks,
	1.2×10^{-3}			1965
	1×10^{-3}			
Hartsville formation	3.3×10^{-5}		Field	Welder and Weeks,
				1965
Ft. Union sandstone	3.7×10^{-4}		Field	Lowry, 1966
	1.2×10^{-4}			

506 355

TABLE M-2. Permeability and porosity of shale, claystone, and siltstone.

Description	Permeability (cm/sec)	Porosity	Type of Test	Reference
Triassic basin, claystone	10^{-12} to 10^{-10}		Lab	Marine, 1973
siltstone	10^{-9} to 10^{-8}			
mudstone	10^{-11} to 10^{-10}			
Deepwells penetrating sandstone, mudstone, conglomerate	10^{-12} to 10^{-10}			
British Columbia, Coldwater Fm.				
claystone	3.2×10^{-4}		Field	Golder, Brawner &
siltstone/sandstone/ conglomerate	7.7×10^{-9}			Assoc., 1976
N. W. Alberta	4×10^{-5}		Field	Golder, Brawner &
very silty sandstone				Assoc., 1976
Colorado, Piceance basin				
Pentz zone, oil shale	2×10^{-6}	0.08	Field	Golder Assoc., 1977
Upper Parachute Creek	1.5×10^{-4}	0.08	Field	
Mahogany	1.2×10^{-5}	0.01	Field	
Lower Parachute Creek	2.14×10^{-4}	0.08	Field	
Leached Zone	2.8×10^{-5}	0.06	Field	
Garden Gulch	2.3×10^{-5}		Field	
N. W. Colorado, silty carbonaceous shale	1.2×10^{-7}		Field	Golder Assoc., 1976
S. W. Wyoming, Lazert Fm. siltstone	9.6×10^{-6} to 6.83×10^{-5}		Field	Golder Assoc., 1976

506 356

TABLE A-2. (concluded)

Description	Permeability (cm/sec)	Porosity	Type of Test	Reference
S. W. Wyoming, Lazert Fm. mudstone	1×10^{-8}		Field	Golder Assoc., 1976
Pennsylvania shale depth 468 ft	9×10^{-11}		Lab	Gondouin and Scala, 1958
Shale (Cretaceous)	4×10^{-7}		Lab	Gondouin and Scala, 1958
Gros Ventre formation shale (Cambrian)		0.111	Lab	Manger, 1963
Graneros shale		0.249	Lab	Manger, 1963
Chanute shale		0.15	Lab	Manger, 1963
Nonesuch shale		0.016	Lab	Manger, 1963

TABLE M-3. Permeability and porosity of salt.

Sample Type/Source	Permeability (cm/sec)	Porosity		Reference
		Average	Range	
Bedded salt[a]	0 to 2.3×10^{-8}[c-i]	0.0059[j]	0.0042-0.0076	Gloyna and
Dome salt[b]	0 to 1.5×10^{-4}[c-i]	0.0171[j]	0.0117-0.0225	Reynolds, 1961
Project Gnome shaft[k]	---	0.028	0.008-0.071	Gard et al., 1962
---	5×10^{-10} to 5×10^{-6}	---	---	Schneider and Platt, 1974

[a]Sample from 645-ft (197-m) depth in Hutchinson, Kansas.
[b]Sample from 700-ft (213-m) depth in Grand Saline, Texas.
[c]Confining pressures of test runs were 500-2500 psi.
[d]Results show permeability largely a function of net confining pressure.
[e]In nearly all liquid tests, permeability decreased with test duration.
[f]Permeability of brine solutions averaged 32% of nonreactive liquid K.
[g]Tests on solid crystals showed no flow possible through crystals themselves.
[h]Lab tests involved 7-14 days consolidation time (period not comparable to geologic consolidation time).
[i]*In situ* permeability is probably lower.
[j]Lower porosity of bedded salt is probably due to greater impurity content.
[k]Samples from various depths: 715-1181 ft (218-360 m).

506 358

TABLE M-4. Range and average permeability of fractured rock in the United States, derived from producing wells.

Rock type	Producing thickness (ft)	Apparent Coefficient of permeability (cm/sec)			No. of Wells
		Min.	Average	Max.	
Gneiss	122	4.7×10^{-8}	6.6×10^{-5}	$2.6 \quad 10^{-3}$	131
Arkosic sandstone, siltstone, and shale	306	4.7×10^{-8}	7.1×10^{-5}	7.1×10^{-3}	326
Undifferentiated igneous and metamorphic rocks	220	9.4×10^{-8}	8.5×10^{-5}	1.9×10^{-4}	556
Shale	110	2.4×10^{-6}	3.5×10^{-4}	5.7×10^{-3}	93
Quartzite	138	1.9×10^{-7}	3.7×10^{-4}	2.6×10^{-3}	135
Coarse-grained igneous rocks (granite, diorite, gabbro)	171	4.7×10^{-7}	4.2×10^{-4}	4.2×10^{-3}	106
Sandstone	134	3.3×10^{-7}	5.1×10^{-4}	5.4×10^{-3}	182
Greenstone	101	5.7×10^{-6}	7.0×10^{-4}	1.0×10^{-2}	134
Tight fine-grained igneous rocks (rhyolite, trachyte, basalt)	96	6.1×10^{-5}	9.6×10^{-4}	1.3×10^{-2}	37
Schist	117	4.7×10^{-7}	1.2×10^{-3}	1.2×10^{-2}	481

Note: from Rasmussen (1963).

506 359

TABLE M-5. Fractured-rock permeabilities from pump tests.

Data source	Rock type	Permeability (10^{-4} cm/sec) Range	Average	No. of tests
	Diorite	0-71.69[a]	2.02	109
79 borings, max. boring depth--368.5 ft	Diabase	0-4.50	0.81	27
	Quartzite	0-1.46	0.31	44
	Schist (quartzose)	0-3.85[a]	0.35	87
	Zone containing at least one contact:			
	diabase/diorite	0-7.22	0.66	51
	diabase/quartzite	0-4.94[a]	[illegible]	47
	diorite/quartzite	0-3.95	[illegible]	17
	diorite/schist	0.14-1.25	0.47	9
	diabase/schist	0-1.12	0.44	20
	quartzite/schist	0.74-0.84	0.79	2
	3-ft-thick welded breccia in quartzite (AIT-39)	0		1
	Quartzite	0-3.11	0.29	38
	Diabase	0-2.17	0.65	18
	Schist	0.08-1.6	0.59	3
	Welded tuff	0-1.37	0.51	7
	Zone containing at least one contact:			
	diabase/quartzite	0.01-5.66	1.46	15
	diabase/schist	0-1.39	0.92	9
	welded tuff/quartzite	0.002-2.47	0.91	4
	welded tuff/diabase	0-1.23	0.27	8

506 360

TABLE M-5 (concluded).

Data source	Rock type	Permeability (10^{-4} cm/sec) Range	Average	No. of tests
	Biotite gneiss			
4 borings, max. boring	and pegmatite veins	0-3.51	0.43	12
depth--273 ft	no pegmatite veins	0.45		1
	Granite to granite gneiss	0.53-0.71	0.62	2
	Zones containing at least one contact:			
	+ pegmatite veins	0.03-2.44	0.55	5
	no pegmatite veins	0-0.04	0.49	3
	Phyllite pelite with	0-9.05	0.77	50
5 borings,	occasional interbeds of		(0.23)[c]	
max. boring	metasiltstone + quartz veins			
depth--202.6 ft	Volcanic tuff to meta-tuff + quartz veins	0-0.01	0.05	2
	Phyllitic pelite, tuff, and quartz veins	0-8.88	1.0 (0.04)[d]	9
			Total	600

[a]Maximum water pressure was limited due to high flow.

[b]Average excluding four exceptionally high permeabilities.

[c]Average excluding four exceptionally high permeabilities.

[d]Average excluding one exceptionally high permeability.

Source: Geotechnical Engineers, Inc., Boston.

506 361

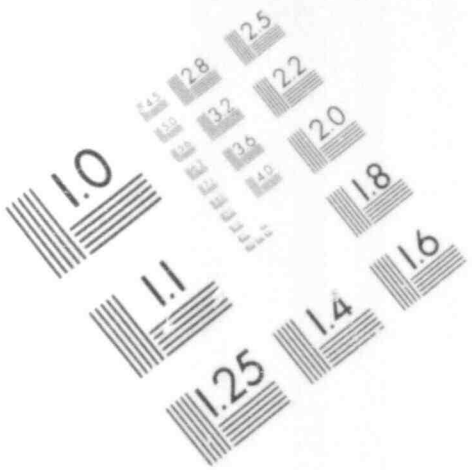

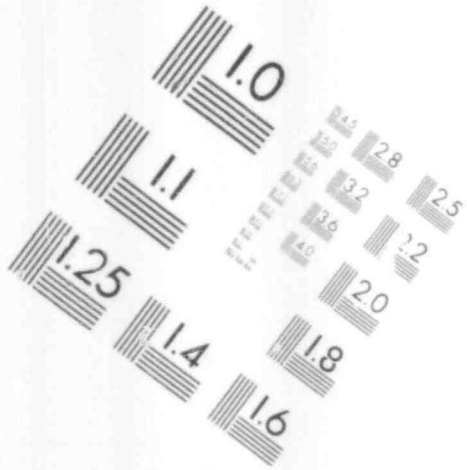

IMAGE EVALUATION TEST TARGET (MT-3)

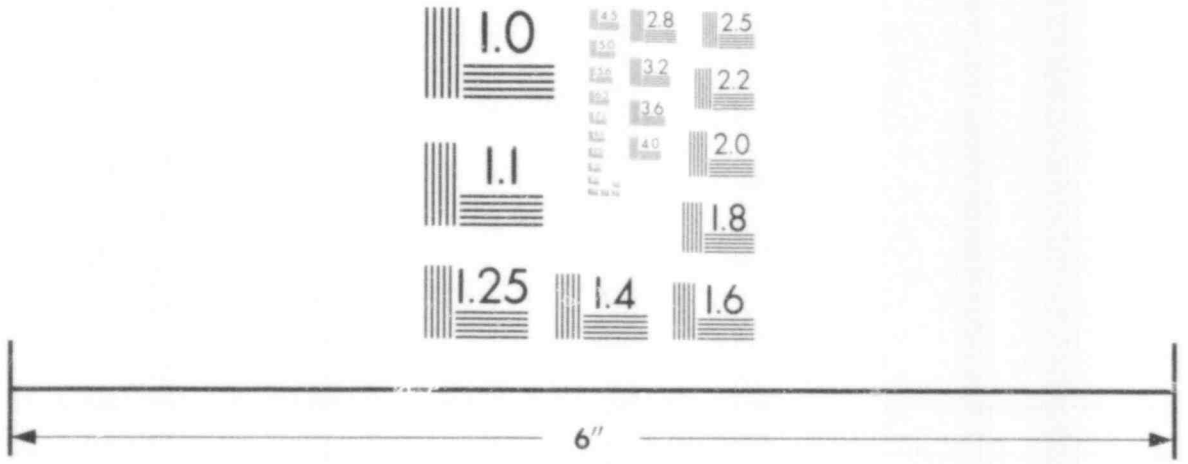

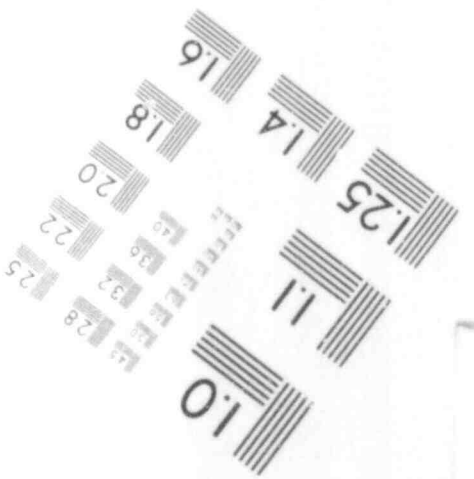

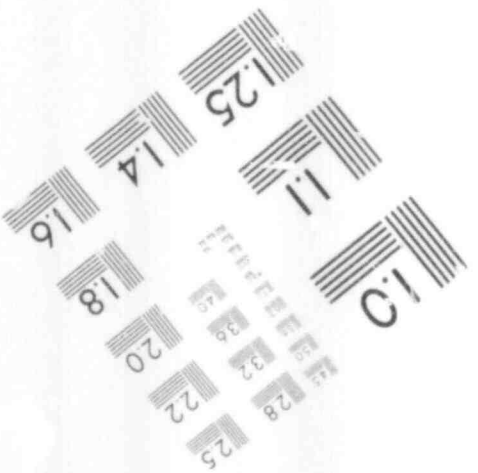

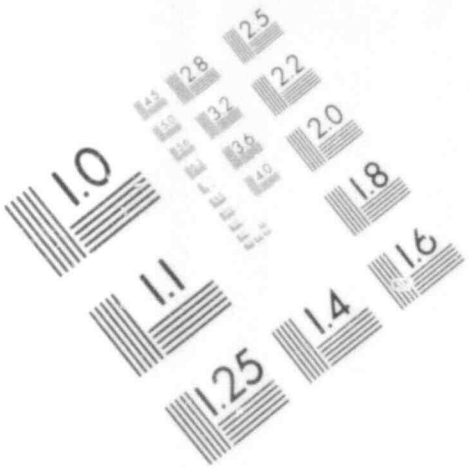

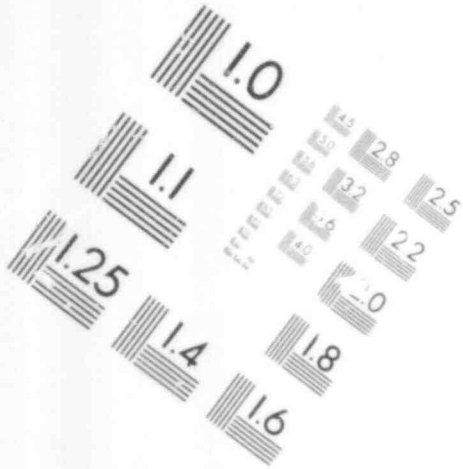

IMAGE EVALUATION TEST TARGET (MT-3)

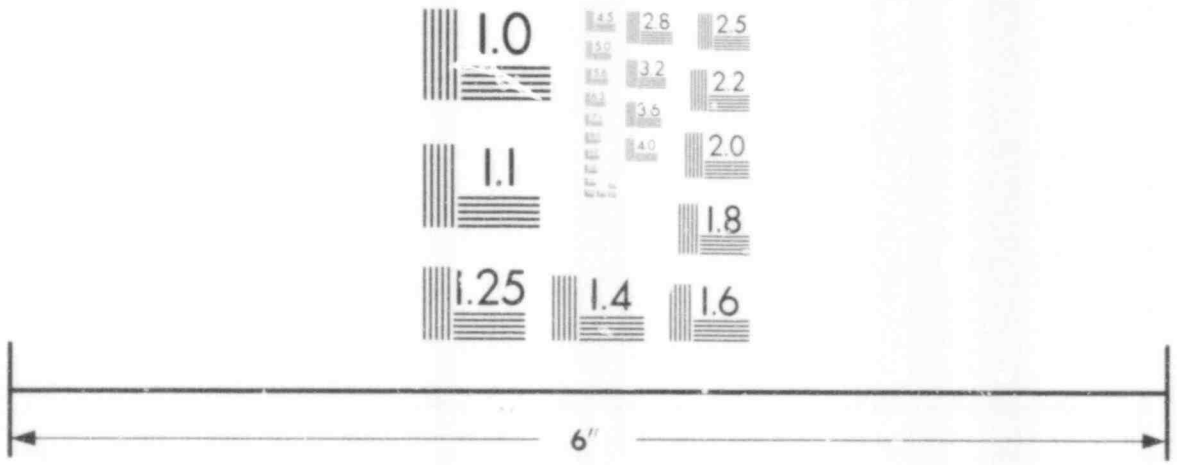

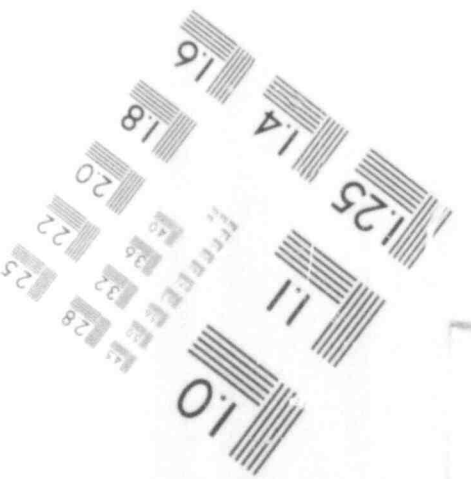

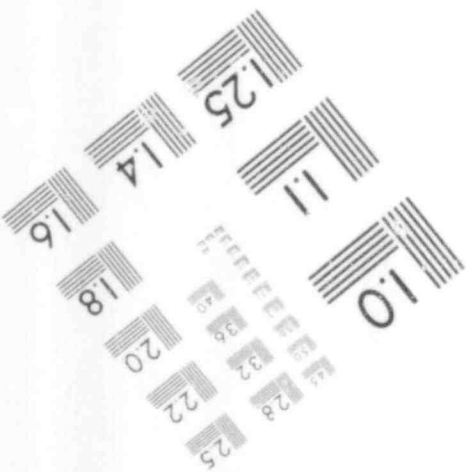

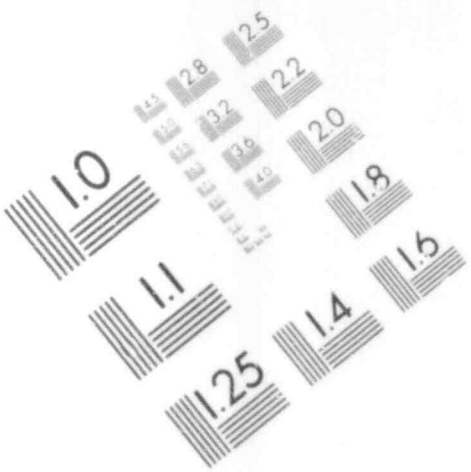

IMAGE EVALUATION TEST TARGET (MT-3)

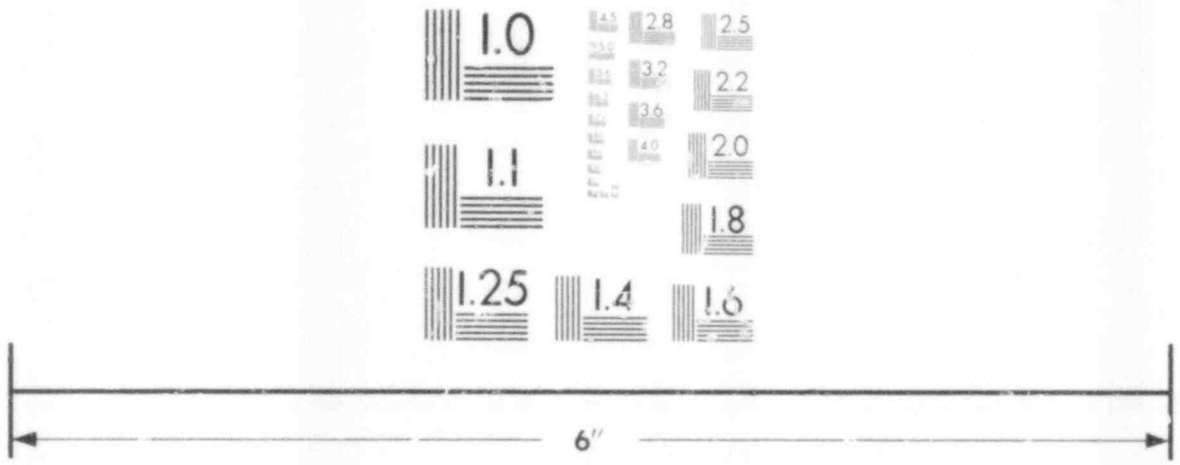

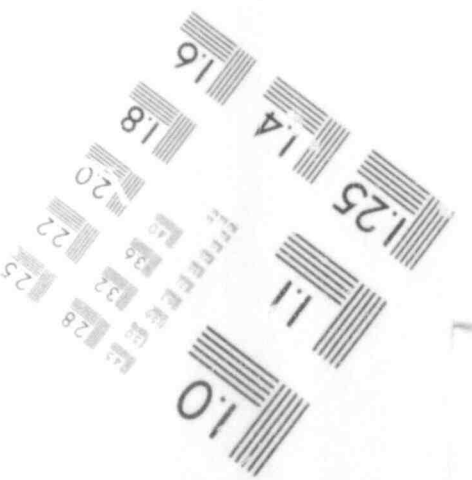

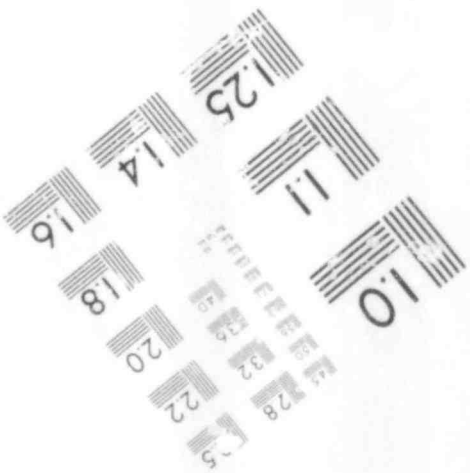

TABLE M-6. Borings with high permeability.

Rock type	Depth (ft)	Permeability (10^{-4} cm/sec)	Rock quality designation[a]	Comments
Diorite	71-93	71.69[b]	96 (ave.)	Fresh and hard; joints and partings clean; tendency to foliated fabric throughout.
	111-133	29.55[b]	90 (ave.)	Fresh and hard; joints and partings clean
	131-153	27.21[b]	99 (ave.)	Fresh and hard; slight powdery weathered effects on joint surfaces at 140.5 ft and 145.5 ft
	153-175	21.92[b]	82 (ave.)	Fresh and hard; slightly weathered on joint set at 158-158.5 ft; hairline solution cavities on some tight joints
Quartzose schist	209-230	3.85[b]	38 (ave.)	Fairly fresh; two 1-in. zones where core lost, probably local severe weathering where core lost; joints have moderate chlorite coating
Diorite with thin diabase dike	137-157	7.22	30 (ave.)	Generally fresh and hard; broken by closely spaced high-angle joints; joints and partings show slight surface weathered effects
Diorite	157-177	6.52	59 (ave.)	Similar to above
Diabase/quartzite contact	240-261	4.94[b]	83 (ave.)	Fresh and hard; joints and partings generally fresh with some minor chlorite locally; 243 ft broken contact dips about 60°

507 001

TABLE M-6 - (concluded)

Rock type	Depth (ft)	Permeability (10^{-4} cm/sec)	Rock quality designation[a]	Comments
Diabase/quartzite contact	43-63	5.66	15 (ave.)	Top of rock is 36 ft; weathered with chips
	53-74	5.28	26 (ave.)	Similar to above to slightly more intact
Phyllitic pelite	48-59	8.47	54 (ave.)	Weathered on foliation, vuggy, slightly weathered
	98-108	9.05	73	Rock is fresh; 99.5 - 100.6 ft is zone of moderate to severe weathering; phyllite is somewhat vuggy, also softened and flaky with minor rusty staining
Phyllitic pelite/tuff contact	81-92	8.88	81 (ave.)	Rock is fresh; minor chips, silicified contact at 88 ft

[a]Percentage of length of core sample made up of core fragments > 10 cm long.

[b]Maximum water pressure was limited due to high flow.

507 002

TABLE M-7. Computed values of porosity and fracture width for given permeabilities and fracture spacing.

Intrinsic permeability (cm^2)	Permeability (cm/sec)	Fracture spacing (cm)	Fracture porosity	Aperture width (cm)
10^{-14}	10^{-9}	10	2.5×10^{-5}	8.4×10^{-5}
10^{-14}	10^{-9}	50	8.7×10^{-6}	1.4×10^{-4}
10^{-14}	10^{-9}	100	5.4×10^{-6}	1.8×10^{-4}
10^{-14}	10^{-9}	500	1.9×10^{-6}	3.1×10^{-4}
10^{-12}	10^{-7}	10	1.2×10^{-4}	3.9×10^{-4}
10^{-12}	10^{-7}	50	4.0×10^{-5}	6.7×10^{-4}
10^{-12}	10^{-7}	100	2.5×10^{-5}	8.4×10^{-4}
10^{-12}	10^{-}	500	8.7×10^{-6}	1.4×10^{-3}
10^{-10}	10^{-5}	10	5.5×10^{-4}	1.8×10^{-3}
10^{-10}	10^{-5}	50	1.9×10^{-4}	3.1×10^{-3}
10^{-10}	10^{-5}	100	1.2×10^{-4}	3.9×10^{-3}
10^{-10}	10^{-5}	500	4.0×10^{-5}	6.7×10^{-3}
10^{-8}	10^{-3}	10	2.5×10^{-3}	8.4×10^{-3}
10^{-8}	10^{-3}	50	8.7×10^{-4}	1.4×10^{-2}
10^{-8}	10^{-3}	100	5.5×10^{-4}	1.8×10^{-2}
10^{-8}	10^{-3}	500	1.9×10^{-4}	3.1×10^{-2}

507 003

APPENDIX N

SENSITIVITY ANALYSIS RESULTS

This appendix presents the model assumptions and results from 85 separate computer runs. Tables N-1 through N-12 present the results of the sensitivity analyses conducted on generic bedded salt and shale repositories with an overlying aquifer and an underlying aquifer under pressure.

Five different baseline cases were defined for the sensitivity analysis of each repository, corresponding to the following situations:

1. An unflawed repository (except for the fracture zone caused by construction) with interstitial flow in the undisturbed portion of all strata.
2. An unflawed repository with fracture flow in shale (for the salt repository, this refers to a shale barrier layer).
3. A repository with deteriorated backfill.
4. A repository with failed borehole seals.
5. A repository in which breccia pipe formation (in the salt case) or fault movement (in the shale case) may occur.

Radionuclide concentrations were calculated assuming a line source in the aquifer with a length of 2 km. Mixing through the full height of the aquifer was assumed. Concentrations were not calculated beyond 3 million y. Therefore, peak concentrations are omitted from the table when the peak occurs beyond 3 million y.

Guide to Using Tables. To understand how population dose or individual radionuclide concentrations are affected by change in parameter, compare the concentration of dose computed for the baseline case with the new value. Table N-1, for example, gives the shale repository baseline value for integrated population dose as 1.3×10^{-3} man-rem/MWe-y. If the dispersion is changed from 50 m to 10 m, the new integrated population dose is 1.53×10^{-3}. This amount represents an 18% increase in population dose. Similar comparisons can be made for changes in peak individual dose or radionuclide concentrations.

507 005

Where the parameter values are not shown, we give a run index number (in parentheses). See the appropriate table in Appendix O for the baseline and new parameter values corresponding to that run index number. For example, Table N-1 does not give the baseline and new parameter values for actinide and fission product sorption factors. Instead, it shows a run index of (1) and refers to Table O-8, which shows that the retardation factors were changed from 10^2 to 1 for the fission products and from 10^4 to 10^2 for the actinides.

ASSUMPTIONS OF TABLES N-1 AND N-2

Tables N-1 and N-2 describe a shale repository with flow paths to the aquifer through a fracture zone surrounding the tunnel and shaft. It is assumed that the flow through the shale is interstitial flow. Flow pathways are shown in Fig. 2.

ASSUMPTIONS OF TABLES N-3 AND N-4

Tables N-3 and N-4 describe a bedded salt repository with flow paths to the aquifer through a fracture zone surrounding the tunnel. It is assumed that the flow through both the salt and a shale barrier layer is interstitial flow. Flow pathways appear in Fig. 2 and baseline parameter values in Table O-2. Changes in parameters varied in the sensitivity analysis, when not shown, are listed in Table O-10 and O-11.

ASSUMPTIONS OF TABLE N-5

Table N-5 describes a shale repository with flow paths to the aquifer through a fracture zone surrounding the tunnel and shaft. It is assumed the flow through both shale layers is fracture flow. Figure 2 shows flow pathways. Baseline parameter values are given in Table O-1, except for flow through the two shale layers, which is described by the values given in Table O-3. Changes in parameters varied in the sensitivity analysis, when not shown, are listed in Table O-6.

507 005

ASSUMPTIONS OF TABLE N-6

Table N-6 describes a bedded salt repository with flow paths to the aquifer through a fracture zone surrounding the tunnel and shaft. It is assumed that the flow through the shale barrier layer is fracture flow, and that the flow through the salt layer is interstitial flow. Flow pathways are shown in Fig. 2. Baseline parameter values are as given in Table 0-2, except for flow through the shale barrier layer, which is described by the values given in the barrier layer entry in Table 0-3.

ASSUMPTIONS OF TABLE N-7 AND N-8

Tables N-7 and N-8 assume the same flow paths as in the shale and salt repositories of Tables N-1 and N-3, respectively, with an additional flow path to the aquifer through the deteriorated backfill in the tunnel and shaft. Partial mixing between the backfill and the surrounding fracture zone is assumed. Flow pathways are shown in Fig. 4. Baseline parameter values for the deteriorated backfill are given in Table 0-4; baselines for other pathways are given in Table 0-1 for Table N-7 and Table 0-2 for Table N-8. Changes in parameters varied in the sensitivity analysis are listed in Tables 0-13 and 0-14, respectively.

ASSUMPTIONS OF TABLES N-9 and N-10

Tables N-9 and N-10 assume the same flow paths as in the baseline shale and salt repositories of Tables N-1 and N-3, respectively, with an additional flow path to the aquifer through borings on which the seal has failed. It is assumed that initially 10% of the borings have failed; after 500 y, 30% have failed, and after 1000 y, 50% have failed. Flow pathways are shown in Fig. 5. Baseline parameter values for the failed borings are given in Table 0-5; baselines for other pathways are given in Table 0-1 for Table N-9 and in Table 0-2 for Table N-10.

507 006

ASSUMPTIONS OF TABLE N-11

Table N-11 describes a shale repository with the possibility that a fault will occur. The probability of the occurrence of a fault in any given year is assumed to be 5×10^{-7} in the baseline case. It is further assumed that when a fault does occur, it will close almost completely after a mean time of 70 y. The opening is assumed to be along an existing fault; we dropped creation of new faults from the analysis because it was less probable, and would result in lesser consequences than movement along an existing fault. Flow pathways are shown in Fig. 3. Baseline parameter values are as given in Table 0-1, with the additions and changes in Table 0-6.

ASSUMPTIONS OF TABLE N-12

Table N-12 describes a salt repository with some probability that a breccia pipe will form between the repository and the aquifer. The probability that a breccia pipe will open in a given year is assumed to be 5×10^{-7} in the baseline case. Figure 3 shows flow pathways. Baseline parameter values are as given in Table 0-2, with the additions and changes in Table 0-7.

507 008

TABLE N-1. Shale repository sensitivity analysis (interstitial flow).

VARIED PARAMETER	BASELINE VALUE	NEW VALUE	INTEGRATED POPULATION DOSE (MAN-REM/MWe-YR)			PEAK INDIVIDUAL DOSE (REM/MWe-YR)				
			WHOLE BODY DOSE	CRITICAL ORGAN DOSE	CRITICAL ORGAN	WHOLE BODY DOSE	TIME	CRITICAL ORGAN DOSE	TIME	CRITICAL ORGAN
BASELINE		-	1.30 E -3	1.60 E -1	GI-LLI	6.19 E -14	1.44 E 4	7.45 E -12	1.44 E 4	GI-LLI
ACTINIDE & FISSION PRODUCT SORPTION FACTORS		(1)	8.98 E -2	3.56 E -1	GI-LLI	2.78 E -12	1.24 E 6	2.31 E -11	1.44 E 4	GI-LLI
DISPERSION	50	10	1.53 E -3	1.88 E -1	GI-LLI	1.07 E -12	1.74 E 5	1.30 E -11	1.74 E 5	GI-LLI
LOW POROSITY EVERYWHERE		(2)	2.36 E -3	2.89 E -1	GI-LLI	2.94 E -13	4.52 E 4	3.56 E -11	4.52 E 4	GI-LLI
LOW POROSITY IN AQUIFER	0.1	0.02	1.35 E -3	1.65 E -1	GI-LLI	6.55 E -14	5.99 E 3	7.93 E -12	5.99 E 3	GI-LLI
POROSITY IN SHALE	0.05	0.01	2.23 E -3	2.74 E -1	GI-LLI	2.94 E -13	5.85 E 4	3.56 E -11	5.85 E 4	GI-LLI
LOW POROSITY IN SHAFT & TUNNEL FRACTURE ZONE		(3)	1.30 E -3	1.60 E -1	GI-LLI	6.53 E -14	1.17 E 4	7.91 E -12	1.17 E 4	GI-LLI
FAST SATURATION	100	20	1.30 E -3	1.60 E -1	GI-LLI	6.19 E -14	1.44 E 4	7.49 E -12	1.44 E 4	GI-LLI
MIN. AREA FRACTURE ZONE IN TUNNEL		(4)	1.29 E -3	1.59 E -1	GI-LLI	5.8 E -14	1.17 E 4	7.01 E -12	1.17 E 4	GI-LLI
MAX. AREA FRACTURE ZONE IN SHAFT AND TUNNEL		(5)	1.72 E -3	2.47 E -1	GI-LLI	7.48 E -13	1.17 E 4	9.05 E -11	1.17 E 4	GI-LLI
SHALE PERMEABILITY		(6)	2.73 E -3	4.14 E -1	GI-LLI	1.59 E -12	1.52 E 4	1.93 E -10	1.52 E 4	GI-LLI
ARTESIAN HEAD	60	150	1.93 E -3	2.37 E -1	GI-LLI	1.42 E -13	8.86 E 4	1.71 E -11	8.86 E 4	GI-LLI
AQUIFER PERMEABILITY	10^{-4}	10^{2}	1.39 E -3	1.67 E -1	GI-LLI	6.57 E -14	3.96 E 3	7.95 E -12	3.96 E 3	GI-LLI
FRACTURE ZONE PERMEABILITY		(7)	1.60 E -3	2.23 E -1	GI-LLI	5.62 E -12	1.17 E 4	6.80 E -11	1.17 E 4	GI-LLI
HEAD GRADIENT IN AQUIFER	0.005	0.05	1.37 E -3	1.66 E -1	GI-LLI	6.64 E -14	4.87 E 3	8.04 E -12	4.87 E 3	GI-LLI
THICKNESS OF DEPOSITORY LAYER	200	20	2.44 E -3	3.12 E -1	GI-LLI	5.35 E -13	3.31 E 4	6.48 E -11	3.31 E 4	GI-LLI
THICKNESS OF BARRIER LAYER	200	20	1.76 E -3	2.26 E -1	GI-LLI	2.43 E -13	1.24 E 4	2.94 E -11	1.24 E 4	GI-LLI
LENGTH OF TUNNEL (INCREASE)	400	6000	1.30 E -3	1.60 E -1	GI-LLI	6.22 E -14	1.52 E 4	7.52 E -12	1.52 E 4	GI-LLI
LENGTH OF TUNNEL	400	200	1.30 E -3	1.60 E -1	GI-LLI	6.19 E -14	1.45 E 4	7.49 E -12	1.45 E 4	GI-LLI
DISSOLUTION RATE OF WASTE	10^{-4}	0.1	1.34 E -3	1.65 E -1	GI-LLI	2.95 E -13	1.21 E 4	3.57 E -11	1.23 E 4	GI-LLI
FISSION PRODUCT SORPTION FACTORS	10^{2}	1	3.39 E -3	3.09 E -1	GI-LLI	6.57 E -13	1.12 E 4	2.30 E -11	1.12 E 4	GI-LLI
ACTINIDE SORPTION FACTORS	10^{4}	10^{2}	8.78 E -2	8.78 E -2	WHOLE BODY	2.78 E -17	1.24 E 6	3.91 E -11	1.24 E 6	BONE
AQUIFER LENGTH	1.6 E 4	1.6 E 3	1.37 E -3	1.66 E -1	GI-LLI	6.52 E -14	5.13 E 3	7.89 E -12	5.13 E 3	GI-LLI

507 008

\BLE N-1. (concluded)

VARIED PARAMETER	PEAK AQUIFER CONCENTRATION (Ci/M^3-MWe-YR)							
	^{99}Tc CONCENTRATION	TIME	^{126}Sn CONCENTRATION	TIME	^{226}Ra CONCENTRATION	TIME	^{239}Pu CONCENTRATION	TIME
BASELINE	2.02 E -11	3.98 E 3	1.31 E -14	2.14 E 5	–	–	–	–
ACTINIDE & FISSION PRODUCT SORPTION FACTORS	2.02 E -11	3.96 E 3	7.50 E -13	3.75 E 3	2.23 E -15	2.25 E 5	1.28 E -14	1.65 E 5
DISPERSION	3.44 E -11	1.65 E 5	2.60 E -14	2.37 E 5	–	–	–	–
LOW POROSITY EVERYWHERE	9.13 E -11	4.29 E 4	3.07 E -13	2.83 E 4	2.07 E -17	1.79 E 6	8.25 E -18	2.20 E 6
LOW POROSITY IN AQUIFER	2.02 E -11	3.95 E 3	1.30 E -14	2.14 E 5	–	–	–	–
POROSITY IN SHALE	9.13 E -11	4.29 E 4	1.30 E -14	2.14 E 5	–	–	–	–
LOW POROSITY IN SHAFT & TUNNEL FRACTURE ZONE	2.37 E -11	5.82 E 2	3.07 E -13	2.83 E 4	2.07 E -17	1.79 E 6	2.44 E -21	2.20 E 6
FAST SATURATION	2.02 E -11	3.88 E 3	1.31 E -14	2.14 E 5	–	–	–	–
MINIMUM AREA FRACTURE ZONE IN TUNNEL	2.15 E -11	2.18 E 2	5.87 E -13	7.37 E 3	8.22 E -16	4.65 E 5	4.81 E -16	3.78 E 5
MAXIMUM AREA FRACTURE ZONE IN SHAFT AND TUNNEL	2.59 E -10	9.28 E 2	2.18 E -12	4.52 E 4	–	–	–	–
SHALE PERMEABILITY	5.04 E -10	4.62 E 3	3.45 E -13	1.41 E 5	–	–	–	–
ARTESIAN HEAD	4.45 E -11	7.98 E 4	7.4 E -14	9.33 E 4	–	–	–	–
AQUIFER PERMEABILITY	2.02 E -13	3.98 E 3	1.30 E -16	2.14 E 5	–	–	–	–
FRACTURE ZONE PERMEABILITY	2.04 E -10	5.82 E 2	2.64 E -12	2.83 E 4	1.73 E -16	1.79 E 6	8.88 E -18	1.98 E 6
HEAD GRADIENT IN AQUIFER	2.02 E -12	3.96 E 3	1.30 E -15	2.14 E 5	–	–	–	–
THICKNESS OF DEPOSITORY LAYER	1.74 E -10	2.43 E 4	1.71 E -15	2.25 E 5	–	–	–	–
THICKNESS OF BARRIER LAYER	8.58 E -11	1.20 E 3	4.91 E -13	6.16 E 4	–	–	–	–
LENGTH OF TUNNEL (INCREASE)	2.08 E -11	4.87 E 3	1.08 E -14	2.77 E 5	–	–	–	–
LENGTH OF TUNNEL	2.02 E -11	3.96 E 3	1.32 E -14	2.14 E 5	–	–	–	–
DISSOLUTION RATE OF WASTE	1.48 E -10	2.24 E 3	1.40 E -14	1.83 E 5	–	–	–	–
FISSION PRODUCT SORPTION FACTORS	2.02 E -11	3.98 E 3	7.50 E -13	3.76 E 3	–	–	–	–
ACTINIDE SORPTION FACTORS	2.02 E -11	3.96 E 3	1.30 E -14	2.14 E 5	2.23 E -15	2.25 E 5	1.28 E -14	1.65 E 5
AQUIFER LENGTH	2.02 E -11	3.96 E 3	1.30 E -14	2.14 E 5	–	–	–	–

507 009

TABLE N-2. Shale repository sensitivity analysis--multiple parameter (interstitial flow).

VARIED PARAMETER	INTEGRATED POPULATION DOSE (MAN-REM/MWe-YR)			PEAK INDIVIDUAL DOSE (REM/MWe-YR)				
	WHOLE BODY DOSE	CRITICAL ORGAN DOSE	CRITICAL ORGAN	WHOLE BODY DOSE	TIME	CRITICAL ORGAN DOSE	TIME	CRITICAL ORGAN
BASELINE	1.30 E -3	1.60 E -1	GI-LLI	6.19 E -14	1.44 E 4	7.48 E -12	1.44 E 4	GI-LLI
PERMEABILITY OF FRACTURE ZONE AND AQUIFER (1)	1.07 E -1	3.4 E -1	GI	2.17 E -12	3.87 E 4	6.54 E -11	3.87 E 4	GI-LLI
PERMEABILITY OF FRACTURE ZONE & AQUIFER AND ACTINIDE SORPTION FACTOR (2)	1.75	1.75	WHOLE BODY	4.48 E -10	4.07 E 4	4.48 E -10	4.07 E 4	WHOLE BODY
SHALE AND AQUIFER PERMEABILITY (3)	4.66 E -3	4.79 E -1	GI-LLI	1.64 E -12	2.59 E 2	1.99 E -10	2.59 E 2	GI-LLI
PERMEABILITY EVERYWHERE (4)	6.55 E -3	4.79 E -1	GI-LLI	1.64 E -12	4.87 E 3	1.98 E -10	4.87 E 3	GI-LLI
SHAFT FRACTURE ZONE AND AQUIFER PERMEABILITY AND TUNNEL FRACTURE ZONE POROSITY (5)	6.80 E -1	6.80 E -1	WHOLE BODY	2.12 E -11	1.24 E 6	1.40 E -10	1.45 E 4	GI-LLI
REDUCED SHALE PERMEABILITY AND INCREASED AQUIFER PERMEABILITY (6)	2.47 E -3	3.60 E -1	GI-LLI	1.27 E -12	8.6 E 3	1.53 E -10	8.6 E 3	GI-LLI

VARIED PARAMETER	PEAK AQUIFER CONCENTRATION (CI/M^3 MWe-YR)							
	^{99}Tc CONCENTRATION	TIME	^{126}Sn CONCENTRATION	TIME	^{226}Ra CONCENTRATION	TIME	^{239}Pu CONCENTRATION	TIME
BASELINE	2.02 E -11	4.00 E 3	1.31 E -14	2.14 E 5	-	-	-	-
PERMEABILITY OF FRACTURE ZONE AND AQUIFER	2.04 E -12	5.82 E 2	2.64 E -14	2.83 E 4	1.73 E -18	1.79 E 6	2.21 E -22	1.98 E 6
PERMEABILITY OF FRACTURE ZONE AND AQUIFER AND ACTINIDE SORPTION FACTOR	2.04 E -12	5.82 E 2	2.64 E -14	2.83 E 4	5.42 E -16	3.14 E 4	1.25 E -13	2.29 E 4
SHALE AND AQUIFER PERMEABILITY	5.04 E -12	4.62 E 3	3.45 E -15	1.41 E 5	-	-	-	-
PERMEABILITY EVERYWHERE	5.02 E -12	4.87 E 3	3.29 E -15	1.41 E 5	3.44 E -20	1.61 E 6	3.04 E -24	1.98 E 6
SHAFT FRACTURE ZONE AND AQUIFER PERMEABILITY AND TUNNEL FRACTURE ZONE POROSITY	1.97 E -12	5.25 E 2	5.85 E -14	4.17 E 3	1.58 E -16	2.60 E 5	5.13 E -16	1.82 E 5
REDUCED SHALE PERMEABILITY AND INCREASED AQUIFER PERMEABILITY	3.90 E -12	8.61 E 3	2.72 E -16	4.19 E 5	-	-	-	-

507 010

TABLE N-3. Salt repository sensitivity analysis (interstitial flow).

VARIED PARAMETER	BASELINE VALUE	NEW VALUE	INTEGRATED POPULATION DOSE (MAN-REM/MWe-YR)			PEAK INDIVIDUAL DOSE (REM/MWe-YR)				
			WHOLE BODY DOSE	CRITICAL ORGAN DOSE	CRITICAL ORGAN	WHOLE BODY DOSE		CRITICAL ORGAN DOSE	TIME	CRITICAL ORGAN
BASELINE	–	–	1.63 E -3	2.86 E -1	GI-LLI	8.15 E -14	1.49 E 5	9.86 E -12	1.49 E 5	GI-LLI
ACTINIDE & FISSION PRODUCT SORPTION FACTOR		(1)	2.61	2.61	WHOLE BODY	7.48 E -11	1.12 E 6	7.48 E -11	1.12 E 6	WHOLE BODY
DISPERSION	50	10	1.63 E -3	3.14 E -1	GI-LLI	1.70 E -13	1.27 E 5	2.06 E -11	1.27 E 5	GI-LLI
LOW POROSITY EVERYWHERE		(2)	4.19 E -3	4.38 E -1	GI-LLI	4.05 E -13	3.87 E 4	4.90 E -11	3.87 E 4	GI-LLI
LOW POROSITY IN ROCK		(3)	2.37 E -3	3.83 E -1	GI-LLI	3.87 E -13	4.58 E 4	4.68 E -11	4.52 E 4	GI-LLI
LOW POROSITY IN SHAFT & TUNNEL FRACTURE ZONE		(4)	1.63 E -3	2.81 E -1	GI-LLI	8.15 E -14	1.48 E 5	9.86 E -12	1.48 E 5	GI-LLI
MINIMUM AREA FRACTURE ZONE IN TUNNEL		(5)	1.63 E -3	2.81 E -1	GI-LLI	8.21 E -14	1.15 E 5	9.93 E -12	1.15 E 5	GI-LLI
MAXIMUM AREA FRACTURE ZONE IN SHAFT AND TUNNEL		(6)	1.64 E -3	2.87 E -1	GI-LLI	8.08 E -14	1.15 E 5	9.77 E -12	1.15 E 5	GI-LLI
SALT PERMEABILITY	10^{-9}	10^{-5}	2.75 E -2	4.29 E -1	GI-LLI	1.48 E -12	1.60 E 4	1.77 E -10	1.60 E 4	GI-LLI
ROCK PERMEABILITY MODERATELY PERMEABLE SALT		(7)	2.76 E -3	4.31 E -1	GI-LLI	1.68 E -12	1.37 E 4	2.03 E -10	1.37 E 4	GI-LLI
ROCK PERMEABILITY EXTREMELY PERMEABLE SALT		(8)	2.77 E -3	4.32 E -1	GI-LLI	1.86 E -12	1.17 E 4	2.27 E -10	1.17 E 4	GI-LLI
ARTESIAN HEAD	60	150	2.17 E -3	3.57 E -1	GI-LLI	2.29 E -13	5.85 E 4	2.78 E -11	5.85 E 4	GI-LLI
AQUIFER PERMEABILITY	10^{-4}	10^{-2}	2.61	2.61	WHOLE BODY	7.48 E -11	1.12 E 6	7.48 E -11	1.12 E 6	WHOLE BODY
FRACTURE ZONE PERMEABILITY		(9)	1.68 E -3	2.90 E -1	GI-LLI	7.89 E -14	1.17 E 6	9.55 E -12	1.17 E 4	GI-LLI
THICKNESS OF DEPOSITORY LAYER	200	20	2.56 E -3	4.06 E -1	GI-LLI	6.52 E -13	2.99 E 4	7.90 E -11	2.99 E 4	GI-LLI
THICKNESS OF BARRIER LAYER	200	20	2.13 E -3	3.52 E -1	GI-LLI	1.97 E -13	4.76 E 4	2.38 E -11	4.76 E 4	GI-LLI
LENGTH OF TUNNEL (INCREASE)	440	6000	1.63 E -3	2.86 E -1	GI-LLI	8.20 E -14	1.15 E 5	9.92 E -12	1.15 E 5	GI-LLI
LENGTH OF TUNNEL	440	200	1.64 E -3	2.87 E -1	GI-LLI	8.12 E -14	1.15 E 5	9.83 E -12	1.15 E 5	GI-LLI
DISSOLUTION RATE OF WASTE	10^{-4}	0.1	1.68 E -3	2.93 E -1	GI-LLI	9.57 E -14	1.09 E 5	1.04 E -11	1.09 E 5	GI-LLI
FISSION PRODUCT SORPTION FACTORS	10^{2}	1	4.46 E -3	3.57 E -1	GI-LLI	6.72 E -13	1.09 E 5	3.51 E -11	1.21 E 5	GI-LLI
ACTINIDE SORPTION FACTORS	10^{4}	10^{2}	2.61	2.61	WHOLE BODY	7.48 E -11	1.12 E 6	7.48 E -11	1.12 E 6	WHOLE BODY
AQUIFER LENGTH	1.6 E 4	1.6 E 3	3.28 E -3	3.42 E -1	GI-LLI	2.97 E -13	2.14 E 5	2.38 E -11	2.14 E 5	GI-LLI

507 017

TABLE N-3. (concluded)

VARIED PARAMETER	PEAK AQUIFER CONCENTRATION (Ci/M^3-MWe-YR)							
	^{99}Tc CONCENTRATION	TIME	^{126}Sn CONCENTRATION	TIME	^{226}Ra CONCENTRATION	TIME	^{239}Pu CONCENTRATION	TIME
BASELINE	2.58 E -11	1.09 E 5	7.04 E -13	1.04 E 5	5.67 E -14	1.15 E 5	1.84 E -12	8.41 E 4
ACTINIDE & FISSION PROD SORPTION	2.58 E -11	1.09 E 5	7.04 E -13	1.04 E 5	5.67 E -14	1.15 E 5	1.84 E -12	8.41 E 4
DISPERSION	5.40 E -11	1.21 E 5	1.42 E -12	1.15 E 5	1.22 E -13	1.21 E 5	2.82 E -12	1.15 E 5
LOW POROSITY EVERYWHERE	1.26 E -10	3.48 E 4	4.19 E -12	3.31 E 4	1.20 E -13	4.52 E 4	1.94 E -11	3.14 E 4
LOW POROSITY IN ROCK	1.26 E -10	3.48 E 4	4.19 E -12	3.31 E 4	1.20 E -12	4.52 E 4	1.94 E -11	3.14 E 4
LOW POROSITY IN SHAFT & TUNNEL FRACTURE ZONE	2.58 E -11	1.09 E 5	7.04 E -13	1.04 E 5	5.67 E -14	1.15 E 5	1.84 E -12	8.41 E 4
MINIMUM AREA FRACTURE ZONE IN TUNNEL	2.60 E -11	1.09 E 5	7.09 E -13	1.04 E 5	5.70 E -14	1.15 E 5	1.84 E -12	7.88 E 4
MAXIMUM AREA FRACTURE ZONE IN SHAFT AND TUNNEL	2.5[illegible] -11	1.09 E 5	6.87 E -13	1.04 E 5	5.62 E -14	1.15 E 5	1.82 E -12	8.41 E 4
SALT PERMEABILITY	4.57 -10	5.69 E 3	1.66 E -11	5.69 E 3	7.51 E -14	1.24 E 4	1.13 E -10	7.37 E 3
ROCK PERMEABILITY MODERATELY PERMEABLE SALT	5.33 E -10	2.57 E 3	2.00 E -11	3.30 E 3	6.21 E -14	1.06 E 4	1.13 E -10	4.87 E 3
ROCK PERMEABILITY EXTREMELY PERMEABLE SALT	7.10 E -10	2.68 E 2	2.74 E -11	2.68 E 2	5.17 E -14	1.17 E 4	1.87 E -10	1.73 E 3
ARTESIAN HEAD	6.39 E -11	5.28 E 4	2.28 E -12	5.01 E 4	9.89 E -14	8.17 E 4	8.51 E -12	4.07 E 4
AQUIFER PERMEABILITY	2.58 E -13	1.09 E 5	7.04 E -16	1.04 E 5	5.67 E -16	1.15 E 5	1.84 E -14	8.41 E 4
FRACTURE ZONE PERMEABILITY	2.87 E -11	5.25 E 2	1.11 E -12	5.25 E 2	5.34 E -14	1.21 E 5	4.48 E -12	4.17 E 3
THICKNESS OF DEPOSITORY LAYER	2.12 E -10	1.97 E 4	7.23 E -12	1.87 E 4	1.11 E -13	2.88 E 4	4.48 E -11	1.52 E 4
THICKNESS OF BARRIER LAYER	6.39 E -11	3.31 E 4	2.14 E -12	3.31 E 4	8.87 E -14	5.01 E 4	1.02 E -11	2.83 E 4
LENGTH OF TUNNEL (INCREASE)	2.60 E -11	1.09 E 5	7.08 E -13	1.04 E 5	5.88 E -14	1.15 E 5	1.85 E -12	7.99 E 4
LENGTH OF TUNNEL	2.57 E -11	1.09 E 5	7.01 E -13	1.04 E 5	5.65 E -14	1.15 E 5	1.83 E -12	8.42 E 4
DISSOLUTION RATE OF WASTE	2.70 E -11	8.82 E 4	8.42 E -12	1.82 E 3	5.77 E -14	1.89 E 5	3.87 E -12	2.02 E 3
FISSION PRODUCT SORPTION FACTORS	2.58 E -11	1.09 E 5	7.04 E -13	1.04 E 5	5.88 E -14	1.15 E 5	1.84 E -12	8.41 E 4
ACTINIDE SORPTION FACTORS	2.58 E -11	[illegible]8 E 5	7.04 E -13	1.04 E 5	5.67 E -14	1.15 E 5	1.84 E -12	8.41 E 4
AQUIFER LENGTH	2.58 E -11	1.09 E 5	7.04 E -13	1.04 E 5	5.67 E -14	1.15 E 5	1.84 E -12	8.41 E 4

507 012

TABLE N-4. Salt repository sensitivity analysis--multiple parameter (interstitital flow).

VARIED PARAMETER	INTEGRATED POPULATION DOSE (MAN-REM/MWe-YR)			PEAK INDIVIDUAL DOSE (REM/MWe-YR)				
	WHOLE BODY DOSE	CRITICAL ORGAN DOSE	CRITICAL ORGAN	WHOLE BODY DOSE	TIME	CRITICAL ORGAN DOSE	TIME	CRITICAL ORGAN
BASELINE	1.83 E -3	2.86 E -1	GI-LLI	8.15 E -14	1.15 E 5	9.86 E -12	1.15 E 5	GI-LLI
PERMEABILITY OF ROCK AND AQUIFER (1)	3.17	3.17	WHOLE BODY	1.22 E -10	8.61 E 5	1.56 E -9	1.01 E 6	BONE
PERMEABILITY OF SHAFT & AQUIFER POROSITY OF TUNNEL (2)	2.61	2.61	WHOLE BODY	7.45 E -11	1.12 E 6	7.45 E -11	1.12 E 6	WHOLE BODY
PERMEABILITY OF SHAFT TUNNEL & AQUIFER (3)	2.63	2.63	WHOLE BODY	7.24 E -11	1.12 E 6	7.24 E -11	1.12 E 6	WHOLE BODY
HIGH PERMEABILITY EVERYWHERE (4)	3.17	3.17	WHOLE BODY	1.22 E -10	8.61 E 5	1.56 E -9	1.01 E 6	BONE

VARIED PARAMETER	PEAK AQUIFER CONCENTRATION (Ci/M^3/MWe-YR)							
	^{99}Tc CONCENTRATION	TIME	^{126}Sn CONCENTRATION	TIME	^{226}Ra CONCENTRATION	TIME	^{239}Pu CONCENTRATION	TIME
BASELINE	2.58 E -11	1.08 E 5	7.04 E -13	1.04 E 5	5.87 E -14	1.15 E 5	1.64 E -12	8.41 E 4
PERMEABILITY OF ROCK & AQUIFER	7.10 E -12	2.68 E 2	2.74 E -13	2.88 E 2	5.17 E -16	1.17 E 4	1.07 E -12	1.73 E 3
PERMEABILITY OF SHAFT & AQUIFER POROSITY OF TUNNEL	2.57 E -13	1.08 E 5	7.00 E -15	1.04 E 5	5.64 E -16	1.15 E 5	1.63 E -14	8.41 E 4
PERMEABILITY OF SHAFT TUNNEL & AQUIFER	2.87 E -13	5.25 E 2	1.11 E -14	5.25 E 2	5.34 E -16	1.21 E 5	4.50 E -14	4.17 E 3
HIGH PERMEABILITY EVERYWHERE	7.10 E -12	2.68 E 2	2.74 E -13	2.87 E 2	5.17 E -16	1.17 E 4	1.07 E -12	1.73 E 3

507 018

TABLE N-5. Shale repository sensitivity analysis (fracture flow).

VARIED PARAMETER	BASELINE VALUE	NEW VALUE	INTEGRATED POPULATION DOSE (MAN-REM/MWe-YR)			PEAK INDIVIDUAL DOSE (REM/MWe-YR)				
			WHOLE BODY DOSE	CRITICAL ORGAN DOSE	CRITICAL ORGAN	WHOLE BODY DOSE	TIME	CRITICAL ORGAN DOSE	TIME	CRITICAL ORGAN
BASELINE	–	–	2.77 E -3	4.32 E -1	GI-LLI	1.86 E -12	1.17 E 4	2.26 E -10	1.17 E 4	GI-LLI
AQUIFER LENGTH	1.6 E 4	1.6 E 3	6.76 E -3	5.15 E -1	GI-LLI	2.09 E -12	1.92 E 3	2.53 E -10	1.92 E 3	GI-LLI
DISPERSION DOWN	50	10	2.77 E -3	4.33 E -1	GI-LLI	2.03 E -12	1.12 E 4	2.45 E -10	1.12 E 4	GI-LLI
ACTINIDE SORPTION	10^5	10^2	3.14	3.14	WHOLE BODY	1.19 E -10	9.61 E 5	1.57 E -9	1.01 E 6	BONE
AQUIFER LENGTH HEAD GRADIENT SIMULTANEOUSLY		(1)	2.32	2.32	WHOLE BODY	2.65 E -11	1.24 E 6	3.63 E -10	1.89 E 4	GI-LLI
PERMEABILITY & ACTINIDE SORPTION SIMULTANEOUSLY		(2)	3.53	3.53	WHOLE BODY	1.47 E -9	1.60 E 4	1.47 E -9	1.60 E 4	WHOLE BODY
DISPERSION UP	50	100	2.77 E -3	4.31 E -1	GI-LLI	1.74 E -12	1.24 E 4	2.11 E -10	1.24 E 4	GI-LLI
ACTINIDE SORPTION, LEACH RATE + AQUIFER PERMEABILITY		(3)	2.49	2.49	WHOLE BODY	4.88 E -9	1.24 E 4	5.16 E -8	2.29 E 2	GI-LLI

VARIED PARAMETER	PEAK AQUIFER CONCENTRATION (Ci/M^3-MWe-YR)							
	^{99}Tc CONCENTRATION	TIME	^{126}Sn CONCENTRATION	TIME	^{226}Ra CONCENTRATION	TIME	^{239}Pu CONCENTRATION	TIME
BASELINE	6.84 E -10	2.29 E 2	1.65 E -11	5.69 E 3	2.92 E -14	1.83 E 5	4.14 E -13	1.27 E 5
AQUIFER LENGTH	6.84 E -10	2.29 E 2	1.65 E -11	5.69 E 3	2.92 E -14	1.83 E 5	4.14 E -13	1.27 E 5
DISPERSION DOWN	6.84 E -10	2.29 E 2	1.65 E -11	5.69 E 3	2.92 E -14	1.83 E 5	4.14 E -13	1.27 E 5
ACTINIDE SORPTION	6.84 E -10	2.29 E 2	1.65 E -11	5.69 E 3	7.36 E -14	1.17 E 4	1.12 E -10	7.37 E 3
AQUIFER LENGTH HEAD GRADIENT SIMULTANEOUSLY	6.84 E -11	2.29 E 2	1.65 E -12	5.69 E 3	2.92 E -15	1.83 E 5	4.14 E -14	1.27 E 5
PERMEABILITY & ACTINIDE SORPTION SIMULTANEOUSLY	6.84 E -12	2.29 E 2	1.65 E -13	5.68 E 3	7.36 E -16	1.17 E 4	1.12 E -12	7.37 E 3
DISPERSION UP	6.84 E -10	2.29 E 2	1.65 E -11	5.69 E 3	2.92 E -14	1.83 E 5	4.14 E -13	1.27 E 5
ACTINIDE SORPTION, LEACH RATE + AQUIFER PERMEABILITY	1.46 E -9	1.23 E 2	7.33 E -13	2.02 E 3	5.70 E -16	3.57 E 3	1.38 E -12	2.13 E 3

507 015

TABLE N-6. Salt repository sensitivity analysis (fracture flow).

VARIED PARAMETER	BASELINE VALUE	NEW VALUE	INTEGRATED POPULATION DOSE (MAN-REM/MWe-YR)			PEAK INDIVIDUAL DOSE (REM/MWe-YR)				
			WHOLE BODY DOSE	CRITICAL ORGAN DOSE	CRITICAL ORGAN	WHOLE BODY DOSE	TIME	CRITICAL ORGAN DOSE	TIME	CRITICAL ORGAN
BASELINE	–	–	2.58 E -3	4.06 E -1	GI-LLI	5.84 E -13	2.58 E 4	7.07 E -11	2.58 E 4	GI-LLI
SALT PERMEABILITY	10^{-9}	10^{-5}	2.77 E -3	4.32 E -1	GI-LLI	1.88 E -12	1.17 E 4	2.27 E -10	1.17 E 4	GI-LLI
DISPERSION	50	10	2.64 E -3	4.18 E -1	GI-LLI	1.00 E -12	2.56 E 4	1.12 E -10	2.56 E 4	GI-LLI

VARIED PARAMETER	PEAK AQUIFER CONCENTRATION (Ci/M^3-MWe-YR)							
	^{99}Tc CONCENTRATION	TIME	^{126}Sn CONCENTRATION	TIME	^{226}Ra CONCENTRATION	TIME	^{239}Pu CONCENTRATION	TIME
BASELINE	1.88 E -10	1.69 E 4	6.5 E -12	1.60 E 4	8.36 E -14	2.69 E 4	4.97 E -11	1.17 E 4
SALT PERMEABILITY	6.82 E -10	2.13 E 2	2.64 E -11	2.13 E 2	5.17 E -14	1.17 E 4	1.12 E -10	1.73 E 3
DISPERSION	3.15 E -10	1.60 E 4	1.11 E -11	1.52 E 4	1.27 E -13	1.97 E 4	7.66 E -11	1.37 E 4

TABLE N-7. Shale repository deteriorated backfill--sensitivity analysis (interstitial flow).

VARIED PARAMETER	INTEGRATED POPULATION DOSE (MAN-REM/MWe-YR)			PEAK INDIVIDUAL DOSE (REM/MWe-YR)				
	WHOLE BODY DOSE	CRITICAL ORGAN DOSE	CRITICAL ORGAN	WHOLE BODY DOSE	TIME	CRITICAL ORGAN DOSE	TIME	CRITICAL ORGAN
BASELINE	1.60 E -3	2.23 E -1	GI-LLI	5.70 E -13	1.18 E 4	6.90 E -11	1.18 E 4	GI-LLI
FURTHER DETERIORATED BACKFILL (1)	2.31 E -3	3.54 E -1	GI-LLI	1.39 E -12	1.18 E 4	1.69 E -10	1.18 E 4	GI-LLI
IMPERMEABLE SHAFT (2)	1.30 E -3	1.80 E -1	GI-LLI	6.78 E -14	1.45 E 4	8.20 E -12	1.45 E 4	GI-LLI
IMPERMEABLE SHAFT & HIGHLY PERMEABLE TUNNEL (3)	1.29 E -3	1.56 E -1	GI-LLI	4.22 E -14	1.74 E 5	5.11 E -12	1.74 E 5	GI-LLI

VARIED PARAMETER	PEAK AQUIFER CONCENTRATION (Ci/M^3-MWe-YR)							
	^{99}Tc CONCENTRATION	TIME	^{126}Sn CONCENTRATION	TIME	^{226}Ra CONCENTRATION	TIME	^{239}Pu CONCENTRATION	TIME
BASELINE	2.20 E -10	5.25 E 2	2.64 E -12	2.99 E 4	1.58 E -16	7.32 E 6	2.09 E -20	2.32 E 6
FURTHER DETERIORATED BACKFILL	5.15 E -10	2.54 E 2	1.26 E -11	1.09 E	1.10 E -14	6.35 E 5	1.19 E -15	4.42 E 5
IMPERMEABLE SHAFT	2.20 E -11	3.76 E 3	1.68 E -14	1.83 E 5	–	–	–	–
IMPERMEABLE SHAFT & HIGHLY PERMEABLE TUNNEL	1.34 E -11	1.57 E 5	1.76 E -18	1.53 E 6	–	–	–	–

507 016

TABLE N-8. Salt repository deteriorated backfill--sensitivity analysis (interstitial flow).

VARIED PARAMETER	INTEGRATED POPULATION DOSE (MAN-REM/MWe-YR)			PEAK INDIVIDUAL DOSE (REM/MWe-YR)				
	WHOLE BODY DOSE	CRITICAL ORGAN DOSE	CRITICAL ORGAN	WHOLE BODY DOSE	TIME	CRITICAL ORGAN DOSE	TIME	CRITICAL ORGAN
BASELINE	1.79 E -3	3.06 E -1	GI-LLI	3.74 E -13	1.75 E 4	4.53 E -11	1.18 E 4	GI-LLI
FURTHER DETERIORATED BACKFILL (1)	2.26 E -3	3.64 E -1	GI-LLI	1.33 E -12	1.24 E 4	1.61 E -10	1.24 E 4	GI-LLI
IMPERMEABLE SHAFT (2)	1.63 E -3	2.86 E -1	GI-LLI	8.28 E -14	1.15 E 5	1.03 E -11	1.15 E 5	GI-LLI
IMPERMEABLE SHAFT HIGHLY PERMEABLE TUNNEL (3)	1.63 E -3	2.86 E -1	GI-LLI	8.26 E -14	1.15 E 5	9.99 E -12	1.15 E 5	GI-LLI
PERMEABLE TUNNEL & SHAFT (4)	2.76 E -3	4.30 E -1	GI-LLI	1.84 E -12	1.18 E 4	2.23 E -10	1.18 E 4	GI-LLI

VARIED PARAMETER	PEAK AQUIFER CONCENTRATION (CUM^3/MWe-YR)							
	^{99}Tc CONCENTRATION	TIME	^{126}Sn CONCENTRATION	TIME	^{226}Ra CONCENTRATION	TIME	^{239}Pu CONCENTRATION	TIME
BASELINE	1.35 E -10	8.37 E 2	5.20 E -12	8.37 E 2	4.02 E -14	1.27 E 5	2.13 E -11	2.02 E 3
FURTHER DETERIORATED BACKFILL	4.63 E -10	1.48 E 3	1.79 E -11	1.48 E 3	4.09 E -14	1.52 E 5	7.89 E -11	2.02 E 3
IMPERMEABLE SHAFT	2.61 E -11	1.09 E 5	7.18 E -13	9.83 E 4	5.73 E -14	1.27 E 5	1.67 E -12	8.41 E 4
IMPERMEABLE SHAFT HIGHLY PERMEABLE TUNNEL	2.61 E -11	1.04 E 5	7.18 E -13	9.83 E 4	5.70 E -14	1.15 E 5	1.69 E -12	7.99 E 4
PERMEABLE TUNNEL & SHAFT	6.61 E -10	9.28 E 2	2.56 E -11	9.28 E 2	6.37 E -14	9.07 E 3	1.06 E -10	2.01 E 3

TABLE N-9. Shale repository boring seal dissolution--sensitivity analysis (interstitial flow).

VARIED PARAMETER	BASELINE VALUE	NEW VALUE	INTEGRATED POPULATION DOSE (MAN-REM/MWe-YR)			PEAK INDIVIDUAL DOSE (REM/MWe-YR)				
			WHOLE BODY DOSE	CRITICAL ORGAN DOSE	CRITICAL ORGAN	WHOLE BODY DOSE	TIME	CRITICAL ORGAN DOSE	TIME	CRITICAL ORGAN
BASELINE	-	-	1.28 E -3	1.58 E -1	GI-LLI	6.11 E -14	1.45 E 4	7.39 E -12	1.45 E 4	GI-LLI
COMPLETE MIXING	-	-	1.29 E -3	1.58 E -1	GI-LLI	6.09 E -14	1.45 E 4	7.37 E -12	1.45 E 4	GI-LLI
MAXIMUM PERMEABILITY MIXING	10^{-4}	10^{-2}	1.37 E -3	1.78 E -1	GI-LLI	2.44 E -13	1.30 E 4	2.96 E -11	1.30 E 4	GI-LLI

507 016

TABLE N-10. Salt repository boring seal dissolution--sensitivity analysis (interstitial flow).

VARIED PARAMETER	BASELINE VALUE	NEW VALUE	INTEGRATED POPULATION DOSE (MAN-REM/MWe-YR)			PEAK INDIVIDUAL DOSE (REM/MWe-YR)				
			WHOLE BODY DOSE	CRITICAL ORGAN DOSE	CRITICAL ORGAN	WHOLE BODY DOSE	TIME	CRITICAL ORGAN DOSE	TIME	CRITICAL ORGAN
BASELINE	–	–	1.63 E -3	2.85 E -1	GI-LLI	7.99 E -14	1.21 E 5	8.87 E -12	1.21 E 5	GI-LLI
COMPLETE MIXING	–	–	1.63 E -3	2.85 E -1	GI-LLI	7.99 E -14	1.21 E 5	8.86 E -12	1.21 E 5	GI-LLI
MAXIMUM PERMEABILITY IN BORING	10^{-4}	10^{-2}	1.65 E -3	2.88 E -1	GI-LLI	1.59 E -13	1.24 E 4	1.83 E -11	1.24 E 4	GI-LLI

TABLE N-11. Shale reposit ry faulting--sensitivity analysis (interstitial flow).

VARIED PARAMETER	BASELINE VALUE	NEW VALUE	INTEGRATED POPULATION DOSE (MAN-REM/MWe-YR)			PEAK INDIVIDUAL DOSE (REM/MWe-YR)				
			WHOLE BODY DOSE	CRITICAL ORGAN DOSE	CRITICAL ORGAN	WHOLE BODY DOSE	TIME	CRITICAL ORGAN DOSE	TIME	CRITICAL ORGAN
BASELINE	–	–	1.27 E 3	1.57 E -1	GI-LLI	6.07 E -14	1.46 E 4	7.32 E -12	1.45 E 4	GI-LLI
FAULT STAYS OPEN AND A HIGHER PROBABILITY OF OCCURRENCE	5. E -7	5. E -5	1.27 E 3	1.57 E -1	GI-LLI	6.34 E -14	1.46 E 4	7.70 E -12	1.45 E 4	GI-LLI

TABLE N-12. Salt repository breccia formation--sensitivity analysis (interstitial flow).

VARIED PARAMETER	BASELINE VALUE	NEW VALUE	INTEGRATED POPULATION DOSE (MAN-REM/MWe-YR)			PEAK INDIVIDUAL DOSE (REM/MWe-YR)				
			WHOLE BODY DOSE	CRITICAL ORGAN DOSE	CRITICAL ORGAN	WHOLE BODY DOSE	TIME	CRITICAL ORGAN DOSE	TIME	CRITICAL ORGAN
BASELINE	–	–	1.62 E -3	2.84 E -1	GI-LLI	8.06 E -14	1.15 E 5	9.74 E -12	1.15 E 5	GI-LLI
HIGH PROBABILITY OF BRECCIA FORMATION	5. E -7	5. E -5	1.18 E -3	1.94 E -1	GI-LLI	1.72 E -13	2.43 E 4	2.08 E -11	2.43 E 4	GI-LLI
BRECCIA PIPE INITIALLY PRESENT	–	–	2.75 E -3	4.29 E -1	GI-LLI	1.48 E -12	1.60 E 4	1.79 E -10	1.60 E 4	GI-LLI

507 018

APPENDIX O

PARAMETER VALUES USED IN SENSITIVITY ANALYSES

The following tables and figures contain a description of the parameter values used to obtain the sensitivity analysis results in Appendix N. Figures 2 through 5 show the flow pathways in the different cases analyzed. Tables O-1 through O-7 list baseline parameter values. Tables O-8 through O-14 describe parameter values tested in the sensitivity analysis when space did not permit their inclusion in Appendix N. The run index numbers in Tables O-8 through O-14 are those referred to in the corresponding tables of Appendix N.

The following variables had the same baseline values in all cases:

- The dissolution rate of the waste was 10^{-4} y.
- The time required for resaturation of the repository was 100 y.
- The hydraulic head of the lower aquifer was 60 m greater than the head of the upper aquifer at the time location.
- The horizontal hydraulic gradient of the upper aquifer was 0.005.

507 018

TABLE O-1. Baseline parameters for Tables N-1 and N-2.

PATHWAY	LENGTH (m)	CROSS SECTION (m^2)	EFFECTIVE POROSITY	PERMEABILITY (cm/sec)	RETARDATION FACTOR		DISPERSION (m)
1st Segment of Tunnel Fracture Zone	1200	316	0.1	0.1	^{129}I, ^{99}Tc: Other Fission Products: Actinides:	1 10^2 10^4	50
2nd Segment of Tunnel Fracture Zone	440	18.96	0.1	0.1	^{129}I, ^{99}Tc: Other Fission Products: Actinides:	1 10^2 10^4	50
Fracture Zone Around Shaft in Repository Layer	100	10	10^{-3}	10^{-4}	^{129}I, ^{99}Tc: Other Fission Products: Actinides:	1 10^2 10^4	50
Fracture Zone Around Shaft in Shale Barrier Layer	200	5	10^{-3}	10^{-4}	^{129}I, ^{99}Tc: Other Fission Products: Actinides:	1 10^2 10^4	50
Repository Layer	100	5×10^6	0.05	10^{-9}	^{129}I, ^{99}Tc: Other Fission Products: Actinides:	1 10^2 10^4	50
Barrier Layer	200	5×10^6	0.0	10^{-7}	^{129}I, ^{99}Tc: Other Fission Products: Actinides:	1 10^2 10^4	50
Aquifer	1.6×10^4	4×10^5	0.1	10^{-4}	^{129}I, ^{99}Tc: Other Fission Products: Actinides:	1 10^2 10^4	50

TABLE O-2. Baseline parameters for Tables N-3 and N-4.

PATHWAY	LENGTH (m)	CROSS SECTION (m^2)	EFFECTIVE POROSITY	PERMEABILITY (cm/sec)	RETARDATION FACTOR		DISPERSION (m)
1st Segment of Tunnel Fracture Zone	1200	3300	10^{-3}	10^{-6}	1		50
2nd Segment of Tunnel Fracture Zone	440	198	10^{-3}	10^{-6}	1		50
Fracture Zone Around Shaft in Repository Layer	100	60	10^{-3}	10^{-6}	1		50
Fracture Zone Around Shaft in Shale Barrier Layer	200	5	10^{-3}	10^{-4}	1		50
Repository Layer	100	5×10^6	10^{-2}	10^{-9}	1		50
Barrier Layer	200	5×10^6	0.05	10^{-7}	1		50
Aquifer	1.6×10^4	4×10^5	0.1	10^{-4}	^{129}I, ^{99}Tc: Other Fission Products: Actinides:	1 10^2 10^4	50

507 089

TABLE O-3. Baseline parameters for shale with fracture flow (Tables N-5 and N-6).

PATHWAY	LENGTH (m)	CROSS SECTION (m^2)	EFFECTIVE POROSITY	PERMEABILITY (cm/sec)	RETARDATION FACTOR	DISPERSION (m)
Repository Layer	100	5×10^6	10^{-5}	10^{-8}	SAME	50
Barrier Layer	200	5×10^6	10^{-4}	10^{-6}	SAME	50

TABLE O-4. Additional baseline parameters for failed backfill cases (Tables N-7 and N-8).

PATHWAY	LENGTH (m)	CROSS SECTION (m^2)	EFFECTIVE POROSITY	PERMEABILITY (cm/sec)	RETARDATION FACTOR	DISPERSION (m)
1st Segment of Tunnel Backfill	1200	3100	10^{-2}	10^{-4}	^{129}I, ^{99}Tc: 1 Other Fission Products: 10^2 Actinides: 10^4	50
2nd Segment of Tunnel Backfill	440	150	10^{-2}	10^{-4}	SAME	50
Shaft Backfill	300	64	10^{-2}	10^{-4}	SAME	50

TABLE O-5. Additional baseline parameters for cases with failed boring seals (Tables N-9 and N-10).

PATHWAY	LENGTH (m)	CROSS SECTION (m^2)	EFFECTIVE POROSITY	PERMEABILITY (cm/sec)	RETARDATION FACTOR	DISPERSION (m)
Borehole Path Less Than 500 Years	300	0.1	10^{-2}	10^{-4}	^{129}I, ^{99}Tc: 1 Other Fission Products: 10^2 Actinides: 10^4	50
Borehole Path Between 500 and 1000 Years	300	0.3	10^{-2}	10^{-4}	SAME	50
Borehole Path After 1000 Years	300	0.5	10^{-2}	10^{-4}	SAME	50

507 020

TABLE O-6. Baseline parameters for case with faults (Table N-11).

PATHWAY	LENGTH (m)	CROSS SECTION (m^2)	EFFECTIVE POROSITY	PERMEABILITY (cm/sec)	RETARDATION FACTOR	DISPERSION (m)
Change from Table H-1						
Depository Layer	100	4.9×10^6	0.05	10^{-9}	SAME	50
Barrier Layer	200	4.9×10^6	0.05	10^{-7}	SAME	50
Add						
*Fault Open in Barrier Layer	200	10^5	10^{-3}	10^{-4}	^{129}I, ^{99}Tc: 1 Other Fission Products: 10^2 Actinides: 10^4	50
Fault Closed in Barrier Layer	200	10^5	10^{-3}	10^{-6}	SAME	50
Fault Open in Depository Layer	100	10^5	10^{-3}	10^{-5}	SAME	50
Fault Closed in Depository Layer	100	10^5	10^{-3}	10^{-7}	SAME	50

*The probability of a fault is 5×10^{-7} per year

TABLE O-7. Baseline parameters for case with breccia pipe (Table N-12).

PATHWAY	LENGTH (m)	CROSS SECTION (m^2)	EFFECTIVE POROSITY	PERMEABILITY (cm/sec)	RETARDATION FACTOR	DISPERSION (m)
Change from Table H-2						
Depository Layer	100	4.9×10^6	10^{-2}	10^{-9}	1	50
Barrier Layer	200	4.9×10^6	0.05	10^{-7}	1	50
Add						
*Breccia Pipe	300	10^5	0.3	10^{-2}	1	50

*The probability of a breccia pipe formation is 5×10^{-7} per year.

507 021

TABLE O-8. Parameters varied in Table N-1.

RUN INDEX NUMBER	VARIED PARAMETER	BASELINE VALUE	NEW VALUE
(1)	Retardation Factor of Fission Products other than I and Tc	10^2	1
	Retardation Factor of Actinides	10^4	10^2
(2)	Porosity of the Tunnel Fracture Zone	10^{-1}	10^{-2}
	Porosity of the Shaft Fracture Zone	10^{-3}	10^{-4}
	Porosity of the Depository Layer	5×10^{-2}	10^{-2}
	Porosity of the Barrier Layer	5×10^{-2}	10^{-2}
	Porosity of the Aquifer	10^{-1}	2×10^{-2}
(3)	Porosity of the Tunnel Fracture Zone	10^{-1}	10^{-2}
	Porosity of the Shaft Fracture Zone	10^{-3}	10^{-4}
(4)	Cross Section of the 1st Segment of the Tunnel Fracture Zone (m^2)	316	580
	Cross Section of the 2nd Segment of the Tunnel Fracture Zone (m^2)	18.91	34.8
	Permeability of the Tunnel Fracture Zone (cm/sec)	10^{-1}	10^{-4}
(5)	Cross Section of the 1st Segment of the Tunnel Fracture Zone (m^2)	316	785
	Cross Section of the 2nd Segment of the Tunnel Fracture Zone (m^2)	18.91	47.1
	Cross Section of the 1st Segment of the Shaft Fracture Zone (m^2)	10	100
	Cross Section of the 2nd Segment of the Shaft Fracture Zone (m^2)	5	100
(6)	Permeability of the Depository Layer (cm/sec)	10^{-9}	10^{-7}
	Permeability of the Barrier Layer (cm/sec)	10^{-7}	10^{-5}
(7)	Permeability of the Tunnel Fracture Zone (cm/sec)	10^{-1}	1
	Permeability of the Shaft Fracture Zone (cm/sec)	10^{-4}	10^{-3}

TABLE O-9. Parameters varied in Table N-2.

RUN INDEX NUMBER	VARIED PARAMETER	BASELINE VALUE	NEW VALUE
(1)	Permeability of the Tunnel Fracture Zone (cm/sec)	10^{-1}	1
	Permeability of the Shaft Fracture Zone (cm/sec)	10^{-4}	10^{-3}
	Permeability of the Aquifer (cm/sec)	10^{-4}	10^{-2}
(2)	Permeability of the Tunnel Fracture Zone (cm/sec)	10^{-1}	1
	Permeability of the Shaft Fracture Zone (cm/sec)	10^{-4}	10^{-3}
	Permeability of the Aquifer (cm/sec)	10^{-4}	10^{-2}
	Actinide Retardation Factor	10^4	10^2
(3)	Permeability of the Aquifer (cm/sec)	10^{-4}	10^{-2}
	Permeability of the Depository Layer (cm/sec)	10^{-9}	10^{-7}
	Permeability of the Barrier Layer (cm/sec)	10^{-7}	10^{-5}
(4)	Permeability of the Tunnel Fracture Zone (cm/sec)	10^{-1}	1
	Permeability of the Shaft Fracture Zone (cm/sec)	10^{-4}	10^{-3}
	Permeability of the Aquifer (cm/sec)	10^{-4}	10^{-2}
	Permeability of the Depository Layer (cm/sec)	10^{-9}	10^{-7}
	Permeability of the Barrier Layer (cm/sec)	10^{-7}	10^{-5}
(5)	Permeability of the Shaft Fracture Zone (cm/sec)	10^{-4}	10^{-3}
	Permeability of the Aquifer (cm/sec)	10^{-4}	10^{-2}
	Porosity of the Tunnel Fracture Zone	10^{-1}	10^{-2}
(6)	Permeability of the Aquifer (cm/sec)	10^{-4}	10^{-2}
	Permeability of the Depository Layer (cm/sec)	10^{-9}	10^{-11}
	Permeability of the Barrier Layer (cm/sec)	10^{-7}	10^{-9}

507 023

TABLE O-10. Parameters varied in Table N-3.

RUN INDEX NUMBER	VARIED PARAMETER	BASELINE VALUE	NEW VALUE
(1)	Retardation Factor of Fission Products (Except I, Tc) in Aquifer	10^{2}	1
	Retardation Factor of Actinides in Aquifer	10^{4}	10^{2}
(2)	Porosity of the Tunnel and Shaft Fracture Zone	10^{-3}	10^{-4}
	Porosity of the Depository Layer	10^{-2}	4×10^{-3}
	Porosity of the Barrier Layer	5×10^{-2}	10^{-2}
(3)	Porosity of the Depository Layer	10^{-2}	4×10^{-3}
	Porosity of the Barrier Layer	5×10^{-2}	10^{-2}
(4)	Porosity of the Tunnel and Shaft Fracture Zone	10^{-3}	10^{-4}
(5)	Cross Section of the 1st Segment of the Tunnel Fracture Zone (m^2)	3.3×10^{3}	190
	Cross Section of the 2nd Segment of the Tunnel Fracture Zone (m^2)	198	11.4
(6)	Cross Section of the 1st Segment of the Tunnel Fracture Zone (m^2)	3.3×10^{3}	6.4×10^{3}
	Cross Section of the 2nd Segment of the Tunnel Fracture Zone (m^2)	198	384
	Cross Section of the 1st Segment of the Shaft Fracture Zone (m^2)	60	110
	Cross Section of the 2nd Segment of the Shaft Fracture Zone (m^2)	5	100
(7)	Permeability of the Depository Layer (cm/sec)	10^{-9}	10^{-7}
	Permeability of the Barrier Layer (cm/sec)	10^{-7}	10^{-5}
(8)	Permeability of the Depository Layer (cm/sec)	10^{-9}	10^{-5}
	Permeability of the Barrier Layer (cm/sec)	10^{-7}	10^{-5}
(9)	Permeability of the Shaft Fracture Zone (cm/sec)	10^{-6}	10^{-5}
	Permeability of the Tunnel Fracture Zone (cm/sec)	10^{-6}	10^{-5}

TABLE O-11. Parameters varied in Table N-4.

RUN INDEX NUMBER	VARIED PARAMETER	BASELINE VALUE	NEW VALUE
(1)	Permeability of the Aquifer (cm/sec)	10^{-4}	10^{-2}
	Permeability of the Depository Layer (cm/sec)	10^{-9}	10^{-5}
	Permeability of the Barrier Layer (cm/sec)	10^{-7}	10^{-5}
(2)	Permeability of the Shaft Fracture Zone (cm/sec)	10^{-6}	10^{-5}
	Porosity of the Tunnel Fracture Zone	10^{-3}	10^{-4}
	Permeability of the Aquifer (cm/sec)	10^{-4}	10^{-2}
(3)	Permeability of the Shaft Fracture Zone (cm/sec)	10^{-6}	10^{-5}
	Permeability of the Tunnel Fracture Zone (cm/sec)	10^{-6}	10^{-5}
	Permeability of the Aquifer (cm/sec)	10^{-4}	10^{-2}
(4)	Permeability of the Shaft Fracture Zone (cm/sec)	10^{-6}	10^{-5}
	Permeability of the Tunnel Fracture Zone (cm/sec)	10^{-6}	10^{-5}
	Permeability of the Depository Layer (cm/sec)	10^{-9}	10^{-5}
	Permeability of the Barrier Layer (cm/sec)	10^{-7}	10^{-5}
	Permeability of the Aquifer (cm/sec)	10^{-4}	10^{-2}

507 023

TABLE O-12. Parameters varied in Table N-5.

RUN INDEX NUMBER	VARIED PARAMETER	BASELINE VALUE	NEW VALUE
(1)	Aquifer Length (m) Head Gradient	1.6×10^{4} 5×10^{-3}	1.6×10^{3} 5×10^{-2}
(2)	Permeability of the Aquifer (cm/sec) Actinide Retardation Factor	10^{-4} 10^{4}	10^{-2} 10^{2}
(3)	Permeability of the Aquifer (cm/sec) Actinide Retardation Factor Leach Rate (yr^{-1})	10^{-4} 10^{4} 10^{-4}	10^{-2} 10^{2} 10^{-1}

TABLE O-13. Parameters varied in Table N-7.

RUN INDEX NUMBER	VARIED PARAMETER	BASELINE VALUE	NEW VALUE
(1)	Permeability of Backfill in the Tunnel (cm/sec) Permeability of Backfill in the Shaft (cm/sec) Porosity of Backfill in the Shaft and Tunnel	10^{-4} 10^{-4} 10^{-2}	10^{-3} 10^{-3} 10^{-1}
(2)	Permeability of Backfill in the Tunnel (cm/sec) Permeability of Backfill in the Shaft (cm/sec) Porosity of Backfill in the Shaft and Tunnel	10^{-4} 10^{-4} 10^{-2}	10^{-3} 10^{-6} 10^{-1}
(3)	Permeability of Backfill in the Tunnel (cm/sec) Permeability of Backfill in the Shaft (cm/sec) Porosity of Backfill in the Shaft and Tunnel	10^{-4} 10^{-4} 10^{-2}	10^{-1} 10^{-6} 10^{-1}

TABLE O-14. Parameters varied in Table N-8.

RUN INDEX NUMBER	VARIED PARAMETER	BASELINE VALUE	NEW VALUE
(1)	Permeability of Backfill in the Tunnel (cm/sec) Permeability of Backfill in the Shaft (cm/sec) Porosity of Backfill in the Shaft and Tunnel	10^{-4} 10^{-4} 10^{-2}	10^{-3} 10^{-3} 10^{-1}
(2)	Permeability of Backfill in the Tunnel (cm/sec) Permeability of Backfill in the Shaft (cm/sec) Porosity of Backfill in the Shaft and Tunnel	10^{-4} 10^{-4} 10^{-2}	10^{-3} 10^{-6} 10^{-1}
(3)	Permeability of Backfill in the Tunnel (cm/sec) Permeability of Backfill in the Shaft (cm/sec) Porosity of Backfill in the Shaft and Tunnel	10^{-4} 10^{-4} 10^{-2}	10^{-1} 10^{-6} 10^{-1}
(4)	Permeability of Backfill in the Tunnel (cm/sec) Permeability of Backfill in the Shaft (cm/sec) Porosity of Backfill in the Shaft and Tunnel	10^{-4} 10^{-4} 10^{-2}	10^{-1} 10^{-1} 10^{-1}

507 025

APPENDIX P

COMPARISON OF SPENT FUEL AND HIGH-LEVEL WASTE

Our source for the composition of high-level waste (HLW) from reprocessed fuel comprising the input to the computer models is the ORIGEN code developed at Oak Ridge National Laboratory (Bell, 1973). We ran this code assuming no reprocessing. The code has the same reactor parameters as had been used previously to calculate the composition of HLW. Standard reactor parameters for a light water reactor are given in ORIGEN. We assumed a fuel of uranium enriched to 3.3% ^{235}U exposed for 1100 days at an average power of 30 MW/Mt. Neutron flux ϕ and reactor spectrum parameters THERM, RES, and FAST are set at 2.92 10^{13} n/cm^2-sec, 0.632, 0.333, and 2.0, respectively.

The main differences between the radionuclide compositions of spent fuel and the HLW from reprocessing can be summarized as follows:

- Spent fuel initially contains about 200 times more uranium and plutonium than does HLW.
- The peak ^{226}Ra content of spent fuel is 43 times that of HLW.
- Spent fuel contains 20 times more ^{241}Am than does HLW at 100 years. By 10 000 years, the amounts of ^{241}Am in the two types of waste are approximately equal.
- Spent fuel contains 755 times as much ^{129}I as does HLW because iodine is volatilized during reprocessing. If the volatilized iodine waste is also stored in the waste repository, this difference between spent fuel and HLW disappears.
- The cladding and structure around the spent fuel contain small additional quantities of radioactive materials, of which ^{59}Ni is the most important. However, this nuclide is of minor importance when compared to the fission products in spent fuel.

Figures 15 and 16 show the potential hazard of spent fuel and HLW from reprocessing as a function of time in terms of population dose to the whole body. Potential hazard is calculated by the method described in earlier.

507 025

Also calculated is the potential hazard in terms of individual and population dose to the GI-LLI thyroid, bone, liver, lung, kidney, and skin.

For most computer runs, use of spent fuel source terms would increase the calculated whole-body doses by less than a factor of 2. However, doses would increase by one to two orders of magnitude for the cases studied in which containment was least effective and the actinides escaped. Similar changes will be observed for critical organ doses, in particular:

- In cases where no fission products other than ^{129}I and ^{99}Tc reached the biosphere, the thyroid dose is increased to a point where it may become the critical organ dose. If retained iodine is emplaced with HLW from a reprocessing plant, the same change will result.
- Where all long-lived fission products reach the biosphere, the thyroid dose due to iodine has the same order of magnitude as the GI dose due to other fission products.
- Where the actinides reach the biosphere, whole-body and critical organ doses increase by factors of 20 to 80.

Other changes may result if differences occur between the dissolution rates of spent fuel and HLW from a reprocessing plant.

The time at which the potential hazard curve first falls below the hazard of radium at 2×10^5 y is reduced by about 100 y for spent fuel. Contrary to the assumption of many published studies, the shape of the potential hazard curve is at no time determined by the half-life of ^{239}Pu. This is true for both HLW and spent fuel. During the time period associated with the decay of ^{239}Pu, the potential hazard of the waste is dominated by ^{226}Ra.

507 026

U.S.GPO:1979-689-060/2018

NRC FORM 335 (7.77)

U.S. NUCLEAR REGULATORY COMMISSION

BIBLIOGRAPHIC DATA SHEET

1. REPORT NUMBER (Assigned by DDC)
NUREG/CR-0578
UCRL-52633

4. TITLE AND SUBTITLE (Add Volume No., if appropriate)
High-Level Waste Repository Site Suitability Study - Status Report

2. (Leave blank)

3. RECIPIENT'S ACCESSION NO.

7. AUTHOR(S) Richard A. Heckman; Donald F. Towse; Dana Isherwood; Ted Harvey; Tom Holdsworth

5. DATE REPORT COMPLETED
MONTH February YEAR 1979

9. PERFORMING ORGANIZATION NAME AND MAILING ADDRESS (Include Zip Code)
Lawrence Livermore Laboratory
Livermore, California 94550

DATE REPORT ISSUED
MONTH July YEAR 1979

6. (Leave blank)

8. (Leave blank)

12. SPONSORING ORGANIZATION NAME AND MAILING ADDRESS (Include Zip Code)
Office of Nuclear Material Safety and Safeguards
U.S. Nuclear Regulatory Commission

10. PROJECT/TASK/WORK UNIT NO.

11. CONTRACT NO.
NRC FIN-A0277

13. TYPE OF REPORT
Status

PERIOD COVERED (Inclusive dates)
October 1976 to January 1978

15. SUPPLEMENTARY NOTES

14. (Leave blank)

16. ABSTRACT (200 words or less)

This report covers the status of site suitability studies performed as part of the Waste Management Technical Support Project which Lawrence Livermore Laboratory is conducting for the Nuclear Regulatory Commission.

This report describes the progress made on site suitability criteria for high-level radioactive waste repositories, through January 1978.

17. KEY WORDS AND DOCUMENT ANALYSIS

17a. DESCRIPTORS

17b. IDENTIFIERS/OPEN-ENDED TERMS

18. AVAILABILITY STATEMENT
Unlimited

19. SECURITY CLASS (This report)

21. NO. OF PAGES

20. SECURITY CLASS (This page)

22. PRICE
$

NRC FORM 335 (7.77)

507 029

UNITED STATES
NUCLEAR REGULATORY COMMISSION
WASHINGTON, D. C. 20555

OFFICIAL BUSINESS
PENALTY FOR PRIVATE USE, $300

POSTAGE AND FEES PAID
U.S. NUCLEAR REGULATORY
COMMISSION

Stan Scott
[illegible]/220

[illegible] PUBLIC DOCUMENT ROOM
[illegible]
[illegible] DC 20555

507 028